

Dissertation zur Erlangung des Doktorgrades  
der Fakultät für Chemie und Pharmazie  
der Ludwig-Maximilians-Universität München



**The innate immune sensors RIG-I and MDA5:  
Identification of *in vivo* ligands and functional investigation  
of the SF2 domain**

Helga Charlotte Lässig

aus

Dresden, Deutschland

2016



## **Erklärung**

Diese Dissertation wurde im Sinne von §7 der Promotionsordnung vom 28. November 2011 von Herrn Prof. Dr. Karl-Peter Hopfner betreut.

## **Eidesstattliche Versicherung**

Diese Dissertation wurde eigenständig und ohne unerlaubte Hilfe erarbeitet.

München, 03. Juni 2016

---

Helga Charlotte Lässig

Dissertation eingereicht am 07. Juni 2016

1. Gutachter: Prof. Dr. Karl-Peter Hopfner
2. Gutachter: Prof. Dr. Karl-Klaus Conzelmann

Mündliche Prüfung am 25. Juli 2016



This thesis has been prepared from July 2012 to May 2016 in the laboratory of Professor Dr. Karl-Peter Hopfner at the Gene Center of the Ludwig-Maximilians-Universität München.

This is a cumulative thesis based on the publications:

Runge S\*, Sparrer KMJ\*, Lässig C\*, Hembach K, Baum A, García-Sastre A, Söding J, Conzelmann K-K, Hopfner K-P (2014) *In vivo* ligands of MDA5 and RIG-I in measles virus-infected cells. PLoS Pathogens 10(4):e1004081.

\* These authors contributed equally.

Lässig C, Matheisl S\*, Sparrer KMJ\*, de Oliveira Mann CC\*, Moldt M, Patel JR, Goldeck M, Hartmann G, García-Sastre A, Hornung V, Conzelmann K-K, Beckmann R, Hopfner K-P (2015) ATP hydrolysis by the viral RNA sensor RIG-I prevents unintentional recognition of self-RNA. eLife 2015;4:e10859.

\* These authors contributed equally.

Lässig C, Hopfner K-P (2016) RIG-I-Like receptors: one STrEP forward. Trends in Microbiology. in press. (spotlight article)



# Table of contents

<b>Summary</b>	<b>1</b>
<b>Introduction</b>	<b>3</b>
1 Basic principles of the immune system . . . . .	3
2 Pattern recognition receptors of the innate immune system . . . . .	4
2.1 Nucleic acid-sensing by Toll-like receptors . . . . .	5
2.2 Recognition of cytosolic DNA . . . . .	6
2.3 RNA-sensing by RIG-I-like receptors . . . . .	7
2.3.1 RIG-I and MDA5 signaling cascade via the adapter protein MAVS . . . . .	8
2.3.2 LGP2 has regulatory functions in RIG-I or MDA5-mediated signaling . . . . .	10
2.3.3 RNA structures recognized by RIG-I-like receptors <i>in vitro</i> and <i>in vivo</i> . . . . .	10
3 Structural basis for antiviral signaling of RIG-I and MDA5 . . . . .	12
3.1 The ligand-free state of RIG-I and MDA5 . . . . .	14
3.2 RIG-I signaling requires a conformational switch that releases the CARDs . . . . .	14
3.3 Cooperative binding of MDA5 on dsRNA stems induces signaling . . . . .	17
3.4 RIG-I and MDA5 are regulated by post-translational modifications . . . . .	18
4 The ATPase domain of RIG-I-like receptors . . . . .	21
4.1 ATPase activity of RIG-I correlates with its binding affinity towards RNA . . . . .	23
4.2 MDA5 forms ATP-sensitive filaments . . . . .	24
4.3 RIG-I forms signaling competent filaments in presence of ATP . . . . .	24
4.4 RIG-I and MDA5 show ATP-dependent effector-like functions in virus-infected cells . . . . .	25
5 Immune evasion strategies of viruses to avoid RIG-I-like receptor-signaling . . . . .	26
6 Mutations within the RIG-I-like receptor SF2 domain can cause autoimmune diseases . . . . .	26
6.1 Type I interferonopathies – the Aicardi-Gutières syndrome and systemic lupus erythematosus . . . . .	27
6.2 Other RIG-I-like receptor-related autoimmune diseases: the Singleton-Merten syndrome and type 1 diabetes . . . . .	29
7 Objectives . . . . .	31
<b>Publications</b>	<b>33</b>
1 <i>In vivo</i> ligands of MDA5 and RIG-I in measles virus-infected cells . . . . .	33
2 ATP hydrolysis by the viral RNA sensor RIG-I prevents unintentional recognition of self-RNA . . . . .	49
<b>Discussion</b>	<b>71</b>
1 Discrimination of self vs non-self by RIG-I and MDA5 . . . . .	71
1.1 What are physiological ligands of RIG-I and MDA5? . . . . .	71
1.2 Is RIG-I's CTD able to bind dsRNA stems? . . . . .	73

2	What role has ATP in RIG-I-like receptor signaling? . . . . .	74
2.1	RNA and ATP binding liberate the RIG-I CARDs, whereas MDA5 activation needs RNA only . . . . .	75
2.2	ATP hydrolysis by RIG-I and MDA5 impedes signaling on endogenous RNA . .	76
2.3	ATP influences LGP2's regulatory function . . . . .	77
3	Translocation of RLRs: a model based on the Hepatitis C virus NS3 protein . . . . .	78
4	The current model of RNA- and ATP-dependent activation of RIG-I and MDA5 . . . .	82
	<b>References</b>	<b>85</b>
	<b>List of abbreviations</b>	<b>109</b>
	<b>Acknowledgments</b>	<b>111</b>

## Summary

The innate immune system provides our body with a first set of rapid defense mechanisms against invading pathogens. Microbial or eukaryotic invaders are sensed by specialized, germline-encoded innate immune receptors that induce the activation of a systemic response in order to fight off the infection. The innate immune system also triggers the activation of the adaptive immune system and modulates the phenotype and function of the adaptive response.

Constitutive activation of innate immune sensors, however, or loss of specificity and therefore misfiring by detection of endogenous molecules can lead to serious autoimmune disorders. Indeed, more and more diseases have been linked to different innate immune pathways. The molecular basis for incorrect signaling, nevertheless, often remains to be determined.

The RIG-I-like receptors (RLRs) RIG-I, MDA5 and LGP2 are cytosolic distributed proteins, that detect foreign double-stranded (ds) RNA. RLRs consist of several domains specialized in dsRNA-recognition as well as in transmitting the recognition event to other proteins in order to start the defense.

Despite the availability of several RLR protein structures accompanied with various *in vitro* and *in vivo* experiments, the exact role of their central Superfamily 2 (SF2) helicase domain, that displays an RNA-dependent ATP hydrolysis function, is still not understood. Furthermore, whereas from *in vitro* experiments it is known that RIG-I favors the recognition of short dsRNA ends containing 5' tri- or diphosphates and MDA5 cooperatively binds within long dsRNA, so far only limited knowledge of *in vivo* ligands and their origin in infected cells is available.

In order to identify physiological ligands of RLRs, in the first part of this thesis, RIG-I and MDA5 protein:RNA complexes from measles virus (MeV)-infected cells were purified and analyzed via deep sequencing. The results were validated by qPCR and are supported by several *in vitro* and *in silico* analyses. Specifically, RIG-I and MDA5 were found to recognize distinct but partly overlapping MeV RNA species: MDA5 preferentially interacted with mRNA species of the MeV polymerase gene. RIG-I additionally bound positive and negative-sense RNA near the genomic and antigenomic 5' ends. Both RIG-I and MDA5 interacted with 5'-copyback defective interfering (DI) sequences as detected by PCR. Further, *in vitro* transcripts covering different regions of the MeV antigenome were used to verify the correlation between actual immunostimulatory potential of RNA and deep sequencing results. Bioinformatics analysis in addition revealed a preference of MDA5 for AU-rich RNA but an anti-correlation of MDA5 ATP hydrolysis rate and RNA AU-content.

Based on this study, a model of how MDA5 preferentially senses AU-rich dsRNA species can be established: In this regard a reduced ATPase function of MDA5 when bound to AU-rich RNA helps to generate stable protein filaments and therefore leads to increased type I interferon signaling.

In the second and major part of this thesis the RIG-I SF2 helicase domain as well as RIG-I variants identified in the multi-system disorder Singleton-Merten syndrome (SMS) were functionally analyzed. RIG-I SF2 mutants deficient in ATP binding severely lost their signaling capabilities in both infected and uninfected cells. In contrast to that, ATP hydrolysis-impaired RIG-I that can still bind ATP, a phenotype that is found in SMS patients as well, constitutively signaled on endogenous RNA. Furthermore, the recognition of a ribosomal expansion segment by ATP hydrolysis-impaired RIG-I could be determined through co-immunopurification from uninfected cells and was visualized by cryo-electron microscopy. Interactions with the ribosome were also found for the respective MDA5 mutant as well as in infected cells. Subsequent biochemical analyses validated reduced binding of wild type RIG-I in presence of ATP, whereas ATP hydrolysis-deficient RIG-I was found to stably interact with this RNA.

The presence of ATP therefore seems to be a prerequisite for RIG-I immune signaling and probably helps to release the CARD domains. ATP hydrolysis by RIG-I, in contrast, weakens the affinity of the protein towards endogenous RNA lacking the 5' triphosphate signature. This renders the ATPase domain of RIG-I to be an essential feature for the discrimination between self and non-self RNA.

Importantly, both studies combined provide the basis for an updated view on ATP-dependent RIG-I-like receptor signaling that is presented and discussed.

# Introduction

## 1 Basic principles of the immune system

All organisms need to continuously protect themselves against invading pathogens. Because of that all domains of life evolved sophisticated defense strategies, including both inherited as well as adaptive mechanisms, known as immune system<sup>1</sup>. Immunity is provided if an organism is able to detect and eliminate foreign molecules or pathogens while tolerating non-harmful self molecules or commensal organisms.

The human body is prepared with two distinct kinds of immune systems: an inherited, rather unspecific system, as well as an adaptive one, that is able to specifically react to changing environmental conditions<sup>2</sup>.

Inherited or innate immune systems are passed from one generation to the next and often provide more general detection mechanisms for several classes of molecules. The innate immune system of multicellular organisms is fairly conserved across evolution and mediated by a limited number of germline-encoded receptors. Similar receptors are found in plants and animals<sup>3</sup>. Innate systems, however, only have a short term memory and need to start from the beginning every time they encounter foreign molecules.

Adaptive immune systems, on the other hand, are typically more specialized and can be acquired in a relatively short period of time<sup>1</sup>. Adaptive immunity of jawed vertebrates is facilitated by antigen specific receptors that are not germ-line encoded, but generated by random genomic recombination of gene segments resulting in many different but individual receptor specificities. Those adaptive systems are characterized by a greater number of reacting receptors, an extended life span and memory, while providing a more rapid response to molecules they might not have seen before. The adaptive response, however, is also more prone for the development of allergy and autoimmunity<sup>4</sup>.

The importance of an intact immune system is frequently emphasized, for instance by the recent Ebola or Zika virus pandemics or by the recurring influenza virus outbreaks. The molecular basis for pathogen recognition and defense of the human body as well as the tricks of pathogens to evade immune recognition and to successfully reproduce, however, are still fairly unknown and subject of recent research.

A precise knowledge about these mechanisms will help to develop better vaccines or therapeutics, but also contributes to our understanding of autoimmune diseases where immune receptors are directed against self.

## 2 Pattern recognition receptors of the innate immune system

If pathogens successfully overcome the physical and chemical barriers of the human body and try to establish an infection, they immediately face different innate immune sensors called pathogen recognition receptors (PRRs). PRRs survey both the intra- and extracellular space, and are activated by unique, so-called pathogen-associated molecular patterns (PAMPs) that are conserved and specific to a wide range of microorganisms<sup>5</sup>.

PAMPs are often to some extent invariable since they represent molecular structures that are essential for the pathogen survival and therefore are not subject to a rapid adaptive evolution of the pathogen<sup>5</sup>. Further, PAMPs are typically either not expressed or modified by the mammalian host, or only occur in certain compartments. Nevertheless, some PRRs also recognize endogenous molecules released from damaged cellular compartments or cells, so-called damage-associated molecular patterns (DAMPs)<sup>6</sup>. Recognition of PAMPs and DAMPs by different PRRs is considerably redundant ensuring that a microbe that evades one mechanism can still be detected by another.

Upon sensing of PAMPs or DAMPs, PRRs activate signaling cascades that start the expression of interferons, cytokines and chemokines, that in turn promote the synthesis of many antiviral proteins<sup>7</sup>. These proteins shut down translation, promote growth arrest or even cell death. Cytokines and chemokines further recruit immune cells to the site of infection in order to control pathogen spread and to initiate an adaptive immune response<sup>7</sup>. Collectively, both innate and adaptive immune response subsequently provide the mechanisms to fight off the infection and to restore homeostasis.

Problems occur, however, if there is no clear cut-off criterion for the distinction between self and non-self. Viruses for example, express only a very limited number of specific molecules and on top exploit the host cell machinery for their reproduction. In order to detect viruses, the immune system thus often relies on the recognition of viral nucleic acids that flood the cell upon an infection, and thereby risks to evolve autoimmunity against very similar self molecules<sup>8</sup>.

The major families of human PRRs are: Toll-like receptors (TLRs), C-type lectin receptors (CLRs), retinoic acid-inducible gene I (RIG-I)-like receptors (RLRs), nucleotide binding oligomerization domain (NOD)-like receptors (NLRs), absent in melanoma 2 (AIM2)-like receptors (ALRs) and the cyclic GMP-AMP synthase (cGAS)/ stimulator of interferon genes (STING) system.

TLRs are membrane bound receptors recognizing a variety of different bacterial, fungal and viral PAMPs ranging from cell wall parts such as lipopolysaccharides and lipopeptides over parts of the bacterial flagellum to different kinds of nucleic acids<sup>9</sup>. CLRs are a large family of soluble and membrane bound receptors recognizing specific carbohydrate structures<sup>10</sup>. RLRs, ALRs and cGAS bind foreign or mislocated cytosolic double-stranded (ds) nucleic acids<sup>11</sup>. NLRs are located within the cytosol as well and provide a back-up defense by recognizing bacterial cell wall components similar to TLRs, but also toxins or host-derived ligands, e.g. uric acids or damaged membranes. Many NLRs assemble into large inflammasome complexes<sup>12</sup>.

This thesis focuses on RIG-I-like receptors and the detection of cytosolic viral RNA. For that purpose, first other nucleic acid-sensing PRRs in general, including TLRs and the cGAS/STING system, are briefly introduced. Afterwards the main attention is drawn towards RLRs signaling.

## 2.1 Nucleic acid-sensing by Toll-like receptors

Toll-like receptors are membrane-bound proteins mostly expressed on immune cells, endothelial and epithelial cells with each cell type expressing a different set of TLRs<sup>13,14</sup>. They reside both on the cell surface as well as on intracellular membranes. 10 human TLRs are known: TLR1, TLR2, TLR4, TLR5, TLR6 and TLR10 are expressed largely on the surface of cells and recognize molecules found outside of pathogens, like e.g. components of the bacterial cell wall. TLR3, TLR7, TLR8 and TLR9 are located within the membrane of the endosomal compartment and generally bind structures that are only available after uptake and destruction of potential pathogens<sup>15</sup>. TLRs all have a characteristic extracellular horseshoe-like shaped leucine-rich repeat (LRP) domain, a transmembrane domain and a cytosolic Toll/interleukin-1 receptor (TIR) domain<sup>16</sup>.

TLRs are activated by simultaneous PAMP binding to two TLRs which leads to homo- or heterodimerization and to the recruitment of several intracellular signaling adapters and kinases. Activated and dimerized TLRs further form higher order clusters in the cell membrane. Specifically, TLRs recognize PAMPs via their extracellular domains. Except for TLR3, which uses TRIF as adapter molecule, all TLRs then directly or indirectly interact through their cytosolic TIR domains with the adapter protein MyD88 for downstream signal transmission (Figure 1). MyD88 in turn promotes the formation of the so-called Myddosome, a large helical assembly of several TLRs and MyD88s, via their death domains that enables the interaction with signal transmitting kinases<sup>18</sup>.

TLR2 forms a heterodimer with either TLR1 or TLR6 in order to bind different kinds of bacterial lipoproteins<sup>19,20</sup>. TLR10 seems to have regulatory roles by competing for ligands with TLR2<sup>21</sup>. TLR4 recognizes lipopolysaccharides (LPS) which is a major component of the outer membrane of Gram-

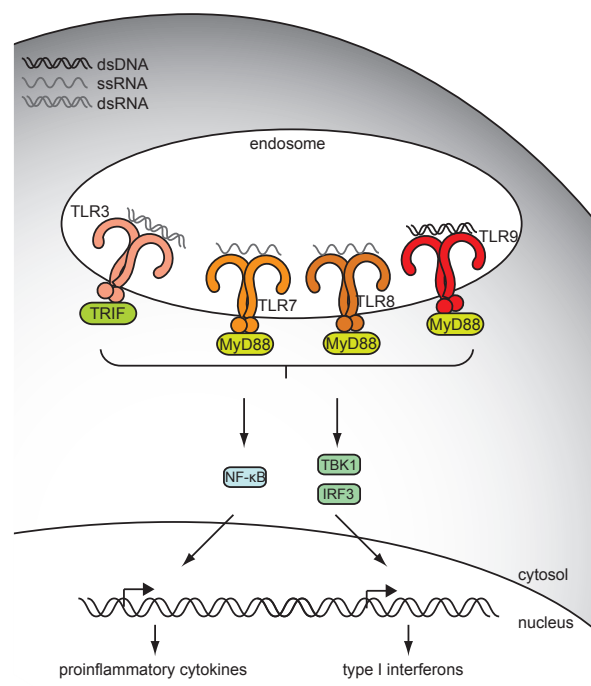


**Figure 1:** Simplified signaling cascade of the endosomal Toll-like receptor pathway. All nucleic acid-sensing TLRs reside in endosomes, dimerize upon ligand binding and signal either via the adapter protein TRIF or MyD88. These in turn activate the NF- $\kappa$ B- and IRF3-dependent expression of proinflammatory cytokines and type I interferons.

Figure adopted from Junt and Barchet<sup>17</sup>.

negative bacteria<sup>22–24</sup> and TLR5 can be activated by a depolymerized form of bacterial flagellin<sup>25</sup>.

Nucleic acid-binding TLRs, however, only reside within the endosomal compartment. Guanosine- and uridine-rich single-stranded (ss) RNA as well as synthetic polyuridines and siRNAs are recognized by TLR7 and TLR8<sup>26–29</sup>. TLR3 responds to dsRNA<sup>30</sup>. TLR9 was originally described to recognize double-stranded, unmethylated CpG-rich DNA<sup>31</sup> but was later shown to only depend on the 2′-deoxyribose backbone of nucleic acids and therefore to respond to all kinds of dsDNA regardless of specific sequences<sup>32,33</sup>.

## 2.2 Recognition of cytosolic DNA

Since the occurrence of DNA within eukaryotic cells is restricted to the nucleus and mitochondria, the appearance of cytosolic DNA in non-dividing cells provides a clear danger signal for potentially invaded pathogens or cellular damage. DNA-sensing TLRs are, however, restricted to plasma membranes, thereby facing the extracellular space or endosomes. Thus several cytosolic DNA sensors, including DNA-dependent activator of IFN-regulatory factors (DAI), DDX41, interferon gamma inducible protein 16 (IFI16), AIM2 and cGAS, exist<sup>11,34–38</sup>. With the exception of cGAS and IFI16, however, they play redundant roles or may be cell type specific.

cGAS is ubiquitously expressed and belongs to the nucleotidyltransferase (NT) family. It consists of a C-terminal NTase and Mab21 domain which is highly conserved in vertebrates, and of a less conserved, long unstructured N-terminal sequence<sup>37</sup>. cGAS is activated by a variety of DNA stimuli, including transfected plasmid DNA, mislocated mitochondrial DNA, and viral DNA generated by infection with DNA viruses as well as retroviruses. For HIV-1 especially, it was shown that cGAS recognizes short Y-shaped cDNA structures with unpaired, flanking guanosines<sup>39</sup>. cGAS was also found to indirectly contribute to the recognition of some RNA viruses, perhaps by inducing a very low basal autoimmune response triggered by endogenous DNA, which ensures the availability of other sensors needed for the primary response to viruses<sup>40</sup>.

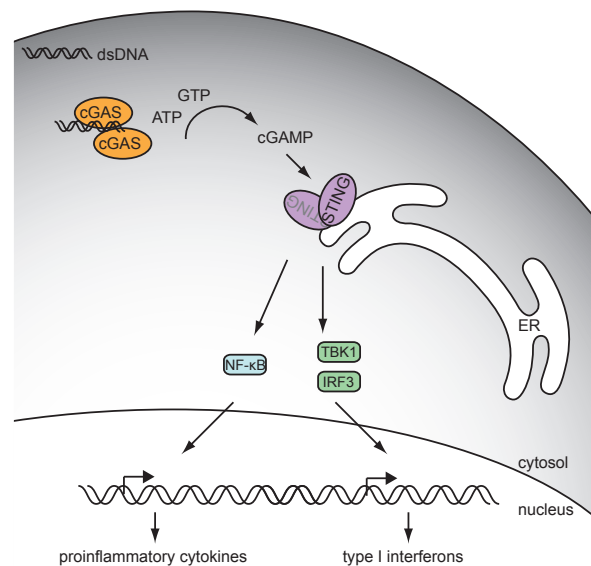
When activated by dsDNA, cGAS catalyzes the production of cyclic AMP-GAMP (cGAMP) from ATP and GTP, which in turn functions as an endogenous second messenger for the activation of the endoplasmic reticulum (ER)-bound adapter protein STING<sup>41</sup> (Figure 2). dsDNA-binding by cGAS is facilitated by a highly positive charged platform as well as a conserved zinc thumb which is furthermore important for DNA-induced dimerization of cGAS<sup>42–45</sup>. Interestingly, the cGAMP produced by cGAS is Gp(2′–5′)Ap(3′–5′) and contains a mixed phosphodiester linkage between the two ring-forming nucleotides<sup>46–48</sup>. STING, however, responds to various cyclic dinucleotides (CDNs) and is, even though to a lesser extent, activated by bacterial CDNs like c-di-GMP or c-di-AMP as well, thereby providing an additional direct immune response to bacterial second messengers<sup>49</sup>.

Upon binding to CDNs, STING in turn triggers the induction of type I interferons in order to start an immune response. Thereby STING was found to dimerize and to relocate from the ER to perinuclear vesicles<sup>50</sup>.

Two other DNA sensors, AIM2 and IFI16, are shown to trigger an immune response through the

**Figure 2:** Simplified signaling cascade of the cGAS/STING pathway. Upon detection of cytosolic dsDNA, cGAS dimerizes and produces the eukaryotic second messenger cGAMP, which activates the adapter protein STING. STING in turn induces the NF- $\kappa$ B- and IRF3-dependent expression of proinflammatory cytokines and type I interferons.

Figure adopted from Junt and Barchet<sup>17</sup>.



activation of the inflammasome<sup>51–53</sup>, which is an intracellular multiprotein complex that mediates the activation of caspase-1 and thereby triggers pyroptotic cell death through an inflammatory response<sup>54</sup>. Both proteins contain a positively charged DNA-binding HIN-200 domain<sup>55</sup> as well as a pyrin domain (PYD) that allows homotypic PYD:PYD interactions with the adapter protein ASC<sup>56</sup>. ASC further possesses a caspase activation and recruitment domain (CARD) and, through CARD-CARD interactions, links the PYD-containing sensor proteins to caspase-1 recruitment, dimerization, and autoproteolytic activation. Caspase-1 in turn processes the inactive precursors of IL-1 $\beta$  and IL-18 into mature cytokines<sup>57</sup>.

In addition IFI16 was reported to detect foreign DNA within the nucleus<sup>58</sup> and might thereby even interact with cGAS<sup>59</sup>.

### 2.3 RNA-sensing by RIG-I-like receptors

In contrast to cytosolic DNA, cytosolic RNA as such is no unusual condition, since translation is facilitated outside the nucleus. Thus several types of endogenous RNAs, including small RNAs, mRNAs, rRNAs and tRNAs are localized in the cytosol and need to be discriminated from foreign, often viral, RNA.

Non-self cytosolic RNA is detected by the RIG-I-like receptors including the eponymous RIG-I, melanoma differentiation-associated gene 5 (MDA5) and laboratory of genetics and physiology 2 (LGP2). RLRs are ubiquitously expressed and thereby ensure that every cell can respond to viral infections. All RLRs specifically recognize foreign dsRNA with slightly different substrate specificities which broadens the spectrum of detected viruses.

RIG-I and MDA5 are composed of three major domains: two N-terminal CARDs necessary for signaling, a central Superfamily 2 (SF2) helicase domain and a C-terminal domain (CTD). Both SF2 helicase domain and CTD are involved in RNA binding<sup>60–62</sup>. Furthermore, an alternative splicing form for each RIG-I and MDA5 exist<sup>63</sup>: RIG-I isoform 2 lacks the amino acids (aa) 36 – 80 within the CARDs,

while MDA5 isoform 2 contains only the CARDS aa 1 – 207 as well as an additional 14 aa tail. LGP2 misses the CARDS entirely but has otherwise a similar domain architecture.

Detection of dsRNA by RIG-I and MDA5 releases the otherwise shielded CARDS<sup>61</sup>, rendering them free to bind to the mitochondrial antiviral signaling protein (MAVS) through CARD-CARD interactions<sup>64–69</sup>. This interaction can further be stabilized by binding of K48-linked ubiquitin chains<sup>69,70</sup>. Translocation of activated cytosolic RIG-I to the membrane bound MAVS is facilitated by 14-3-3 $\epsilon$  chaperons<sup>71</sup>. Activation of MAVS by RIG-I or MDA5 in turn starts an innate immune response that aims to clear the cell of the invading virus, to attract specialized immune cells, and to alert and protect uninfected neighboring cells.

LGP2 is thought to have regulatory functions within this process, since it lacks the signal promoting CARDS<sup>72,73</sup>.

### 2.3.1 RIG-I and MDA5 signaling cascade via the adapter protein MAVS

Similar to MyD88 within the TLR pathway or STING within the cGAS axis, MAVS integrates the RLR immune response signal, and promotes the activation of several transcription factors. These include nuclear factor  $\kappa$ -light-chain-enhancer of activated B cells (NF- $\kappa$ B) and various interferon regulatory factors (IRFs), all of which together act to create an antiviral state of the cell (Figure 3).

MAVS itself contains a C-terminal transmembrane domain anchoring it to mitochondria, peroxisomes and mitochondrion-associated membranes<sup>74</sup>, a long unstructured region and an N-terminal CARD domain. Binding of the RIG-I or MDA5 CARDS to the MAVS CARD, leads to conformational changes within MAVS and to multimerization into prion-like functional aggregates. Thereby MAVS polymers recruit more MAVS molecules and that in turn activate downstream proteins<sup>75</sup>.

MAVS is, depending on its localization, able to induce a sequential antiviral response. Peroxisome-bound MAVS triggers an immediate interferon-independent antiviral response that provides short-term protection by inducing type III interferons and the rapid expression of antiviral genes<sup>76</sup>. Mitochondrion-located MAVS, apart from that, triggers type I interferon (IFN) gene expression ensuring a long-term containment of the infection<sup>74</sup>. In the latter case, MAVS polymers recruit several redundantly acting tumor necrosis factor (TNF) receptor-associated factors (TRAF) ubiquitin E3 ligases through proline-rich repeats within the unstructured region to synthesize linear K63-linked polyubiquitin chains<sup>77</sup>. These polyubiquitin chains in turn bind the regulatory subunits of I $\kappa$ B kinase (IKK) and TANK-binding kinase 1 (TBK1) complexes thereby activating them<sup>78–81</sup>. Active IKK phosphorylates the inhibitor of NF- $\kappa$ B (I $\kappa$ B) resulting in its degradative K48-linked polyubiquitination and subsequent proteasome-mediated digestion. Active TBK1, in contrast, phosphorylates the MAVS polymer, which is then able to recruit IRF3 that harbors a positively charged phospho-binding domain<sup>82</sup>. This recruitment enables TBK1 to phosphorylate IRF3 as well, thereby resulting in its dimerization and activation. Finally, activated NF- $\kappa$ B and IRF3 translocate into the nucleus and activate the expression of interferons and multiple cytokines or chemokines.

Cytokines and chemokines help to recruit immune cells to the site of viral infection in order to control

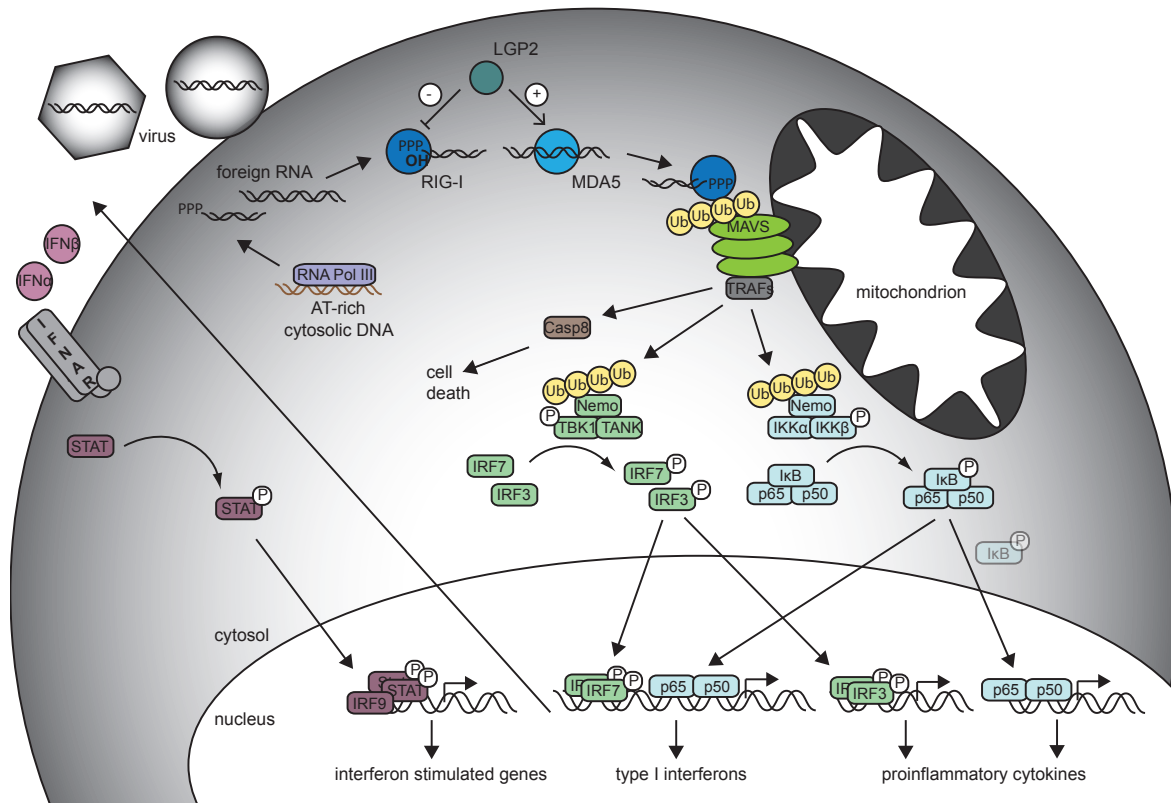


**Figure 3:** Signaling cascade initiated by RIG-I-like receptors. RIG-I and MDA5 recognize different foreign cytosolic dsRNA species or RNA polymerase III transcripts. LGP2 is thought to have regulatory functions. Activation and tetramerization of RIG-I and MDA5, followed by subsequent K63-linked ubiquitination or ubiquitin binding (see section 3.4), induces to MAVS polymerization. MAVS polymers recruit several TRAF proteins that synthesize K63-linked ubiquitin chains and thereby activate IKK and TBK1 complexes. IKK and TBK1 phosphorylate different IRFs or I $\kappa$ B and thus induce their translocation into the nucleus in order to activate the expression of type I interferons and proinflammatory cytokines.

Released interferons in turn initiate the expression of hundreds of interferon stimulated genes via the STAT pathway.

virus spread and to initiate the adaptive immune response. IFNs activate the janus kinase/signal transducers and activators of transcription (JAK/STAT) pathway and lead in turn to the expression of several hundreds interferon regulated genes (ISGs) in both the infected and surrounding uninfected cells<sup>83</sup> (Figure 3). ISGs encode additional cytokines and chemokines, antibacterial effectors, pro- and anti-apoptotic molecules, as well as molecules involved in metabolic processes, that amplify and stabilize the antiviral response. In addition, all RLRs are ISGs themselves and are upregulated in order to boost or control the immune response<sup>84</sup>.

Other ISGs comprise the RIG-I splice variant lacking aa 36-80 within the first CARD domain<sup>85</sup>. This variant competes with full-length RIG-I for RNA substrates, but potentially suppresses the CARD-CARD interactions with MAVS and therefore interferon signaling. Further, an N-terminally shortened isoform of MAVS that entirely misses the CARD domain is upregulated during infections and might interfere with the immune response by competing with downstream signaling factors of MAVS<sup>86</sup>. Both shortened molecules thus provide a negative feed-back loops and help to modulate the im-

mune response.

RLRs were further shown to co-localize to virus-induced stress granules (SGs) upon phosphorylation of eukaryotic translation initiation factor  $2\alpha$  (eIF2 $\alpha$ ) by dsRNA-dependent protein kinase (PKR) or general control non-derepressible-2 (GCN2) during some viral infections<sup>87-89</sup>. Phosphorylation of eIF2 $\alpha$  terminates the initiation of translation, stalls mRNAs and thereby inhibits mRNA translation until eIF2 $\alpha$  is dephosphorylated again. Several viruses are implicated in inducing SG formation or even shown to exploit them for replicating their own RNAs<sup>90,91</sup>. Other viruses however, like measles virus, are shown to inhibit SGs by promoting RNA editing thereby decreasing the amount of PKR substrates<sup>92</sup>. SGs could thus represent a platform for viral RNA recognition and immune response activation by RLRs.

### 2.3.2 LGP2 has regulatory functions in RIG-I or MDA5-mediated signaling

In contrast to RIG-I and MDA5, there is still relatively little known about LGP2. LGP2 was originally discovered as highly expressed gene in a mammary tissue<sup>93</sup> and later shown to be involved in anti-viral signaling<sup>94</sup>. Since then mostly controversial literature regarding LGP2's function has been published. Even though, of all RLRs, LGP2 has the highest affinity for RNA and it might bind to the same RNA substrates as RIG-I or MDA5 or both<sup>95</sup>, the role of LGP2 within the RLR signaling pathway is contradictory. Since LGP2 lacks CARDs it might function as a negative feedback regulator by competitive binding of stimulatory RNA<sup>68,72</sup>. Later studies, however, suggested that LGP2 might have different regulatory roles depending on the virus and the RLR it might interact with<sup>96</sup>.

In that regard, limited levels of LGP2 are reported to have a positive regulatory role for MDA5 by promoting cooperative dsRNA binding<sup>97-99</sup>. Higher levels of LGP2, however, negatively regulate RIG-I and to a lesser extent MDA5-mediated signaling<sup>99</sup>. Furthermore, LGP2 was shown to be required for T cell survival during virus infection by blocking death-receptor-mediated cell death<sup>100</sup>. This might be related to the inhibition of RIG-I-mediated signaling at high protein concentrations in order to terminate the immune response and to prevent cell death.

### 2.3.3 RNA structures recognized by RIG-I-like receptors *in vitro* and *in vivo*

Despite their structural similarities, RLRs recognize distinct dsRNA species *in vitro*. At the same time, they have overlapping functions in virus recognition. Many negative-sense RNA viruses including orthomyxoviruses, rhabdoviruses and bunyaviruses are predominantly recognized by RIG-I. MDA5, in contrast, detects picornaviruses and caliciviruses. Several flaviviruses, paramyxoviruses and reoviruses are sensed by both RIG-I and MDA5<sup>101</sup>.

In order to allow a distinction of both RNA strands within the duplex, this thesis will refer to the strand that is mainly recognized by the SF2 helicase domain as "bottom strand". The complementary strand, that might harbor the phosphorylation mark, will be referred to as "top strand" of the RNA duplex (compare to Figure 4).

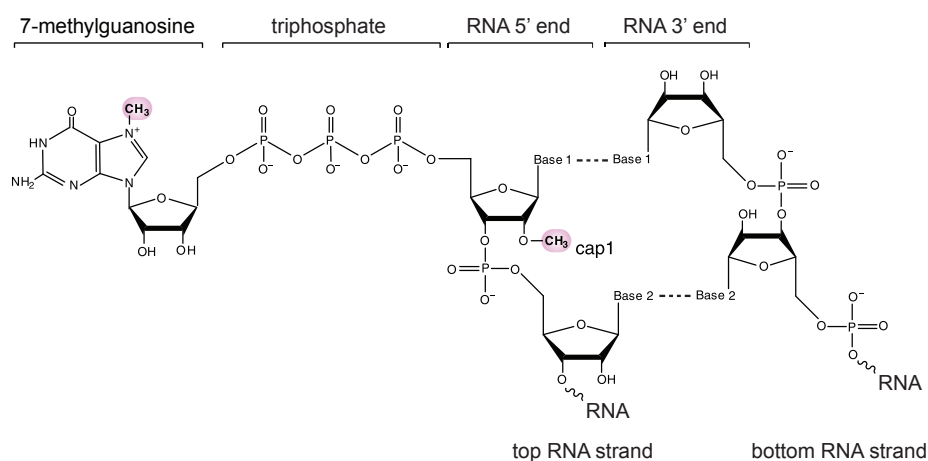


**Figure 4:** The first two base pairs of a potential RIG-I dsRNA substrate. RIG-I preferentially recognizes short dsRNA ends. Methylation of the cap structure as well as of the first 5' ribose (depicted in pink) reduces recognition.

The top and bottom RNA strand of the duplex, as used in this thesis, are indicated. Figure adopted from Leung and Amarasinghe<sup>112</sup>.

Numerous *in vitro* experiments defined the optimal RIG-I ligand as short 5' tri- or diphosphorylated dsRNA with at least 10 base pairs length and the phosphate-carrying nucleoside being part of a Watson-Crick base pairing<sup>102–106</sup>. Binding affinities of RIG-I towards 5' phosphorylated dsRNA are in the low nanomolar range<sup>107,108</sup>. However, with only slightly lower affinities RIG-I recognizes blunt-ended dsRNA without phosphates<sup>108</sup> and also tolerates unmethylated 5' cap-structures<sup>105,109</sup>. Methylation at N7 of the capping guanosine or the top strand first ribose, however, drastically decreases signaling<sup>105</sup> (compare with Figure 4). Further, RIG-I accepts RNA:DNA hybrids as well, while only tracking the OH-groups of the bottom RNA strand<sup>110,111</sup>. 3' overhangs at the phosphorylated end are better tolerated by RIG-I than 5' overhangs<sup>102</sup>.

Despite the variety of RNAs that RIG-I is able to recognize *in vitro*, *in vivo* ligands are still controversial. Several transfection assays validated the preference for tri- or diphosphorylated dsRNA<sup>102–104</sup>. The minimal RNA duplex length, however, varies and might depend on the stage of infection or the amount of available RIG-I or RNA substrates, respectively<sup>111,113</sup>. In that regard, even unphosphorylated dsRNAs like ribonuclease L (RNase L) cleavage products of endogenous or viral RNAs amplify RIG-I signaling<sup>114–116</sup>.

Likewise, different infection assays confirm RIG-I activation by 5' tri- or diphosphorylated dsRNA structures, as these are present on viral genomes<sup>102,104</sup> or incoming viral nucleocapsids that are detected by RIG-I<sup>117,118</sup>. RIG-I also recognizes viral replicating RNA products as for instance stem-loop structures in defective interfering (DI) RNA genomes, short internal deletion defective interfering particles<sup>119,120</sup> or abortive replication products. Further, viral or even endogenous mRNAs might represent RIG-I agonists and thereby especially their 3' untranslated regions (UTR)<sup>114,121–123</sup>.

In addition, RIG-I indirectly senses cytosolic DNA through RNA polymerase III that transcribes AT-rich DNA as for instance present in Epstein-Barr virus, adenoviruses and Herpes simplex virus-1, or in

intracellular bacteria like *Legionella pneumophila*, promoter-independently into dsRNA containing a 5' triphosphate<sup>124–126</sup>. RIG-I is further implicated to be involved in the recognition of cytosolic uncapped and unphosphorylated bacterial mRNA<sup>127</sup>.

In contrast to RIG-I, MDA5 has a lower affinity to dsRNA in general, but cooperatively recognizes long dsRNA stems and branched or higher-order structured RNAs<sup>128–130</sup>. Similar to RIG-I, MDA5 is described to discriminate self from non-self based on ribose 2'-OH methylation marks as well<sup>131</sup>. Further, MDA5 is like RIG-I implicated to take part in the recognition of intracellular bacteria, like *Plasmodium* species, probably by detecting double-stranded non-coding RNAs<sup>132</sup>.

In addition, both RIG-I and MDA5 might prefer U- and AU-rich RNA respectively<sup>114,119,133–135</sup>.

Furthermore, RIG-I and MDA5 might respond to viral infections in a temporal manner<sup>136</sup>. For instance, early occurring triphosphate-containing replication intermediates of West Nile Virus are recognized by RIG-I, whereas MDA5 responded to later produced dsRNA species<sup>137</sup>.

Ligands of LGP2 are not well described. Similar to RIG-I, LGP2 preferentially recognizes RNA ends but does not discriminate the phosphorylation state<sup>138</sup>. Furthermore, in infected cells, LGP2 was shown to have overlapping binding sites with MDA5 since LGP2 co-immunopurified RNA was found to stimulate in a MDA5-dependent manner<sup>95</sup>.

### 3 Structural basis for antiviral signaling of RIG-I and MDA5

RIG-I-like receptors are a subfamily of SF2 helicases owing to their central DECH box RNA helicase domain that consists of two structurally almost identical RecA-like domains (domain 1a and domain 2a, Figure 5). Both domains 1a and 2a form an active site for ATP binding and hydrolysis between their interfaces, which defines SF1 and SF2 helicases and distinguishes them from SF3 – SF6 helicases that form hexameric toroids. Compared to other SF2 helicases, the RLR helicase domain further harbors an unusual helical insertion domain (domain 2b) within domain 2a as well as an elbow-like helical pincer domain that also emerges from 2a. The helicase domain is structurally related to the archaeal Hef helicase/nuclease<sup>139</sup>.

Functional specificity of RLRs comes from their accessory domains that augment the SF2 helicase domain (Figure 5): All RLRs possess a CTD that supports the helicase domain in RNA binding and that confers RNA substrate specificity. The CTD further contains a conserved zinc-binding site essential for the structural integrity of the domain<sup>85,140</sup>. Structurally, the CTD resembles GDP/GTP exchange factors of Rab-like GTPases<sup>140</sup>. Furthermore, except for LGP2, RLRs harbor two N-terminal CARDS belonging to the death domain (DD)-fold superfamily<sup>141</sup> that elicit the downstream signal. Similar DD-fold domains can be found in various other immune signaling pathways.

Other RLR homologue proteins include Dicer as well as the DNA-binding protein Fanconi anemia, complementation group M (FANCM)<sup>142</sup>.

Upon RNA and ATP binding large conformational changes are induced with all subdomains moving

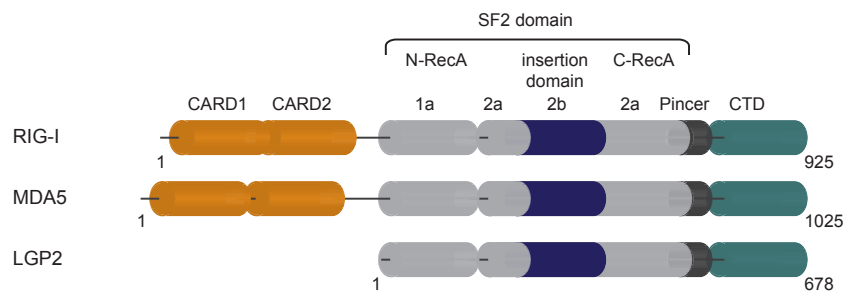


**Figure 5:** Domain organization of the RIG-I-like receptors RIG-I, MDA5 and LGP2. Individual domains are depicted as cylinders, long linkers are shown as lines. SF2 helicase domain notations are according to Singleton et al.<sup>143</sup>.

relative to each other (Figure 6). RIG-I, MDA5 and LGP2 completely encircle the RNA double-strand within a large network of interactions between RNA, SF2 helicase domain and CTD<sup>60–62,144,145</sup>. The dsRNA itself, maintains an A-form conformation without any structural evidence of RNA destabilization or partial unwinding<sup>60–62</sup>. In addition, RLRs miss a characteristic phenylalanine-loop motif, that is conserved in other SF2 helicases with nucleic acid unwinding activity<sup>62</sup>. In *in vitro* experiments, nevertheless, RNA unwinding was reported and thereby preferentially takes place on 3' overhangs and independently whether the bottom strand consists of RNA or DNA<sup>146</sup>.

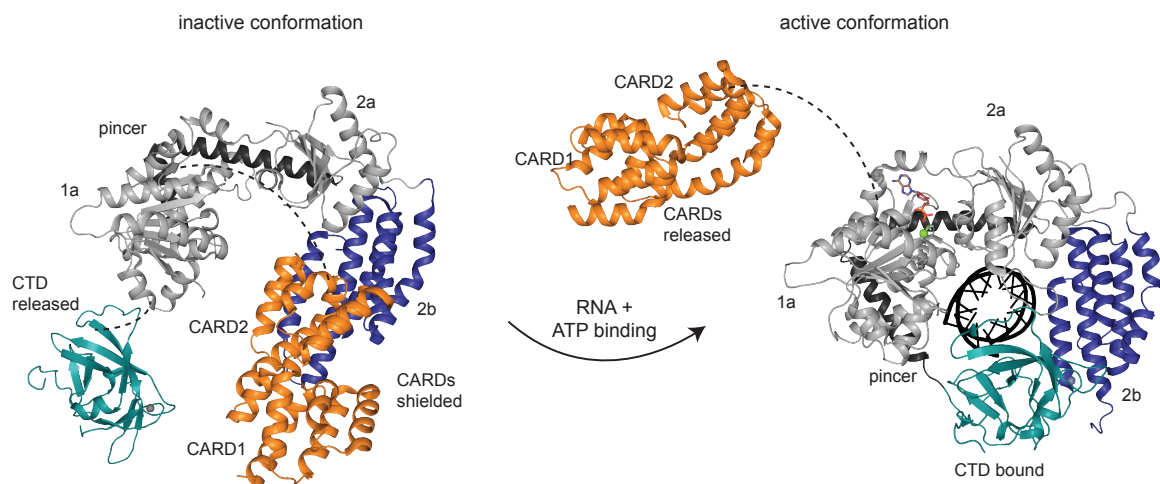


**Figure 6:** RIG-I three-dimensional reorganization upon RNA and ATP binding. In the ligand-free state RIG-I adopts an inactive conformation with CARD2 bound to the insertion domain 2b, whereas the CTD is flexibly linked and free to survey the cytoplasm. Upon RNA binding, the CTD presents bound dsRNA to the helicase domain and subsequent ATP binding establishes the active conformation with released CARDs that are able to transmit the signal. Colors of individual domains are according to Figure 5. Flexible linkers are shown as dashed lines.

RCSB PDB codes for the depicted structures are: 2qfb (CTD released, human), 4a2q (CARDs bound to SF2 helicase, duck), 3tmi (RIG-I  $\Delta$ CARDs bound to dsRNA and ADP·BeF<sub>3</sub>, human).

### 3.1 The ligand-free state of RIG-I and MDA5

In the ligand-free state the SF2 helicase domain of RIG-I is shown to be in an extended flexible conformation with only domains 2a and 2b rigidly attached to each other<sup>60,61,147,148</sup>. Domain 1a is stabilized by the pincer arm, but otherwise only in loose contact to domain 2a. Without RNA, ATP can bind to domain 1a, but cannot be hydrolyzed because domain 2a is rotated and too far away<sup>147</sup>. In addition, several interstrand loops for ATP binding or hydrolysis, particularly within domain 2a, are disordered. The CTD is flexibly linked to the rest of protein and is thus available for RNA-sensing and capturing<sup>61,106</sup>. The CARDS, in contrast, form a rigid head-to tail unit and are bound via CARD2 to domain 2b<sup>61,106</sup>.

The insertion domain 2b, hence, has a very pivotal role in maintaining the non-signaling state: while attached to domain 2b, CARD2 is shielded from interactions with other cytosolic proteins and thus unable to interact with the MAVS CARD. In addition, the binding site of CARD2 to domain 2b partially overlaps with an RNA binding site of domain 2b and would sterically clash with both CTD and RNA in the ligand-bound state<sup>61</sup>. The domain 2b:CARD2 interface is thus thought to provide a checkpoint for RNA selection, which only tightly CTD-bound 5' tri- or diphosphorylated dsRNAs can disrupt<sup>108</sup>.

The helicase domain of ligand-free MDA5 adopts an open conformation similar to RIG-I and the CTD is flexibly linked as well. Domain 1a is, as in RIG-I, stabilized by the pincer arm. In contrast to RIG-I, however, a longer linker between CARD2 and domain 1a, as well as several variations within domain 2b lead to reduced intramolecular autoinhibitory interactions and partially released CARDS even in absence of ligands. To that effect, the length of several domain 2b helices is reduced and a critical phenylalanine within 2b, which is responsible for CARD2 binding in RIG-I, is not conserved in MDA5<sup>149</sup>. The MDA5 CARDS thus do not as tightly associate with domain 2b<sup>106,130</sup>. In contrast to RIG-I, MDA5 is therefore thought to alternate in a conformational equilibrium between bound- and extended-CARDS with the bound state being favored<sup>149</sup>. This in turn results in a higher background activity of MDA5 compared to RIG-I.

The crucial role of the CARDS in triggering an antiviral response is emphasized by the fact that over-expression of the isolated RIG-I or MDA5 CARDS is sufficient for immune response activation<sup>70,72</sup>. Release of the CARDS as well as the establishment of CARD-CARD interactions with MAVS, therefore, need to be carefully controlled.

### 3.2 RIG-I signaling requires a conformational switch that releases the CARDS

RIG-I binds dsRNA as a monomer without forming protein-protein mediated oligomers<sup>113</sup>. RNA binding to RIG-I induces a closure of the SF2 domain and creates the mature ATP binding pocket. Yet, RNA binding alone is not sufficient to entirely free the CARDS, but rather slowly destabilizes the CARD2:domain 2b interface and leads to a partial release<sup>106</sup>. RNA-induced ATP binding, however, induces further conformational changes within the protein resulting in a switchlike compaction of the SF2 helicase domain that brings domains 1a and 2a into very close proximity<sup>61,62</sup>. ATP hydrolysis was further suggested to induce an intramolecular domain repositioning that is needed to release

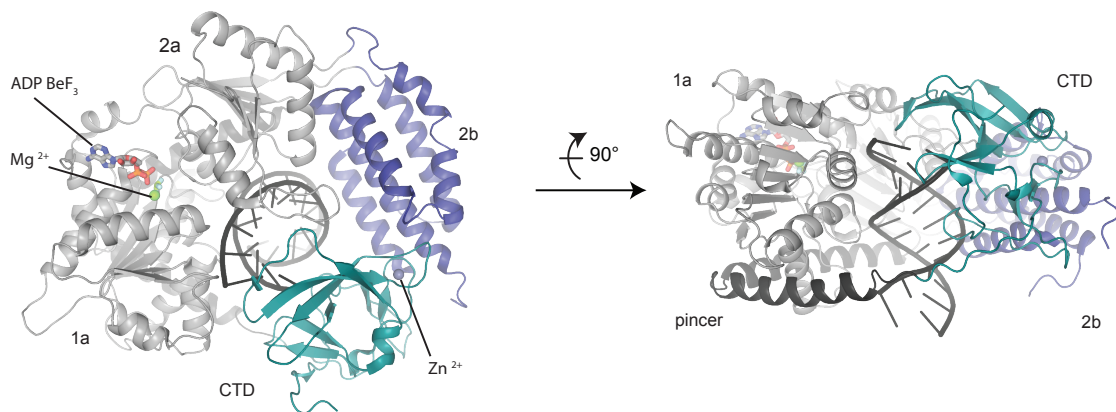


**Figure 7:** RIG-I  $\Delta$ CARDs bound to dsRNA and the ATP analogue ADP·BeF<sub>3</sub> (RCSB PDB code 3tmi, human). RIG-I completely encircles the dsRNA and especially caps one RNA end via the CTD. Coloring according to Figure 5.

the CARDs, since ATP binding-deficient RIG-I is unable to induce signaling, even though the protein has no altered RNA binding properties<sup>73</sup>. Nevertheless, the exact activation mechanism remained elusive until recently and will be discussed in detail later.

An overview of dsRNA encircled by RIG-I  $\Delta$ CARDs is shown in Figure 7.

Most of the dsRNA contacts are provided by domains 1a and 2a of the helicase domain (Figure 8A-1), which mainly track the bottom RNA strand. Thereby, almost every helix from RIG-I's SF2 domain that reaches into the RNA-binding tunnel provides potential binding partners to the RNA phosphodiester backbone thus creating an extensive network of protein:RNA interactions. The insertion domain 2b also participates in RNA binding with an  $\alpha$ -helix that runs perpendicular to the minor RNA groove and contacts both RNA strands (Figure 8A-2). ATP is coordinated within a pocket between domain 1a and 2a distant from the RNA binding sites (Figure 8A-3).

The pincer domain further establishes comprehensive contacts between domains 1a, 2a and CTD, thereby providing a mechanical connection that might transmit information between different parts of the molecule<sup>60-62</sup> (Figure 6, 7). Thus, the pincer domain might allosterically control the ATPase core and probably plays an important role by mediating the enzymatic and signaling activities of RIG-I<sup>150</sup>. In accordance with this, disruption of the domain 1a:pincer interface results in loss of immune signaling because of defects in RNA dissociation and ATP hydrolysis while ATP and RNA binding are still intact<sup>150</sup>.

The RIG-I CTD mainly captures the very 5' dsRNA end via a positively charged end-capping loop (Figure 8B-4/5). This loop contains several lysines that either contact the phosphate backbone or the 5' phosphate groups of RNA<sup>107,140,151</sup>. Thereby, specific contacts to the phosphates are varying between different crystallized RIG-I CTD:RNA constructs and even capped RNA ends can be flexibly accommodated<sup>109</sup> (Figure 8B-4). F853 within the end-capping loop stacks to the terminal base pair explaining the preferred nucleic acid end recognition of RIG-I<sup>60,62,107</sup>. S854 (also part of the end-capping loop) and H830 contribute to preference for RNA over DNA by hydrogen bonding with the ribose hydroxyl groups of the first base pair<sup>62</sup>. H830 further sterically hinders binding of 2'-OH-methylated RNA<sup>105,107,109</sup>.

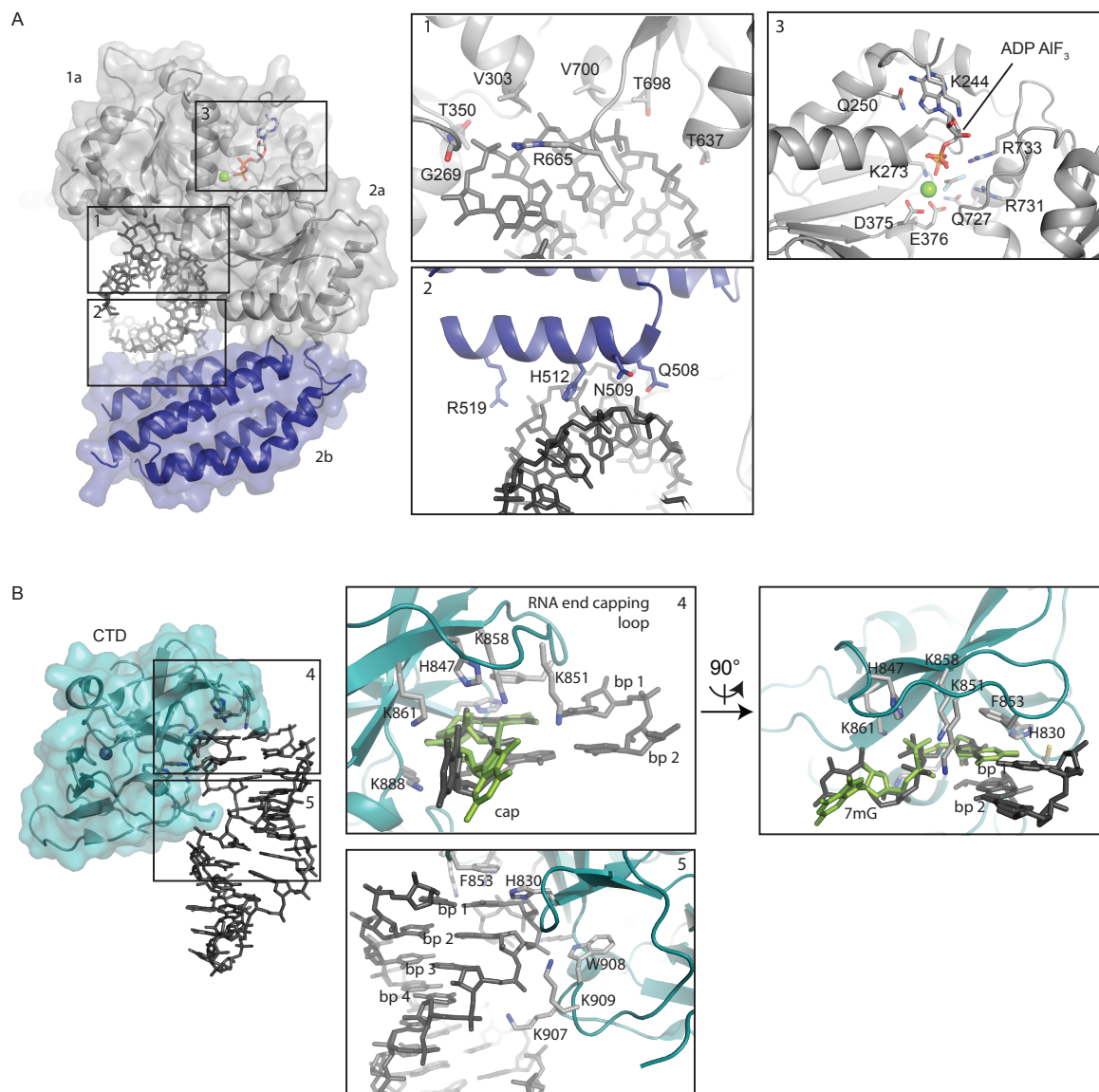


**Figure 8:** Contacts of RIG-I's helicase domain (A) and CTD (B) to dsRNA as well as to ADP·AlF<sub>3</sub>. (1) Potential contacts of domains 1a and 2a to the dsRNA backbone. (2) Potential contacts of domain 2b to the dsRNA backbone. (3) Coordination of the ATP analogue ADP·AlF<sub>3</sub> by several residues of the ATP binding pocket. (4) Several residues of the RNA end-capping loop coordinate the first nucleotide base pair including the phosphates. The cap itself, however, is not coordinated and therefore found in different conformations (green and black). (5) RIG-I CTD contacts to the dsRNA backbone via a second positively charged loop. Domain coloring according to Figure 5. RCSB PDB codes for the depicted structures are: 4a36 (RIG-I helicase, duck), 5f98 (RIG-I  $\Delta$ CARDs, human, only CTD is shown).

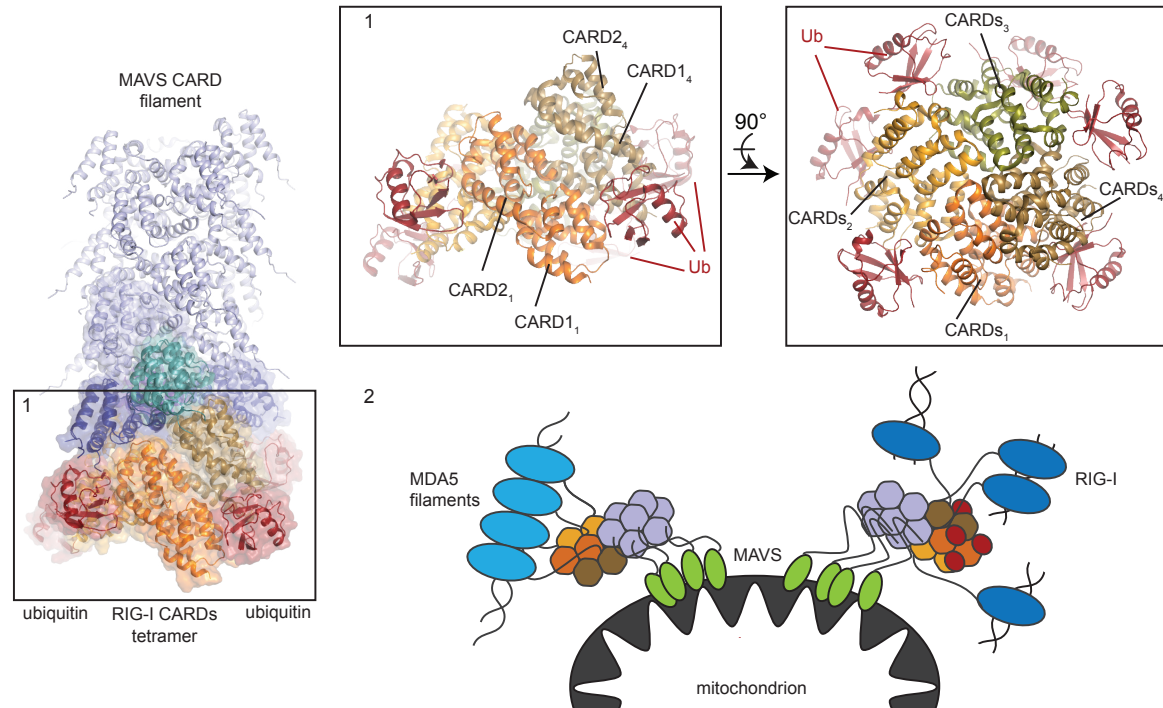


**Figure 9:** Helical assembly of RIG-I CARDs bound to ubiquitin (1, RCSB PDB code 4nqk, human) and building the scaffold for the MAVS CARD assembly into large filaments (model of RCSB PDB code 2ms7, human, docked onto 4nqk using pymol). Structural stability of the RIG-I CARDs tetramer is provided by several ubiquitin chains wrapping around the complex. (2) Model of RIG-I and MDA5 nucleating signaling competent MAVS filaments. Whereas MDA5 cooperatively assembles onto long dsRNA, RIG-I preferentially recognizes shorter dsRNAs or RNA ends and therefore requires stabilization by ubiquitin chains.

Due to the disruption of the CARD2:domain 2b interface, the CARDs are released and accessible for the interaction with the MAVS CARD or other proteins<sup>69</sup> (Figure 9). Thereby, each four RIG-I molecules oligomerize via their CARD domains to build a tetrameric complex<sup>70</sup>. In particular, left-handed helical CARDs tetramers with a 5Å rise per CARDs module and a total rise of one CARD per turn are formed<sup>152</sup>. In addition, covalently or transiently-linked ubiquitin chains can wrap around the CARDs tetramer and thus further stabilize the complex<sup>152</sup> (Figure 9). The CARDs tetramer in turn constitutes the scaffold for the assembly of large MAVS-CARD filaments starting at the surface of the second RIG-I CARD and extending the helix in a counter-clockwise manner<sup>153</sup>. Similar large assemblies have as well been shown to arise from other death domain-fold proteins including the death domains of the Myddosome and inflammasome<sup>154,155</sup>.

### 3.3 Cooperative binding of MDA5 on dsRNA stems induces signaling

In contrast to RIG-I's preference for RNA ends, MDA5 nucleates within the RNA duplex and cooperatively assembles into long filaments on dsRNA<sup>130,149,156</sup>. Protein:protein contacts are induced upon RNA binding<sup>106</sup> and are dynamically regulated via the ATPase activity of MDA5.

Similar to RIG-I, MDA5 interacts with dsRNA using the helicase domain as well as the CTD. RNA con-

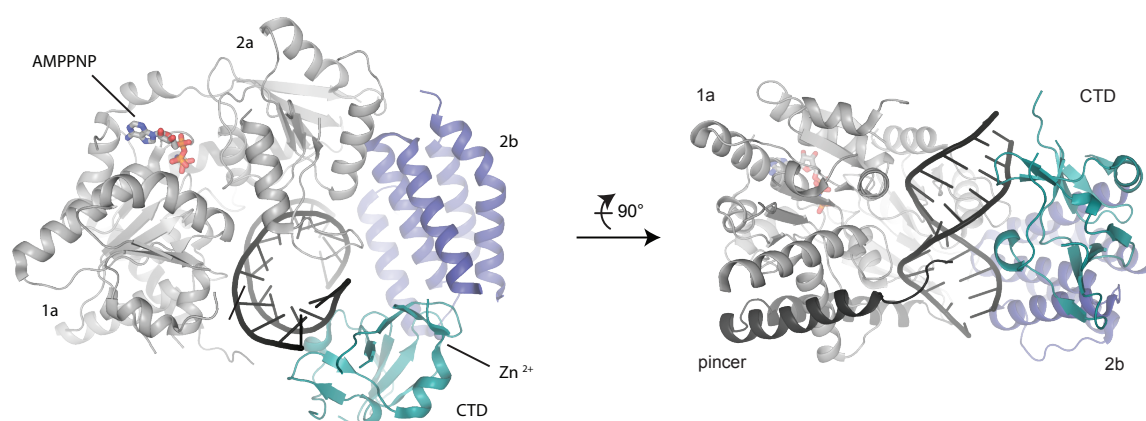


**Figure 10:** MDA5  $\Delta$ CARDs bound to dsRNA and the non-hydrolyzable ATP analogue AMPPNP (RCSB PDB code 4gl2, human). MDA5 completely encircles the dsRNA similar to RIG-I, but instead of binding to the RNA end, it rather recognizes the dsRNA stem. Coloring according to Figure 5.

tacts to the RNA backbone and 2' hydroxyl groups are, except for the CTD:RNA contacts, conserved in MDA5 and RIG-I<sup>144</sup> (Figure 10).

The orientation of the MDA5 CTD, however, is 20° rotated compared with the RIG-I CTD and runs parallel to the dsRNA stem thus leaving a gap of approximately 30° (Figure 10). This results in an open, C-shaped structure of MDA5 and preferential binding to the dsRNA stem through recognition of internal duplexes<sup>130,144</sup>. In NMR experiments, the isolated MDA5 CTD was shown to have a similar fold compared to the RIG-I CTD and seemed also be able to bind RNA ends via its end-capping loop<sup>157</sup>. MDA5  $\Delta$ CARDs co-crystallized with dsRNA, however, was found to recognize the RNA stem via a flat surface with the end-capping loop being unfolded<sup>144</sup>. The intrinsic flexibility of the MDA5 CTD might thus allow alternative binding modes.

MDA5 filaments build up by stacking of individual monomers in a head to tail arrangement<sup>144</sup> (Figure 11). In the current model, each monomer is rotated by 70° and each helicase domain is in close contact with the adjacent helicase domain resulting in extensive protein:protein interactions. These interactions explain the cooperativity of MDA5 upon dsRNA binding and lead to higher affinity for long dsRNA<sup>144</sup>.

Filament formation brings several MDA5 CARDs into close spatial proximity in order start immune signaling (Figure 9). As detailed earlier, release of the MDA5 CARDs, however, seems not as strictly coupled to ATP as the RIG-I CARDs<sup>106,149</sup> (see Discussion as well).

### 3.4 RIG-I and MDA5 are regulated by post-translational modifications

As aberrant or premature immune signaling as well as sustained activation maybe harmful to the host, control mechanisms are required that prevent RLR activation in uninfected cells or that shut down signaling in infected cell once the infection is cleared. Therefore, signal-transducing activities of RIG-I and MDA5 are tightly regulated by various post-translational modifications (PTMs) that act

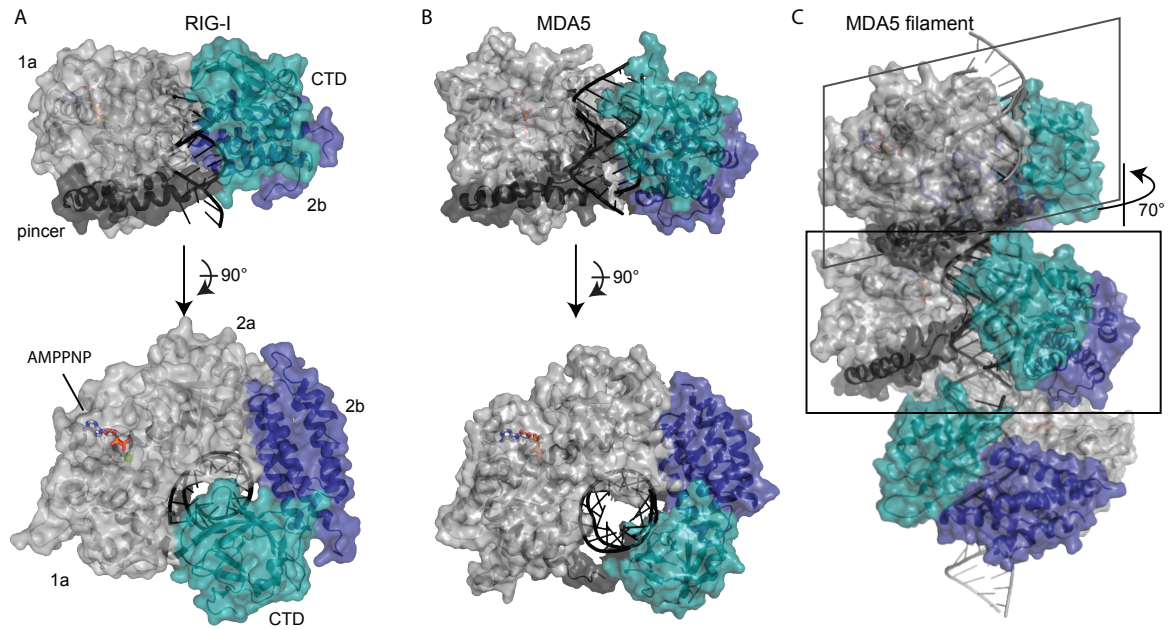


**Figure 11:** Structural basis for filament formation of MDA5. (A) and (B) Surface representation of RIG-I  $\Delta$ CARDs bound to dsRNA (A, RCSB PDB code 3tmi, human) and MDA5  $\Delta$ CARDs bound to dsRNA (B, RCSB PDB code 4gl2, human). (A) The RNA end-capping mode of RIG-I does not allow filament formation on dsRNAs. (B) MDA5's O-shaped structure that recognizes dsRNA stems is compatible with filament formation. (C) Model of a head-to-tail MDA5 filament with a 70° turn per molecule based on the monomer crystal structure in B and built with pymol. Bridging RNA (gray) was added to assemble monomers while preserving the dsRNA continuity. Coloring according to Figure 5.

on protein activation and degradation. Regulation occurs by phosphorylation, acetylation, ISGylation, SUMOylation and polyubiquitination or binding of free ubiquitin chains respectively. The latter can be distinguished into eight different linkage types of ubiquitin chains<sup>158</sup>, of which K48-linked, i.e. degradative, and K63-linked, i.e. signal-transducing, ubiquitination are reported for RLRs. Most post-translational modifications are identified within the CARDs or the CTD of RLRs and are again best studied for RIG-I (Figure 12).

In uninfected cells RIG-I is constitutively phosphorylated at serine 8 of the first CARD and threonines 170 and 197 of the second CARD by protein kinases C- $\alpha$  (PKC- $\alpha$ ) and PKC- $\beta$ <sup>159,160</sup>. Threonine 770 within the RIG-I pincer kink as well as serines 854 and 855 within the CTD RNA end-capping loop are shown to be phosphorylated by casein kinase II (CK2) or IKK subunit  $\epsilon$ <sup>161-163</sup>. Furthermore, lysines 858 and 909 are acetylated by a so far unknown acetyl transferase<sup>162,164</sup>. All modifications are thought to help keeping RIG-I in an inactive state by either stabilizing the RNA unbound state, interfering with RNA binding, or by suppressing other modifications that help to activate RIG-I. Besides these experimentally validated post-translational modification sites, several other sites have been found in mass spectrometry-based assays: serine 468 and tyrosine 473 have been found to be phosphorylated, and lysines 99, 169, 181, 190, 193, 644 and 796 might be ubiquitinated<sup>69,162,165</sup>. The *in vivo* relevance, however, is not determined.

In infected cells and upon RNA and ATP binding, conformational changes of RIG-I allow access of phosphoprotein phosphatase (PP) 1 $\alpha$  and PP1 $\gamma$  to the CARDs, which dephosphorylate serine 8

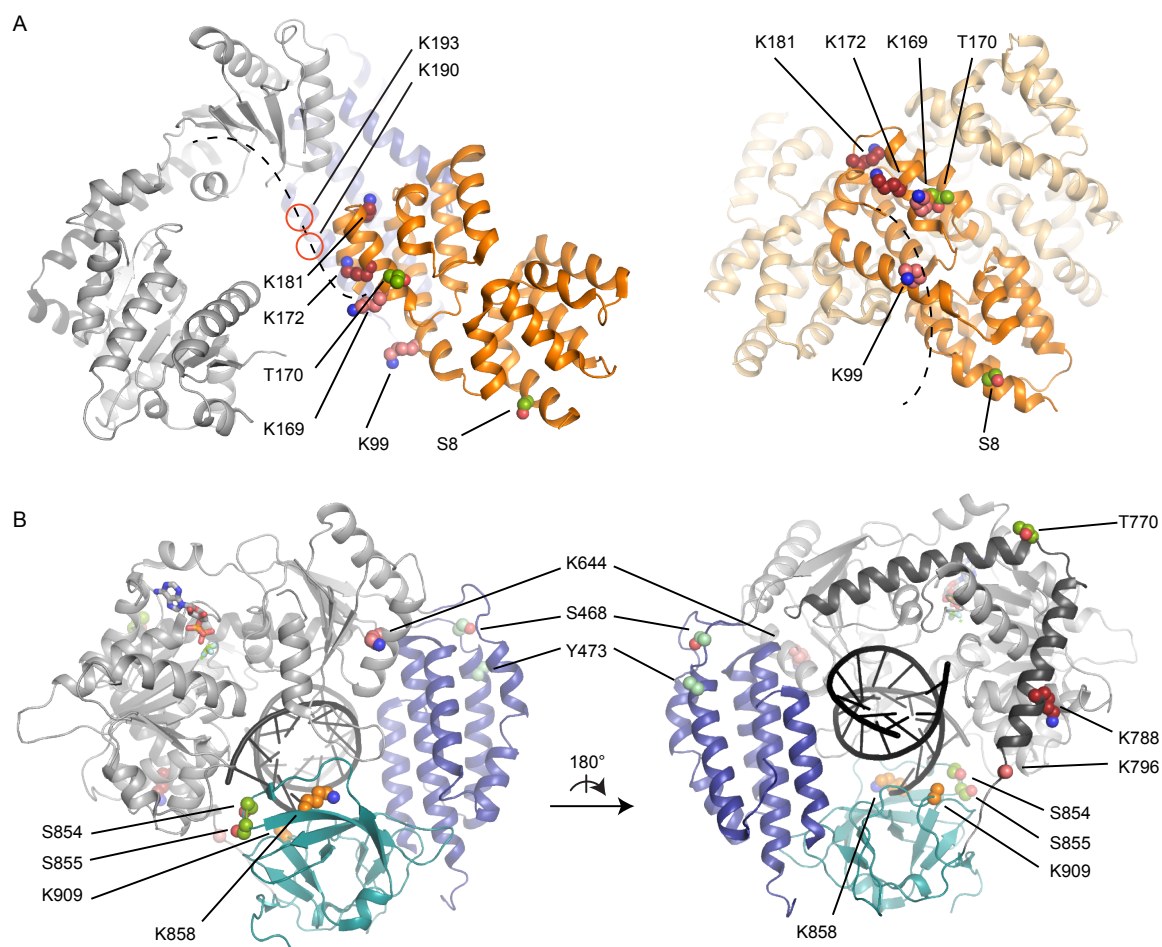


**Figure 12:** Known post-translational modifications of RIG-I. (putative) phosphorylation sites: (light) green; (putative) ubiquitination sites: (light) red; acetylation sites: orange. (A) Left: RIG-I PTMs within the CARDs (RIG-I ligand-free state). Estimated localization of PTMs within the unstructured linker are marked as red circles. Right: Localization of PTMs on a CARDs tetramer (RIG-I ligand-bound state). (B) RIG-I PTMs within the helicase domain as well as within the CTD. Domain coloring according to Figure 5 and residue labeling according to the human RIG-I sequence. Flexible linkers are shown as dashed lines. RCSB PDB codes for the depicted structures are: 4a2q (CARDs bound to SF2 helicase, duck), 4nqk (CARDs tetramer, human), 3tmi (RIG-I  $\Delta$ CARDs bound to dsRNA and ADP·BeF<sub>3</sub>, human).

and threonine 170<sup>166</sup>. This in turn renders the CARDs free to interact with K63-linked polyubiquitin chains<sup>159,167</sup>. Several kinds of RIG-I:ubiquitin or ubiquitin-like protein interactions have been described, emphasizing the apparent importance of this process during RLR signaling: RIG-I was found to be either polyubiquitinated by tripartite motif 25 (TRIM25) at lysine 172<sup>69,85</sup>, to bind short unanchored cytosolic polyubiquitin chains<sup>70,168</sup> or to interact with the tandem ubiquitin-like domain (UBL) of the human IFN-inducible oligoadenylate synthetases-like (OASL) protein that mimics polyubiquitin chains<sup>169–171</sup>. RIG-I was further shown to be modified by small ubiquitin-like modifier-1 (SUMO-1), which promotes ubiquitination and the interaction with MAVS as well<sup>172</sup>.

Ubiquitination or ubiquitin binding is thought to be critical for efficient interactions with MAVS<sup>69</sup> and a prerequisite for stable antiviral signal transduction since it prevents rebinding of the CARDs to domain 2b due to steric reasons<sup>61</sup>. Polyubiquitin binding further induces RIG-I oligomerization and stabilizes the CARDs cluster which in turn interact with the MAVS CARD, thereby activating the

immune response<sup>70,75</sup>.

Other ubiquitin ligases, that have been described to promote K63-linked ubiquitination of the RIG-I CARDs and that might complement TRIM25 in cells where it is not present, are RING finger protein leading to RIG-I activation (Riplet, also called RIG-I E3 ubiquitin ligase/ REUL or Ring Finger Protein 135/ RNF135, ubiquitination of lysines 154, 164)<sup>173</sup>, TRIM4<sup>174</sup> and the stress granule associated ligase MEX3C<sup>175</sup>. In addition to ubiquitination of the CARDs, Riplet was shown to attach K63-linked ubiquitin chains to lysine 788 within the pincer region of RIG-I, which like ubiquitination of the CARDs promotes RIG-I signaling<sup>176,177</sup>.

Furthermore, during an infection, lysine 909 of the RIG-I CTD is deacetylated by histone deacetylase 6 (HDAC6), which was shown to promote recognition of viral RNA<sup>178</sup>. The phosphatase that is responsible for pincer and CTD dephosphorylation as well as the biological significance still need to be investigated.

Proteasomal degradation of RIG-I and thus negative regulation, on the other hand, is facilitated by the interferon inducible ubiquitin ligase Ring Finger Protein 125 (RNF125) and guided by the p97 chaperon complex<sup>179,180</sup>. RNF125 conjugates K48-linked ubiquitin to RIG-I lysine 181<sup>179</sup>. This can be reversed by USP4 that removes K48-linked poly-ubiquitination chains and thereby stabilizes RIG-I<sup>181</sup>. RIG-I is further shown to be ISGylated with ISG15<sup>182</sup>, which is as well an ubiquitin-like protein negatively regulating antiviral signaling<sup>183</sup>. Another suppressor is the linear ubiquitin assembly complex (LUBAC) that targets both TRIM25 and RIG-I. LUBAC induces proteasomal degradation of TRIM25 and competes with TRIM25 for RIG-I leading to inhibition of RIG-I ubiquitination and suppression antiviral signaling<sup>184</sup>. In addition cylindromatosis (CYLD)<sup>185,186</sup>, USP3<sup>187</sup>, USP15<sup>188</sup> and USP21<sup>189</sup> remove K63-linked polyubiquitin chains from RIG-I and therefore constitute a negative regulatory mechanism as well.

Post-translational modifications of MDA5 are less well investigated, even though also MDA5 is heavily modified<sup>a</sup>. For instance, in uninfected cells, the MDA5 CARDs are similar to the RIG-I CARDs phosphorylated at serines 88 and 104 in order to inhibit downstream signaling<sup>166</sup>. Dephosphorylation upon infection is accomplished by PP1 $\alpha$  and PP1 $\gamma$  as well<sup>166</sup>. The MDA5 CARDs were, as RIG-I, found to bind K63-linked polyubiquitin chains<sup>70,168</sup> as well as SUMO-1<sup>191</sup>. In addition, also proteasomal degradation of MDA5 due to K48-linked ubiquitination was shown to be mediated by RNF125<sup>179</sup>.

## 4 The ATPase domain of RIG-I-like receptors

RIG-I-like receptors are often termed "RIG-I-like helicases" due to their classification as SF2 helicases. RNA or DNA helicases are usually found to unwind duplex nucleic acids by translocation on one of the product single strands in an ATP-dependent manner<sup>110</sup>. Their ATPase activity is therefore stimulated in presence of single-stranded nucleic acids. RLRs, in contrast, hydrolyze ATP upon detection of

<sup>a</sup>for an overview see also <http://www.phosphosite.org><sup>190</sup>

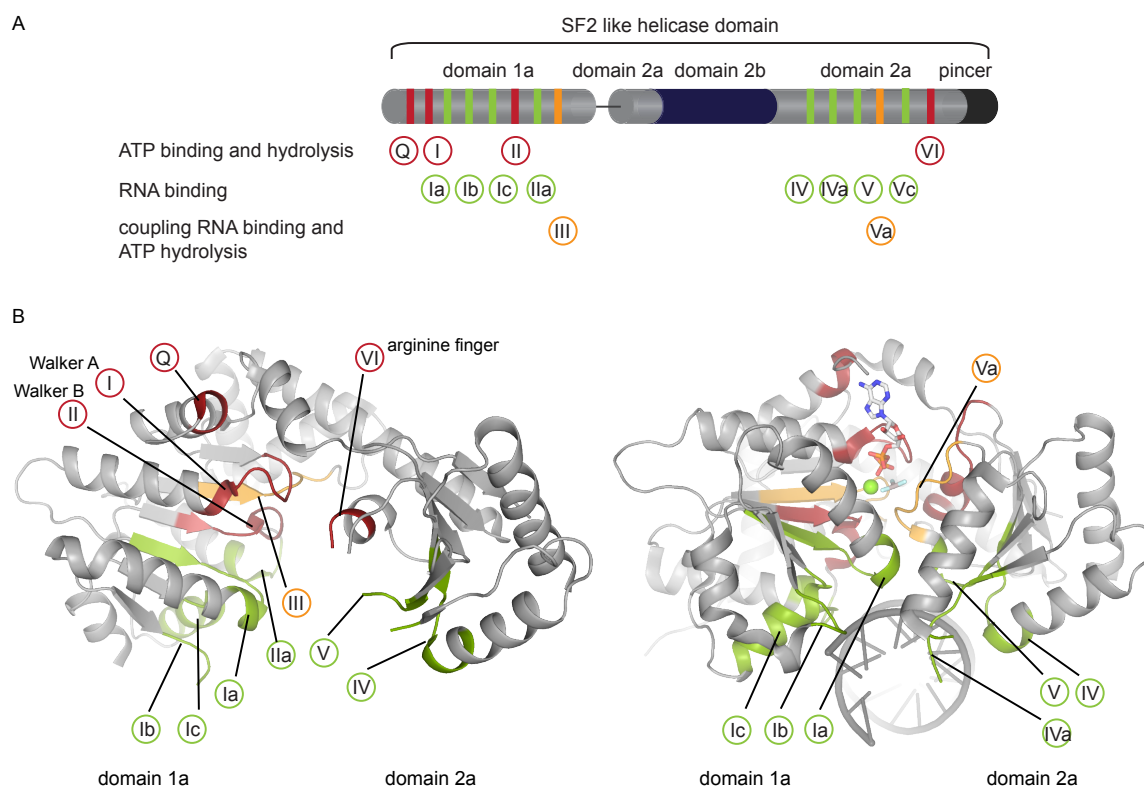


**Figure 13:** RIG-I-like receptor helicase motifs and their three-dimensional arrangement. (A) Motif localization within the primary amino acid sequence and their respective function. (B) Left: Mapping of motifs onto the ligand-free, inactive conformation of RIG-I. Right: Mapping of motifs onto the RNA- and ADP-AIF<sub>3</sub>-bound active conformation of RIG-I.

RCSB PDB codes for the depicted structures are: 4a2q (RIG-I CARDS bound to helicase domain, duck), 4a36 (RIG-I  $\Delta$ CARDS bound to dsRNA and ADP-AIF<sub>3</sub>, duck), only domains 1a and 2a are shown.

double-stranded RNA<sup>102,103</sup> and their helicase activity is controversial<sup>62,146</sup>.

ATP hydrolysis occurs within an ATP binding pocket between both RecA-like domains in presence of RNA. RLRs are thus as well termed dsRNA-dependent ATPases (DRAs)<sup>192</sup>. Sequence and structure analysis of different SF2 helicases including RLRs revealed a common arrangement of several conserved motifs for ATP hydrolysis and RNA binding which are distributed between the domains 1a and 2a of the helicase core<sup>193</sup> (Figure 13). Motifs for ATP binding and hydrolysis include the Q motif, motif I ("Walker A motif") and motif II ("Walker B motif") within domain 1a, and motif VI ("arginine finger") within domain 2a. Residues of the Q and Walker A motifs primarily coordinate the nucleotide-triphosphate for hydrolysis and provide specificity for the adenine base. Furthermore, Walker A motif residues, but mainly the Walker B motif bind a magnesium ion, that in turn coordinates the  $\beta$  and  $\gamma$ -phosphate of the nucleotide and thereby helps stabilizing the ATP conformation needed for hydrolysis. In addition, a residue of the Walker B motif usually serves as a catalytic base by activating the water residue that participates in hydrolysis of ATP. The arginine finger of domain 2a of the opposing side of the ATP binding pocket stabilizes the ATP hydrolysis transition state. Conserved SF2 motifs involved in binding of the bottom RNA strand are the motifs Ia, Ib and Ic within domain 1a as well as motifs IV, IVa and V of domain 2a. Motifs III within domain 1a and Va within

domain 2a help to couple RNA binding and ATP hydrolysis<sup>143,193,194</sup>. Furthermore, in contrast to other SF2 helicases, two other possible RNA binding motifs, motif IIa within domain 1a and motif Vc within domain 2a, were suggested<sup>192</sup>. Both of them help to recognize the complementary top RNA strand and thus explain the double-stranded RNA binding mode of RLRs.

ATP hydrolysis, however, does not occur on the isolated SF2 domain, but requires besides RNA also the C-terminal domain<sup>62,195</sup>. Presence of the CARDs, on the other hand, decreases the ATPase function and emphasizes a negative regulatory role for the CARDs.

The role of ATP hydrolysis in RNA binding and signaling, however, is still controversial. Already early studies found a strict dependence of *in vivo* signaling on the presence of ATP, since RIG-I and MDA5 Walker A mutants, that are defect in ATP binding are impaired in immune signaling as well<sup>68,72,73</sup>. Later on, both protein gain-of-function, i.e. increased signaling, as well as loss-of-function, i.e. reduced signaling, have been described for different ATPase motif mutants<sup>196,197</sup>. ATPase activity of RLR was further reported to lead to either unwinding of RNA duplexes<sup>146</sup>, translocation on dsRNA, oligomerization<sup>110,198–200</sup> or dissociation from RNA<sup>149</sup>.

#### 4.1 ATPase activity of RIG-I correlates with its binding affinity towards RNA

In order to infer a possible *in vivo* relevance, several studies addressed the *in vitro* biochemical properties of RIG-I in presence or absence of ATP, RNA or both.

*In vitro* ATP turnover rates of RIG-I under saturating ATP and RNA conditions are shown to be mostly independent of RNA length, the presence of a 5' triphosphate motif or even an RNA end<sup>108,113</sup>. ATP binding under dsRNA saturating conditions, however, decreases with increasing RNA length but is still independent of RNA-end phosphorylation<sup>113</sup>. Whereas the maximal ATP hydrolysis rate, thus, seems to be independent of the RNA substrate, only ATP binding conditions, i.e. RNA-dependent formation of the ATP binding pocket, impact hydrolysis.

*In vitro* RNA binding, on the other hand, is dependent on the availability of ATP<sup>108</sup>. The only exception are short triphosphorylated RNA with a very high affinity at nanomolar range, that is not significantly changed in presence of ATP<sup>108</sup>. The affinity towards short blunt-ended dsRNA is slightly weaker and was shown to further decrease under ATP saturating conditions<sup>108</sup>. Therefore, ATP, as present in cells, might help decreasing the affinity of RIG-I towards RNA without phosphorylated ends.

In addition, ATPase activity of RIG-I under saturating ATP conditions was shown to correlate with the RNA binding affinity. Blunt-ended or triphosphorylated dsRNAs induce the highest ATPase rates, whereas hairpin RNAs have a reduced potential<sup>108</sup>. Nevertheless, ATPase activity and RNA binding do not correlate with immune signaling<sup>106</sup>. Blunt ended dsRNAs, for instance, show very tight binding affinities to RIG-I and stimulate ATP hydrolysis rates comparable to triphosphorylated RNA, but do not induce an immune response *in vivo*<sup>102,103,106</sup>. The presence of a 5' triphosphate on dsRNA might therefore be important at the initial steps of RNA- and ATP-binding as well as for release of CARDs. The lack of immune system stimulation by blunt-ended dsRNAs, also excludes the possibility

that ATP hydrolysis of RIG-I would provide the energy to directly liberate the CARDs.

## 4.2 MDA5 forms ATP-sensitive filaments

For MDA5 comparably little biochemical data concerning the ATPase activity is available so far. Nevertheless, several *in vitro* studies showed that filament formation of MDA5 on long double-stranded RNA becomes unstable upon addition of ATP. ATP hydrolysis by MDA5 is thus found to weaken the protein:RNA interaction similar to RIG-I. This is thought to confer MDA5 filament disassembly on RNA ends and thus mainly effects the stability on short dsRNA<sup>130</sup>. By that, MDA5 improves length discrimination of dsRNA and it explains the preference for long double-stranded RNAs<sup>201</sup>. Repeated cycles of ATP hydrolysis and hence filament assembly and disassembly, however, can fill gaps within filaments and promote a more efficient coating of the dsRNA (Figure 14).

Since MDA5 immune signaling requires filament formation and subsequent CARDs oligomerization, ATP thereby controls the MDA5 antiviral immune response to different types of RNAs<sup>130,149</sup>. The non-hydrolyzable ATP analogue AMPPNP or the reaction product ADP have no effect on filament formation<sup>149</sup>. This emphasizes the importance of a functional ATPase activity, rather than the need to bind ATP.

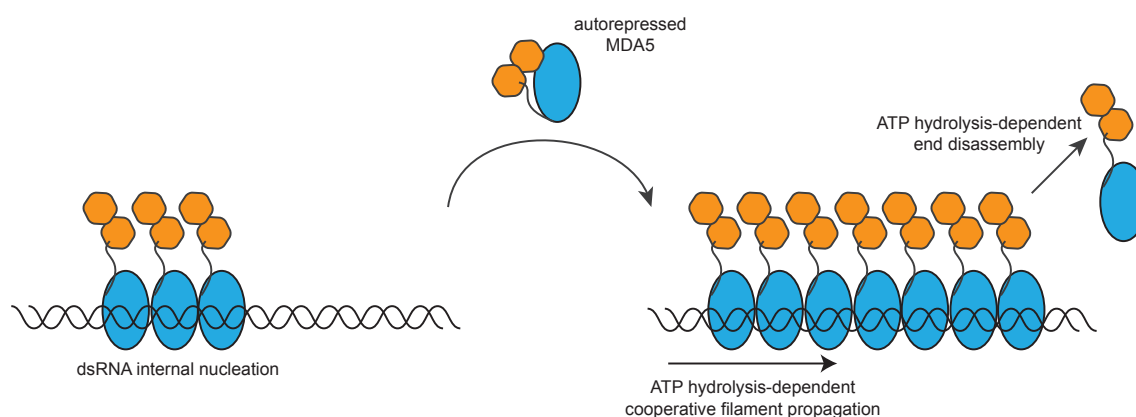


**Figure 14:** Model of MDA5 ATP-dependent filament formation. MDA5 cooperatively assembles on dsRNA stems. ATP hydrolysis helps to efficiently coat the dsRNA stems and leads to disassembly on dsRNA ends. The longer an RNA is, the more stable MDA5 can bind. Figure adopted from Peisley et al.<sup>199</sup>.

## 4.3 RIG-I forms signaling competent filaments in presence of ATP

Similar to MDA5, RIG-I was recently found to form filaments on dsRNA as well. RIG-I filament formation is ATP-dependent and correlates with immune signaling<sup>198,199</sup>. Mechanistically, monomeric RIG-I binds to the RNA end, translocates inward thereby hydrolyzing ATP, and stacks along the translocation track (Figure 15). During that process, the RIG-I CTD needs to adopt a different orientation towards the dsRNA stem and the RNA capping loop is most likely not involved in RNA binding, resulting in loss of affinity<sup>106</sup>. In addition, RIG-I filaments propagate with only very limited cooperativity leading to inefficient coating and poor recognition of longer dsRNA<sup>198,199</sup>. Nevertheless,

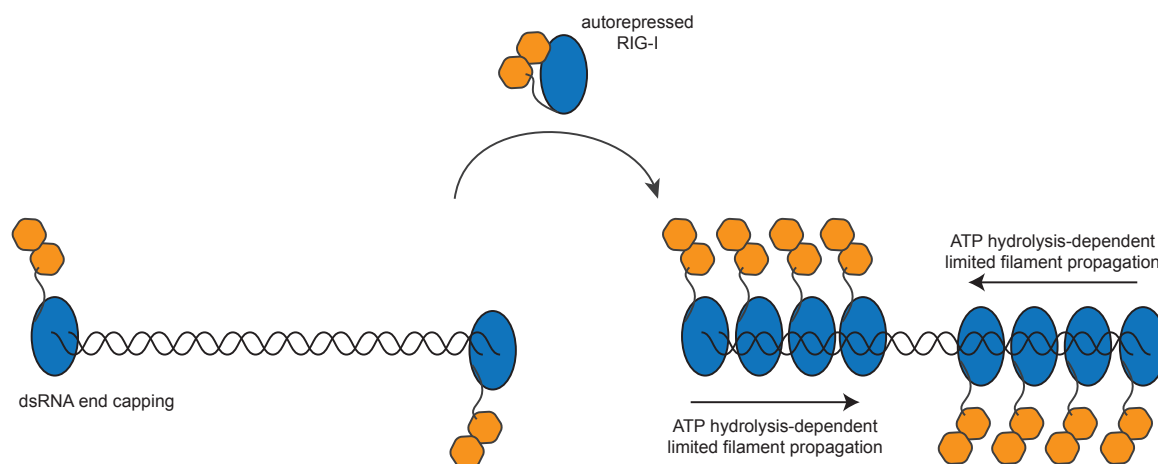


**Figure 15:** Model of RIG-I ATP-dependent filament formation. RIG-I preferentially binds to dsRNA ends, but is able to translocate into the dsRNA interior by hydrolyzing ATP irrespective of a triphosphate PAMP. RIG-I filaments propagate only with very limited cooperativity. Figure adopted from Peisley et al.<sup>199</sup>.

the 50 aa linker between the RIG-I's CARDS and the SF2 helicase domain is in theory long enough to allow direct contacts between CARDS that are six molecules apart.

The RIG-I filaments have been shown to be signaling competent without further binding of ubiquitin chains<sup>199</sup>. Ubiquitination, however, could help stabilizing CARD-oligomers that do not arise from one long double-stranded RNA and are therefore more prone to dissociate again (compare with Figure 9).

#### 4.4 RIG-I and MDA5 show ATP-dependent effector-like functions in virus-infected cells

The translocation function of RLRs might provide a direct, interferon-independent mechanism by remodeling of protein:nucleic acid complexes and by displacing viral proteins bound to dsRNA<sup>200</sup>. In accordance to this RIG-I and MDA5 CARD-less proteins, that are impaired in downstream signaling and induction if ISG expression, were shown to have an antiviral activity against several RNA viruses<sup>200</sup>. This was not true for their respective ATP binding-deficient Walker A mutants, which again illustrates the relevance of an intact RLR SF2 helicase domain.

Further effector functions of RIG-I and MDA5 were found in hepatitis B virus (HBV) infected cells, where RIG-I might counteract the HBV polymerase by binding to the 5'  $\epsilon$  region of the pregenomic RNA and suppresses replication<sup>202</sup>. Similar results have been reported for influenza A virus-infected cells, where RIG-I was shown to recognize the incoming fully encapsidated, 5' triphosphate-containing genome and inhibits infection probably by competing with the nucleocapsid proteins<sup>203</sup>.

## 5 Immune evasion strategies of viruses to avoid RIG-I-like receptor-signaling

In order to avoid detection and subsequent signaling of RLRs, viruses evolved an immense arsenal of counteracting strategies. These include modification of their own RNA in order to decrease RLR binding and the prevention of RLR immune response activation.

The simplest case of viral RNA modifications is probably processing of 5' termini of genomes and replication intermediates in order to avoid RIG-I detection. This can include either processing to a monophosphate, trimming of the 5' end in order to produce 3' overhangs or usage of a more sophisticated "prime and realign" mechanism during genome and antigenome synthesis that produces a 5' G overhang<sup>117,204–207</sup>. Furthermore some viruses modify their 5' RNA termini by capping and 2'-O-methylation in order to appear like host mRNA, or by protecting the end with covalently linked viral proteins<sup>131,208,209</sup>. Another strategy is to coat the viral dsRNA with proteins that out-compete binding by RIG-I and MDA5<sup>210</sup>, or to degrade dsRNA replication intermediates and thus to remove potential PAMPs<sup>211</sup>.

Some viruses reduce activation of RLRs by manipulating post-translational modifications of RIG-I or MDA5. Examples are the viral blockage of TRIM25-mediated ubiquitination of RIG-I or the expression of deubiquitination enzymes that remove covalently-linked K63-linked ubiquitin residues of the CARDs<sup>212–214</sup>. Also PP1- $\alpha/\gamma$  is a viral target and blockage of MDA5 dephosphorylation was shown to impede its signaling activation<sup>215</sup>. Other viruses were shown to attack MDA5 by inserting into the three-dimensional structure and unfolding the protein<sup>216,217</sup>, or to cleave RIG-I or MDA5 either by exploiting cellular caspases and the proteasome or by expressing viral proteinases<sup>218–220</sup>.

## 6 Mutations within the RIG-I-like receptor SF2 domain can cause autoimmune diseases

A comparably new field within RLR research are RIG-I- and MDA5-related autoimmune diseases. Due to the growing field of genome-wide association studies (GWAS) of human diseases, an increasing number of genetic variants become available. GWAS usually compare genetic data of healthy people to those of people carrying a certain disease phenotype and look for single-nucleotide polymorphisms (SNPs) that are more frequent within the disease genomes. Thereby more and more attention is also drawn to RLRs.

Examples for RLR-related diseases are the Aicardi-Gutières syndrome, diabetes mellitus type 1, multiple sclerosis, systemic lupus erythematosus, the Singleton-Merten syndrome, psoriatic arthritis or cutaneous psoriasis, dermatomyositis, selective IgA deficiency and dilated cardiomyopathy<sup>221,222</sup>. In most cases the involved RLR is MDA5, with only a few known disease-correlated SNPs for RIG-I and so far non for LGP2. Interestingly, almost all of the so far identified pathogenic SNPs are either non-coding or are located within the RLR helicase domain (Table 1 and Figure 16).

**Table 1:** *DDX58* (encodes RIG-I) and *IFIH1* (encodes MDA5) single nucleotide polymorphisms associated with autoimmune diseases.

SMS: Singleton-Merten syndrome, AGS: Aicardi-Gutières syndrome, SLE: Systemic lupus erythematosus, T1D: type 1 diabetes, NA: not available

protein	SNP	nucleotide change	amino acid change	SNP location	disease
RIG-I	rs786204848	G to T	C268F	domain 1a	SMS
	rs786204847	A to C	E373A	domain 1a	SMS
MDA5	rs587777447	A to G	R337G	domain 1a	AGS
	rs587777576	C to T	L372F	domain 1a	AGS
	rs587777449	A to T	D393V	domain 1a	AGS
	rs587777575	G to A	A452T	domain 1a	AGS
	rs10930046	G to A	R460H	domain 1a	SLE
	rs672601336	G to A	G495R	domain 1a	AGS
	rs35744605	G to T	E627X	domain 2b	T1D <sup>1</sup>
	rs587777445	G to A	R720Q	domain 2a	AGS
	rs587777446	G to A	R779H	domain 2a	AGS, SLE
	rs587777448	C to T	R779C	domain 2a	AGS
	rs376048533	G to A	R822Q	domain 2a	SMS
	NA	G to A	R824K	domain 2a	AGS
	rs3747517	A to G	R843H	pincer, AP-1 binding site	T1D
	rs35667974	A to G	I923V	CTD	T1D <sup>1</sup>
	rs1990760	G to A	A946T	CTD, HNF-3bFOXA2 binding site	T1D, SLE
	rs13023380	G to A	intronic	intron	SLE
	rs2111485	T to C	intergenic	13 kb 3' of <i>IFIH1</i> gene	T1D
rs13422767	C to T	intergenic	23 kb 3' of <i>IFIH1</i> gene	T1D	
rs35337543	G to A	intronic	intron 8+1	T1D <sup>1</sup>	
rs35732034	G to A	intronic	intron 14+1	T1D <sup>1</sup>	

<sup>1</sup> The indicated SNPs confer protection against T1D.

### 6.1 Type I interferonopathies – the Aicardi-Gutières syndrome and systemic lupus erythematosus

The term "type I interferonopathies" is only recently emerging in literature and is used to describe a group of (mono)genetic diseases in which a constitutive upregulation of type I IFN production is considered to be directly relevant to pathogenesis<sup>223</sup>. As detailed earlier, type I interferon production and the expression of ISGs controls virus replication and spread in infected cell. Aberrant stimulation, however, or unregulated control of the type I interferon system can lead to inappropriate or sustained IFN production and might thus result in autoimmune diseases.

Known RLR-related diseases that are associated with the activation of type I interferon production include the Aicardi-Gutières syndrome and systemic lupus erythematosus.

#### Aicardi-Gutières syndrome:

The Aicardi-Gutières syndrome (AGS) is a rare monogenetic, inflammatory disease affecting the skin and brain, and is manifested by the degeneration of white matter due to the deterioration of myelinated nerve fibers<sup>224</sup>. The majority of affected patients are profoundly disabled with significant

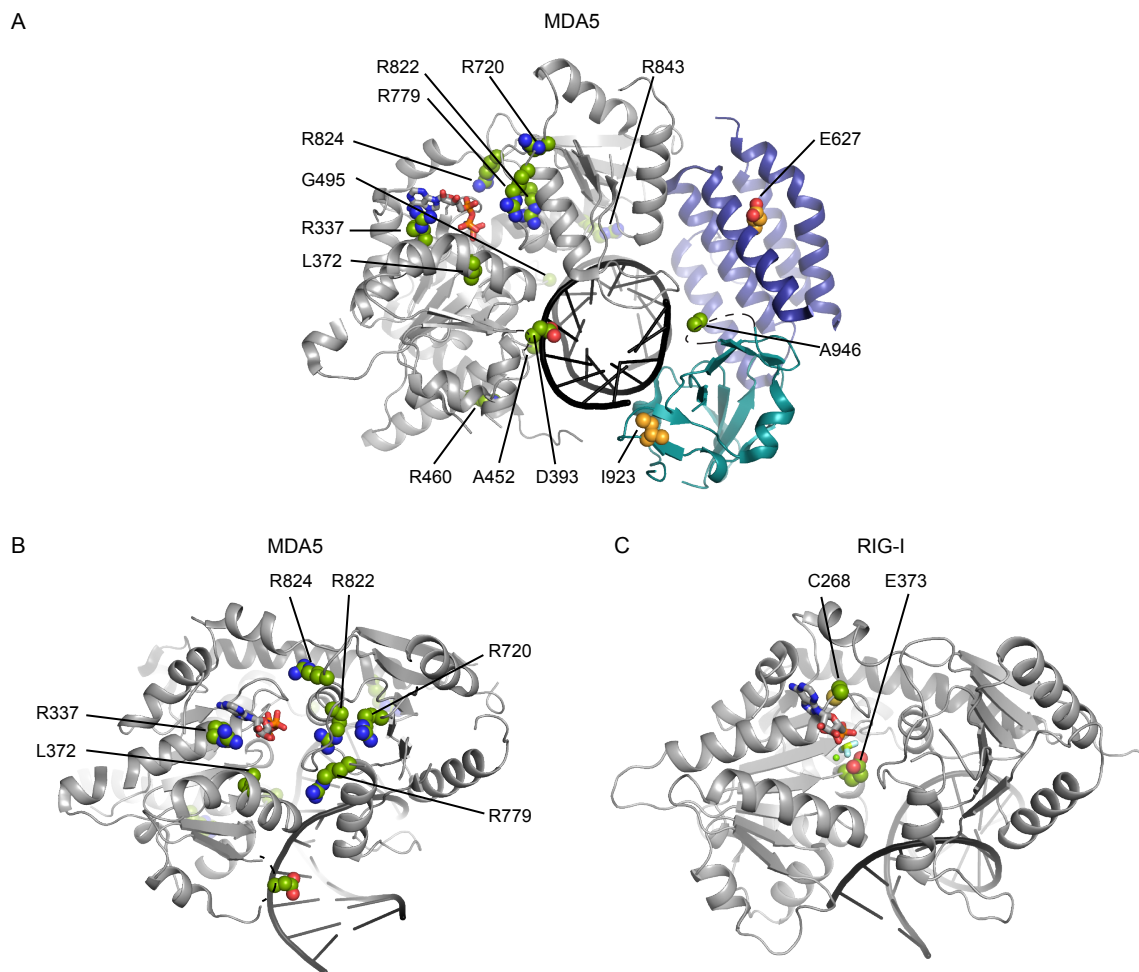


**Figure 16:** Mapping of known RLR disease-related susceptibility loci to the three-dimensional protein structure. Amino acids connected to a disease-promoting prognosis are depicted in green, potential disease-protecting sites are shown in orange. Dashed lines: invisible linkers containing susceptibility loci. (A) Overview of MDA5 susceptibility loci. (B) and (C) Susceptibility loci that map to residues within the ATP binding pocket between domains 1a and 2a of MDA5 or RIG-I respectively. RCSB PDB codes for the structures depicted are: 4gl2 (MDA5  $\Delta$ CARDs) and 3tmi (RIG-I  $\Delta$ CARDs).

intellectual and physical problems<sup>225</sup>. Other symptoms that are consistently associated with AGS include skin lesions referred to as chilblains and raised intraocular pressure (glaucoma). All patients show a constitutive upregulation of type I IFN production that is considered to cause pathogenesis<sup>226</sup>.

So far, AGS is known to be induced by mutations in one or several of the genes encoding the following seven proteins: the DNA 3' repair exonuclease 1 (TREX1)<sup>227</sup>, the subunits H2A, H2B and H2C of the ribonuclease H2 (RNase H2) endonuclease complex<sup>228</sup>, the deoxynucleoside triphosphate triphosphohydrolase and ribonuclease SAM domain and HD domain 1 (SAMHD1)<sup>229</sup>, the adenosine deaminase acting on RNA 1 (ADAR1)<sup>230</sup> and the gene encoding MDA5<sup>197</sup>. A deficiency in these genes may result in the accumulation of immune stimulatory RNA or DNA, leading to the chronic production of IFN via nucleic acid sensors like TLRs, RLRs or cGAS<sup>221</sup>.

In total 8 susceptibility loci within domains 1a and 2a of MDA5 have been related to AGS<sup>197,225,231</sup> (see Figure 16 and Table 1). All SNPs are described as gain-of-function mutations due to increased IFN

signaling<sup>197</sup>. In contrast to all other so far identified AGS-related SNPs, mutations in MDA5 display an autosomal dominant pattern of inheritance and occur exclusively heterozygous<sup>225</sup>. Nevertheless, some of the patients inherited the mutation from their parents or grandparents that were symptom-free despite also having elevated IFN levels<sup>197</sup>. A monogenetic background, therefore, seems not necessarily be sufficient to develop AGS.

Interestingly, increased IFN signaling of ADAR1 mutations within AGS patients is also dependent on MDA5. ADAR1 converts adenosine to inosine within endogenous RNAs and is essential for the maintenance of both fetal and adult hematopoietic stem cells by protecting against IFN-mediated apoptosis<sup>232</sup>. ADAR1-edited RNA has immunosuppressive properties<sup>233</sup> and altered binding affinities to RLRs<sup>234</sup>. Specifically, ADAR1 was shown to deaminate adenosine to inosine preferentially at the 3' UTR of mRNA thereby remodeling RNA secondary structure and preventing the formation of long dsRNA regions which are potential MDA5 binding sites<sup>235</sup>.

#### **Systemic lupus erythematosus:**

Systemic lupus erythematosus (SLE) is a chronic systemic inflammatory disease characterized by multi-organ damage caused by hyperactive T and B cells and autoantibody production against self nucleic acids and small nuclear RNA-binding proteins<sup>223,236</sup>. Affected organs are for instance the skin, kidney, joints, lungs, various blood elements, heart and the central and peripheral nervous system<sup>237</sup>. Like AGS, SLE is characterized by high IFN levels and dysregulated expression of genes of the IFN pathway with both the innate and the adaptive immune system being activated<sup>238</sup>. 90% of the SLE incidences affect women of child-bearing age between 20 and 30 years<sup>239</sup>.

For SLE there are so far more than 40 genetic susceptibility loci identified<sup>240</sup>. Many of these loci are shared with other autoimmune diseases like type 1 diabetes or AGS. The most prominent loci are HLA genes, especially class II genes, and the Fc $\gamma$  receptor. MDA5 is also shown to be a risk factor and especially the SNP that results in the MDA5 A946T mismatch<sup>241,242</sup> as well as MDA5 R779H<sup>243</sup>, R460H and an intronic SNP<sup>244</sup> have been linked to SLE (see Figure 16 and Table 1).

## **6.2 Other RIG-I-like receptor-related autoimmune diseases: the Singleton-Merten syndrome and type 1 diabetes**

So far, not all RLR-related immune diseases are connected to elevated levels of type I IFN in patients. Examples, where no interferon signature is described are the Singleton-Merten syndrome as well as Type I diabetes.

#### **Singleton-Merten syndrome:**

The Singleton-Merten syndrome (SMS) is a multi-system disorder mainly characterized by dental dysplasia, thoracic aortic calcification, osteoporosis, psoriasis, glaucoma and skeletal abnormalities<sup>245,246</sup>. SMS has an autosomal dominant pattern of inheritance<sup>246</sup>.

Recently, two mutations of RIG-I and one of MDA5 were found to be associated with SMS<sup>247,248</sup>. All mutations are located within the ATP binding pocket (Figure 12 and Table 1) and led to enhanced IFN signaling in cells, even without stimulus<sup>247,248</sup>. Clinical features of SMS patients harboring the identified mutations, however, are very diverse with for instance RIG-I-associated SNPs resulting in

atypical SMS which lacks the dental dysplasia phenotype.

The RIG-I SMS variant C268F and E373A affect key aa residues within the ATPase motifs I (Walker A) and II (Walker B) of domain 1a, respectively (see Figure 16). MDA5 R822 is located in motif VI (the "arginine finger") of domain 2a. The molecular basis for increased IFN production of SMS mutants was so far not understood, but is addressed in the second part of thesis and will be discussed later.

### **Type 1 diabetes:**

Type 1 diabetes (T1D) is a type of the metabolic disorder diabetes mellitus that is developed during childhood or adolescence. It is characterized by chronic hyperglycaemia with disturbances of carbohydrate, fat and protein metabolism resulting from defects in insulin secretion, insulin action, or both. During T1D the body develops amongst others autoantibodies against insulin-producing  $\beta$ -cells in pancreatic islets and insulin itself<sup>249</sup>. The trigger for the occurrence of those autoantibodies is still highly controversial and might, amongst others, be connected to enterovirus infections<sup>249–251</sup>. Statistically, the development of T1D has a seasonal pattern, being more common during the cold season, and has a higher incidence in industrialized countries where the sanitary conditions are better and, paradoxically, the prevalence of enteroviral infections is lower<sup>249,252</sup>.

The enteroviruses mainly implicated with T1D are Coxsackie type B viruses<sup>253</sup> and are sensed by MDA5<sup>254</sup>. It is speculated that the appearance of autoantibodies is connected to either an enhanced production of type I IFNs and subsequent inflammation induced tissue damage, or to a weak response that might favor viral replication and spread and therefore tissue damage<sup>255</sup>. In any case, the upregulation of type I IFNs helps to activate the adaptive immune response by enhancing the expression of major histocompatibility complex (MHC) molecules. By that cells become highly susceptible to recognition and destruction by adaptive immune cells<sup>256</sup>. Infections with enteroviruses might therefore contribute either to the initiation of autoimmunity or to the progression from islet autoimmunity to T1D or both<sup>255</sup>.

So far, more than 50 susceptibility loci for T1D have been identified<sup>257</sup>. Implicated genetic factors are mainly mutations within human leukocyte antigen (HLA) genes with class II genes being the strongest genetic contributors. Less prominent associations have been found for example for MDA5, which could therefore provide a link between genetic susceptibility, viral infections and the innate immune response, all being believed to contribute to T1D pathogenesis<sup>250</sup>.

In case of MDA5 the A946T and R843H substitutions as well as two intergenic SNPs were implicated in being a risk factor for T1D<sup>258,259</sup> (Figure 16 and Table 1). These four mutations, however, are found in a strong linkage disequilibrium and are reported to have cumulative effects<sup>259,260</sup>. Furthermore, MDA5 gene expression in unstimulated cells is increased<sup>260</sup>. Opposed to that, the mutations I923V, E627X and two variants with SNPs at an intron first nucleotide position are suspected to confer lower risk for T1D<sup>261</sup> (Figure 16 and Table 1). *In vitro* I923V and E627X show decreased IFN production after poly(I:C) stimulation<sup>262,263</sup> and except for I923V all protective MDA5 SNPs have lower mRNA levels<sup>264</sup>. A decrease in MDA5 driven production of type I IFNs might thus have protective effects on T1D development.

## 7 Objectives

RIG-I and MDA5 are the key immune receptors for defending many viral infections. Over the last decade, an immense number of studies focused on the molecular characterization of RIG-I-like receptors and their respective agonists *in vitro*. Several crystal structures of RIG-I and MDA5 successfully explain different binding preferences of both proteins towards distinct kinds of dsRNA, and build together with biochemical and cellular assays the foundation for their particular mode of action. The optimal RIG-I agonist, as defined *in vitro*, is short 5' di- or triphosphorylated, but unmethylated, dsRNA. MDA5 ligands, however, are less well understood and only characterized as long unmethylated dsRNA without any further particular discriminating element. In contrast to their distinct binding partners *in vitro*, RLRs show nevertheless overlapping functions when it comes to virus detection *in vivo*. The precise nature and origin of viral RLR agonists are thus still enigmatic. In addition, the function of the central SF2 helicase domain of RLRs remained mysterious. This became even more important, since recently several autoimmune disease variants, including single nucleotide polymorphisms causing Singleton-Merton syndrome (SMS), have been identified within the RLR helicase domain and particular within ATP binding or hydrolysis motifs of RIG-I and MDA5.

The aim of the first part of this thesis was the isolation and characterization of *in vivo* occurring ligands of RIG-I and MDA5 in measles virus-infected cells. Because of the comparably low affinity of MDA5 towards dsRNA a protein:RNA crosslinking approach with subsequent co-immunopurification from infected cells was established. In order to elucidate the nature of physiological RLR agonists, the recovered RNA was analyzed via Next Generation Sequencing. In addition, different biochemical assays were used to validate the sequencing results.

The second, and major, aim of this thesis was the functional characterization of the SF2 domain of RIG-I. For that purpose designed Walker A and Walker B mutants as well as RIG-I SMS variants were used. The impact of these mutations onto the RLR signaling pathway was analyzed in cellular assays with both infected and uninfected RIG-I KO cells. In addition, physiological ligands of the RIG-I Walker B mutant, that shows constitutive activity, and of SMS variants were investigated by co-immunopurification. The interaction of one putative endogenous ligand, that was found to be recognized by the RIG-I Walker B mutant, was visualized by cryo-electron microscopy. Again, biochemical experiments with purified proteins were used to independently validate the results.



# Publications

## 1 *In vivo* ligands of MDA5 and RIG-I in measles virus-infected cells

Runge S\*, Sparrer KMJ\*, Lässig C\*, Hembach K, Baum A, García-Sastre A, Söding J, Conzelmann K-K, Hopfner K-P (2014) *In vivo* ligands of MDA5 and RIG-I in measles virus-infected cells. PLOS Pathogens 10(4):e1004081.

\* These authors contributed equally.

DOI: 10.1371/journal.ppat.1004081

<http://journals.plos.org/plospathogens/article?id=10.1371/journal.ppat.1004081>

### Summary

In this publication we report the purification and characterization of physiological ligands of MDA5 and RIG-I in measles virus-infected cells. Since MDA5 shows only comparably poor affinity towards RNA ligands, we established a protein:RNA crosslinking approach aiming at improving the nucleic acid yield. Thereby incorporation of photoactivatable nucleosides into newly-synthesized RNA allows a subsequent selective UV light linkage to interacting proteins. Afterwards, we analyzed MDA5 and RIG-I co-immunopurified RNAs by next generation deep sequencing and compared the obtained reads to the measles virus genome.

In accordance with previous literature, RIG-I mainly interacted with measles virus genomic (i.e. negative-sense) RNA or antigenomic (i.e. positive-sense) RNA close to the 5' end. These RNA species most likely represent leader read-through transcripts or abortive replication products. For MDA5 on the other hand, we were for the first time able to purify *in vivo* relevant RNA and show that it solely interacted with antigenomic RNA/ mRNA excluding the end, but otherwise similar regions as RIG-I. For both proteins most interactions were found to occur within the measles virus L gene encoding the viral polymerase. We confirmed the sequencing results by quantitative PCR. Furthermore, by PCR, in both sequencing libraries measles virus copyback DI sequences could be detected. By bioinformatics evaluation of the sequencing data we found a direct connection between sequencing read number and AU base composition for MDA5. With subsequent cellular analysis of dephosphorylated *in vitro* transcribed (IVT) RNA spanning different regions of the measles virus antigenome, we could recapitulate this finding: IVTs with higher AU content exhibited also higher immunostimulatory potential. We further confirmed this correlation with Mengo virus IVTs. Finally, using *in vitro* ATP hydrolysis assays of purified MDA5 interacting with measles virus IVTs we show a negative correlation

of MDA5's ATPase function with AU base composition, indicating that ATP hydrolysis might disturb immunopurification of MDA5 associated RNA.

Based on our results we conclude that MDA5 preferentially senses AU-rich RNA species because they are poorer activators of its ATPase domain and therefore result in more stable MDA5 filaments, which in turn are better activators of type I interferon signaling.

#### **Author contributions**

I generated measles and Mengo virus *in vitro* transcripts together with Konstantin M. J. Sparrer and analyzed their ATP hydrolysis potential together with Simon Runge. I generated RIG-I and MDA5 mutants and performed luciferase reporter gene assays. Together with Katharina Hembach I analyzed the sequencing data and calculated correlation coefficients for different biochemical RNA parameters or assay results. I revised the manuscript together with Simon Runge, Konstantin M. J. Sparrer and Karl-Peter Hopfner.



# *In Vivo* Ligands of MDA5 and RIG-I in Measles Virus-Infected Cells

Simon Runge<sup>1,9</sup>, Konstantin M. J. Sparrer<sup>2,9</sup>, Charlotte Lässig<sup>1,9</sup>, Katharina Hembach<sup>1</sup>, Alina Baum<sup>3</sup>, Adolfo García-Sastre<sup>4</sup>, Johannes Söding<sup>1,5</sup>, Karl-Klaus Conzelmann<sup>2</sup>, Karl-Peter Hopfner<sup>1,5,9\*</sup>

**1** Gene Center and Department of Biochemistry, Ludwig-Maximilians University Munich, Munich, Germany, **2** Max von Pettenkofer-Institute, Gene Center, Ludwig-Maximilians University Munich, Munich, Germany, **3** Center for the Study of Hepatitis C, Laboratory of Virology and Infectious Disease, The Rockefeller University, New York, New York, United States of America, **4** Department of Microbiology, Department of Medicine, Division of Infectious Diseases and Global Health and Emerging Pathogens Institute, Icahn School of Medicine at Mount Sinai, New York, New York, United States of America, **5** Center for Integrated Protein Science Munich, Munich, Germany

## Abstract

RIG-I-like receptors (RLRs: RIG-I, MDA5 and LGP2) play a major role in the innate immune response against viral infections and detect patterns on viral RNA molecules that are typically absent from host RNA. Upon RNA binding, RLRs trigger a complex downstream signaling cascade resulting in the expression of type I interferons and proinflammatory cytokines. In the past decade extensive efforts were made to elucidate the nature of putative RLR ligands. *In vitro* and transfection studies identified 5'-triphosphate containing blunt-ended double-strand RNAs as potent RIG-I inducers and these findings were confirmed by next-generation sequencing of RIG-I associated RNAs from virus-infected cells. The nature of RNA ligands of MDA5 is less clear. Several studies suggest that double-stranded RNAs are the preferred agonists for the protein. However, the exact nature of physiological MDA5 ligands from virus-infected cells needs to be elucidated. In this work, we combine a crosslinking technique with next-generation sequencing in order to shed light on MDA5-associated RNAs from human cells infected with measles virus. Our findings suggest that RIG-I and MDA5 associate with AU-rich RNA species originating from the mRNA of the measles virus L gene. Corresponding sequences are poorer activators of ATP-hydrolysis by MDA5 *in vitro*, suggesting that they result in more stable MDA5 filaments. These data provide a possible model of how AU-rich sequences could activate type I interferon signaling.

**Citation:** Runge S, Sparrer KMJ, Lässig C, Hembach K, Baum A, et al. (2014) *In Vivo* Ligands of MDA5 and RIG-I in Measles Virus-Infected Cells. *PLoS Pathog* 10(4): e1004081. doi:10.1371/journal.ppat.1004081

**Editor:** Karen L. Mossman, McMaster University, Canada

**Received:** September 18, 2013; **Accepted:** March 6, 2014; **Published:** April 17, 2014

**Copyright:** © 2014 Runge et al. This is an open-access article distributed under the terms of the Creative Commons Attribution License, which permits unrestricted use, distribution, and reproduction in any medium, provided the original author and source are credited.

**Funding:** This work is funded by grants from the German Research Council (Deutsche Forschungsgemeinschaft, DFG GRK1721) and the Excellence Initiative of the German Ministry of Education and Science (Center for Integrated Proteins Science Munich, CIPSM) to KPH, the National Institutes of Health (NIH U19AI083025) to KPH and AGS, the Bavarian government (BioSysNet) to KPH and JS, the DFG SFB646 to JS and K-PH and the DFG GRK1202 to KPH, KKC, SR and KS. The funders had no role in study design, data collection and analysis, decision to publish, or preparation of the manuscript.

**Competing Interests:** The authors have declared that no competing interests exist.

\* E-mail: hopfner@genzentrum.lmu.de

9 These authors contributed equally to this work.

## Introduction

The retinoic acid inducible gene I (RIG-I)-like receptor (RLR) proteins are key players in innate immunity and act by recognizing viral RNA (vRNA) in the cytosol. The RLR family consists of the members retinoic acid inducible gene I (RIG-I), melanoma differentiation associated protein 5 (MDA5), and laboratory of genetics and physiology 2 (LGP2) [1–3]. *In vitro* studies have shown that RIG-I and MDA5 recognize the majority of viruses in a complementary manner. While many negative-strand RNA viruses like rabies and influenza viruses are predominantly sensed by RIG-I, picornaviruses are predominantly recognized by MDA5. The observed preferences are, however, unlikely to be exclusive and the exact role of LGP2 still needs to be investigated [4–9]. In case of MDA5, a minor contribution to recognition of measles, rabies, vesicular stomatitis and Sendai virus has been reported [10–13].

The RLR proteins belong to the DExD/H-box ATPases sharing a central ATP-dependent helicase domain and a C-terminal regulatory domain (RD) that is responsible for initial

RNA binding. In addition, RIG-I and MDA5 possess N-terminal tandem caspase activation and recruitment domains (CARDs) that are responsible for downstream signaling transduction [2,14,15]. Several crystal structures of RIG-I have shown that, in the absence of virus, the protein exists in an auto-inhibited state where the RD domain folds back to the CARDs, thereby shielding them from the cytosol. Upon viral infection and initial vRNA binding, the protein undergoes large conformational changes leading to the interaction with the mitochondrial associated signaling protein (MAVS) [16–19]. This leads to the activation of a downstream signaling cascade and finally to the induction of type I interferon (IFN) expression and the establishment of an anti-viral state. Although the exact nature of RLR ligands is not yet fully understood, several studies report that RIG-I preferentially binds to relatively short (between 25 to 1000–2000 bp) 5'-triphosphate double-stranded RNAs (5'-triphosphate dsRNA) like those of Sendai virus (SeV) defective interfering (DI) particles [20–23]. In contrast, MDA5 seems to have a preference for long (more than 1000–2000 bp) dsRNA stretches [24,25]. Upon binding to dsRNA, MDA5 is thought to cooperatively form polar helical filaments leading to association

### Author Summary

RIG-I-like receptors (RLRs) are helicase-like molecules that detect cytosolic RNAs that are absent in the non-infected host. Upon binding to specific RNA patterns, RLRs elicit a signaling cascade that leads to host defense via the production of antiviral molecules. To understand how RLRs sense RNA, it is important to characterize the nature and origin of RLR-associated RNA from virus-infected cells. While it is well established that RIG-I binds 5'-triphosphate containing double-stranded RNA, the *in vivo* occurring ligand for MDA5 is poorly characterized. A major challenge in examining MDA5 agonists is the apparently transient interaction between the protein and its ligand. To improve the stability of interaction, we have used an approach to crosslink MDA5 to RNA in measles virus-infected cells. The virus-infected cells were treated with the photoactivatable nucleoside analog 4-thiouridine, which is incorporated in newly synthesized RNA. Upon 365 nm UV light exposure of living cells, a covalent linkage between the labeled RNA and the receptor protein is induced, resulting in a higher RNA recovery from RLR immunoprecipitates. Based on next generation sequencing, bioinformatics and *in vitro* approaches, we observed a correlation between the AU-composition of viral RNA and its ability to induce an MDA5-dependent immune response.

with MAVS and activation of the downstream signaling cascade [26–28].

Viruses have developed numerous strategies to evade the immune system. For instance, viruses of the paramyxovirus family (e.g. measles, parainfluenza, Sendai and Nipah viruses) encode V inhibitor proteins that specifically bind to MDA5 and LGP2, but not always to RIG-I [29–31]. By determining the structure of MDA5 in complex with parainfluenza virus V-protein, we previously showed that the viral protein unfolds the ATPase domain of MDA5. This leads to the disruption of the MDA5 ATP-hydrolysis site and prevents RNA bound MDA5 filament formation [32].

One of the remaining key questions in this field is how RLR proteins are able to distinguish between self and non-self RNA in the cytosol. Recently, several studies showed that 5'-triphosphate RNA is not the only RNA ligand for RIG-I. Specific poly U/C-rich regions within certain viral genomes seem to contribute to efficient recognition by the protein [33,34]. In case of MDA5, it is not known which features of vRNA are required in order to induce an immune response. Expression of subgenomic and subgenic RNA from parainfluenza virus 5 (PIV5) indicated that MDA5 recognizes a specific region within the L mRNA [35]. For picornaviruses, it is speculated that MDA5 binds to long dsRNA that represents replicative intermediates composed of the positive genome and the negative antigenome [36]. These studies were, however, based on *in vitro* transfection experiments and it has so far not been possible to isolate a natural RNA ligand for MDA5 directly from virus-infected cells.

In this study we combined different methods, including RNA-protein crosslinking and deep sequencing, to investigate *in vivo* RNA ligands for RLR proteins from virus-infected cells. Based on the crosslinking we were able to co-purify immunostimulatory RNA in a RIG-I and MDA5 dependent manner from measles virus (MeV)-infected cells. Deep sequencing and bioinformatics analysis revealed that RIG-I and MDA5 bind RNA of positive polarity originating from the L gene of the MeV genome. In addition, RIG-I binds to the 5' ends of genomic and antigenomic RNAs, which probably represent 5'-triphosphate RNA, and are

therefore not recognized by MDA5. Furthermore, we showed that RIG-I, but not MDA5, binds RNA of negative polarity, indicating that MDA5 does not efficiently recognize the MeV genome. Based on bioinformatics analysis, we observed a correlation between MDA5-enriched RNA sequences and the AU content and this was confirmed by *in vitro* transcription assays. In summary, we report the isolation of MDA5-associated RNA from virus-infected cells and the discovery of *in vivo* occurring activating viral RNA ligands for MDA5.

### Results

#### 4-thiouridine treatment and 365 nm UV light exposure lead to improved RLR-associated RNA recovery from virus-infected cells

Several *in vitro* studies showed that MDA5 preferably recognizes long dsRNA stretches [24,25]. However, it is still unclear if the protein has a preference for specific RNA sequences. The main reason for this may lie in the weak interaction between the protein and its ligand resulting in very poor RNA levels that co-purify from MDA5 immunoprecipitates. In order to address this problem, we established an RNA-protein crosslinking approach adapted from the PAR-CLIP (Photoactivatable-Ribonucleoside-Enhanced Crosslinking and Immunoprecipitation) methodology [37]. With this approach, we intended to improve RNA recovery from RLR immunoprecipitates in the context of a viral infection. For validation of the method, we compared the crosslinking approach with a conventional pull-down technique previously used for the identification of SeV DI particles as potent RIG-I inducers [20]. We infected A549 human lung carcinoma cells with SeV at a high multiplicity of infection (MOI) in the presence of 4-thiouridine (4SU) and allowed infection to occur over 24 h. A part of the cells was then exposed to 365 nm UV light and endogenous RIG-I was immunopurified (Figure 1a). The recovered RNA was isolated and subjected to quantitative PCR (qPCR) analysis and immunoactivity experiments. The data indicate that treatment of cells with 4SU and exposure to 365 nm UV light lead to a reduction of immunostimulatory activity of RIG-I-associated RNA to 50% (Figure 1b). However, the results of qPCR analysis showed that the crosslinking approach yields a quantitatively improved RNA recovery, with an increase of 50% in SeV DI particles in comparison to the non-crosslinking approach (Figure 1c and d). Furthermore, we confirmed that treatment of cells with the photoreactive nucleoside does not affect cell viability or virus replication (data not shown). Taken together, our data indicate that the crosslinking technique is a promising tool to study *in vivo* occurring RNA ligands for RLR proteins.

Next, we validated the crosslinking approach on cells that were infected with a variety of viruses, including negative-stranded (–) RNA viruses (MeV [38] and rabies [39]) and positive-stranded (+) RNA viruses (Encephalomyocarditis virus (EMCV [40]) and Mengo virus [41]). In all cases, we infected A549 cells at an MOI of 1.0 in the presence of 4SU. Cells were crosslinked 24 h post infection (hpi) and RIG-I and MDA5 were immunopurified. The recovered RNA was subjected to immunoactivity experiments. Based on the data, we concluded that immunoactive RNA was co-purified in a RIG-I- and MDA5-dependent manner from MeV-infected cells. This induction was significant in comparison to the negative control (Figure 2). In the case of RIG-I-associated RNA, we obtained an immunostimulatory effect that was 2600-fold higher in comparison to the control. For MDA5, we observed an 800-fold induction. The data show that the approach yields RIG-I- and MDA5-specific immunoactive RNA from MeV-infected cells in a RIG-I- and MDA5-dependent manner.

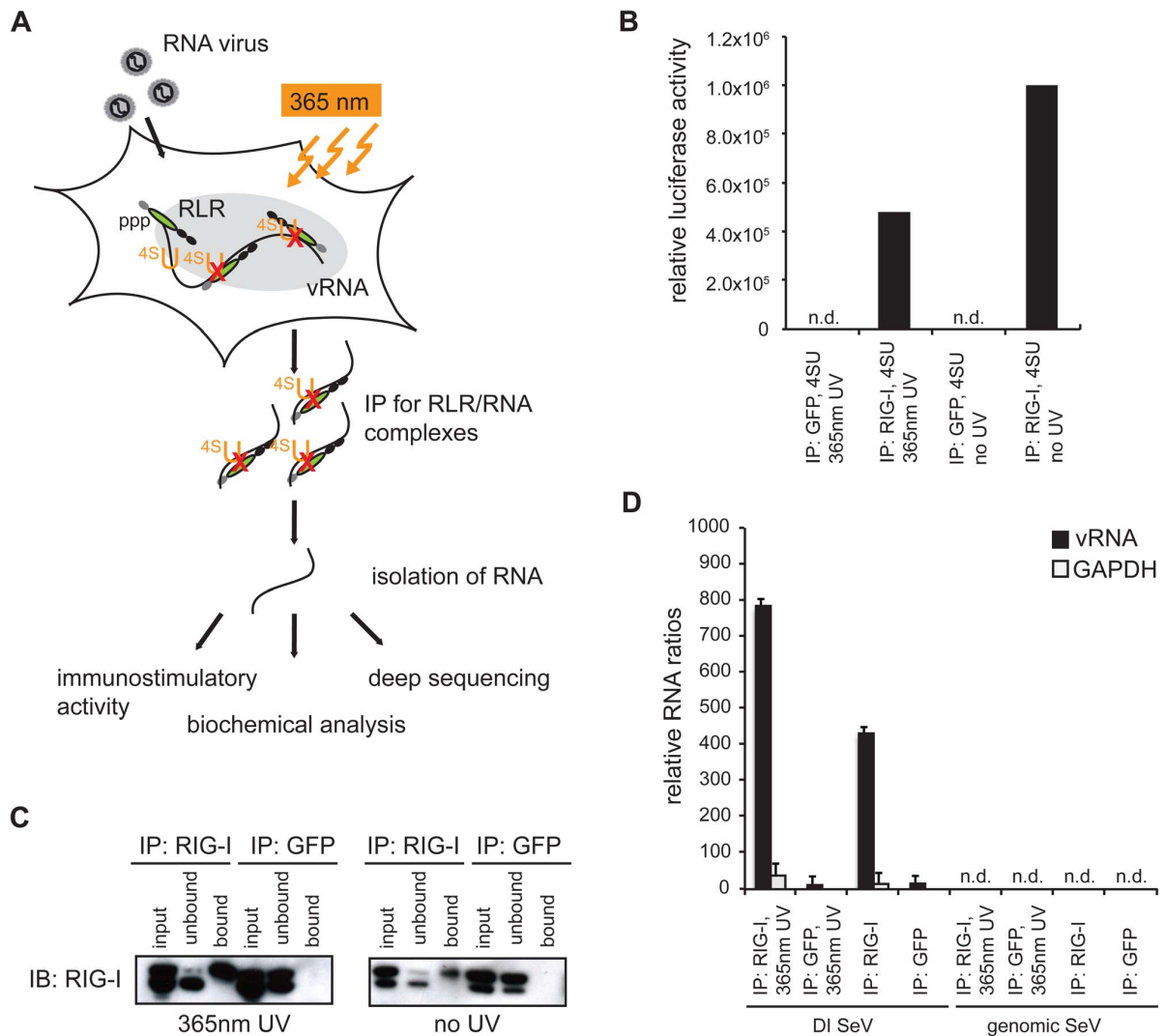


**Figure 1. Validation of crosslinking and immunoprecipitation of RLR/RNA complexes from 24 h virus-infected cells.** **A:** Schematic representation of the experimental procedure for characterization of RLR-associated RNA molecules. **B:** Immunostimulatory activity of RNA from RIG-I and control (GFP) crosslinking samples in comparison to non-crosslinking immunoprecipitates. **C:** Western blot analysis of crosslinked and non-crosslinked RIG-I and control (GFP) pull-down experiments. **D:** Comparison of RNA recovery levels by quantitative PCR analysis of RIG-I-associated RNA from SeV-infected cells (n=3). n.d.=not detectable. doi:10.1371/journal.ppat.1004081.g001

Although we detected significant immunostimulatory activity for RLR-associated RNAs from MeV-infected cells, the experimental set up is currently unsuitable for the isolation of RLR RNA ligands from the other viruses (Figure S1). The reason for this may lie in the heterogeneity and the need for precise timing of viral replication cycles or in the efficiency of 4SU incorporation and crosslinking. Utilization of this technique for other viruses may require adjustment of parameters, such as the time points of 4SU addition, crosslinking and harvesting after infection.

### Deep sequencing reveals regions within the measles virus genome recognized by RIG-I and MDA5

Based on the above-mentioned results, we focused our studies on MeV, which belongs to the order of *Paramyxoviridae*. MeV has a single-stranded RNA genome of negative polarity consisting of

15,894 nucleotides. It comprises six non-overlapping genes, which are flanked by small terminal non-coding regions known as leader (*le*) and trailer (*tr*) sequences. These sequences serve as promoter regions during viral replication and transcription [42,43]. While the replication of the genome and antigenome is performed in a continuous process, viral transcription is carried out in a sequential manner, giving rise to an mRNA gradient declining in the 3' to 5' direction (Figure S2), as previously published [44]. Since (-) RNA virus polymerases eventually fail in transcription termination, they generate, in addition to monocistronic mRNAs, numerous alternative RNA species including read-through transcripts, such as leader-N, bi- or tricistronic mRNAs [45]. Furthermore, replication can give rise to abortive replication products and DI RNA with large internal deletions or copy-back genomes [46]. Due to the complex RNA composition of

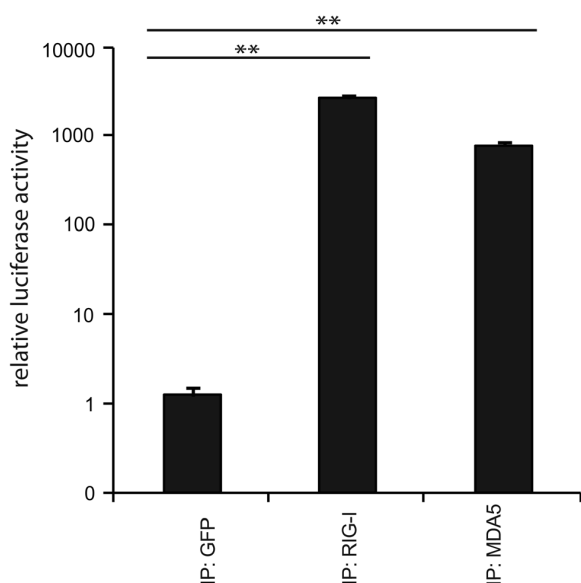


**Figure 2. Immunoprecipitation of RLR-associated RNA from 24 h MeV infections.** Validation of immunostimulatory activity of RNA from RIG-I, MDA5, and GFP immunoprecipitates upon transfection into 293T ISRE-FF reporter cells ( $n = 3$ ,  $** P < 0.01$ ). doi:10.1371/journal.ppat.1004081.g002

a virus-infected cell, the analysis of specific RNA ligands for RLR proteins is challenging.

In order to shed light on the exact nature of RIG-I and MDA5-associated RNAs derived from MeV-infected cells, we performed a deep sequencing analysis on isolated RNA species from co-immunoprecipitations with antibodies against endogenous RIG-I and MDA5. As a control, we used an antibody against GFP (GFP protein was not present). The MeV strain used for the studies presented here was a recombinant measles virus rescued from cDNA with the exact sequence of the Schwarz vaccine strain (Genbank AF266291.1) [38].

Obtained sequences were mapped to the MeV antigenome and the relative abundances of these sequences between RIG-I pull-down, MDA5 pull-down, and GFP pull-down were compared. Analysis of the reads showed that RIG-I and MDA5 bind to similar regions within the L gene-derived RNAs. In addition, RIG-I, but not MDA5, binds to RNAs derived from the 3' and the 5' ends of the MeV genome (Figure 3a and b). These regions probably represent *le* or *tr*RNA generated in the course of replication or transcription. Additionally, internal genomic and antigenomic sequences found in the pull-downs could potentially originate from MeV DI particles [46–51]. To address this question, we performed a PCR analysis of RLR libraries in which we specifically amplified copyback DI RNA of MeV [47–49]. Indeed, we detected copyback DI particles not only in the RIG-I pull-down but also within RNA recovered from MDA5 immunoprecipitates (Figure S3). We did not find DIs in the GFP control pull-downs.

Consistent with previous work, the higher copy numbers of reads indicate that RIG-I binds MeV RNA with higher affinity than MDA5 [11]. This observation is in good agreement with the increased immunostimulatory activity of isolated RNA from RIG-I pull-down samples in comparison to MDA5. Regarding the immunostimulatory activity, RIG-I-associated RNA gives a 4-fold higher induction in comparison to MDA5-associated RNA (Figure 3d and e).

### Analysis of deep sequencing data reveals remarkable differences in the strand-specificity of RIG-I and MDA5

Based on the protocol used for cDNA library preparation, sequencing reads could be separated according to their strand orientation. During cDNA synthesis, adaptors were specifically ligated to the 3' or 5' ends, thereby keeping the information of strand specificity during the deep sequencing run. Separation of sequences revealed remarkable differences between both protein immunoprecipitations. RIG-I associated RNA sequences of positive polarity, which represent either antigenomic RNA or mRNA transcripts, are enriched in regions close to the 5' end of the viral antigenome (leader) but also in distinct regions within the L gene. In contrast, sequences of negative polarity, representing the viral genome, are exclusively enriched in the 5' end of the genome (trailer region) and in regions of the L gene (Figure 4a).

Analysis of MDA5-associated RNA revealed that sequences of positive polarity were enriched within the L gene originating from similar regions as (+) RNA from the RIG-I library (Figure 4b). In contrast to RIG-I, however, MDA5 did not bind to RNA sequences comprising the 5' end of the antigenome or leader RNA. Comparison of (–) RNA from RIG-I and MDA5 libraries further revealed that, in contrast to RIG-I, MDA5 did not enrich sequences of negative polarity, including trailer sequences.

According to the analysis of strand specific enrichment, it appears that MDA5 does not bind vRNA of negative polarity that represents the MeV genome. Furthermore, the data evidently rule out the possibility that MDA5 recognizes RNA duplexes of (+) and (–) RNA that might represent replication intermediates, as previously suggested for a positive-strand RNA virus [36]. In fact, the result suggests that MDA5 binds (+) RNA that could either represent mRNA or the MeV antigenome.

To further validate the specificity of the accumulation of RIG-I and MDA5-associated RNA, we calculated specific read enrichments [52] of the RLR libraries compared to the control library (Figure S4). Enrichment (greater than  $2\times$  compared to the control library) of RIG-I-associated RNA of positive polarity can be found across the whole genome, whereas only few reads of negative polarity are enriched within the N and L segment. In contrast, enriched sequences of MDA5-associated RNA are exclusively present within the L segment of positive polarity, whereas no specific enrichment was observed for (–) RNA.

Based on the data, we observed a good correlation between the deep sequencing analysis and enrichment calculations, indicating that distinct regions within the MeV genome are indeed specifically enriched in a RIG-I- and MDA5-dependent manner in comparison to the control.

### Confirmation of deep sequencing data with quantitative PCR

To independently validate the relative amount of RLR-associated RNA, qPCR amplification was performed. The obtained copy read numbers were normalized to the GFP negative control in order to compare the genomic segments in the RIG-I and MDA5 samples (Figure 5a). Analysis of relative abundances confirmed that RIG-I specifically enriches sequences from the 3' and 5' regions of the MeV genome, representing either antigenome or viral mRNA. Interestingly, the analysis showed that RIG-I-associated RNA from the genomic 3' end most likely represents leader read-through transcripts or abortive replication products and not N mRNA. In MDA5 pull-downs, RNA was enriched in the case of the L mRNAs and partly in the case of H mRNAs, while no relevant copy numbers were obtained at other genomic positions. This is in good agreement with the results of

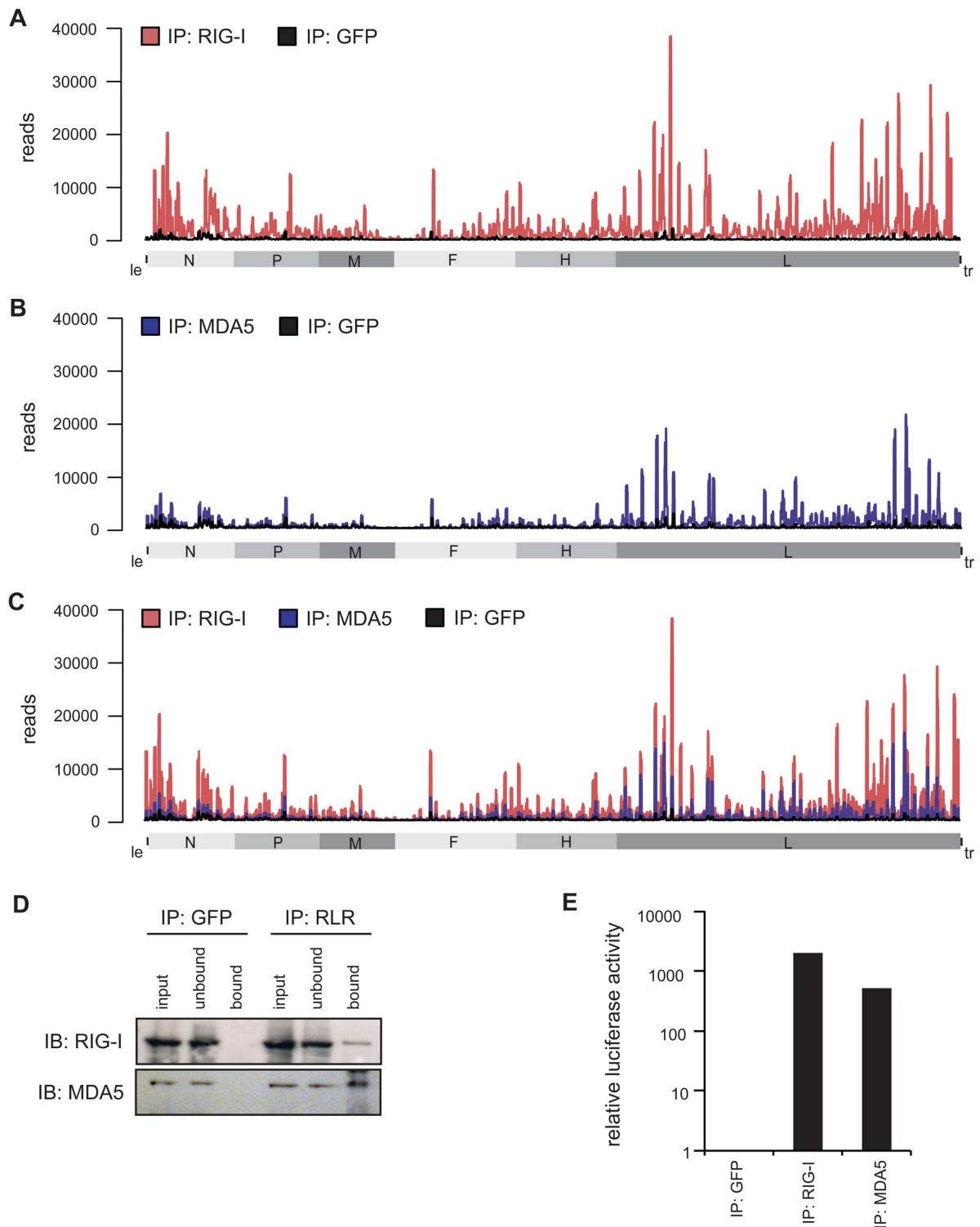


**Figure 3. Deep sequencing analysis of RLR-associated RNA from MeV-infected cells.** **A–C:** RNA from RIG-I pull-down (red), MDA5 pull-down (blue), and control (GFP) pull-down (black) from MeV-infected cells were subjected to Illumina deep sequencing analysis. Obtained sequencing reads are mapped to their position on the viral antigenome. The x-axis corresponds to all possible 15,894 positions in the MeV antigenome and the y-axis shows the number of reads at the respective position. (A) RIG-I-associated sequences in comparison to the control mapped to the viral antigenome. (B) MDA5-associated sequences in comparison to the control mapped to the viral antigenome. (C) Overlay of RIG-I associated and MDA5-associated sequences. **D:** Western blot analysis of RIG-I and MDA5 immunoprecipitation in comparison to the GFP pull-down. **E:** Validation of immunostimulatory activity of RNA from RIG-I, MDA5, and GFP immunoprecipitates upon transfection into 293T ISRE-FF reporter cells. doi:10.1371/journal.ppat.1004081.g003

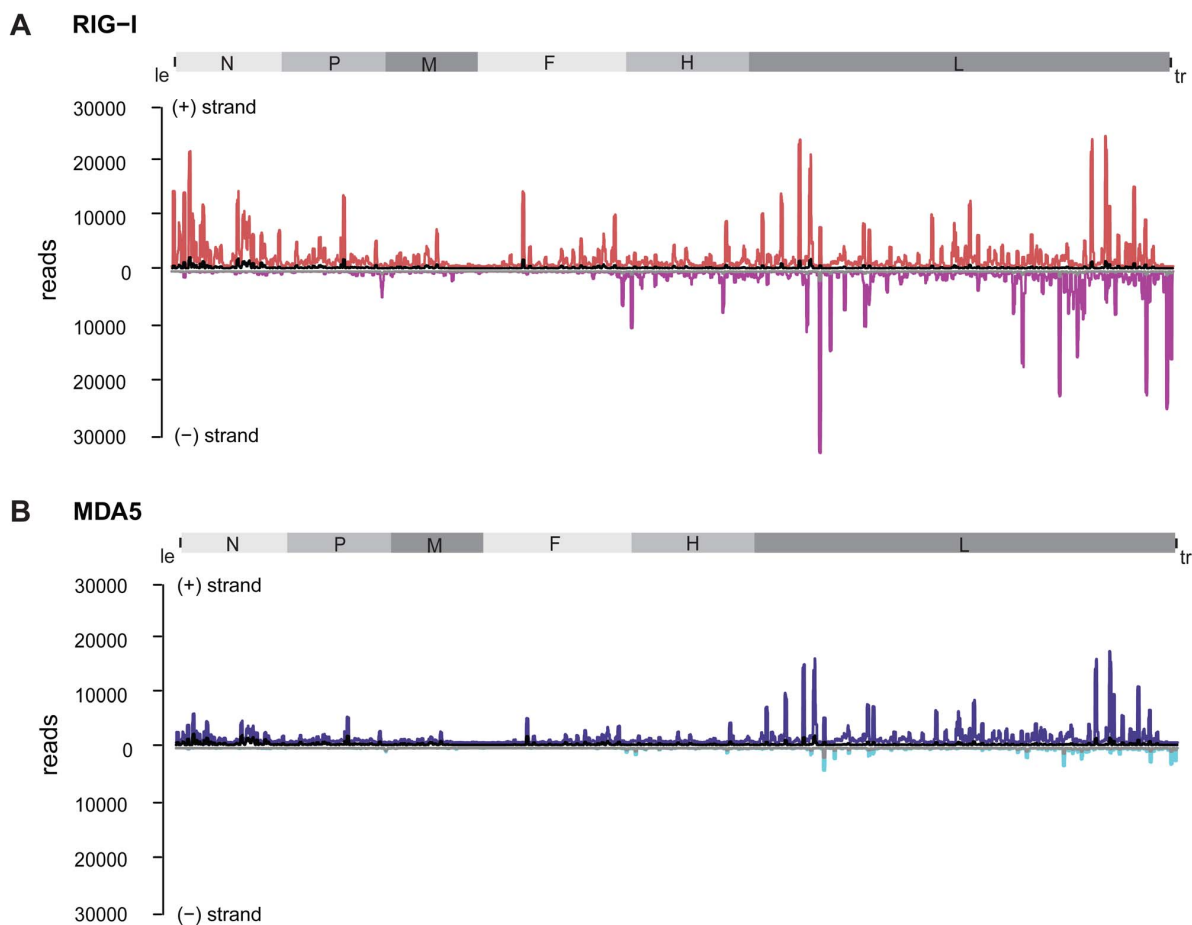


**Figure 4. Strand separation of sequencing libraries into (+) and (-) MeV RNA.** RNA deep sequencing libraries were generated based on the strand-specific mRNA sample preparation protocol from Epicentre. The Epicentre protocol encompasses sequential ligation of 5' and 3' adapters to RNA molecules, thus preserving strandness information. **A:** RIG-I-associated sequences in comparison to the control mapped to the viral antigenome. (+) RNA is shown in red; (-) RNA is shown in magenta; the control library is shown in black and grey. **B:** MDA5-associated sequences in comparison to the control mapped to the viral antigenome. (+) RNA is shown in blue, (-) RNA is shown in cyan; the control library is shown in black and grey. doi:10.1371/journal.ppat.1004081.g004

the deep sequencing analysis, indicating that MDA5 indeed recognizes RNA originating from the L gene of the MeV genome. Furthermore, comparison of the relative copy numbers between RIG-I and MDA5 revealed remarkable differences between both proteins. The relative abundances in the RIG-I sample were up to 40-fold higher in comparison to MDA5. This observation again indicates that RIG-I has a higher affinity for MeV RNA sequences in comparison to MDA5. Our conclusion is further supported by immunoactivity experiments, where the relative immunostimulatory activity of RIG-I-associated RNA was 20-fold higher in comparison to MDA5 (**Figure 5b and c**).

#### Bioinformatics analysis reveals a preferred binding of RIG-I and MDA5 to RNA species with a higher AU composition

To elucidate the exact nature of sequences enriched by RIG-I and MDA5 immunoprecipitations, we conducted a bioinformatics analysis. For this, the complete genome was divided into fragments of size 201 nt with a shifting window of 5 nt. Each sequence was folded *in silico* (RNAfold [53]) and several RNA primary and

secondary structure features were analyzed. The analyzed parameters were set in relation to the mean coverage of sequencing reads from RIG-I and MDA5 pull-down experiments. Heat scatter plots indicate that sequences rich in AU correlate with a high mean coverage of sequencing reads in both the RIG-I (cor = 0.273, cor = 0.334) and MDA5 (cor = 0.358, cor = 0.348) libraries (**Figure 6a and b**). These data suggest that RIG-I and MDA5 preferably bind to AU-rich sequences originating from the viral genome. Although we further analyzed a variety of secondary structure parameters, including paired nucleotides and bulges, we did not see any other relevant correlation with the mean coverage of sequencing reads (**Figure S5 and Figure S6**).

#### Confirmation of deep sequencing analysis by immunoactive experiments on *in vitro* transcripts

To further confirm the obtained sequencing data, we generated 17 single-stranded, 200 nucleotide long *in vitro* transcripts (IVTs) covering different regions of the MeV antigenome (**Table S1**). RNAs were double-phosphorylated in order to ensure that 5'-triphosphate groups were removed. For immunoactivity

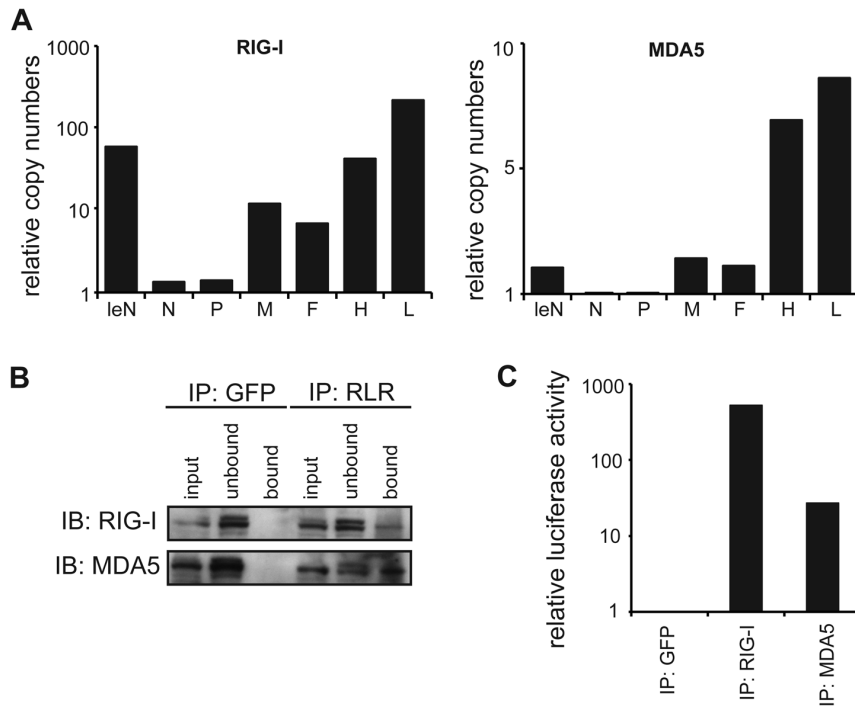


**Figure 5. Quantitative PCR analysis of RLR-associated RNA from MeV-infected cells.** **A:** Comparison of RNA levels between RIG-I and MDA5 immunoprecipitates for each genomic segment at 24 hpi. Relative RNA ratios were normalized against the control (GFP) library (mean values, n = 2). **B:** Western blot analysis of RLR pull-down experiments in comparison to the GFP pull-down. **C:** Immunostimulatory activity of RLR-associated RNA at 24 hpi. doi:10.1371/journal.ppat.1004081.g005

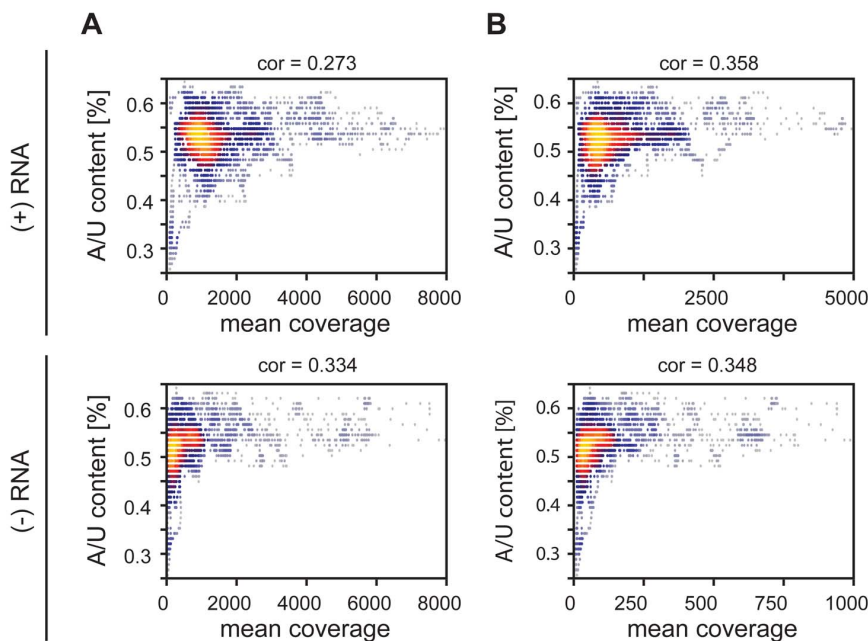


**Figure 6. Heatscatter plots of AU content of 201 nucleotide MeV RNA fragments and the fragment's mean coverage.** The linear correlation is expressed via the Pearson coefficient. Every dot corresponds to one fragment with its respective AU content and mean coverage within an RLR library. The more yellow the plot, the more data points overlap. **A:** Correlation between AU composition and coverage of RIG-I-associated RNA of positive and negative RNA respectively. **B:** Correlation between AU composition and coverage of MDA5-associated RNA of positive and negative RNA respectively. doi:10.1371/journal.ppat.1004081.g006

experiments IVTs were transfected into 293T ISRE-FF reporter cells. The stimulatory effect revealed a correlation of high read numbers from deep sequencing analysis and high stimulatory activity of the IVT sequences (Figure 7). According to the immunostimulatory experiment, we observed increased immunostimulatory activities for transcripts 8, 9, and 12 (Figure 7a). These transcripts correspond to regions at the 5' end of the L gene, which is also the region with the highest copy numbers of reads (Figure 3). In general, IVTs representing regions within the L gene have higher immunostimulatory activity in comparison to the upstream genomic segments. This is in good agreement to the deep sequencing analysis. Furthermore, calculated Pearson correlations showed that the best correlation between maximal numbers of sequencing reads and the immunostimulatory activity of RNA transcripts can be found in the MDA5 sequencing data ( $\text{cor} = 0.526$ ), while RIG-I and GFP samples showed less correlation ( $\text{cor} = 0.369$  and  $\text{cor} = 0.217$ ) (Figure 7b). In order to find a possible explanation for the different immunostimulatory potentials of IVTs, several characteristics of the transcripts were analyzed *in silico*. The obtained data revealed that the immunostimulatory potential correlates with the AU content of IVTs ( $\text{cor} = 0.599$ ) (Figure 7d), which is consistent with the results from the deep sequencing analysis. Visualization of transcripts on an Agilent bioanalyzer RNA chip indicates that no higher-order structures due to the sequence composition were formed that might explain differences in immunostimulatory activity (data not shown).

In order to get a more general conclusion about the contribution of the AU content to the immunostimulatory potential of RNAs, *in vitro* transcripts from Mengo virus (Table S3) were tested for their immunostimulatory activity. The transcripts were generated according to the protocol for MeV RNA sequences. We again observed a correlation ( $\text{cor} = 0.583$ ) of the AU content of the tested sequences and their immunostimulatory potential (Figure S 7a and b). These data are consistent with the *in vitro* analysis of MeV RNA sequences indicating that the AU composition of RNA might play a general role in activating RLR signaling.

### In vitro transcripts with a low proportion of AU strongly stimulate ATP hydrolysis by MDA5

Finally, we asked whether the ATP hydrolysis activity of MDA5 correlates with the immunostimulatory potential of the tested IVTs. We measured the ATP hydrolysis rate of recombinant mouse MDA5 in the presence of RNA transcripts (Figure 7 and Figure S8) and observed a negative correlation between the maximum number of sequencing reads in the MDA5 library and the ATP hydrolysis rate ( $\text{cor} = -0.414$ , Figure 7c). Analysis of the *in vitro* data revealed that AU-rich sequences lead to a decrease in ATP hydrolysis activity of MDA5 ( $\text{cor} = -0.445$ ). Furthermore, the ATP hydrolysis rate negatively correlates with the immunostimulatory potential of RNA transcripts ( $\text{cor} = -0.426$ ) (Figure 7d). This result suggests that the ATPase hydrolysis activity of MDA5 is not correlated to the binding and the immunostimulatory potential of the RNA transcripts and could therefore provide a model of RNA recognition by the protein. The data are consistent with previous work on MDA5 filament formation upon dsRNA binding [26,27]. In structural and biophysical studies, Berke *et al* showed that ATP hydrolysis by MDA5 causes filaments to disassemble, perhaps by inducing translocation along the RNA or triggering a conformational change in the protein. According to our data, this may explain the observed inverse correlation between the immunostimulatory

activity of IVTs and their potential to induce the ATPase activity of MDA5.

## Discussion

Until now, *in vivo* RLR ligands were poorly understood and a naturally occurring MDA5 ligand could only be purified indirectly by immunoprecipitation of LGP2:RNA complexes from virus-infected cells overexpressing LGP2 [54]. By applying a combination of RNA-protein crosslinking, immunoprecipitation of endogenous proteins and RNA deep sequencing analysis, we were able to investigate RLR-associated RNA from MeV infected cells. We compared our results to the empty GFP antibody control resembling a previously published immunoprecipitation strategy [20].

Our approach reveals that MDA5 preferentially binds measles virus RNA of positive polarity, whereas RIG-I additionally binds to (−) sense RNA within the trailer region as well as in the adjacent L gene. We propose that enriched RNA of positive polarity most likely represents mRNA species, since antigenomic RNA is only generated during replication and is immediately packed into nucleocapsids [55–57]. For *Mononegavirales*, these RNA-protein complexes are considered inaccessible for cytoplasmic proteins [55,58] and might not be ligands for RLR proteins unless they become released. We show that, unlike MDA5, RIG-I binds (+) sense RNA originating from not only the L genomic segment, but also from the 3' end of the MeV genome, which could be either *le-N* read-through transcripts or abortive replication products comprising 5'-triphosphate ends [45,46]. Furthermore, we hypothesize that RIG-I specific enriched RNA of negative polarity represents abortive replication products also having 5'-triphosphate ends [20–23]. Additionally, 5'-copyback DI sequences combining vRNA of positive and negative polarity were found both in RIG-I and MDA5 immunoprecipitates and may contribute to recognition [49].

Bioinformatics analysis and *in vitro* transcription experiments revealed a correlation between AU content and read coverage of the obtained sequences or IVTs, respectively. As shown before [59], this indicates that RNA rich in AU could serve as a putative ligand for RIG-I and MDA5, or in a secondary manner lead to a specific structure that is recognized by both proteins. The slightly weaker correlation of RIG-I associated sequences with their AU content compared to MDA5 bound RNAs could be explained by additional sequences or triphosphate RNAs recognized by RIG-I that originate from regions less rich in AU.

Interestingly, ATP hydrolysis assays performed with recombinant MDA5 and RNA transcripts indicate that the AU content of RNA negatively correlates with the ATP hydrolysis rate of the protein. This inverse correlation between the immunostimulatory potential of RNAs and their capability to stimulate ATP hydrolysis by MDA5 lets us speculate that the ATPase activity might not be necessary for, or even interfere with, the immunoactivity of RNA ligands. Although this observation disagrees with recent findings about the role of ATP hydrolysis in RIG-I oligomerization on 5'-triphosphate dsRNA [60], we assume that MDA5 and RIG-I differ markedly in their mechanical activation and the role of ATP hydrolysis. Our data is supported by results suggesting that MDA5 filament formation is abrogated in an ATP-sensitive manner. By electron microscopy (EM) analysis it was shown that MDA5 filaments disassemble in the presence of ATP, indicating that ATP hydrolysis triggers the translocation of the protein along the dsRNA molecule or reduces the binding affinity, thereby interfering with downstream signaling [26,27]. In light of the available data in the literature we therefore hypothesize that the

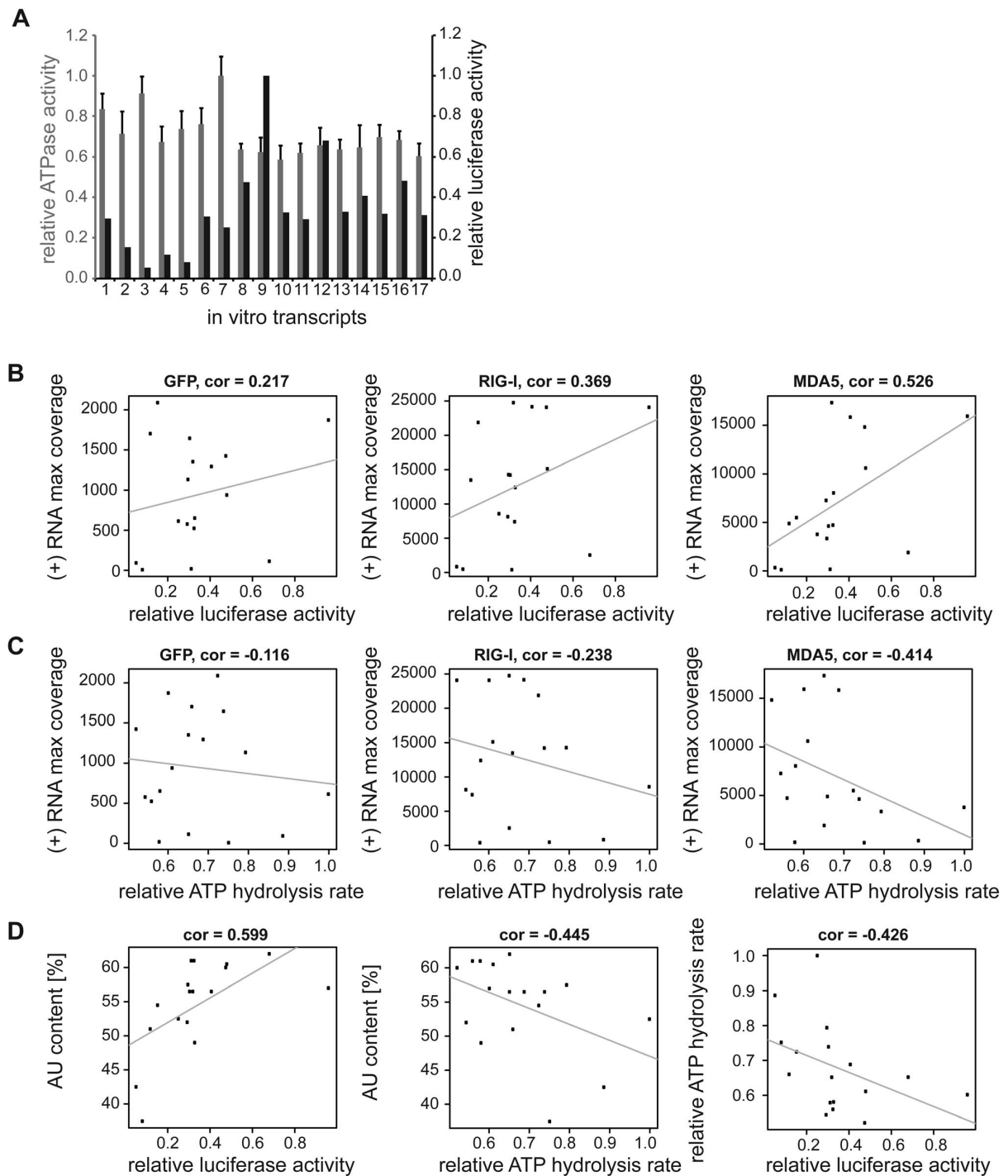


**Figure 7. Analysis of *in vitro* transcribed RNA of the measles virus genome.** Sequences were generated according to deep sequencing data. The transcripts were either transfected into 293T ISRE-FF reporter cells in order to validate the immunostimulatory potential or ATPase hydrolysis experiments were performed in presence of recombinant *mMDA5*. **A:** Comparison of relative luciferase activities (black) and relative ATPase activities (grey) of *in vitro* transcribed RNAs (n=3 and n=2 respectively, values were normalized to the highest mean value of each replicate). **B:** Pearson correlation between (+) RNA maximal coverage and relative luciferase activity. **C:** Pearson correlation between (+) RNA maximal coverage and relative ATPase activity. **D:** Correlation analysis between AU content and luciferase or ATPase activity, and between ATPase and luciferase activity. doi:10.1371/journal.ppat.1004081.g007

ATPase activity of the MDA5 helicase domain contributes to substrate specificity by detaching the protein from low affinity substrates. To further test this hypothesis we generated RIG-I<sup>E373Q</sup> and MDA5<sup>E444Q</sup>, which are mutated in the “Walker B” ATP hydrolysis motif [61], slowing down or abrogating the ATP hydrolysis activity of the proteins, while preserving formation of ATP complexes. Overexpression of these mutant proteins from transfected plasmids showed a dramatic increase in their immunostimulatory potential in the absence of any viral ligands in comparison to expressed wild-type MDA5 (Figure S9). Furthermore, pull-down studies with the RIG-I Walker B mutant revealed an increase in the amount of recovered RNA while their immunostimulatory potential decreased (data not shown). The increased immunostimulation of ATPase deficient RLRs is consistent with the model that RNAs that lead to a reduced ATP-hydrolysis rate are more proficient in immunostimulation, possibly by stabilizing RLR:RNA complexes. The negative correlation between AU-rich sequences and the ATP hydrolysis rate suggests that MDA5 binds AU-rich RNA in preference to GC-rich RNA. This would lead to a stronger interaction between RNA and MDA5 and result in a higher immunostimulatory signal. In order to test this hypothesis, we performed binding assays with MDA5 and IVTs but we were not able to demonstrate differences in the binding affinities between the different transcripts that might support this theory (data not shown). Finally, we speculate that RNA ligands for RLR proteins could be divided into two classes. The first class would comprise RNA molecules originating from the 5'-triphosphate ends of the genome or antigenome. These molecules could be generated in the course of read-through transcription and abortive replication [45,46] and could therefore represent preferred ligands of RIG-I, as shown previously [20]. The second class of RNA molecules could be recognized by both receptor proteins. Our data suggest that recognition of these RNAs might occur through the AU composition of sequences [34]. This second class might also prominently include defective interfering (DI) particles generated during MeV replication. For MDA5, however, our deep sequencing data show that the (-) strand portion of the DIs is either relatively short or the fraction of DIs binding to MDA5 is magnitudes lower than the binding to L derived (+) sense RNAs and therefore not easily detectable during sequencing. A more detailed analysis of the deep sequencing data is currently ongoing in order to shed more light on the complex nature of the DIs involved.

It will be interesting to see what types of RNA associate with RIG-I and MDA5 during infections with different viruses and to what extent the AU composition and DI generation contributes to RNA recognition in these types of viruses. In particular, the finding that both RIG-I and MDA5 localize to AU rich regions suggests partially overlapping roles in detection of different viruses. The specificity of RIG-I and MDA5 for certain viruses may lie not only in the detection of 5'-triphosphate by RIG-I, but also in the heterogeneity of viral evasion strategies [62]. Our findings support a model for the recognition of AU-rich sequences by RIG-I and MDA5 from MeV-infected cells. Consistently, we find a similar correlation for *in vitro* transcribed RNA from the Mengo virus genome.

In general, the data support previous experiments indicating that MeV is mainly recognized by RIG-I, while MDA5 seems to play a minor role [4,5,13,63]. It could be possible that RIG-I initially recognizes *le-N* read-through transcripts or abortive replication products containing 5'-triphosphate ends, leading to the activation of the signaling cascade. In a second round of recognition, RIG-I and MDA5 then recognize viral transcripts that are rich in AU. To further test this hypothesis, time dependent experiments need to be carried out.

One feature of the applied crosslinking technique is the introduction of specific T to C transitions at the interaction sites of 4SU-labeled RNA and the protein upon UV light exposure [37]. By identifying these point mutations in the deep sequencing data, one can exactly pinpoint the RNA sequences that interact with the protein of interest. However, our bioinformatics analysis did not reveal significant enrichment of T to C mutations, which could be explained by the rather low incorporation efficiency of the photoreactive nucleoside into viral RNA, consistent with the low incorporation level of 4SU into host RNA. Nevertheless, by increasing the incorporation efficiency in future studies, the identification of point mutants could further narrow down the precise binding sites of RLRs.

In summary, our approach provides a first insight into the molecular basis of vRNA derived from MeV interaction with MDA5 in living cells and reveals a preference for binding of AU-rich regions originated from (+)-sense RNA of the L gene. *In vitro*, these RNA molecules appear to be a poorer stimulator of the ATPase activity of MDA5, and result in more stable MDA5 filaments and support better downstream signaling.

## Materials and Methods

### Cell lines, viruses and antibodies

Infection experiments were carried out in A459 human lung carcinoma cells. HEK 293T ISRE-FF reporter cells (stable expression of firefly luciferase under the control of an interferon stimulated response element) were used for interferon stimulation luciferase reporter gene assays. All cells were maintained in Dulbecco's Modified Eagle Medium supplemented with 2 mM L-glutamine, 1% Penicillin-Streptomycin and 10% FBS (all purchased from Invitrogen). Viruses used for infections were recombinant measles virus with a sequence identical to the vaccine strain Schwarz (AF266291.1.), Sendai virus, Sendai virus defective interfering particles H4 (kindly provided by Dominique Garcin, Geneva, Switzerland), Mengo virus strain pMC0 (kindly provided by Anne Krug, TU Munich, Germany) and EMCV. Primary antibodies to human MDA5 (AT113) and RIG-I (Alme-1) were purchased from Enzo Life Science (Loerrach, Germany). Antibody to GFP (ab1218) was obtained from Abcam (Cambridge, UK). Secondary antibodies were supplied by GE Healthcare (Buckinghamshire, UK).

### Crosslinking and immunoprecipitation of RLR-associated RNA from virus-infected cells

A549 cells were infected with virus with an MOI of 1.0 in the presence of 400  $\mu$ M 4SU. Infection was allowed to proceed for 24 h and living cells were washed with PBS (10 mM phosphate, 137 mM NaCl, 2.7 mM KCl, pH 7.5) and exposed to 1 J/cm<sup>2</sup> 365 nm UV light using a photocrosslinker (Vilbert Lourmat). Cells were harvested and incubated in Nonidet P-40 lysis buffer (50 mM HEPES, 150 mM KCl, 1 mM NaF, 10  $\mu$ M ZnCl<sub>2</sub>, 0.5% NP-40, 0.5 mM DTT, protease inhibitor, pH 7.5) for 10 min on ice. The lysate was cleared by centrifugation and endogenous proteins were immunoprecipitated for 4 h with the respective antibodies (1  $\mu$ g/mL) bound to protein G Dynabeads (Life Technologies). The beads were washed five times with high-salt wash buffer (50 mM HEPES, 500 mM KCl, 0.05% NP-40, 0.5 mM DTT, protease inhibitor, pH 7.5) and incubated with proteinase K (Thermo Scientific) for 30 min at 55°C. The RNA was isolated by phenol/chloroform/isoamylalcohol extraction and subjected to further analysis.

### Total RNA isolation from virus infected cells

A549 cells were infected with MeV with an MOI of 1. Cells were harvested 24 hpi. Total RNA was isolated according to

manufacturer's protocol of the RNeasy Protect Mini Kit (Qiagen) and subjected to Illumina deep sequencing.

### Luciferase transfection assay

Immunoactivity experiments were carried out in 24-well plates.  $2.5 \times 10^5$  HEK 293T ISRE-FF reporter cells were transfected with 250 ng of recovered RNA, 500 ng *in vitro* transcripts or 500 ng plasmid DNA using Lipofectamine 2000 (Invitrogen) according to manufacturer's protocol. After 24 h incubation, cells were subjected to immunoactivity experiments using the Dual-Glo luciferase assay system (Promega) according to manufacturer's instructions. The luciferase activity was determined in a 96-well plate reader. Significance of differences in luciferase activity between samples were determined via an unpaired t-test.

### cDNA library preparation and deep sequencing analysis

Isolated RNA was prepared for Illumina sequencing using the mRNA-Seq library preparation kit (Epicentre) according to manufacturer's protocol. To remove ribosomal RNA species from the sequencing libraries a Ribo-Zero rRNA removal kit (Epicentre) was used. Quality of RNA-Seq libraries was validated on a DNA1500 chip for the Bioanalyzer 2100 (Agilent). Sequencing was performed on the Illumina Genome Analyzer in the Gene Center sequencing facility (LAFUGA). Obtained sequences were processed with the FASTX toolkit ([http://hannonlab.cshl.edu/fastx\\_toolkit/](http://hannonlab.cshl.edu/fastx_toolkit/)) in order to remove adapter sequences and reads with PHRED scores below 30. Remaining sequences were mapped to human and viral genomes by utilization of the Bowtie algorithm [64], allowing maximal one mismatch per unique read. The Bowtie sequence alignments were converted with SAMtools [65] to pileup format, which was subsequently used for further data analysis. Relative sequence abundances were analyzed between RLR pull-down samples and the GFP control. Specific read enrichments were calculated by determining the relative sequence abundance at each position on the genomic segment and calculating the average of the RLR/GFP ratios over a dynamic window of 200 reads. Relative sequence abundances with  $\log_2$  ratios above +1 were defined as significantly enriched in the RLR library.

### Analysis of RNA sequences

RNA secondary structure prediction from measles virus genome or *in vitro* transcripts was performed by utilization of RNAfold from the ViennaRNA package [53] using standard parameter settings. For this purpose, the genome was divided into 201 nt fragments with a shifting window size of 5 nt. The sequences were folded *in silico* and the linear relationship between different data sets was quantified with the Pearson correlation coefficient.

### SYBR green quantitative PCR analysis

DNase treatment of the immunoprecipitated RNAs and qPCR was performed as previously described [66]. The primer pairs used for quantification were identical to those published [67]. For cDNA synthesis a random hexanucleotide mix was used (Roche). Full length MeV vac2 cDNA with a known concentration was used for standard generation. Copy number values obtained for MDA5 and RIG-I were normalized to the control GFP.

### PCR for 5'-copyback defective interfering genome detection

Specific primers for reverse transcription (Roche transcriptase) and the subsequent PCR (Biozym Phusion Polymerase) were adapted from Calain et al [47]. PCR products were analyzed on agarose gels and stained with ethidium bromide.

### T7 RNA transcription

Templates were generated for *in vitro* transcription in a PCR adding the T7 promoter sequence (TAATACGACTCACTATA GGG) to the 5' end of the desired MeV or Mengo virus genomic fragment, respectively (for oligonucleotides see **Tables S2 and S4** respectively). PCR products were subsequently purified on agarose gels. RNA was transcribed using the Ambion Megashortscript T7 Kit according to the manufacturer's protocols. The reaction was incubated overnight at 37°C and RNA was precipitated using LiCl at -20°C for 30 minutes. Afterwards, RNA was subjected to triphosphate digestion using FastAP (Fermentas) according to the manufacturer's instructions and purified on denaturing 8 M urea/10% polyacrylamide gels at 25 mA constant current. Gel slices containing RNA were incubated overnight with 450  $\mu$ L probe elution buffer (0.5 M ammonium acetate, 1 mM EDTA, 0.2% SDS). Eluted RNA was isolated by phenol/chloroform/isoamylalcohol extraction and precipitated with ethanol.

### ATPase hydrolysis assays

ATPase hydrolysis activity was determined using [ $\gamma$ - $P^{32}$ ] ATP. Mouse MDA5 was purified as described previously [32] and 1.6  $\mu$ M of protein was preincubated with 80 nM *in vitro* transcribed RNA for 10 min at room temperature. The reaction was initiated by addition of ATPase hydrolysis buffer (20 mM HEPES, pH 7.5, 150 mM NaCl, 1.5 mM  $MgCl_2$ , and 2 mM DTT) containing 2 mM ATP and 0.2  $\mu$ Ci [ $\gamma$ - $P^{32}$ ] ATP. The hydrolysis rate was monitored over 1 h and analyzed by thin layer chromatography (TLC).

### Generation of RLR mutants

Sequences encoding full-length human RIG-I with N-terminal FLAG-tag and full-length human MDA5 with N-terminal FLAG-tag were cloned into pcDNA5 FRT/TO (Invitrogen). Mutants (FLAG-RIG-I E373Q and FLAG-MDA5 E444Q) were generated by site directed mutagenesis with PfuUltra (Agilent).

### Supporting Information

**Figure S1 Validation of immunostimulatory activity of RNA from RIG-I, MDA5, and GFP immunoprecipitates upon transfection into 293T ISRE-FF reporter cells** (n = 3, \*\* P < 0.01). (TIF)

**Figure S2 Deep sequencing analysis of total RNA from MeV-infected cells 24 hpi.** RNA was isolated according to manufacturer's protocol of the RNeasy Protect Mini Kit (Qiagen) and total RNA was subjected to Illumina deep sequencing. The data show an mRNA gradient declining in the 5' to 3' direction, while RNA of negative polarity has no relevant copy numbers. (TIF)

**Figure S3 Qualitative PCR analysis of MeV copyback DI RNA.** Following a specific reverse transcription of RNA with a primer binding at the 3'-terminus of the antigenome, 5'-copyback DI genomes were specifically amplified using another primer in the same direction 600 nt downstream. The PCR was afterwards analyzed on agarose gels to separate the amplicons of specific copyback DIs with different length and branching points. The RNA used for these experiments is indicated on the lanes (RIG-I, MDA5 and GFP immunoprecipitates). (TIF)

**Figure S4 Enrichments in RLR sequencing libraries.** Binary logarithms of RLR to GFP ratios of sequence reads ( $\log_2$ [read number RLR/read number GFP] \* [total read number

GFP/total read number RLR)) were calculated in order to determine specific accumulations within the RLR libraries. Data points with  $\log_2$  ratios above 1 represent sequencing reads that were enriched in comparison to the control (GFP) library. **A:** Enrichments within the whole RIG-I (+) or (-) stranded sequencing library. **B:** Enrichments within the whole MDA5 (+) or (-) stranded sequencing library. **C:** Similar to A and B, but zoomed in view of the enrichments for positive polarity (le)N and L segments. Mean values for RIG-I and MDA5  $\log_2$  ratios are shown in red and blue, respectively. Standard deviations are represented in grey. The mean coverage of (+) RNA sequences is shown for the RIG-I (red), MDA5 (blue), and GFP (black) libraries below each graph. (TIF)

**Figure S5 Secondary structure analysis of several features from *in silico* folded 201 nucleotide MeV RNA fragments and correlation to the fragment's mean coverage within the RIG-I sequencing library.** *In silico* folding was done with RNAfold using standard parameters. The analysis is visualized in heatscatter plots and the linear correlation is expressed via the Pearson coefficient. Every dot corresponds to one fragment with its depicted feature and mean coverage. The more yellow the plot, the more data points overlap. Analyzed RNA features are: number of paired nucleotides, longest paired stretch, number of stem-loops, mean size of stem-loops, number of bulges, mean size of bulges and mean number of paired nucleotides per branch. **A:** Correlation analysis of RNA secondary structure features with the RIG-I associated RNA of positive polarity. **B:** Correlation analysis of RNA secondary structure features with the RIG-I associated RNA of negative polarity. (TIF)

**Figure S6 RNA secondary structure analysis of several features from *in silico* folded 201 nucleotide MeV RNA fragments and correlation to the fragment's mean coverage within the RIG-I sequencing library.** Foldings were performed with RNAfold using standard parameters. The analysis is visualized in heatscatter plots and the linear correlation is expressed via the Pearson coefficient. Every dot corresponds to one fragment with its depicted feature and mean coverage. The more yellow the plot, the more data points overlap. Analyzed RNA features are: number of paired nucleotides, longest paired stretch, number of stem-loops, mean size of stem-loops, number of bulges, mean size of bulges and mean number of paired nucleotides per branch. **A:** Correlation analysis of RNA secondary structure features with the RIG-I associated RNA of positive polarity. **B:** Correlation analysis of RNA secondary structure features with the RIG-I associated RNA of negative polarity. (TIF)

**Figure S7 Analysis of *in vitro* transcribed RNA of the Mengo virus genome.** Six 201 nt fragments were chosen to include low and high AU content. Transcripts were transfected

into 293T ISRE-FF reporter cells in order to validate the immunostimulatory potential. **A:** Relative luciferase activity of transfected RNA (n = 3). **B:** Pearson correlation between (+) RNA maximal coverage and the relative luciferase activity. (TIF)

**Figure S8 MDA5 ATPase activity assay.** Free phosphate was separated by thin layer chromatography (TLC) and visualized on a Storm PhosphorImager from Molecular Dynamics. The ATPase hydrolysis rate was determined by quantifying free phosphate in comparison to non-hydrolyzed ATP 15 min after adding [ $\gamma$ - $P^{32}$ ] ATP to the reaction mixture. (TIF)

**Figure S9 Immunostimulatory activity of overexpressed Walker B mutants RIG-I<sup>E373Q</sup> and MDA5<sup>E444Q</sup> compared to wildtype proteins in 293T ISRE-FF reporter cells** (n = 3, \*\* P<0.01, \*\*\* P<0.001). (TIF)

**Table S1 Sequences of *in vitro* transcribed MeV RNAs.** The gene annotation with the exact nucleotide position on the MeV genome is shown in brackets. (DOCX)

**Table S2 Oligonucleotides used for generation of *in vitro* transcribed MeV sequences.** (DOCX)

**Table S3 Sequences of *in vitro* transcribed Mengo RNAs.** The gene annotation with the exact nucleotide position on the Mengo virus genome is shown in brackets. (DOCX)

**Table S4 Oligonucleotides used for generation of *in vitro* transcribed Mengo sequences.** (DOCX)

## Acknowledgments

We kindly thank Dr. Luis Martinez-Sorbido (University of Rochester, Rochester, NY) for the 293T ISRE-FF cell line, Dominique Garcin (University of Geneva, Switzerland) for providing SeV defective interfering particles H4 and Anne Krug (TU Munich, Germany) for providing Mengo virus, Manuela Moldt for purifying mMDA5, LAFUGA and especially Stefan Krebs for help with sequencing, Phillip Torkler and Alexander Graf for help with data analysis, Richard Cadagan and Osman Lizardo for technical assistance and Robert Byrne for critically reading our manuscript.

## Author Contributions

Conceived and designed the experiments: SR KMJS CL. Performed the experiments: SR KMJS CL AB. Analyzed the data: SR CL KH. Contributed reagents/materials/analysis tools: KPH KKC AGS JS. Wrote the paper: SR KMJS CL KPH KKC AGS. Designed the bioinformatical tools used in analysis: KH JS.

## References

- Loo Y-M, Gale Jr M (2011) Immune signaling by RIG-I-like receptors. *Immunity* 34: 680–692.
- Yoneyama M, Kikuchi M, Natsukawa T, Shinobu N, Imaizumi T, et al. (2004) The RNA helicase RIG-I has an essential function in double-stranded RNA-induced innate antiviral responses. *Nat Immunol* 5: 730–737.
- Kato H, Takahashi K, Fujita T (2011) RIG-I-like receptors: cytoplasmic sensors for non-self RNA. *Immunol Rev* 243: 91–98.
- Kato H, Takeuchi O, Sato S, Yoneyama M, Yamamoto M, et al. (2006) Differential roles of MDA5 and RIG-I helicases in the recognition of RNA viruses. *Nature* 441: 101–105.
- Loo Y-M, Fornek J, Crochet N, Bajwa G, Perwitasari O, et al. (2008) Distinct RIG-I and MDA5 signaling by RNA viruses in innate immunity. *J Virol* 82: 335–345.
- Plumet S, Herschke F, Bourhis J-M, Valentin H, Longhi S, et al. (2007) Cytosolic 5'-triphosphate ended viral leader transcript of measles virus as activator of the RIG I-mediated interferon response. *PLoS One* 2: e279.
- Saito T, Hirai R, Loo Y-M, Owen D, Johnson CL, et al. (2007) Regulation of innate antiviral defenses through a shared repressor domain in RIG-I and LGP2. *Proc Natl Acad Sci USA* 104: 582–587.
- Satoh T, Kato H, Kumagai Y, Yoneyama M, Sato S, et al. (2010) LGP2 is a positive regulator of RIG-I- and MDA5-mediated antiviral responses. *Proc Natl Acad Sci USA* 107: 1512–1517.
- Wilkins C, Gale M (2010) Recognition of viruses by cytoplasmic sensors. *Curr Opin Immunol* 22: 41–47.
- Faul EJ, Wanjalla CN, Suthar MS, Gale Jr M, Wirblich C, et al. (2010) Rabies virus infection induces type I interferon production in an IPS-1 dependent

- manner while dendritic cell activation relies on IFNAR signaling. *PLoS Path* 6: e1001016.
11. Ikegame S, Takeda M, Ohno S, Nakatsu Y, Nakanishi Y, et al. (2010) Both RIG-I and MDA5 RNA helicases contribute to the induction of alpha/beta interferon in measles virus-infected human cells. *J Virol* 84: 372–379.
  12. Saito T, Gale Jr M (2007) Principles of intracellular viral recognition. *Curr Opin Immunol* 19: 17–23.
  13. Yount JS, Gitlin L, Moran TM, López CB (2008) MDA5 participates in the detection of paramyxovirus infection and is essential for the early activation of dendritic cells in response to Sendai virus defective interfering particles. *J Immunol* 180: 4910–4918.
  14. Fujita T, Onoguchi K, Onomoto K, Hirai R, Yoneyama M (2007) Triggering antiviral response by RIG-I-related RNA helicases. *Biochimie* 89: 754–760.
  15. Wang Y, Ludwig J, Schubert C, Goldeck M, Schlee M, et al. (2010) Structural and functional insights into 5'-ppp RNA pattern recognition by the innate immune receptor RIG-I. *Nat Struct Mol Biol* 17: 781–787.
  16. Civril F, Bennett M, Moldt M, Deimling T, Witte G, et al. (2011) The RIG-I ATPase domain structure reveals insights into ATP-dependent antiviral signalling. *EMBO reports* 12: 1127–1134.
  17. Jiang F, Ramanathan A, Miller MT, Tang G-Q, Gale M, et al. (2011) Structural basis of RNA recognition and activation by innate immune receptor RIG-I. *Nature* 479: 423–427.
  18. Kowalinski E, Lunardi T, McCarthy AA, Loubser J, Brunel J, et al. (2011) Structural basis for the activation of innate immune pattern-recognition receptor RIG-I by viral RNA. *Cell* 147: 423–435.
  19. Luo D, Ding SC, Vela A, Kohlway A, Lindenbach BD, et al. (2011) Structural insights into RNA recognition by RIG-I. *Cell* 147: 409–422.
  20. Baum A, Sachidanandam R, Garcia-Sastre A (2010) Preference of RIG-I for short viral RNA molecules in infected cells revealed by next-generation sequencing. *Proc Natl Acad Sci USA* 107: 16303–16308.
  21. Hornung V, Ellegast J, Kim S, Brzózka K, Jung A, et al. (2006) 5'-Triphosphate RNA is the ligand for RIG-I. *Science* 314: 994–997.
  22. Pichlmair A, Schulz O, Tan CP, Näslund TI, Liljeström P, et al. (2006) RIG-I-mediated antiviral responses to single-stranded RNA bearing 5'-phosphates. *Science* 314: 997–1001.
  23. Schlee M, Roth A, Hornung V, Hagmann CA, Wimmenauer V, et al. (2009) Recognition of 5' triphosphate by RIG-I helicase requires short blunt double-stranded RNA as contained in panhandle of negative-strand virus. *Immunity* 31: 25–34.
  24. Kato H, Takeuchi O, Mikamo-Sato H, Hirai R, Kawai T, et al. (2008) Length-dependent recognition of double-stranded ribonucleic acids by retinoic acid-inducible gene-I and melanoma differentiation-associated gene 5. *J Exp Med* 205: 1601–1610.
  25. Pichlmair A, Schulz O, Tan C-P, Rehwinkel J, Kato H, et al. (2009) Activation of MDA5 requires higher-order RNA structures generated during virus infection. *J Virol* 83: 10761–10769.
  26. Berke IC, Modis Y (2012) MDA5 cooperatively forms dimers and ATP-sensitive filaments upon binding double-stranded RNA. *EMBO J* 31: 1714–1726.
  27. Berke IC, Yu X, Modis Y, Egelman EH (2012) MDA5 assembles into a polar helical filament on dsRNA. *Proc Natl Acad Sci USA* 109: 18437–18441.
  28. Peisley A, Lin C, Wu B, Orme-Johnson M, Liu M, et al. (2011) Cooperative assembly and dynamic disassembly of MDA5 filaments for viral dsRNA recognition. *Proc Natl Acad Sci USA* 108: 21010–21015.
  29. Andrejeva J, Childs KS, Young DF, Carlos TS, Stock N, et al. (2004) The V proteins of paramyxoviruses bind the IFN-inducible RNA helicase, mda-5, and inhibit its activation of the IFN- $\beta$  promoter. *Proc Natl Acad Sci USA* 101: 17264–17269.
  30. Childs K, Stock N, Ross C, Andrejeva J, Hilton L, et al. (2007) mda-5, but not RIG-I, is a common target for paramyxovirus V proteins. *Virology* 359: 190–200.
  31. Parisien J-P, Bamming D, Komuro A, Ramachandran A, Rodriguez JJ, et al. (2009) A Shared Interface Mediates Paramyxovirus Interference with Antiviral RNA Helicases MDA5 and LGP2. *J Virol* 83: 7252–7260.
  32. Motz C, Schuhmann KM, Kirchhofer A, Moldt M, Witte G, et al. (2013) Paramyxovirus V proteins disrupt the fold of the RNA sensor MDA5 to inhibit antiviral signaling. *Science* 339: 690–693.
  33. Saito T, Owen DM, Jiang F, Marcotrigiano J, Gale Jr M (2008) Innate immunity induced by composition-dependent RIG-I recognition of hepatitis C virus RNA. *Nature* 454: 523–527.
  34. Schnell G, Loo Y-M, Marcotrigiano J, Gale Jr M (2012) Uridine composition of the poly-U/UC tract of HCV RNA defines non-self recognition by RIG-I. *PLoS Path* 8: e1002839.
  35. Luthra P, Sun D, Silverman RH, He B (2011) Activation of IFN- $\beta$  expression by a viral mRNA through RNase L and MDA5. *Proc Natl Acad Sci USA* 108: 2118–2123.
  36. Feng Q, Hato SV, Langereis MA, Zoll J, Virgen-Slane R, et al. (2012) MDA5 Detects the double-stranded RNA replicative form in picornavirus-infected cells. *Cell reports* 2: 1187–1196.
  37. Hafner M, Landthaler M, Burger L, Khorshid M, Haussler J, et al. (2010) Transcriptome-wide identification of RNA-binding protein and microRNA target sites by PAR-CLIP. *Cell* 141: 129–141.
  38. del Valle JR, Devaux P, Hodge G, Wegner NJ, McChesney MB, et al. (2007) A vectored measles virus induces hepatitis B surface antigen antibodies while protecting macaques against measles virus challenge. *J Virol* 81: 10597–10605.
  39. Schnell MJ, Mebatsion T, Conzelmann K-K (1994) Infectious rabies viruses from cloned cDNA. *EMBO J* 13: 4195.
  40. Hoskins J, Sanders F (1957) Propagation of mouse encephalomyocarditis virus in ascites tumour cells maintained in vitro. *Br J Exp Pathol* 38: 268.
  41. Osorio JE, Martin LR, Palmenberg AC (1996) The immunogenic and pathogenic potential of short poly (C) tract Mengo viruses. *Virology* 223: 344–350.
  42. Colonno RJ, Banerjee AK (1976) A unique RNA species involved in initiation of vesicular stomatitis virus RNA transcription in vitro. *Cell* 8: 197–204.
  43. Leppert M, Rittenhouse L, Perrault J, Summers DF, Kolakofsky D (1979) Plus and minus strand leader RNAs in negative strand virus-infected cells. *Cell* 18: 735–747.
  44. Cattaneo R, Rebmann G, Schmid A, Baczeko K, Ter Meulen V, et al. (1987) Altered transcription of a defective measles virus genome derived from a diseased human brain. *EMBO J* 6: 681.
  45. Plumet S, Duprex WP, Gerlier D (2005) Dynamics of viral RNA synthesis during measles virus infection. *J Virol* 79: 6900–6908.
  46. Mottet G, Curran J, Roux L (1990) Intracellular stability of nonreplicating paramyxovirus nucleocapsids. *Virology* 176: 1–7.
  47. Calain P, Curran J, Kolakofsky D, Roux L (1992) Molecular cloning of natural paramyxovirus copy-back defective interfering RNAs and their expression from DNA. *Virology* 191: 62–71.
  48. Calain P, Roux L (1988) Generation of measles virus defective interfering particles and their presence in a preparation of attenuated live-virus vaccine. *J Virol* 62: 2859–2866.
  49. Pfaller CK, Radeke MJ, Cattaneo R, Samuel CE (2014) Measles Virus C Protein Impairs Production of Defective Copyback Double-Stranded Viral RNA and Activation of Protein Kinase R. *J Virol* 88: 456–468.
  50. Rima B, Davidson W, Martin S (1977) The role of defective interfering particles in persistent infection of Vero cells by measles virus. *J Gen Virol* 35: 89–97.
  51. Whistler T, Bellini WJ, Rota P (1996) Generation of defective interfering particles by two vaccine strains of measles virus. *Virology* 220: 480–484.
  52. Wood HM, Belvedere O, Conway C, Daly C, Chalkley R, et al. (2010) Using next-generation sequencing for high resolution multiplex analysis of copy number variation from nanogram quantities of DNA from formalin-fixed paraffin-embedded specimens. *Nucleic Acids Res* 38: e151–e151.
  53. Lorenz R, Bernhart SH, Zu Siederdisen CH, Tafer H, Flamm C, et al. (2011) ViennaRNA Package 2.0. *Algorithms Mol Biol* 6: 26.
  54. Deddouche S, Goubau D, Rehwinkel J, Chakravarty P, Begum S, et al. (2014) Identification of an LGP2-associated MDA5 agonist in picornavirus-infected cells. *eLife* 3: e01535.
  55. Blumberg BM, Leppert M, Kolakofsky D (1981) Interaction of VSV leader RNA and nucleocapsid protein may control VSV genome replication. *Cell* 23: 837–845.
  56. Mottet-Osman G, Iseni F, Pelet T, Wiznerowicz M, Garcin D, et al. (2007) Suppression of the Sendai virus M protein through a novel short interfering RNA approach inhibits viral particle production but does not affect viral RNA synthesis. *J Virol* 81: 2861–2868.
  57. Reuter T, Weissbrich B, Schneider-Schaulies S, Schneider-Schaulies J (2006) RNA interference with measles virus N, P, and L mRNAs efficiently prevents and with matrix protein mRNA enhances viral transcription. *J Virol* 80: 5951–5957.
  58. Vidal S, Kolakofsky D (1989) Modified model for the switch from Sendai virus transcription to replication. *J Virol* 63: 1951–1958.
  59. Ablasser A, Bauernfeind F, Hartmann G, Latz E, Fitzgerald KA, et al. (2009) RIG-I-dependent sensing of poly (dA: dT) through the induction of an RNA polymerase III-transcribed RNA intermediate. *Nat Immunol* 10: 1065–1072.
  60. Patel JR, Jain A, Chou Yy, Baum A, Ha T, et al. (2013) ATPase-driven oligomerization of RIG-I on RNA allows optimal activation of type-I interferon. *EMBO reports* 14: 780–787.
  61. Gorbalenya AE, Koonin EV, Donchenko AP, Blinov VM (1989) Two related superfamilies of putative helicases involved in replication, recombination, repair and expression of DNA and RNA genomes. *Nucleic Acids Res* 17: 4713–4730.
  62. Randall RE, Goodbourn S (2008) Interferons and viruses: an interplay between induction, signalling, antiviral responses and virus countermeasures. *J Gen Virol* 89: 1–47.
  63. Gerlier D, Valentin H (2009) Measles virus interaction with host cells and impact on innate immunity. *Measles: Springer*, pp. 163–191.
  64. Langmead B, Trapnell C, Pop M, Salzberg SL (2009) Ultrafast and memory-efficient alignment of short DNA sequences to the human genome. *Genome Biol* 10: R25.
  65. Li H, Handsaker B, Wysoker A, Fennell T, Ruan J, et al. (2009) The sequence alignment/map format and SAMtools. *Bioinformatics* 25: 2078–2079.
  66. Plumet S, Gerlier D (2005) Optimized SYBR green real-time PCR assay to quantify the absolute copy number of measles virus RNAs using gene specific primers. *J Virol Methods* 128: 79–87.
  67. Sparrer KM, Pfaller CK, Conzelmann K-K (2012) Measles virus C protein interferes with Beta interferon transcription in the nucleus. *J Virol* 86: 796–805.



## 2 ATP hydrolysis by the viral RNA sensor RIG-I prevents unintentional recognition of self-RNA

Lässig C, Matheisl S\* , Sparrer KMJ\* , de Oliveira Mann CC\* , Moldt M, Patel JR, Goldeck M, Hartmann G, García-Sastre A, Hornung V, Conzelmann K-K, Beckmann R, Hopfner K-P (2015) ATP hydrolysis by the viral RNA sensor RIG-I prevents unintentional recognition of self-RNA. *eLife* 2015;4:e10859.

\* These authors contributed equally.

DOI: <http://dx.doi.org/10.7554/eLife.10859>

<http://elifesciences.org/content/4/e10859v3>

### Summary

In this publication we analyze the SF2 helicase domain of RIG-I like receptors. We engineered several single amino acid point mutations in SF2 motifs or found in patients with the multi-system disease Singleton-Merten syndrome (SMS) into RIG-I. We are thus able to dissect ATP binding and ATP hydrolysis for the function of RIG-I as an innate immune sensor of non-self RNA.

By luciferase reporter gene assays in cells lacking endogenous RIG-I we show that, regardless of the presence of an infection, ATP binding-deficient RIG-I is not able to induce any immune response at all. ATP hydrolysis-deficient RIG-I on the other hand, as for instance found in SMS patients, constitutively signals in an RNA binding-dependent manner. We exclude structural protein alterations of the hydrolysis-deficient mutant by thermofluor assays and SAXS with purified proteins, and by cellular competition assays with wild type RIG-I. In addition, we were able to purify a physiological ligand for ATP hydrolysis-deficient RIG-I, i.e. an expansion segment of the big ribosomal subunit, by co-immunoprecipitation and visualize the interaction by cryo-electron microscopy. Similar co-immunoprecipitation results were obtained for infected cells as well as for the respective MDA5 mutant. Subsequent biochemical studies with wild type RIG-I or the ATPase-dead mutant and either purified human ribosomes or a derived hairpin-RNA verified binding of the mutated protein and confirmed a loss of interaction of wild type RIG-I in presence of ATP. By EMSA and fluorescence anisotropy we further show that, in contrast to the hairpin-RNA, dsRNA binding of wild type RIG-I is enhanced under ATP hydrolyzing conditions.

Based on our studies and previous literature, we conclude that ATP hydrolysis of RIG-I confers a proof-reading step in order to discriminate between self- and non-self RNA by testing the CTD affinity towards the respective RNA. RNAs providing a high affinity CTD anchor, like a triphosphate motif, bind very stable to RIG-I regardless of the presence of ATP. Endogenous RNAs lacking an anchor, however, are removed from the protein through ATP hydrolysis.

Our results further provide the molecular basis of RLR signaling for the development of autoimmune diseases like the Singleton-Merten syndrome and emphasize the importance of an intact RLR ATPase domain in discrimination between self and non-self RNA.

**Author contributions**

I performed luciferase reporter assays with all RIG-I constructs in presence or absence of additional RNA or competitor protein. I co-immunopurified RNA bound to RIG-I mutants from cells together with Carina C. de Oliveira Mann. I further analyzed the purified RNA on gels, with the Bioanalyzer or back-transfected them into a reporter cell line. I purified RIG-I proteins with help of Manuela Moldt and analyzed their binding behavior in presence or absence of ATP to different kinds of RNA by EMSA and Fluorescence anisotropy. Furthermore, I tested ATP binding and hydrolysis of RIG-I mutants in presence or absence of several RNA ligands. Together with Karl-Peter Hopfner I wrote the paper.



# ATP hydrolysis by the viral RNA sensor RIG-I prevents unintentional recognition of self-RNA

Charlotte Lässig<sup>1</sup>, Sarah Matheisl<sup>1†</sup>, Konstantin MJ Sparrer<sup>2†‡</sup>, Carina C de Oliveira Mann<sup>1†</sup>, Manuela Moldt<sup>1</sup>, Jenish R Patel<sup>3,4</sup>, Marion Goldeck<sup>5</sup>, Gunther Hartmann<sup>5</sup>, Adolfo García-Sastre<sup>3,4,6</sup>, Veit Hornung<sup>7</sup>, Karl-Klaus Conzelmann<sup>2</sup>, Roland Beckmann<sup>1,8</sup>, Karl-Peter Hopfner<sup>1,8\*</sup>

<sup>1</sup>Gene Center, Department of Biochemistry, Ludwig Maximilian University of Munich, Munich, Germany; <sup>2</sup>Max von Pettenkofer-Institute, Gene Center, Ludwig Maximilian University of Munich, Munich, Germany; <sup>3</sup>Department of Microbiology, Icahn School of Medicine at Mount Sinai, New York, United States; <sup>4</sup>Global Health and Emerging Pathogens Institute, Icahn School of Medicine at Mount Sinai, New York, United States; <sup>5</sup>Institute for Clinical Chemistry and Clinical Pharmacology, University Hospital Bonn, University of Bonn, Bonn, Germany; <sup>6</sup>Department of Medicine, Division of Infectious Diseases, Icahn School of Medicine at Mount Sinai, New York, United States; <sup>7</sup>Institute of Molecular Medicine, University Hospital Bonn, University of Bonn, Bonn, Germany; <sup>8</sup>Center for Integrated Protein Science Munich, Munich, Germany

\*For correspondence: hopfner@genzentrum.lmu.de

†These authors contributed equally to this work

**Present address:** ‡ Department of Microbiology and Immunobiology, Harvard Medical School, Boston, United States

**Competing interest:** See page 16

**Funding:** See page 16

**Received:** 14 August 2015

**Accepted:** 25 November 2015

**Published:** 26 November 2015

**Reviewing editor:** Stephen C Kowalczykowski, University of California, Davis, United States

© Copyright Lässig et al. This article is distributed under the terms of the [Creative Commons Attribution License](#), which permits unrestricted use and redistribution provided that the original author and source are credited.

**Abstract** The cytosolic antiviral innate immune sensor RIG-I distinguishes 5' tri- or diphosphate containing viral double-stranded (ds) RNA from self-RNA by an incompletely understood mechanism that involves ATP hydrolysis by RIG-I's RNA translocase domain. Recently discovered mutations in ATPase motifs can lead to the multi-system disorder Singleton-Merten Syndrome (SMS) and increased interferon levels, suggesting misregulated signaling by RIG-I. Here we report that SMS mutations phenocopy a mutation that allows ATP binding but prevents hydrolysis. ATPase deficient RIG-I constitutively signals through endogenous RNA and co-purifies with self-RNA even from virus infected cells. Biochemical studies and cryo-electron microscopy identify a 60S ribosomal expansion segment as a dominant self-RNA that is stably bound by ATPase deficient RIG-I. ATP hydrolysis displaces wild-type RIG-I from this self-RNA but not from 5' triphosphate dsRNA. Our results indicate that ATP-hydrolysis prevents recognition of self-RNA and suggest that SMS mutations lead to unintentional signaling through prolonged RNA binding.

DOI: [10.7554/eLife.10859.001](https://doi.org/10.7554/eLife.10859.001)

## Introduction

The innate immune system provides a rapid initial reaction to invading pathogens and also stimulates the adaptive immune system (*Iwasaki and Medzhitov, 2015*). Pattern recognition receptors (PRRs) of the innate immune system sense pathogen- or danger-associated molecular patterns (PAMPs or DAMPs) and trigger molecular cascades that together initiate and orchestrate the cellular response through activation of e.g. interferon regulatory factors and nuclear factor  $\kappa$ B (*Brubaker et al., 2015; Pandey et al., 2015; Wu and Chen, 2014*).

Retinoic-acid inducible gene 1 (RIG-I), melanoma differentiation-associated gene 5 (MDA5) and laboratory of physiology and genetics 2 (LGP2) are three structurally related PRRs – denoted RIG-I

**eLife digest** Living cells produce long, strand-like molecules of RNA that carry the instructions needed to make proteins. Viruses also make use of RNA molecules to hijack an infected cell's protein-production machinery and create new copies of the virus. RNA molecules from viruses have a number of features that distinguish them from a cell's own RNAs, and human cells contain receptors called RLRs that can start an immune response whenever they detect viral RNAs. All of these receptors break down molecules of ATP, a process that releases useable energy. However, so far it is not understood how this activity helps the receptors to distinguish viral RNA from the cell's own RNA molecules (called self-RNA).

Recently, some autoimmune diseases (including Singleton-Merten Syndrome) were linked to mutations in the parts of RLRs that allow the receptors to break down ATP. Now, Lässig et al. have studied the effects of specific mutations in an RLR called RIG-I in human cells. The experiments showed that mutations that disrupt RIG-I's ability to bind to ATP also prevented the receptor from becoming activated. However, mutations linked to Singleton-Merten Syndrome don't stop ATP from binding but instead slow its breakdown; this effectively locks the receptor in an ATP-bound state. Lässig et al. found that similar mutations in RIG-I caused human cells to trigger a constant immune response against the self-RNAs.

Further experiments then suggested that the breakdown of ATP helps to remove RIG-I that has bound to double-stranded sections of self-RNAs. This activity frees the receptor, making it more able to detect double-stranded viral RNAs and preventing unintentional signaling. Lässig et al. also identified a specific double-stranded section of a human RNA that may be recognized by the mutated version of RIG-I in people with Singleton-Merten Syndrome.

The next steps following on from this work are to extend the analysis to also include other RLRs and further explore the underlying mutations within the three-dimensional structures of the receptors and RNA molecules involved.

DOI: [10.7554/eLife.10859.002](https://doi.org/10.7554/eLife.10859.002)

like receptors (RLRs) – that recognize cytosolic foreign RNA. RIG-I senses RNA from a broad range of viruses including measles virus and Sendai virus (both paramyxoviridae), Influenza A virus, Japanese encephalitis virus and Hepatitis C virus, whereas MDA5 is activated for example by picornavirus RNA. LGP2 has augmenting and regulatory roles in MDA5 and RIG-I dependent signaling (Bruns et al., 2014; Satoh et al., 2010; Sparrer and Gack, 2015).

RIG-I preferentially detects base-paired double-stranded RNA (dsRNA) ends containing either 5' triphosphate (ppp) or 5' diphosphate (pp) moieties (Goubau et al., 2014; Hornung et al., 2006; Pichlmair et al., 2006; Schlee et al., 2009; Schmidt et al., 2009) and not 2' OH methylated at the first 5' terminal nucleotide (Schuberth-Wagner et al., 2015). ppp-dsRNA arises, for example, at panhandle structures of influenza virus nucleocapsids, or during measles or Sendai virus transcription (Liu et al., 2015; Weber et al., 2013). 5' diphosphates are found on genomic RNA of reoviruses (Banerjee and Shatkin, 1971). RIG-I can also detect poly-U/UC-rich dsRNA (Schnell et al., 2012). Ligands of MDA5 are less well characterized but include dsRNA longer than 1000 bp (Kato et al., 2008), higher-order dsRNA structures (Pichlmair et al., 2009), or AU-rich RNA (Runge et al., 2014).

RLRs are members of the superfamily II (SF2) of ATPases, helicases or nucleic acid translocases. RIG-I and MDA5 consist of two N-terminal tandem caspase activation and recruitment domains (2CARD), a central ATPase/translocase domain and a C-terminal regulatory domain (RD). LGP2 lacks the 2CARD module but otherwise has a similar domain architecture. Binding of RNA induces a conformational change in RIG-I. If activated, the RD binds the ppp- or pp-dsRNA end, while the SF2 domain interacts with the adjacent RNA duplex and forms an active ATPase site (Civril et al., 2011). In this conformation, the 2CARD module is sterically displaced from its auto-inhibited state (Jiang et al., 2011; Kowalinski et al., 2011; Luo et al., 2011) and can be K63-linked poly-ubiquitinated (Gack et al., 2007). Multiple Ub-2CARD complexes assemble to form a nucleation site for the polymerization of mitochondrial antiviral-signaling adaptor protein (MAVS) into long helical filaments (Hou et al., 2011; Wu et al., 2014; Xu et al., 2014). Instead of recognizing terminal structures like

RIG-I, MDA5 cooperatively polymerizes along dsRNA (Berke and Modis, 2012), which is suggested to trigger MAVS polymerization.

The SF2 ATPase domain plays a critical part in RIG-I activation, although the role of the ATPase activity is still debated. Mutation of the seven SF2 “helicase” motifs resulted in RLRs that are either inactive or signal constitutively (Bamming and Horvath, 2009; Louber et al., 2015). On the other hand, overexpression of the 2CARD module alone is sufficient for signaling (Yoneyama et al., 2004). Further studies revealed that the SF2 domain is an ATP-dependent dsRNA translocase (Myong et al., 2009) that can help enhance signaling by loading multiple RIG-I on dsRNA (Patel et al., 2013) and may execute anti-viral “effector” functions through displacement of viral proteins (Yao et al., 2015). Finally, RIG-I ATPase activity promotes recycling of RIG-I:dsRNA complexes in vitro, suggesting a kinetic discrimination between self and non-self RNA (Anchisi et al., 2015; Louber et al., 2015).

Several autoimmune diseases, including the Aicardi-Goutières and Singleton-Merten syndromes (SMS), were linked to single amino acid mutations in the SF2 domains of MDA5 and RIG-I (Funabiki et al., 2014; Jang et al., 2015; Rice et al., 2014; Rutsch et al., 2015). Two point mutations within the Walker A (motif I) or Walker B (motif II) of RIG-I are linked to atypical SMS and functional studies indicated constitutive RIG-I activation (Jang et al., 2015). Thus, these mutations have been described as a gain of function, which is puzzling considering previous mutations in motif I led to loss of RIG-I function, while mutations in motif II led to either gain or loss of function, depending on the type of mutation (Bamming and Horvath, 2009; Louber et al., 2015).

In order to clarify the role of RIG-I’s ATPase in antiviral signaling and RLR associated human diseases, we engineered structure-derived and patient-identified mutations into RIG-I and tested the resulting proteins in different types of cell-based and in vitro analyses. Collectively, we find that SMS mutations phenocopy the structure-derived E373Q mutation in motif II, which is designed to trap RIG-I in an ATP-bound state. Freezing this state results in a dramatic autoimmune response because the enzyme binds self-RNA and signals. An unexpected, strongly enriched self-RNA is the ribosomal large subunit, which contains large, dsRNA expansion segments. Collectively, our results suggest that a biomedical and functional critical role of RIG-I’s ATPase is to prevent spontaneous and unintended activation by self-RNA. Thus, the SF2 translocase likely increases the sensitivity of the system by reducing background signaling. Furthermore, our studies suggest that in SMS, RIG-I is trapped in an ATP-bound state and signals through self-ligands.

## Results

### Prevention of ATP hydrolysis in RIG-I leads to a constitutive activation of the interferon- $\beta$ promoter by recognition of self-RNA

To address the roles of ATP binding and hydrolysis by the SF2 domain of RIG-I, we studied RIG-I variants containing structure-based mutations designed to i) prevent ATP binding and formation of a functional ATP-bound complex, ii) allow ATP binding and ATP-induced conformational changes but prevent ATP hydrolysis, or iii) disable interaction of the RNA with either the 1A or 2A domain of SF2 (Figure 1A, B). The structure of RIG-I in complex with RNA and ADP-BeF<sub>x</sub> served as guide for these mutations (Jiang et al., 2011], PDB code 3TMI, Figure 1B).

In order to dissect the influence of these mutations on the ability of RIG-I to elicit downstream signaling, we used an interferon- $\beta$  (IFN $\beta$ ) promoter activity assay carried out in HEK 293T RIG-I KO cells (Figure 1—figure supplement 1A,B). Overexpressed wild-type RIG-I (wtRIG-I) is able to induce a slight activation of the IFN $\beta$  promoter, which can be further amplified by stimulation with Sendai virus defective interfering particles (SeV DIs) (Figure 1C). The 2CARD module (RIG-I 1-229) induced a strong activation in both non-infected and SeV DI-stimulated cells and is crucial since constructs lacking these domains ( $\Delta$ 2CARD, RIG-I 230-925) cannot conduct any downstream signaling. RIG-I K270I, carrying a mutation in the motif I lysine that reduces ATP binding (Rozen et al., 1989), signaled in neither uninfected nor SeV DIs stimulated cells, consistent with previous studies. Remarkably, the E373Q substitution in motif II had a strikingly different effect. RIG E373Q, which has a stabilized ATP-bound state by slowed-down ATP hydrolysis, strongly signaled in both non-infected and SeV DIs stimulated cells. Western blots validated correct expression of all mutants (Figure 1—figure supplement 1C).

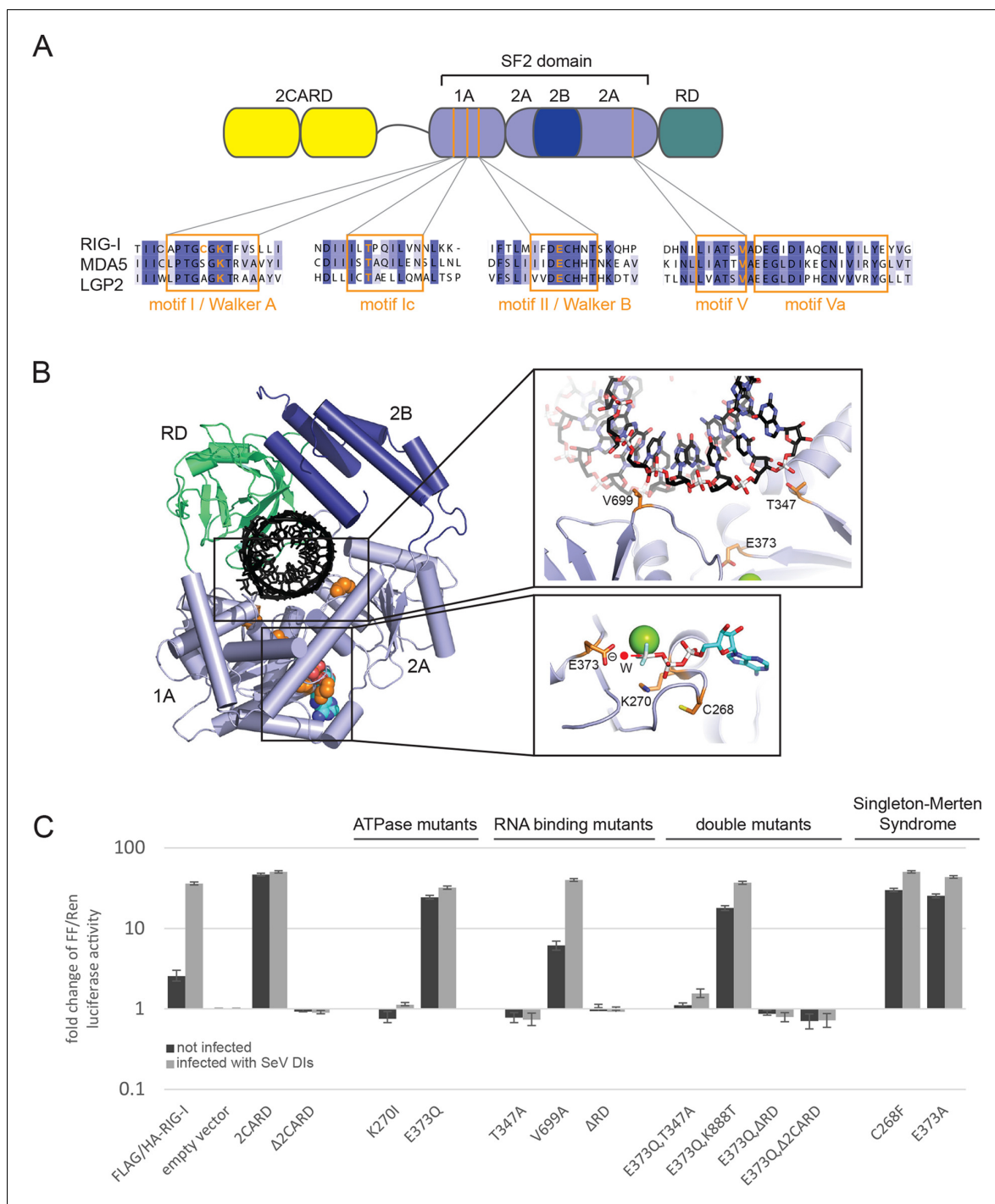


**Figure 1.** Cellular studies of RIG-I ATPase mutants in infected or non-infected cells. (A) Location of amino acid substitutions of RIG-I SF2 domain variants used in this study (orange lines) within different RLR helicase motifs (orange squares). (B) Single amino acid substitutions (orange) within the RIG-I 3D structure (PDB: 3TMI). (C) Fold change of interferon-β (IFNβ) promoter driven luciferase activity in uninfected HEK 293T RIG-I KO cells or in cells challenged with Sendai virus defective interfering particles (SeV DIs). Cells were co-transfected with RIG-I expression vectors and p125-luc/ pCMV-RL reporter plasmids, and infected with SeV DIs 6 hr post transfection. Firefly (FF) luciferase activities were determined in respect to Renilla (Ren) luciferase activities 24 hpi. All ratios were normalized to the empty vector control. n=3–12, error bars represent mean values ± standard deviation.

Figure 1 continued on next page

To rule out a “constitutive” active conformation of RIG-I E373Q due to an exposed 2CARD module (e.g. from an unfolded SF2) we performed small angle X-ray scattering with purified wtRIG-I and RIG-I E373Q demonstrating that both proteins have the same solution structure (**Figure 1—figure supplement 2A, B**). In addition, thermal unfolding assays show that the E373Q mutation does not destabilize RIG-I (**Figure 1—figure supplement 2C**). Finally, RIG-I  $\Delta$ 2CARD,E373Q has a dominant negative effect on signaling by RIG-I E373Q (**Figure 1, Figure 1—figure supplement 2D, E**). Taken together, these data show that RIG-I E373Q is neither destabilized nor constitutively active, suggesting it needs productive RNA interactions.

To test whether E373Q signals in non-infected (and perhaps also infected cells) because of interaction with self-RNA, we additionally introduced mutations in various RNA binding sites, in particular a  $\Delta$ RD variant (RIG-I 1-798) and mutations in two RNA-interacting residues in domains 1A (T347A) and 2A (V699A) of SF2. The single mutation RIG-I T347A did not signal in either infected or non-infected cells, showing that the interaction of RNA with this specific amino acid is critical for signaling (**Figure 1C**). Interestingly, we find that the single mutation V699A slightly increases the signaling activity of RIG-I in non-infected cells (**Figure 1C**), which could be explained by a putative reduction of translocation activity instead of a prevention of RNA binding to SF2 (see discussion). Finally, deletion of the regulatory domain ( $\Delta$ RD) inactivates signaling in both infected and non-infected cells as previously observed (**Cui et al., 2008**). As expected, both combination mutants RIG-I E373Q,T347A and RIG-I E373Q, $\Delta$ RD failed to signal in both SeV DIs infected and non-infected cells. These data show that the increased immunostimulatory effect of E373Q requires a productive RNA interaction of SF2 and RD.

Since RD is also required for the displacement of the 2CARD module from SF2, we additionally analyzed a point mutation in RD. K888 mediates triphosphate binding in RD and mutations in this residue inactivate recognition of viral RNA (**Cui et al., 2008; Wang et al., 2010**). Of note RIG-I E373Q,K888T is still constitutively active in non-infected cells. This effect indicates that the increased signaling capacity on endogenous RNA is independent from the ppp-dsRNA or pp-dsRNA epitopes that RIG-I recognizes on viral RNA via the RD.

Finally, we addressed the effect of the Singleton-Merten mutations C268F and E373A. E373A is at the same position as our structure-derived E373Q mutant. Consistent with this, we observed that this substitution leads to a constitutive activation of the IFN $\beta$  promoter (**Jang et al., 2015**) (**Figure 1C**). Interestingly, although C268 is located in motif I, it also leads to constitutive signaling, whereas motif I mutation of K270 (which coordinates the  $\beta$ -phosphate of ATP) blocks ATP binding and renders RIG-I inactive. Thus, mutation of the non-ATP binding C268 in motif I appears to phenocopy a mutation that prevents ATP hydrolysis.

In summary, our studies show that signaling of RIG-I requires both ATP and RNA binding. ATP hydrolysis, on the other hand, appears to be critical to dissolve the signaling state and to prevent activation of RIG-I by self-RNA.

### RIG-I ATP hydrolysis defective mutant E373Q shows increased interaction with ribosomal RNA

We hypothesized that E373Q traps RIG-I in an ATP bound high affinity conformation that is activated already by self-RNA. To test this idea, we immunoprecipitated RIG-I and its mutants from non-infected HEK 293T RIG-I KO cells or cells infected with measles or Sendai virus and analyzed the co-purified RNA molecules. Regardless of whether co-purified from infected or non-infected cells, the amount of RNA recovered from RIG-I E373Q was about 3 times higher than that from RIG-I (**Figure 2A**). Similarly increased amounts of RNA co-purified with the SMS mutants C268F and E373A from uninfected cells, reflecting the same altered RNA binding properties as in RIG-I E373Q (**Figure 2—figure supplement 1A**).

When analyzed on a Bioanalyzer RNA chip or on agarose gels, we found that the increased amount of RNA is to a large extent due to the presence of 28S rRNA, while 18S rRNA remains unaltered (**Figure 2B**). Control analysis of the total RNA content ruled out an alteration of ribosome subunit ratio in RIG-I E373Q transfected cells (**Figure 2C**). Both increased amount of RNA and specific enrichment of 28S rRNA were also observed for the equivalent MDA5 E444Q Walker B mutant (**Figure 2—figure supplement 1B, C**).

In order to determine the immunostimulatory potential of the RNA co-purified from virus-infected cells, we back-transfected the RNA into HEK 293T ISRE-FF/RFP reporter cells (which contain

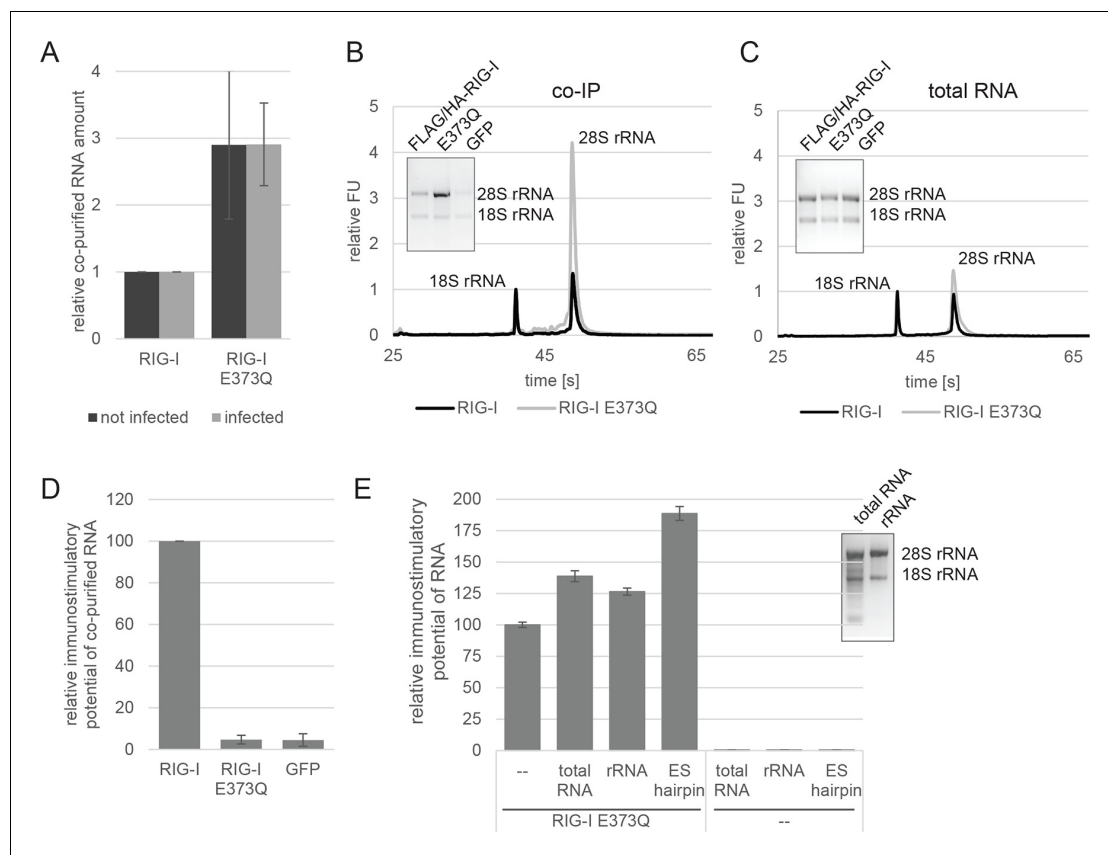


**Figure 2.** RIG-I ATP hydrolysis defective mutant E373Q recognizes the 60S ribosomal subunit in vivo. (A) Relative RNA amount co-purified with overexpressed RIG-I or RIG-I E373Q from virus infected or non-infected HEK 293T RIG-I KO cells.  $n=4$  (infected) or  $n=10$  (non-infected), error bars represent mean values  $\pm$  standard deviation. (B) Bioanalyzer evaluation and agarose gel separation of RNA co-purified with overexpressed RIG-I or RIG-I E373Q from non-infected HEK 293T RIG-I KO cells. Curves are normalized in respect to 18S rRNA peaks. (C) Bioanalyzer evaluation and agarose gel separation of total RNA content of non-infected HEK 293T RIG-I KO cells overexpressing RIG-I or RIG-I E373Q. Curves were normalized as in panel B. (D) Immunostimulatory potential of co-purified RNA from RIG-I, RIG-I E373Q or GFP overexpressed in measles virus (MeV), MeV-Cko-ATU-Cs or Sendai virus Cantell (SeV) infected HEK 293T RIG-I KO cells. RNA was back-transfected into HEK 293T ISRE-FF/RFP cells together with pTK-RL transfection control. Firefly luciferase (FF) activities were determined 24 hr after transfection in respect to Renilla luciferase (Ren) activity and were normalized to the immunostimulatory potential of RIG-I associated RNA.  $n=4$ , error bars represent mean values  $\pm$  standard deviation. (E) Immunostimulatory potential of endogenous RNA in cells overexpressing RIG-I E373Q. RNA was co-transfected into HEK 293T RIG-I KO cells together with a RIG-I E373Q expression vector and p125-luc/ pCMV-RL reporter plasmids. FF luciferase activities were determined in respect to Ren luciferase activities 24 hr after transfection. All ratios are normalized to the RIG-I E373Q control without RNA stimulation. Purified RNA was in addition analyzed on agarose gels.  $n=3$ , error bars represent mean values  $\pm$  standard deviation.

DOI: [10.7554/eLife.10859.006](https://doi.org/10.7554/eLife.10859.006)

The following figure supplements are available for figure 2:

**Figure supplement 1.** Analysis of RNA co-purified with RIG-I SMS or MDA5 variants.

DOI: [10.7554/eLife.10859.007](https://doi.org/10.7554/eLife.10859.007)

**Figure supplement 2.** Assay for defining the immunostimulatory potential of different RNAs.

DOI: [10.7554/eLife.10859.008](https://doi.org/10.7554/eLife.10859.008)

**Figure supplement 3.** Immunostimulatory potential of co-purified RNA from Sendai virus Cantell (SeV) infected cells.

DOI: [10.7554/eLife.10859.009](https://doi.org/10.7554/eLife.10859.009)

endogenous RIG-I, see **Figure 2—figure supplement 2A**). RNA co-purified with wtRIG-I and RIG-I lacking the 2CARD module induced an immune response in these cells (**Figure 2—figure supplement 3A**). RNA co-purified with RIG-I K270I (ATP binding deficient) and V699A (putative translocation deficient) was also able to stimulate the ISRE reporter in an amount comparable to wtRIG-I, indicating no altered RNA binding properties in these mutants under virus infected conditions. In

contrast, RNA that co-purified with the RNA-binding deficient RIG-I T347A (mutation in SF2 domain), RIG-I K858E (mutation in RD domain that reduces triphosphate recognition) or RIG-I  $\Delta$ RD poorly stimulated the ISRE promoter and probably represents background RNA (**Figure 2—figure supplement 3A**). These data suggest that RIG-I recognizes immunostimulatory RNA via the SF2 and RD domains, but does not require ATP binding for this process. ATP binding is necessary, however, because RIG-I K270I expression alone does not stimulate the IFN $\beta$  promoter (compare with **Figure 1C**). Interestingly, RNA co-purified with RIG-I E373Q failed to induce reporter gene expression (**Figure 2D**, **Figure 2—figure supplement 3A**). Thus, despite the observation that RIG-I E373Q co-purifies with approximately threefold more RNA than wtRIG-I from infected cells, the co-purified RNA is not immunostimulatory in a wtRIG-I background. However, cells that transiently express RIG-I E373Q can be further stimulated by transfection of total RNA extracts and purified ribosomal RNA (**Figure 2E**), suggesting that ribosomal RNA can activate RIG-I E373Q. Cells lacking wtRIG-I or RIG-I E373Q on the other hand do not respond to those RNAs. We conclude that host-RNA, which does not activate wtRIG-I, can apparently compete with viral RNA for RIG-I E373Q.

In order to verify a higher affinity of the RIG-I ATP hydrolysis defective mutant towards ribosomal RNA, we purified full-length human RIG-I and RIG-I E373Q, as well as human 80S ribosomes, and tested for a direct interaction. We confirmed that while both RIG-I E373Q and the wild-type protein are able to bind ATP, only wtRIG-I can hydrolyze ATP (**Figure 3A, B**). We subsequently conducted sedimentation assays via ultra-centrifugation of sucrose cushions loaded with 80S ribosomes that have been pre-incubated with wtRIG-I or RIG-I E373Q in presence or absence of ATP or the non-hydrolysable ATP analogue ADP·BeF<sub>3</sub>. In presence of ATP a minor binding of wtRIG-I to the ribosome could be observed, whereas RIG-I E373Q bound in a near stoichiometric manner. In absence of ATP or in presence of ADP·BeF<sub>3</sub> binding of wtRIG-I was greatly enhanced and showed similar levels compared to RIG-I E373Q (**Figure 3C**).

We next analyzed RIG-I E373Q:80S ribosome complexes by cryo-electron microscopy and single particle 3D reconstruction (**Figure 3D**). The average resolution was estimated to be 17.7 Å based on the Fourier shell correlation cut-off criterion at 0.5. When compared with the reconstruction of the human 80S ribosome alone (**Figure 3E**), the ribosome:RIG-I E373Q complex revealed an additional density located at rRNA expansion segment (ES) 7L, which is located at the back of the large ribosomal subunit. Calculation of a statistical difference map between the two reconstructions confirmed that this distinct region contained significant additional density (**Figure 3F**). Human ribosomes contain several long, G:C rich, base-paired RNA expansion segments forming large tentacle-like hairpin structures of substantial double-stranded nature (**Anger et al., 2013**). A large part of the double-stranded RNA in these segments is not covered by ribosomal proteins and accessible for cytosolic proteins. The crystal structure of ADP·BeF<sub>x</sub>-bound RIG-I  $\Delta$ 2CARD:RNA complex (**Jiang et al., 2011**), PDB code 3TMI) fits well into the density observed at ES7L and is located at the root of the solvent exposed portion of helix A of ES7L that contains a contiguous stretch of seven G:C/C:G base pairs (**Figure 3G**).

In summary, we conclude that stabilizing the ATP-bound state of RIG-I induces a conformation where RIG-I binds to ribosomes, presumably at exposed dsRNA expansion segments.

### Specificity of RIG-I towards double-stranded RNA is increased in presence of ATP

To further evaluate the role of ATP binding and hydrolysis of RIG-I we performed electrophoretic mobility shift assays (EMSAs), fluorescence anisotropy experiments and ATP hydrolysis assays in presence and absence of ATP or ADP·BeF<sub>3</sub> with different RNAs. These RNAs mimic different types of endogenous or viral RNAs and help dissecting contributions of RD's binding to the RNA end and SF2's binding to the stem. In addition to a 24mer or 12mer blunt-ended dsRNA or ppp-dsRNA (**Goldeck et al., 2014**), we also used a 60 nucleotide hairpin RNA (denoted as ES hairpin) derived from the ribosomal expansion segment ES7L, which contains several bulges and a non-pairing end (**Figure 4—figure supplement 1A**). The hairpin at one end and the added Y-structure at the other end are used to minimize RNA end binding by RIG-I's RD because RD has a high affinity for blunt RNA ends.

RIG-I and RIG-I E373Q bound to the 24mer blunt ended dsRNA with a slightly higher affinity in presence of ATP or ADP·BeF<sub>3</sub> than in its absence (**Figure 4A**), suggesting that ATP binding to the SF2 domain positively contributes to the overall affinity in addition to RD. A similar result was

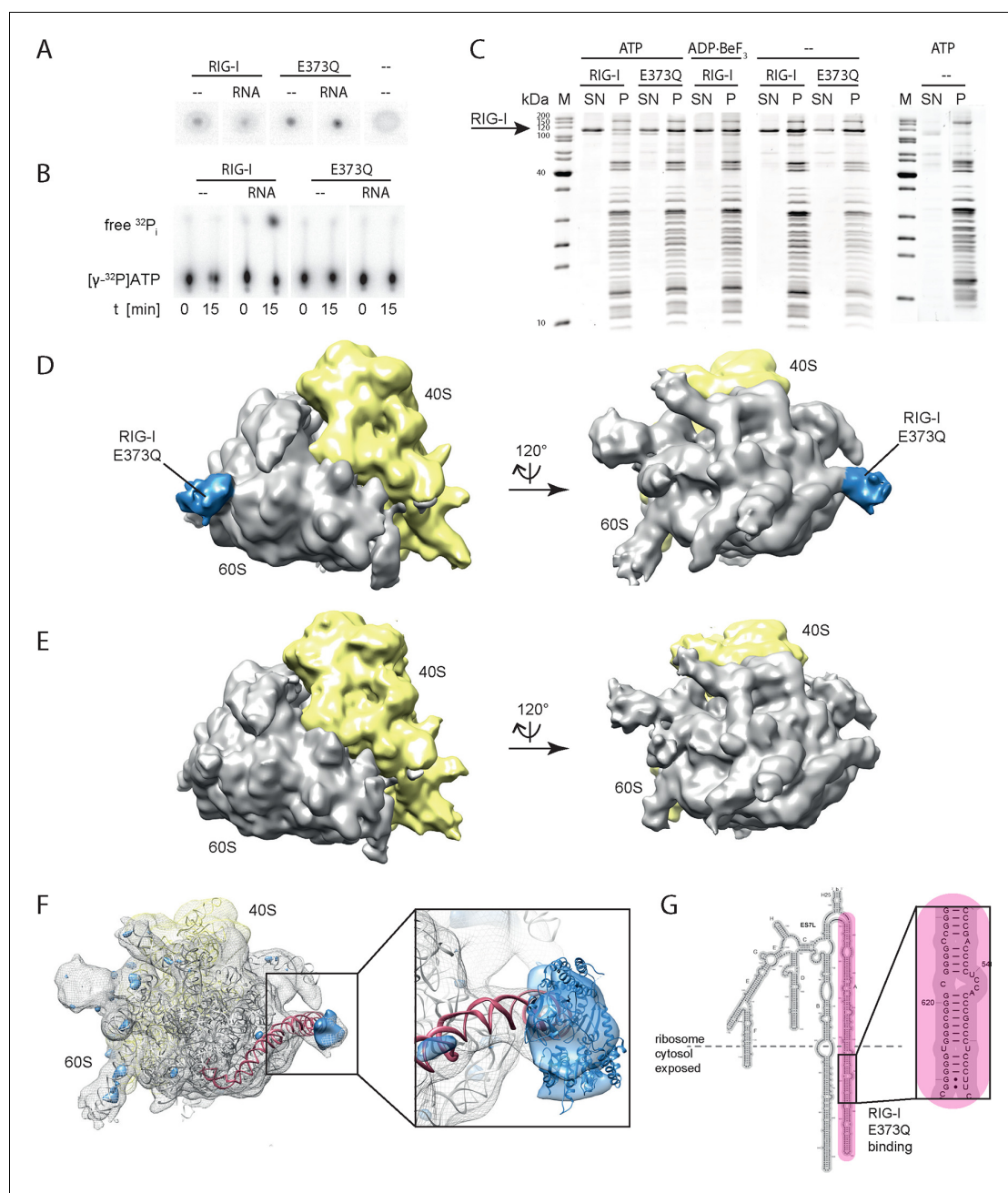


**Figure 3.** RIG-I ATP hydrolysis defective mutant E373Q recognizes the 60S ribosomal subunit in vitro. (A) DRaCALA ATP binding assay of RIG-I or RIG-I E373Q in presence or absence of RNA. (B) ATP hydrolysis assay of RIG-I or RIG-I E373Q in presence and absence of RNA. (C) Binding studies of human 80S ribosomes with RIG-I or RIG-I E373Q in presence or absence of ATP or ADP-BeF<sub>3</sub>. Pre-formed complexes were separated on sucrose cushions via ultracentrifugation and pellet (P) as well as supernatant (SN) fractions were analyzed by SDS-PAGE. (D) Side views of a cryo-EM reconstruction of RIG-I E373Q (blue) bound to the human 80S ribosome (yellow: 40S subunit, gray: 60S subunit). Data was low pass-filtered at 15 Å. (E) Side views of a cryo-EM reconstruction of the human 80S ribosome without prior RIG-I E373Q incubation. Data filtering and color coding as in panel D. (F) Statistical difference map (left,  $\sigma = 2$ ) of cryo-EM reconstructions in panels D and E reveals a significant additional density at expansion segment 7L A (ES7L-A, pink) into which RIG-I (PDB 3TMI) can be fitted (right,  $\sigma = 1.51$ ). (G) Secondary structure map of the 28S rRNA ES7L (derived from (Anger et al., 2013) and zoom into RIG-I E373Q binding area. ES7L-A is indicated in pink (as in panel F).

DOI: 10.7554/eLife.10859.010

obtained when we used a 12mer dsRNA in fluorescence anisotropy experiments in order to further dissect the influence of different RNA ends (**Figure 4B**). Interestingly, the positive effect of ATP was not observed when we used the corresponding ppp-dsRNA 12mer (**Figure 4C**), most likely because the RD dominates RNA binding under these conditions. Thus, it is plausible that RIG-I dissociates from unphosphorylated RNA termini with an increased rate after ATP hydrolysis than from triphosphorylated termini.

We next tested the role of ATP on binding of wtRIG-I, RIG-I E373Q, RIG-I T347A,E373Q and the SMS variant RIG-I C268F to the ES hairpin RNA mimicking the base of the ribosomal E57L. In presence of ATP we observed moderately increased binding of RIG-I E373Q and of RIG-I C268F to this hairpin, however wtRIG-I displayed a strikingly opposing effect (**Figure 4D**, **Figure 4—figure supplement 1C**). For this RNA, ATP reduced rather than increased the affinity of wtRIG-I. The addition of ADP·BeF<sub>3</sub> to RIG-I could reconstitute the high affinity state of RIG-I E373Q. The RIG-I T347A,E373Q double mutant, on the other hand, showed binding affinities similar to RIG-I in presence of ATP, probably caused by residual binding of RD (**Figure 4D**).

Consistent with this, the ES hairpin RNA could induce signaling in RIG-I E373Q transfected HEK 293T RIG-I KO cells (**Figure 2F**) and could also stimulate the ATPase activity of RIG-I Δ2CARD, and to a lesser extent wtRIG-I (which is auto-inhibited by the 2CARD module) (**Figure 5A**, **Figure 5—figure supplement 1A**). A comparable stimulatory effect on the ATPase activity of RIG-I could also be detected with whole human ribosomes (**Figure 5A**). Control assays with the ATP hydrolysis defective mutants RIG-I E373Q and RIG-I T347A,E373Q confirmed the lacking ability of those proteins to hydrolyze ATP even in the presence of triphosphorylated RNA (**Figure 5A**, **Figure 5—figure supplement 1B**).

In summary, our results show that ATP hydrolysis leads to a moderately increased binding of RNA containing base-paired ends, but decreased binding of RNA lacking base-paired ends. These in vitro data are also consistent with our co-immunopurification studies of RNA from cells, where we observed that the ATP hydrolysis deficient RIG-I E373Q mutant co-purified with increased amounts of endogenous RNA.

## Discussion

Here we show that mutations that slow down or inhibit RIG-I's ATPase lead to an increased interaction of RIG-I with endogenous RNA, including double-stranded RNA expansion segments of the human large ribosomal subunit. Our results suggest that RIG-I's ATPase confers specificity to viral RNA by preventing signaling through the abundant background of self-RNA and provide a molecular framework for understanding the pathology of atypical Singleton-Merton syndrome.

Recently, several autoimmune diseases, including the Aicardi-Goutières and Singleton-Merten syndromes, have been linked to RLRs through whole exome sequencing, which discovered single amino acid mutations that are mostly found within the ATPase domain of RLRs (**Jang et al., 2015**; **Rice et al., 2014**; **Rutsch et al., 2015**). Increased interferon levels suggest that an increased activation of MDA5 or RIG-I underlies the molecular pathology of these diseases. Indeed we find that not only E373Q, consistent with recent results, leads to an increased activation of RIG-I in non-infected cells, but also the SMS mutations E373A and C268F (**Jang et al., 2015**) (**Figure 1C**). While this could have been expected for E373A, because of its similarity to E373Q, the increased immunostimulatory effect of C268F in motif I comes as a surprise. Prior mutations in motif I studied by others and us led to an inactivation of RIG-I, rather than constitutive activation. The precise structural reason for the increased signaling of C268F needs to be addressed in future studies, but our co-immunoprecipitation and in vitro binding assay results suggest that this mutation may also lock RIG-I in an RNA-bound, active conformation (**Figure 2—figure supplement 1A**, **Figure 4—figure supplement 1C**).

Mutational and biochemical analyses previously suggested a kinetic model for RIG-I's specificity towards viral RNA, where the ATP-dependent recycling helps to discriminate ppp-dsRNA from endogenous RNA (**Anchisi et al., 2015**; **Louber et al., 2015**; **Runge et al., 2014**) (**Figure 6A**). Our studies show that, in case of base-paired triphosphate containing RNA ends, the RIG-I RD dominates binding. Although RIG-I's ATPase is very active, we do not see a strong effect of ATP on the affinity for the RNA (**Figure 4C**, **Figure 5A**). ATP hydrolysis may under the assayed conditions not efficiently displace RIG-I from ppp-dsRNA because RD might prevent full dissociation even after ATP-hydrolysis displaced SF2. Importantly, ATP reduces the affinity towards self-RNA containing a duplex region

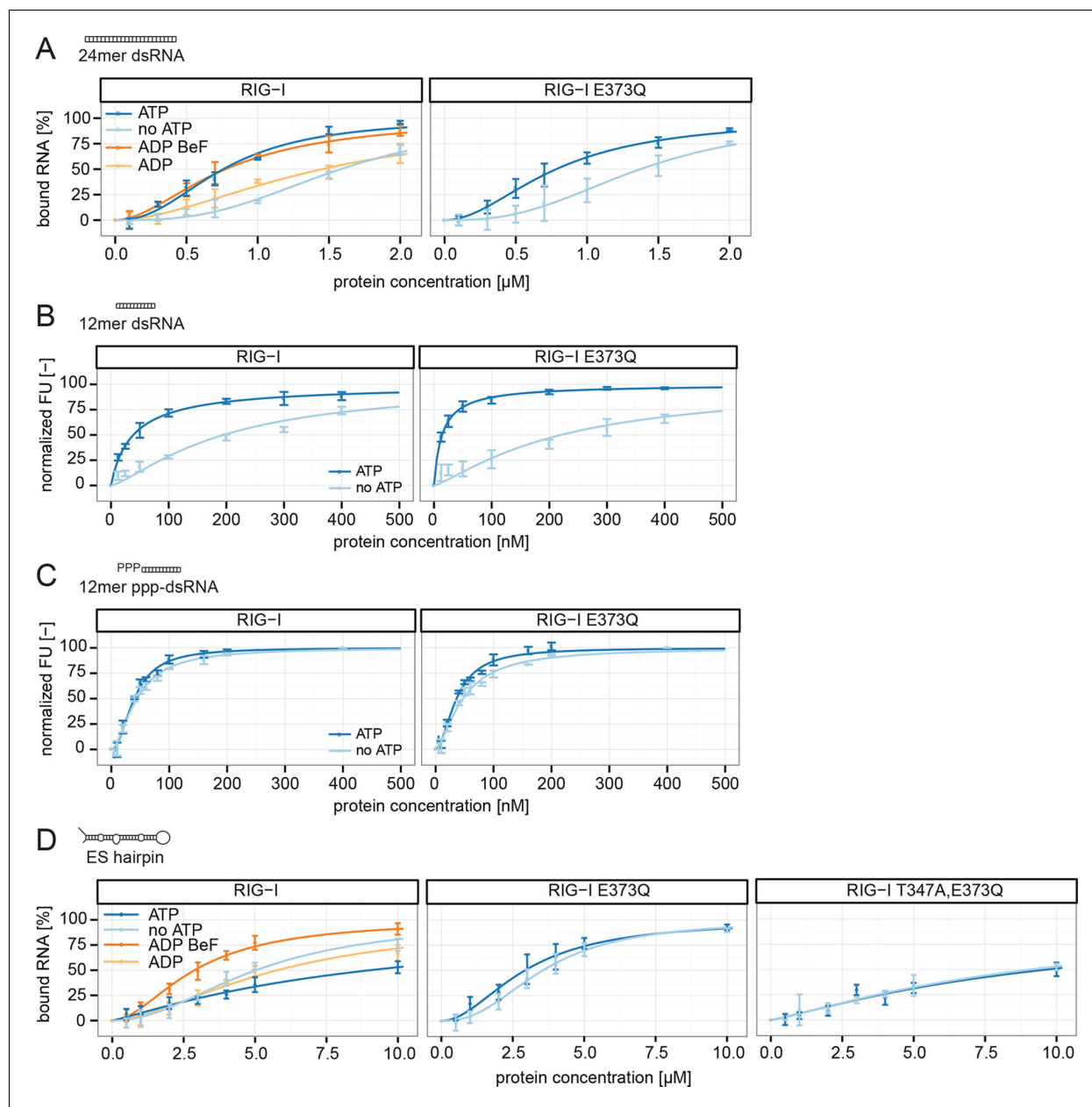


**Figure 4.** RIG-I's ATP hydrolysis enhances RNA end recognition and removes RIG-I from RNA stems. (A) Quantification of electrophoretic mobility shift assays of RIG-I or RIG-I E373Q incubated with 24mer dsRNA in presence or absence of ATP, ADP or ADP·BeF<sub>3</sub> (compare with **Figure 4—Figure supplement 1B**). (B) Fluorescence anisotropy changes measured by titrating RIG-I or RIG-I E373Q in presence or absence of ATP into solutions containing fluorescently labeled 12mer dsRNA. (C) Fluorescence anisotropy changes measured by titrating RIG-I or RIG-I E373Q in presence or absence of ATP into solutions containing fluorescently labeled 12mer ppp-dsRNA. (D) Quantification of electrophoretic mobility shift assays of RIG-I, RIG-I E373Q or RIG-I T347A, E373Q incubated with an RNA hairpin derived from helix A of the human ribosome expansion segment 7L (ES hairpin) in presence or absence of ATP, ADP or ADP·BeF<sub>3</sub> (compare with **Figure 4—Figure supplement 1C**). All binding curves were fitted using the LL.2 function of the R drc package (Cedergreen et al., 2005). n=3-6, error bars represent mean values ± standard deviation.  
DOI: 10.7554/eLife.10859.011

The following figure supplement is available for figure 4:

**Figure supplement 1.** Design of the ribosomal expansion segment derived hairpin RNA, EMSA raw figures and control experiments with RIG-I C268F SMS mutant.  
DOI: 10.7554/eLife.10859.012

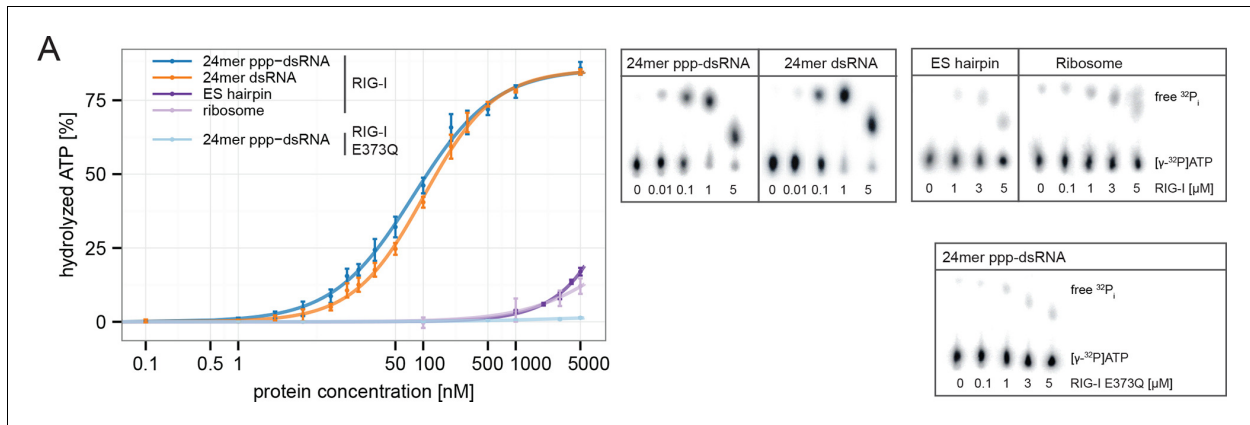


**Figure 5.** RIG-I's ATPase activity correlates with its RNA binding affinity. (A) Quantification of hydrolyzed  $[\gamma\text{-}^{32}\text{P}]\text{ATP}$  by RIG-I or RIG-I E373Q in presence of different RNA substrates. Reactions were allowed to proceed for 20 min at 37 °C and free phosphate was separated from ATP via thin layer chromatography. Spots corresponding to labeled ATP and labeled  $\text{P}_i$  were quantified using ImageJ. All curves were fitted using the LL.2 function of the R drc package.  $n=3$ , error bars represent mean values  $\pm$  standard deviation.

DOI: [10.7554/eLife.10859.013](https://doi.org/10.7554/eLife.10859.013)

The following figure supplement is available for figure 5:

**Figure supplement 1.** RIG-I's 2CARD module reduces the ATP hydrolysis activity.

DOI: [10.7554/eLife.10859.014](https://doi.org/10.7554/eLife.10859.014)

but not a “proper” ppp-dsRNA end (Figure 4D). Thus, if RD is unable to tether RIG-I to ppp-dsRNA ends the ATPase could rapidly remove RIG-I from RNA duplex regions via its translocase and therefore prevents an autoimmune response towards self-RNA (Figure 6B). Our cellular studies are consistent with this biochemical observation, because a point mutation in K888, a residue that is critical for recognizing ppp-dsRNA ends, did not reduce the constitutive activation of ATP hydrolysis-deficient RIG-I (Figure 1C). However, RD and ATP binding are clearly important for signaling, as shown by  $\Delta\text{RD}$  and K270I mutations by us and others (Loubser et al., 2015) (Figure 1C), suggesting that a ring-like, ATP-bound structure is also involved in signaling caused by self-RNA (Figure 6C). In this conformation, the RD likely helps to displace the 2CARD module from the SF2 domain but may not have a high affinity for the RNA itself. Of note, the mutation in V699 of motif V also leads to increased constitutive signaling (Figure 1C). A plausible explanation could be that this mutation in RecA2 decouples RNA-binding induced ATP hydrolysis from translocation or displacement of RNA. In summary, our results suggest a model where RIG-I's translocase removes SF2 from dsRNA, perhaps at nearby bulges, unless high-affinity binding by the RD on RNA ends containing di- or triphosphates tethers RIG-I despite ATP-hydrolysis and leads to repeated or prolonged exposure of the 2CARD module.

An unexpected finding was that trapping the ATP state of RIG-I leads to a particularly increased interaction with the large ribosomal subunit via the expansion segment ES7L (Figure 3D, F). This expansion segment is present in metazoan ribosomes, however its length is substantially increased in human compared to drosophila ribosomes. The function of these expansion segments is not understood, but since helix E (ES7L-E) was recently found to interact with the selenoprotein synthesis factor SBP2, it is likely that the RNA in these elements is accessible to cytosolic proteins (Kossinova et al., 2014). The specific enrichment of the large ribosomal subunit under conditions where ribosomal subunits disengage argues for rather specific interactions of RIG-I E373Q with RNA present on the large but not the small subunit. The dominant binding of ribosomes by RIG-I E373Q can be explained by the high abundance of ribosomal RNA compared to other potential RIG-I ligands in the cytosol. We could directly visualize RIG-I E373Q on the ribosome at the solvent exposed root of ES7L-A (Figure 3F, G). This site contains a stretch of seven G:C/G base pairs, which approximately matches the footprint of dsRNA across the two SF2 RecA domains in the crystal structure of ADP-BeF<sub>x</sub>-bound RIG-I (Jiang et al., 2011; Kohlway et al., 2013; Kowalinski et al., 2011; Luo et al., 2011) and also meets the requirements for activation of RIG-I's ATPase

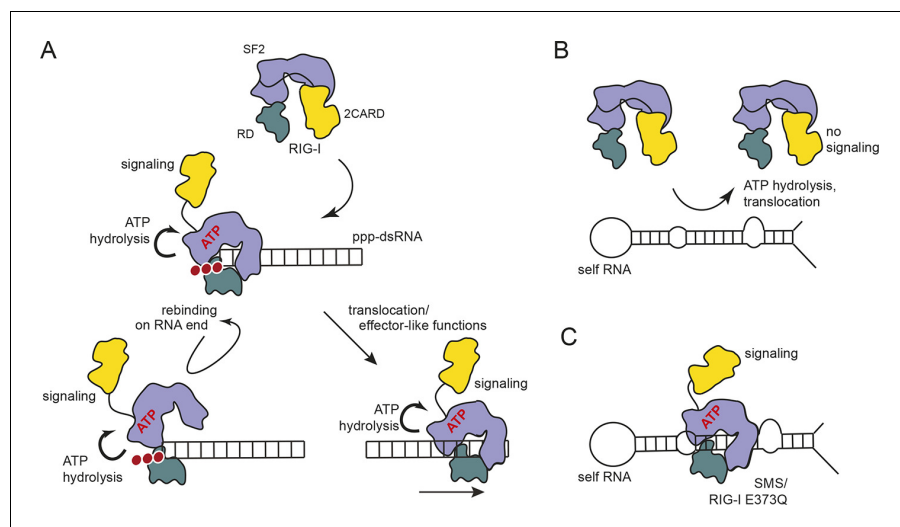


**Figure 6.** Proposed model for impact of ATP on RIG-I signaling on different RNAs. (A) RIG-I recognizes tri- or diphosphorylated double-stranded RNA and preferentially binds to the RNA end through its regulatory domain (RD, green). Binding of ATP-SF2 (purple) to the dsRNA releases the 2CARD module (yellow) and activates the downstream signaling process. ATP hydrolysis displaces the SF2 domain from dsRNA leading to either rebinding at the RNA end (tethered by RD) or to translocation along the RNA. (B) In healthy cells, sustained binding of RIG-I to self-RNA containing dsRNA stretches is prevented by ATP hydrolysis. The SF2 domain can be sufficiently displaced because the RD does not provide a high affinity tether. (C) Mutations that allow ATP promoted binding of dsRNA and displacement of the 2CARD module, but prevent ATP hydrolysis dependent dissociation of SF2 from dsRNA, such as those underlying atypical Singleton-Merten Syndrome, will result in an unintended signaling through self-RNA.

DOI: [10.7554/eLife.10859.015](https://doi.org/10.7554/eLife.10859.015)

(Anchisi *et al.*, 2015). Since 40% of the particles had this additional density, it is conceivable that additional binding sites could contribute to the interaction with RIG-I E737Q as well. However, the peripheral parts of the expansion segments are flexible and not visible in the 3D reconstructions, preventing us from observing RIG-I at other regions.

The RNA corresponding to the observed binding region of ES7L-A is also bound by RIG-I *in vitro* and can moderately stimulate RIG-I's ATPase (Figure 4D, Figure 5A). The much more efficient stimulation of RIG-I's ATPase by ppp-dsRNA is likely due to the high affinity towards RD, which could repeatedly "present" the RNA to SF2 (i.e. increasing the "local" concentration of RNA at SF2). Of note, while the addition of ATP to RIG-I reduces the interaction with the ES hairpin RNA, consistent with a role of the ATPase in preventing interaction with self-RNA, RIG-I E373Q binds with a moderately increased affinity to the ES-hairpin RNA in presence of ATP. Because of the large number of ribosomes in the cytosol it is therefore conceivable that RIG-I binds to double-stranded ribosomal RNA, including ES7L-A, under conditions where the ATPase is not able to efficiently displace the protein, such as those arising in patients with atypical SMS. In addition, the high local concentration of ribosomes in polysomes as well as a potential binding of RIG-I to other expansion segments could bring multiple RIG-I E373Q in contact, such that their exposed 2CARD module could interact for downstream signaling (Peisley *et al.*, 2014; Wu *et al.*, 2014). We do not, however, want to rule out contributions by other self-ligands as well. For instance, RIG-I can bind to endogenous mRNA (Zhang *et al.*, 2013) or RNase-L cleavage products (Malathi *et al.*, 2007), while MDA5 was shown to be activated by mRNA stem loop structures under conditions where reduction of A:T base-paired RNA is not prevented by ADAR1 (Liddicoat *et al.*, 2015).

In any case, there are two levels of control to limit RIG-I mediated signaling to viral RNA. On one hand, RNA editing (Liddicoat *et al.*, 2015) and methylation (Schuberth-Wagner *et al.*, 2015) modifies particular types of self-RNA that would otherwise form reasonable ligands for RIG-I or MDA5. On the other hand, the intrinsic ATPase and translocase activity removes RIG-I from short, but abundant endogenous dsRNA stretches, thereby reducing background signaling and increasing the sensitivity of the system.

## Materials and methods

### Cell lines, viruses and antibodies

Luciferase assays and RIG-I:RNA co-immunopurifications were carried out in HEK 293T cells (purchased from ATCC, CRL-11268) or HEK 293T RIG-I KO cells (Zhu *et al.*, 2014). HEK 293T ISRE-FF/RFP reporter cells (stable expression of firefly luciferase and RFP under the control of an ISRE promoter, kindly provided by Luis Martinez-Sorbid, University of Rochester, Rochester, NY) were used for interferon stimulated luciferase reporter gene assays of recovered RNA. HEK cells were maintained in high glucose Dulbecco's Modified Eagle Medium supplemented with GlutaMAX, pyruvate and 10% FBS (all purchased from Gibco, UK). Human ribosomes were purified from HeLa S3 cells cultured in SMEM (Sigma, Germany) supplemented with 10% FBS, Penicillin (100 U/mL)/ Streptomycin (100 µg/mL) and 1x GlutaMAX (all purchased from Gibco, UK) using a spinner flask at 40 rpm. All cell lines were routinely checked for Mycoplasmas by PCR and were, except for the HEK 293T ISRE-FF/RFP cell line, tested to be negative. Mycoplasma contaminations were suppressed using Plasmocin (InvivoGen, France) according to the manufacturer's protocol. Viruses used for infections were Sendai virus Cantell, Sendai virus defective interfering particles H4 (kindly provided by Dominique Garcin, Geneva, Switzerland), recombinant measles virus (MeV) with a sequence identical to the vaccine strain Schwarz (AF266291.1.) (del Valle *et al.*, 2007; Devaux *et al.*, 2007) and recombinant MeV-Cko-ATU-Cs. MeV-Cko-ATU-Cs expresses the C Schwarz protein from an additional transcription unit (ATU) located between the M and the P gene, while expression of C from the P gene is abrogated. Specifically, three stop codons were introduced into the P gene for the C ORF while leaving P and V protein expression intact. Cloning was done as described previously (Pfaller and Conzelmann, 2008; Sparrer *et al.*, 2012). Additionally, an ATU was introduced between the P and M gene by duplicating the gene borders of the P gene. The ORF of the C (Schwarz) protein was cloned into that ATU and the virus rescued from cDNA using helper plasmids in 293-3-46 cells (Radecke *et al.*, 1995) and propagated on Vero cells as described previously (Parks *et al.*, 1999; Pfaller *et al.*, 2014). Primary antibodies to human MDA5 (AT113) and RIG-I (Alme-1) were purchased from Enzo Life Science (Loerrach, Germany). Antibodies to FLAG (M2), HA (HA-7) and  $\beta$ -tubulin (TUB 2.1) were obtained from Sigma-Aldrich (Saint Luis, MO, USA). Secondary antibodies were supplied by GE Healthcare (Buckinghamshire, UK).

### Generation of RLR mutants

Sequences encoding full-length human RIG-I or MDA5 with N- or C-terminal FLAG/HA-tag were cloned into pcDNA5 FRT/TO (Invitrogen, Carlsbad, CA, USA). Mutants were generated by site-directed mutagenesis with PfuUltra polymerase (Agilent, Santa Clara, CA, USA).

### Immunoprecipitation of RLR-associated RNA from infected or non-infected cells

$6 \times 10^6$  HEK 293T or HEK 293T RIG-I KO cells were transfected with 10 µg pcDNA5 vector coding for different FLAG/HA tagged RLR proteins. Non-infected cells were harvested 24 h after transfection. Infections were carried out 6h after transfection with an MOI of 0.05 for measles virus or high MOI for Sendai virus and were allowed to proceed for 40 or 24 hr, respectively. Cells were harvested and incubated in Nonidet P-40 lysis buffer (50 mM HEPES, 150 mM KCl, 1 mM NaF, 0.5% NP-40, 0.5 mM DTT, protease inhibitor (Sigma, Saint Luis, MO, USA), pH 7.5) for 10 min on ice. Lysates were cleared by centrifugation and proteins were immunoprecipitated for 2.5 - 4 hr with anti-DDK magnetic beads (OriGene, Rockville, MD, USA) or anti-FLAG (M2) bound to magnetic protein G Dynabeads (Novex, Life Technologies, Carlsbad, CA, USA). Beads were washed five times with washing buffer (50 mM HEPES, 300 mM KCl, 0.05% NP-40, 0.5 mM DTT, protease inhibitor, pH 7.5) and incubated with proteinase K (Thermo Scientific, Vilnius, Lithuania) for 30 min at 50 °C. RNA was isolated by phenol/ chloroform/ isoamyl alcohol extraction using Phase Lock Gel Heavy tubes (5 PRIME, Germany). The quality of the isolated RNA was validated on an Agilent RNA 6000 Nano chip.

### Luciferase transfection assays

Immunoactivity experiments were carried out in 24-well plates seeded with  $2.5 \times 10^5$  HEK 293T RIG-I KO or  $2.5 \times 10^5$  HEK 293T ISRE-FF/RFP reporter cells per well using Lipofectamine 2000 (Invitrogen, Carlsbad, CA, USA) as transfection reagent according to the manufacturer's protocol. For downstream signaling assays HEK 293T RIG-I KO cells were co-transfected with 500 ng protein expression vector, 100 ng p125-luc, 10 ng pCMV-RL and 50 ng empty expression vector. For RIG-I E373Q/RIG-I  $\Delta$ 2CARD,E373Q competition assays HEK 293T RIG-I KO cells were co-transfected with 100 ng RIG-I E373Q expression vector, varying concentrations of the RIG-I  $\Delta$ 2CARD,E373Q expression vector, 100 ng p125-luc and 10 ng pCMV-RL. DNA concentrations were held constant by adding empty expression vector if necessary. For determination of the immunostimulatory potential of recovered RNA from co-immunoprecipitations, HEK 293T ISRE-FF/RFP cells were transfected with 250 ng RNA in Opti-MEM (Gibco, UK). For RNA stimulation of cells overexpressing RIG-I E373Q  $2.5 \times 10^5$  HEK 293T RIG-I KO cells were transfected with 100 ng RIG-I E373Q expression vector, 100 ng p125-luc, 10 ng pCMV-RL and 1000 ng total RNA/ rRNA or ES hairpin RNA in Opti-MEM. All cells were harvested 24 h after transfection using 200  $\mu$ L PLB (Promega, Madison, WI, USA) and subjected to immunoactivity experiments using the Dual-Glo luciferase assay system (Promega, Madison, WI, USA) as previously described (Runge *et al.*, 2014). The luciferase activity was determined with a Berthold Luminometer in 96-well plates using 20  $\mu$ L cell lysate.

### Protein expression and purification

RIG-I and RIG-I E373Q were expressed and purified from insect cells as described previously (Cui *et al.*, 2008). Briefly, sequences encoding RIG-I were cloned into pFBDM vectors and transformed into *E. coli* DH10MultiBac cells. Bacmids were extracted for transfection into SF9 insect cells and propagated virus was used for protein expression in High Five insect cells. Seventy-two hours after infection cells were harvested and flash frozen in liquid nitrogen. RIG-I  $\Delta$ 2CARD was expressed in *E. coli* BL21 Rosetta (DE3), using pET expression vectors as described earlier (Cui *et al.*, 2008). All recombinant proteins were purified using metal affinity (QIAGEN, Germany), heparin affinity and gel filtration chromatography (both GE Healthcare, Buckinghamshire, UK). Fractions containing RIG-I were concentrated to 6 mg/mL and flash-frozen in liquid nitrogen.

### Thermal unfolding assay

Thermal stability of RIG-I or RIG-I E373Q in presence or absence of ATP was analyzed by fluorescence thermal shift assays. Proteins (20  $\mu$ M) were incubated in 25 mM HEPES pH 7, 150 mM NaCl, 10 mM  $MgCl_2$ , 5 mM TCEP, 5% glycerol and 5 mM ATP. After addition of SYPRO orange (Invitrogen, Carlsbad, CA, USA, final concentration: 2.5x) the fluorescence signal was detected using a gradient from 5  $^{\circ}C$  to 100  $^{\circ}C$  with 0.5 K/30 s and one scan each 0.5 K in a real-time thermal cycler (Biorad, Germany, CFX96 touch) using the FRET mode.

### Small-angle X-ray scattering

SAXS experiments were conducted at the PETRA3 P12 beamline of the European Molecular Biology Laboratory/ Deutsches Elektronen-Synchrotron, Hamburg, Germany. Samples were measured in absence or presence of 5 mM ATP in size exclusion buffer (25 mM HEPES pH 7, 150 mM NaCl, 5 mM  $MgCl_2$ , 5 mM  $\beta$ -Mercaptoethanol, 5% glycerol). RIG-I samples were measured at protein concentrations of 1.28, 2.65 and 8.35 mg/mL and RIG-I E373Q samples with concentrations of 0.87, 2.13 and 6.84 mg/mL. The respective scattering of the corresponding buffer was used for buffer subtraction. The samples did not show signs of radiation damage, which was assessed by automatic and manual comparison of consecutive exposure frames. The data was processed using PRIMUS from the ATSAS package (Konarev *et al.*, 2006) and the radius of gyration was determined by Guinier plot [ $\ln I(s)$  versus  $s^2$ ] analysis obeying the Guinier approximation for globular proteins ( $s \times R_g < 1.3$ ).

### Human 80S ribosome preparation

HeLa S3 cells were harvested (2 min, 650 x g), washed with PBS (Invitrogen, Carlsbad, CA, USA) and incubated with 1.5x vol Buffer 1 (10 mM HEPES/KOH, pH 7.2/4  $^{\circ}C$ , 10 mM KOAc, 1 mM  $Mg(OAc)_2$  and 1 mM DTT) for 15 min on ice, followed by disruption with nitrogen pressure (300 psi, 30 min, 4  $^{\circ}C$ ) in a cell disruption vessel (Parr Instrument, Moline, IL, USA). The cell lysate was cleared (10 min,

14,000 rpm, Eppendorf 5417R, 4 °C) and the resulting supernatant was loaded onto a sucrose cushion (Buffer 1 supplemented with 35% sucrose). Subsequent spinning (98 min, 75,000 rpm, TLA 120.2, 4 °C) was performed. After resuspension of the ribosomal pellet, a high-salt purification by centrifugation through a 500 mM sucrose cushion (50 mM Tris/HCl, pH 7.0/4 °C, 500 mM KOAc, 25 mM Mg(OAc)<sub>2</sub>, 5 mM β-mercaptoethanol, 1 M sucrose, 1 μg/mL cycloheximide and 0.1% Nikkol) was conducted (45 min, 100,000 rpm, TLA120.2, 4 °C). The ribosomal pellet was resuspended in Ribosome Buffer (50 mM Tris/HCl, pH 7.0/4 °C, 100 mM KOAc, 6 mM Mg(OAc)<sub>2</sub>, 1 mM DTT, 1/200 EDTA-free Complete protease inhibitor (Roche, Germany), 0.2 U/mL RNasin (Promega, Madison, WI, USA)), quickly centrifuged, frozen in liquid nitrogen and stored at -80 °C.

### Total RNA and ribosomal RNA isolation

For total RNA isolation 2.5 × 10<sup>5</sup> HEK 293T were seeded per well of 24 well plates. After 24 h cells were harvested in PBS, collected by centrifugation and lysed in Nonidet P-40 lysis buffer for 10 min on ice. Supernatant was cleared by centrifugation and DNA was digested with TURBO DNase (Ambion, Life Technologies, Carlsbad, CA, USA) for 3 min at 37 °C. Proteins were digested and RNA was extracted as described above. For ribosomal RNA isolation purified human ribosomes were proteinase K digested and RNA was extracted accordingly.

### Ribosomal binding studies

Human 80S ribosomes were incubated with or without 2.5x molar excess of RIG-I or RIG-I E373Q in binding buffer (50 mM HEPES/KOH, pH 7.5/ 4 °C, 100 mM KCl, 2.5 mM Mg(OAc)<sub>2</sub>, 2 mM DTT, 1 mM ATP, 0.1% DDM, 10% Glycerol) for 15 min at room temperature and then for 15 min at 4 °C. The mixture was loaded onto a sucrose cushion (binding buffer with 750 mM sucrose) and spun (3 h, 40,000 rpm, SW55Ti, 4 °C). Supernatant and pellet fractions were separated and TCA precipitated. The resulting samples were analyzed by SDS-PAGE and visualized using SYPRO Orange Staining (Molecular Probes, Eugene, OR, USA).

### Cryo-grid preparation

5 OD/mL human 80S ribosomes were incubated with or without 2.5x molar excess of RIG-I E373Q. Each sample (50 mM HEPES / KOH, pH 7.5 / 4 °C, 100 mM KCl, 2.5 mM Mg(OAc)<sub>2</sub>, 2 mM DTT, 1 mM ATP, 0.1% DDM, 5% glycerol) was applied to 2 nm pre-coated Quantifoil R3/3 holey carbon supported grids and vitrified using a Vitrobot Mark IV (FEI Company, Germany).

### Cryo-electron microscopy and single particle reconstruction

Data were collected on a 120 keV TECNAI SPIRIT cryo-electron microscope with a pixel size of 2.85 Å/pixel at a defocus range between 1.4 μm and 4.6 μm (with RIG-I E373Q ligand) or between 1.8 μm and 5.3 μm (without ligand) under low dose conditions. Particles were detected with SIGNATURE (Chen and Grigorieff, 2007). Initial alignment resulted in 61,067 particles (with ligand) and 29,959 particles (without ligand). Subsequent data processing and single particle analysis was performed using the SPIDER software package (Frank et al., 1996). Non-ribosomal particles (19,080 particles, 31% (with ligand) and 10,663 particles, 35% (without ligand)) were removed from each data set by unsupervised 3D sorting (Loerke et al., 2010). The remaining particles were further sorted, resulting in a volume with additional density (with ligand: 23,715 particles, 39%). The identical sorting scheme was applied to the control 80S ribosome without ligand, resulting in final 11,727 particles (39%). The final 80S structures with and without ligand were refined to an overall resolution (FCS<sub>0.5</sub>) of 17.7 Å and 21.9 Å, respectively. For comparison of the two final volumes, a statistical difference map between the two reconstructions was calculated.

### Figure preparations and model docking

We used the crystal structure of the human RIG-I protein (PDB code 3TMI) (Jiang et al., 2011) and the human ribosome (PDB 4V6X) (Anger, et al., 2013) for rigid-body fitting into the additional density. Figures depicting atomic models with and without density were prepared using UCSF Chimera (Pettersen et al., 2004).

### Differential radial capillary action of ligand assay

ATP binding was determined by DRaCALA using [ $\alpha$ - $^{32}$ P]ATP (Hartmann Analytik, Germany). 12  $\mu$ M RIG-I or RIG-I E373Q were incubated in 50 mM HEPES, pH 7.5, 150 mM KCl, 5 mM MgCl<sub>2</sub>, 2.5 mM TCEP, 0.1 mg/mL BSA supplemented with 2.5 nM [ $\alpha$ - $^{32}$ P]ATP for 10 min at room temperature in presence or absence of 100 nM RNA. 2.5  $\mu$ L of reaction mixture was spotted on nitrocellulose membranes (0.22  $\mu$ M pores, GE Healthcare, Buckinghamshire, UK), air-dried and [ $\alpha$ - $^{32}$ P]ATP was detected using a phosphor-imaging system (GE Healthcare, Germany).

### Electrophoretic mobility shift assay

Proteins at different concentrations were pre-incubated with ATP, ADP or ADP·BeF<sub>3</sub> (all 3 mM end concentration, ADP·BeF<sub>3</sub> was generated using ADP, NaF and BeCl<sub>2</sub> in a 1:1:5 molar ratio) and added to 0.5  $\mu$ M ES hairpin RNA or 0.2  $\mu$ M 24mer RNA in EMSA buffer (50 mM Tris pH 7.5, 50 mM KCl, 5 mM MgCl<sub>2</sub>, 5 mM TCEP, 7.5  $\mu$ M ZnCl<sub>2</sub>, 3 mM ATP, 5% glycerol). Reactions were incubated for 20 min at 37 °C. Samples were separated on TB agarose gels (89 mM Tris, 89 mM boric acid, 0.8% agarose) and stained with Gel-Red (Biotium, Hayward, CA, USA). Unbound RNA bands were quantified with ImageJ.

### Fluorescence anisotropy assays

Different RIG-I or RIG-I E373Q protein concentrations were titrated into EMSA buffer without ATP and glycerol. Reactions were started by addition of 5 mM ATP and 20 nM Cy3- or Cy5-labeled RNA and fluorescence anisotropy was measured with a TECAN M1000 plate reader after incubation at room temperature for 20 min.

### ATPase hydrolysis assays

ATPase hydrolysis activity was determined using [ $\gamma$ - $^{32}$ P]ATP (Hartmann Analytik, Germany). Proteins at different concentrations were pre-incubated with 100 nM RNA or purified ribosomes for 10 min at room temperature in EMSA buffer without ATP. The reaction was initiated by addition of 1.5 mM unlabeled and 10 nM [ $\gamma$ - $^{32}$ P]ATP and incubated for 20 min at 37 °C. Free phosphate was separated from ATP by thin layer chromatography in TLC running buffer (1 M formic acid, 0.5 M LiCl) on polyethyleneimine cellulose TLC plates (Sigma-Aldrich, Germany). [ $\gamma$ - $^{32}$ P]P<sub>i</sub> and [ $\gamma$ - $^{32}$ P]ATP were detected using a phosphor-imaging system (GE Healthcare, Germany) and quantified using ImageJ.

### Acknowledgements

We thank Simon Runge for help with RNA co-purification during initial stages of the project and Filiz Civril for the RIG-I insect cell expression vector. We thank Luis Martinez-Sorbido (University of Rochester, Rochester, NY) for the HEK 293T ISRE-FF/RFP cell line and Dominique Garcin (University of Geneva, Switzerland) for providing SeV defective interfering particles H4. We thank Stefan Krebs and Andrea Klanner for support in RNA analysis and Andrea Gilmozzi for help with ribosome purification and binding assays. Furthermore, we thank the staff of the EMBL/DESY PETRA3 P12 beamline for support in SAXS measurements, Gregor Witte for help with SAXS data analysis, Tobias Deimling for help with EMSAs and ATPase assays and Robert Byrne for critically reading the manuscript.

### Additional information

#### Competing interests

GH, VH co-founder and shareholder of the Rigontec GmbH. The other authors declare that no competing interests exist.

#### Funding

Funder	Grant reference number	Author
National Institutes of Health	T32 training grant 5T32AI007647-13	Jenish R Patel
German Excellence Initiative	CIPSM	Roland Beckmann Karl-Peter Hopfner

Graduate School of Quantitative Biosciences Munich		Roland Beckmann Karl-Peter Hopfner
European Research Council	Advanced Grant CRYOTRANSLATION	Roland Beckmann
Deutsche Forschungsgemeinschaft	FOR 1805	Roland Beckmann
Deutsche Forschungsgemeinschaft	SFB646	Roland Beckmann Karl-Peter Hopfner
Deutsche Forschungsgemeinschaft	GRK1721	Karl-Peter Hopfner Roland Beckmann
Bavarian network for Molecular Biosystems		Karl-Peter Hopfner

The funders had no role in study design, data collection and interpretation, or the decision to submit the work for publication.

#### Author contributions

CL, Planned and performed luciferase assays and co-IP experiments, purified proteins, performed in vitro assays and wrote the paper; SM, Purified human ribosomes, carried out ribosome binding studies and analyzed the cryo-EM structure; KMJS, Produced measles virus and planned the luciferase assays and co-IPs; CCdOM, Carried out co-IP experiments and thermal shift assays; MM, Purified proteins; JRP, Provided Sendai virus Cantell; MG, GH, Provided synthetic 24mer and 12mer ppp-RNAs; AGS, K-KC, RB, Supervised the study and critically read the manuscript; VH, Provided the 293T RIG-I KO cell line and critically read the manuscript; K-PH, Designed the research, supervised experiments and wrote the paper

#### Author ORCIDs

Karl-Peter Hopfner, <http://orcid.org/0000-0002-4528-8357>

## Additional files

#### Major datasets

The following previously published datasets were used:

Author(s)	Year	Dataset title	Dataset URL	Database, license, and accessibility information
Jiang F, Ramanathan A, Miller MT, Tang GQ, Gale M, Patel SS, Marcotrigiano J	2011	Structural basis of RNA recognition and activation by innate immune receptor RIG-I	<a href="http://www.rcsb.org/pdb/explore/explore.do?structureId=3TMI">http://www.rcsb.org/pdb/explore/explore.do?structureId=3TMI</a>	Publicly available at the RCSB Protein Data Bank (Accession no: 3TMI).
Anger AM, Armache JP, Beringhausen O, Habeck M, Subklewe M, Wilson DN, Beckmann R	2013	Structures of the human and Drosophila 80S ribosome	<a href="http://www.rcsb.org/pdb/explore/explore.do?structureId=4V6X">http://www.rcsb.org/pdb/explore/explore.do?structureId=4V6X</a>	Publicly available at the RCSB Protein Data Bank (Accession no: 4V6X).

## References

- Anchisi S, Guerra J, Garcin D. 2015. RIG-I ATPase activity and discrimination of self-RNA versus non-self-RNA. *mBio* **6**:e02349-14. doi: [10.1128/mBio.02349-14](https://doi.org/10.1128/mBio.02349-14)
- Anger AM, Armache J-P, Beringhausen O, Habeck M, Subklewe M, Wilson DN, Beckmann R. 2013. Structures of the human and drosophila 80S ribosome. *Nature* **497**:80–85. doi: [10.1038/nature12104](https://doi.org/10.1038/nature12104)
- Bamming D, Horvath CM. 2009. Regulation of signal transduction by enzymatically inactive antiviral RNA helicase proteins MDA5, RIG-I, and LGP2. *Journal of Biological Chemistry* **284**:9700–9712. doi: [10.1074/jbc.M807365200](https://doi.org/10.1074/jbc.M807365200)

- Banerjee AK**, Shatkin AJ. 1971. Guanosine-5'-diphosphate at the 5' termini of reovirus RNA: evidence for a segmented genome within the virion. *Journal of Molecular Biology* **61**:643–653. doi: [10.1016/0022-2836\(71\)90069-6](https://doi.org/10.1016/0022-2836(71)90069-6)
- Berke IC**, Modis Y. 2012. MDA5 cooperatively forms dimers and ATP-sensitive filaments upon binding double-stranded RNA. *The EMBO Journal* **31**:1714–1726. doi: [10.1038/emboj.2012.19](https://doi.org/10.1038/emboj.2012.19)
- Brubaker SW**, Bonham KS, Zanoni I, Kagan JC. 2015. Innate immune pattern recognition: a cell biological perspective. *Annual Review of Immunology* **33**:257–290. doi: [10.1146/annurev-immunol-032414-112240](https://doi.org/10.1146/annurev-immunol-032414-112240)
- Bruns AM**, Leser GP, Lamb RA, Horvath CM. 2014. The innate immune sensor LGP2 activates antiviral signaling by regulating MDA5-RNA interaction and filament assembly. *Molecular Cell* **55**:771–781. doi: [10.1016/j.molcel.2014.07.003](https://doi.org/10.1016/j.molcel.2014.07.003)
- Cedergreen N**, Ritz C, Streibig JC. 2005. Improved empirical models describing hormesis. *Environmental Toxicology and Chemistry* **24**:3166–3172. doi: [10.1897/05-014R.1](https://doi.org/10.1897/05-014R.1)
- Chen JZ**, Grigorieff N. 2007. SIGNATURE: a single-particle selection system for molecular electron microscopy. *Journal of Structural Biology* **157**:168–173. doi: [10.1016/j.jsb.2006.06.001](https://doi.org/10.1016/j.jsb.2006.06.001)
- Civril F**, Bennett M, Moldt M, Deimling T, Witte G, Schiesser S, Carell T, Hopfner K-P. 2011. The RIG-I ATPase domain structure reveals insights into ATP-dependent antiviral signalling. *EMBO Reports* **12**:1127–1134. doi: [10.1038/embor.2011.190](https://doi.org/10.1038/embor.2011.190)
- Cui S**, Eisenächer K, Kirchofer A, Brzózka K, Lammens A, Lammens K, Fujita T, Conzelmann K-K, Krug A, Hopfner K-P. 2008. The C-terminal regulatory domain is the RNA 5'-triphosphate sensor of RIG-I. *Molecular Cell* **29**:169–179. doi: [10.1016/j.molcel.2007.10.032](https://doi.org/10.1016/j.molcel.2007.10.032)
- del Valle JR**, Devaux P, Hodge G, Wegner NJ, McChesney MB, Cattaneo R. 2007. A vectored measles virus induces hepatitis B surface antigen antibodies while protecting macaques against measles virus challenge. *Journal of Virology* **81**:10597–10605. doi: [10.1128/JVI.00923-07](https://doi.org/10.1128/JVI.00923-07)
- Devaux P**, von Messling V, Songsunthong W, Springfield C, Cattaneo R. 2007. Tyrosine 110 in the measles virus phosphoprotein is required to block STAT1 phosphorylation. *Virology* **360**:72–83. doi: [10.1016/j.virol.2006.09.049](https://doi.org/10.1016/j.virol.2006.09.049)
- Frank J**, Radermacher M, Penczek P, Zhu J, Li Y, Ladjadj M, Leith A. 1996. SPIDER and WEB: processing and visualization of images in 3D electron microscopy and related fields. *Journal of Structural Biology* **116**:190–199. doi: [10.1006/jsbi.1996.0030](https://doi.org/10.1006/jsbi.1996.0030)
- Funabiki M**, Kato H, Miyachi Y, Toki H, Motegi H, Inoue M, Minowa O, Yoshida A, Deguchi K, Sato H, Ito S, Shiroishi T, Takeyasu K, Noda T, Fujita T. 2014. Autoimmune disorders associated with gain of function of the intracellular sensor MDA5. *Immunity* **40**:199–212. doi: [10.1016/j.immuni.2013.12.014](https://doi.org/10.1016/j.immuni.2013.12.014)
- Gack MU**, Shin YC, Joo C-H, Urano T, Liang C, Sun L, Takeuchi O, Akira S, Chen Z, Inoue S, Jung JU. 2007. TRIM25 RING-finger E3 ubiquitin ligase is essential for RIG-I-mediated antiviral activity. *Nature* **446**:916–920. doi: [10.1038/nature05732](https://doi.org/10.1038/nature05732)
- Goldeck M**, Tuschl T, Hartmann G, Ludwig J. 2014. Efficient solid-phase synthesis of pppRNA by using product-specific labeling. *Angewandte Chemie* **126**:4782–4786. doi: [10.1002/ange.201400672](https://doi.org/10.1002/ange.201400672)
- Goubau D**, Schlee M, Deddouche S, Pruijssers AJ, Zillinger T, Goldeck M, Schuberth C, Van der Veen AG, Fujimura T, Rehwinkel J, Iskarpatyoti JA, Barchet W, Ludwig J, Dermody TS, Hartmann G, Reis e Sousa C. 2014. Antiviral immunity via RIG-I-mediated recognition of RNA bearing 5'-diphosphates. *Nature* **514**:372–375. doi: [10.1038/nature13590](https://doi.org/10.1038/nature13590)
- Gruber AR**, Lorenz R, Bernhart SH, Neubock R, Hofacker IL. 2008. The vienna RNA websuite. *Nucleic Acids Research* **36**:W70–W74. doi: [10.1093/nar/gkn188](https://doi.org/10.1093/nar/gkn188)
- Hornung V**, Ellegast J, Kim S, Brzózka K, Jung A, Kato H, Poeck H, Akira S, Conzelmann K-K, Schlee M, Endres S, Hartmann G. 2006. 5'-triphosphate RNA is the ligand for RIG-I. *Science* **314**:994–997. doi: [10.1126/science.1132505](https://doi.org/10.1126/science.1132505)
- Hou F**, Sun L, Zheng H, Skaug B, Jiang Q-X, Chen ZJ. 2011. MAVS forms functional prion-like aggregates to activate and propagate antiviral innate immune response. *Cell* **146**:448–461. doi: [10.1016/j.cell.2011.06.041](https://doi.org/10.1016/j.cell.2011.06.041)
- Iwasaki A**, Medzhitov R. 2015. Control of adaptive immunity by the innate immune system. *Nature Immunology* **16**:343–353. doi: [10.1038/ni.3123](https://doi.org/10.1038/ni.3123)
- Jang M-A**, Kim EK, Now H, Nguyen NTH, Kim W-J, Yoo J-Y, Lee J, Jeong Y-M, Kim C-H, Kim O-H, Sohn S, Nam S-H, Hong Y, Lee YS, Chang S-A, Jang SY, Kim J-W, Lee M-S, Lim SY, Sung K-S, Park K-T, Kim BJ, Lee J-H, Kim D-K, Kee C, Ki C-S. 2015. Mutations in DDX58, which encodes RIG-I, cause atypical Singleton-Merten syndrome. *The American Journal of Human Genetics* **96**:266–274. doi: [10.1016/j.ajhg.2014.11.019](https://doi.org/10.1016/j.ajhg.2014.11.019)
- Jiang F**, Ramanathan A, Miller MT, Tang G-Q, Gale M, Patel SS, Marcotrigiano J. 2011. Structural basis of RNA recognition and activation by innate immune receptor RIG-I. *Nature* **479**:423–427. doi: [10.1038/nature10537](https://doi.org/10.1038/nature10537)
- Kato H**, Takeuchi O, Mikamo-Sato E, Hirai R, Kawai T, Matsushita K, Hiiragi A, Dermody TS, Fujita T, Akira S. 2008. Length-dependent recognition of double-stranded ribonucleic acids by retinoic acid-inducible gene I and melanoma differentiation-associated gene 5. *Journal of Experimental Medicine* **205**:1601–1610. doi: [10.1084/jem.20080091](https://doi.org/10.1084/jem.20080091)
- Kohlway A**, Luo D, Rawling DC, Ding SC, Pyle AM. 2013. Defining the functional determinants for RNA surveillance by RIG-I. *EMBO Reports* **14**:772–779. doi: [10.1038/embor.2013.108](https://doi.org/10.1038/embor.2013.108)
- Konarev PV**, Petoukhov MV, Volkov VV, Svergun DI. 2006. ATSAS 2.1, a program package for small-angle scattering data analysis. *Journal of Applied Crystallography* **39**:277–286. doi: [10.1107/S0021889806004699](https://doi.org/10.1107/S0021889806004699)

- Kossinova O**, Malygin A, Krol A, Karpova G. 2014. The SBP2 protein central to selenoprotein synthesis contacts the human ribosome at expansion segment 7L of the 28S rRNA. *RNA* **20**:1046–1056. doi: [10.1261/rna.044917.114](https://doi.org/10.1261/rna.044917.114)
- Kowalinski E**, Lunardi T, McCarthy AA, Louber J, Brunel J, Grigorov B, Gerlier D, Cusack S. 2011. Structural basis for the activation of innate immune pattern-recognition receptor RIG-I by viral RNA. *Cell* **147**:423–435. doi: [10.1016/j.cell.2011.09.039](https://doi.org/10.1016/j.cell.2011.09.039)
- Liddicoat BJ**, Piskol R, Chalk AM, Ramaswami G, Higuchi M, Hartner JC, Li JB, Seeburg PH, Walkley CR. 2015. RNA editing by ADAR1 prevents MDA5 sensing of endogenous dsRNA as nonself. *Science* **349**:1115–1120. doi: [10.1126/science.aac7049](https://doi.org/10.1126/science.aac7049)
- Liu G**, Park H-S, Pyo H-M, Liu Q, Zhou Y, Lyles DS. 2015. Influenza A virus panhandle structure is directly involved in RIG-I activation and interferon induction. *Journal of Virology* **89**:6067–6079. doi: [10.1128/JVI.00232-15](https://doi.org/10.1128/JVI.00232-15)
- Loerke J**, Giesebrecht J, Spahn CMT. 2010. Multiparticle cryo-EM of ribosomes. *Methods Enzymol* **483**:161–177. doi: [10.1016/S0076-6879\(10\)83008-3](https://doi.org/10.1016/S0076-6879(10)83008-3)
- Louber J**, Brunel J, Uchikawa E, Cusack S, Gerlier D. 2015. Kinetic discrimination of self/non-self RNA by the ATPase activity of RIG-I and MDA5. *BMC Biology* **13**. doi: [10.1186/s12915-015-0166-9](https://doi.org/10.1186/s12915-015-0166-9)
- Luo D**, Ding SC, Vela A, Kohlway A, Lindenbach BD, Pyle AM. 2011. Structural insights into RNA recognition by RIG-I. *Cell* **147**:409–422. doi: [10.1016/j.cell.2011.09.023](https://doi.org/10.1016/j.cell.2011.09.023)
- Malathi K**, Dong B, Gale M, Silverman RH. 2007. Small self-RNA generated by RNase I amplifies antiviral innate immunity. *Nature* **448**:816–819. doi: [10.1038/nature06042](https://doi.org/10.1038/nature06042)
- Myong S**, Cui S, Cornish PV, Kirchhofer A, Gack MU, Jung JU, Hopfner K-P, Ha T. 2009. Cytosolic viral sensor RIG-I is a 5'-triphosphate-dependent translocase on double-stranded RNA. *Science* **323**:1070–1074. doi: [10.1126/science.1168352](https://doi.org/10.1126/science.1168352)
- Pandey S**, Kawai T, Akira S. 2015. Microbial sensing by toll-like receptors and intracellular nucleic acid sensors. *Cold Spring Harbor Perspectives in Biology* **7**:a016246. doi: [10.1101/cshperspect.a016246](https://doi.org/10.1101/cshperspect.a016246)
- Parks CL**, Lerch RA, Walpita P, Sidhu MS, Udem SA. 1999. Enhanced measles virus cDNA rescue and gene expression after heat shock. *Journal of Virology* **73**:3560–3566.
- Patel JR**, Jain A, Chou Yi-ying, Baum A, Ha T, García-Sastre A. 2013. ATPase-driven oligomerization of RIG-I on RNA allows optimal activation of type-I interferon. *EMBO Reports* **14**:780–787. doi: [10.1038/embor.2013.102](https://doi.org/10.1038/embor.2013.102)
- Peisley A**, Wu B, Xu H, Chen ZJ, Hur S. 2014. Structural basis for ubiquitin-mediated antiviral signal activation by RIG-I. *Nature* **509**:110–114. doi: [10.1038/nature13140](https://doi.org/10.1038/nature13140)
- Petersen EF**, Goddard TD, Huang CC, Couch GS, Greenblatt DM, Meng EC, Ferrin TE. 2004. UCSF chimera – a visualization system for exploratory research and analysis. *Journal of Computational Chemistry* **25**:1605–1612. doi: [10.1002/jcc.20084](https://doi.org/10.1002/jcc.20084)
- Pfaller CK**, Conzelmann K-K. 2008. Measles virus V protein is a decoy substrate for I $\kappa$ B kinase and prevents toll-like receptor 7/9-mediated interferon induction. *Journal of Virology* **82**:12365–12373. doi: [10.1128/JVI.01321-08](https://doi.org/10.1128/JVI.01321-08)
- Pfaller CK**, Radeke MJ, Cattaneo R, Samuel CE. 2014. Measles virus C protein impairs production of defective copyback double-stranded viral RNA and activation of protein kinase R. *Journal of Virology* **88**:456–468. doi: [10.1128/JVI.02572-13](https://doi.org/10.1128/JVI.02572-13)
- Pichlmair A**, Schulz O, Tan C-P, Rehwinkel J, Kato H, Takeuchi O, Akira S, Way M, Schiavo G, Reis e Sousa C. 2009. Activation of MDA5 requires higher-order RNA structures generated during virus infection. *Journal of Virology* **83**:10761–10769. doi: [10.1128/JVI.00770-09](https://doi.org/10.1128/JVI.00770-09)
- Pichlmair A**, Schulz O, Tan CP, Naslund TI, Liljestrom P, Weber F, Reis e Sousa C. 2006. RIG-I-mediated antiviral responses to single-stranded RNA bearing 5'-phosphates. *Science* **314**:997–1001. doi: [10.1126/science.1132998](https://doi.org/10.1126/science.1132998)
- Radecke F**, Spielhofer P, Schneider H, Kaelin K, Huber M, Dötsch C, Christiansen G, Billeter MA. 1995. Rescue of measles viruses from cloned DNA. *The EMBO Journal* **14**.
- Rice GI**, del Toro Duany Y, Jenkinson EM, Forte GMA, Anderson BH, Ariaudo G, Bader-Meunier B, Baildam EM, Battini R, Beresford MW, Casarano M, Chouchane M, Cimaz R, Collins AE, Cordeiro NJV, Dale RC, Davidson JE, De Waele L, Desguerre I, Faivre L, Fazzi E, Isidor B, Lagae L, Latchman AR, Lebon P, Li C, Livingston JH, Lourenço CM, Mancardi MM, Masurel-Paulet A, McInnes IB, Menezes MP, Mignot C, O'Sullivan J, Orcesi S, Picco PP, Riva E, Robinson RA, Rodriguez D, Salvatici E, Scott C, Szybowska M, Tolmie JL, Vanderver A, Vanhulle C, Vieira JP, Webb K, Whitney RN, Williams SG, Wolfe LA, Zuberi SM, Hur S, Crow YJ. 2014. Gain-of-function mutations in IFIH1 cause a spectrum of human disease phenotypes associated with upregulated type I interferon signaling. *Nature Genetics* **46**:503–509. doi: [10.1038/ng.2933](https://doi.org/10.1038/ng.2933)
- Rozen F**, Pelletier J, Trachsel H, Sonenberg N. 1989. A lysine substitution in the ATP-binding site of eucaryotic initiation factor 4A abrogates nucleotide-binding activity. *Molecular and Cellular Biology* **9**:4061–4063. doi: [10.1128/MCB.9.9.4061](https://doi.org/10.1128/MCB.9.9.4061)
- Runge S**, Sparrer KMJ, Lässig C, Hembach K, Baum A, García-Sastre A, Söding J, Conzelmann K-K, Hopfner K-P, Mossman KL. 2014. In vivo ligands of MDA5 and RIG-I in measles virus-infected cells. *PLoS Pathogens* **10**:e1004081. doi: [10.1371/journal.ppat.1004081](https://doi.org/10.1371/journal.ppat.1004081)
- Rutsch F**, MacDougall M, Lu C, Buers I, Mamaeva O, Nitschke Y, Rice GI, Erlandsen H, Kehl HG, Thiele H, Nürnberg P, Höhne W, Crow YJ, Feigenbaum A, Hennekam RC. 2015. A specific IFIH1 gain-of-function mutation causes Singleton-Merten syndrome. *The American Journal of Human Genetics* **96**:275–282. doi: [10.1016/j.ajhg.2014.12.014](https://doi.org/10.1016/j.ajhg.2014.12.014)

- Satoh T**, Kato H, Kumagai Y, Yoneyama M, Sato S, Matsushita K, Tsujimura T, Fujita T, Akira S, Takeuchi O. 2010. LGP2 is a positive regulator of RIG-I- and MDA5-mediated antiviral responses. *Proceedings of the National Academy of Sciences of the United States of America* **107**:1512–1517. doi: [10.1073/pnas.0912986107](https://doi.org/10.1073/pnas.0912986107)
- Schlee M**, Roth A, Hornung V, Hagmann CA, Wimmenauer V, Barchet W, Coch C, Janke M, Mihailovic A, Wardle G, Juraneck S, Kato H, Kawai T, Poeck H, Fitzgerald KA, Takeuchi O, Akira S, Tuschl T, Latz E, Ludwig J, Hartmann G. 2009. Recognition of 5' triphosphate by RIG-I helicase requires short blunt double-stranded RNA as contained in panhandle of negative-strand virus. *Immunity* **31**:25–34. doi: [10.1016/j.immuni.2009.05.008](https://doi.org/10.1016/j.immuni.2009.05.008)
- Schmidt A**, Schwerdt T, Hamm W, Hellmuth JC, Cui S, Wenzel M, Hoffmann FS, Michallet M-C, Besch R, Hopfner K-P, Endres S, Rothenfusser S. 2009. 5'-triphosphate RNA requires base-paired structures to activate antiviral signaling via RIG-I. *Proceedings of the National Academy of Sciences of the United States of America* **106**:12067–12072. doi: [10.1073/pnas.0900971106](https://doi.org/10.1073/pnas.0900971106)
- Schnell G**, Loo Y-M, Marcotrigiano J, Gale M, Mossman KL. 2012. Uridine composition of the poly-U/UC tract of HCV RNA defines non-self recognition by RIG-I. *PLoS Pathogens* **8**:e1002839. doi: [10.1371/journal.ppat.1002839](https://doi.org/10.1371/journal.ppat.1002839)
- Schuberth-Wagner C**, Ludwig J, Bruder AK, Herzner A-M, Zillinger T, Goldeck M, Schmidt T, Schmid-Burgk JL, Kerber R, Wolter S, Stümpel J-P, Roth A, Bartok E, Drosten C, Coch C, Hornung V, Barchet W, Kümmerer BM, Hartmann G, Schlee M. 2015. A conserved histidine in the RNA sensor RIG-I controls immune tolerance to N1-2'-O-methylated self RNA. *Immunity* **43**:41–51. doi: [10.1016/j.immuni.2015.06.015](https://doi.org/10.1016/j.immuni.2015.06.015)
- Sparrer KMJ**, Gack MU. 2015. Intracellular detection of viral nucleic acids. *Current Opinion in Microbiology* **26**:1–9. doi: [10.1016/j.mib.2015.03.001](https://doi.org/10.1016/j.mib.2015.03.001)
- Sparrer KMJ**, Pfaller CK, Conzelmann K-K. 2012. Measles virus C protein interferes with beta interferon transcription in the nucleus. *Journal of Virology* **86**:796–805. doi: [10.1128/JVI.05899-11](https://doi.org/10.1128/JVI.05899-11)
- Wang Y**, Ludwig J, Schuberth C, Goldeck M, Schlee M, Li H, Juraneck S, Sheng G, Micura R, Tuschl T, Hartmann G, Patel DJ. 2010. Structural and functional insights into 5'-ppp RNA pattern recognition by the innate immune receptor RIG-I. *Nature Structural & Molecular Biology* **17**:781–787. doi: [10.1038/nsmb.1863](https://doi.org/10.1038/nsmb.1863)
- Weber M**, Gawanbacht A, Habjan M, Rang A, Borner C, Schmidt AM, Veitinger S, Jacob R, Devignot S, Kochs G, García-Sastre A, Weber F. 2013. Incoming RNA virus nucleocapsids containing a 5'-triphosphorylated genome activate RIG-I and antiviral signaling. *Cell Host & Microbe* **13**:336–346. doi: [10.1016/j.chom.2013.01.012](https://doi.org/10.1016/j.chom.2013.01.012)
- Wu B**, Peisley A, Tetrault D, Li Z, Egelman EH, Magor KE, Walz T, Penczek PA, Hur S. 2014. Molecular imprinting as a signal-activation mechanism of the viral RNA sensor RIG-I. *Molecular Cell* **55**:511–523. doi: [10.1016/j.molcel.2014.06.010](https://doi.org/10.1016/j.molcel.2014.06.010)
- Wu J**, Chen ZJ. 2014. Innate immune sensing and signaling of cytosolic nucleic acids. *Annual Review of Immunology* **32**:461–488. doi: [10.1146/annurev-immunol-032713-120156](https://doi.org/10.1146/annurev-immunol-032713-120156)
- Xu H**, He X, Zheng H, Huang LJ, Hou F, Yu Z, de la Cruz MJ, Borkowski B, Zhang X, Chen ZJ, Jiang Q-X. 2014. Structural basis for the prion-like MAVS filaments in antiviral innate immunity. *eLife* **3**:e01489. doi: [10.7554/eLife.01489](https://doi.org/10.7554/eLife.01489)
- Yao H**, Dittmann M, Peisley A, Hoffmann H-H, Gilmore RH, Schmidt T, Schmid-Burgk JL, Hornung V, Rice CM, Hur S. 2015. ATP-dependent effector-like functions of RIG-I-like receptors. *Molecular Cell* **58**:541–548. doi: [10.1016/j.molcel.2015.03.014](https://doi.org/10.1016/j.molcel.2015.03.014)
- Yoneyama M**, Kikuchi M, Natsukawa T, Shinobu N, Imaizumi T, Miyagishi M, Taira K, Akira S, Fujita T. 2004. The RNA helicase RIG-I has an essential function in double-stranded RNA-induced innate antiviral responses. *Nature Immunology* **5**:730–737. doi: [10.1038/ni1087](https://doi.org/10.1038/ni1087)
- Zhang H-X**, Liu Z-X, Sun Y-P, Zhu J, Lu S-Y, Liu X-S, Huang Q-H, Xie Y-Y, Zhu H-B, Dang S-Y, Chen H-F, Zheng G-Y, Li Y-X, Kuang Y, Fei J, Chen S-J, Chen Z, Wang Z-G, Lu SY, Liu XS, Huang QH, Xie YY, Zhu HB, Dang SY. 2013. RIG-I regulates NF- $\kappa$ B activity through binding to nf-kappab1 3'-UTR mRNA. *Proceedings of the National Academy of Sciences of the United States of America* **110**:6459–6464. doi: [10.1073/pnas.1304432110](https://doi.org/10.1073/pnas.1304432110)
- Zhu J**, Zhang Y, Ghosh A, Cuevas RA, Forero A, Dhar J, Ibsen MS, Schmid-Burgk JL, Schmidt T, Ganapathiraju MK, Fujita T, Hartmann R, Barik S, Hornung V, Coyne CB, Sarkar SN. 2014. Antiviral activity of human OASL protein is mediated by enhancing signaling of the RIG-I RNA sensor. *Immunity* **40**:936–948. doi: [10.1016/j.immuni.2014.05.007](https://doi.org/10.1016/j.immuni.2014.05.007)

# Discussion

## 1 Discrimination of self vs non-self by RIG-I and MDA5

### 1.1 What are physiological ligands of RIG-I and MDA5?

One of the main unsolved questions within the field of RIG-I like receptors is still addressing *in vivo* occurring ligands of RIG-I and MDA5. Even though several *in vitro* experiments successfully defined optimal RNA substrates for both proteins, data under infectious conditions are so far only sparse and often raise more questions than they answer. Regarding the present knowledge, how do RIG-I and MDA5 ligands look like? When, if ever, do they occur *in vivo*? And how does the cell protect itself from generating these ligands?

Optimal RIG-I ligands are described as short blunt-ended dsRNA containing 5' tri- or diphosphates<sup>265,266</sup>. Naturally such RNAs could occur within the nucleus, but are typically masked before they are transported to the cytosol. mRNAs modifications that are believed to abolish cytosolic immune activation include capping of the 5' end with a guanosine residue methylated at N<sub>7</sub>, and methylation of the first 5' nucleotide ribose<sup>267</sup>. Methylation of the 5' cap is mainly important for translation initiation and was recently shown to only partly suppress RIG-I activation<sup>105</sup>. This is due to the flexible incorporation of the cap within RIG-I's CTD where contacts to the RNA were demonstrated to be limited to the  $\alpha$  and  $\beta$ -phosphates<sup>105,109</sup>. In this regard, capped but unmethylated RNA have been shown to fully activate RIG-I similar to non-capped triphosphorylated RNA<sup>105</sup> (compare to Figure 4). Methylation of the first 5' nucleotide however, effectively inactivates RIG-I-dependent signaling by introducing a steric clash with the CTD<sup>105</sup>. This efficiently prevents binding of RIG-I to folded mRNA 5' ends or even capturing of mRNAs by the RIG-I CTD. Other potential endogenous ligands like tRNAs are cleaved to produce 5' monophosphate ends<sup>268</sup> and ribosomal RNA is mainly masked by ribonucleoprotein complexes and modified ribonucleotides. Furthermore, miRNAs and siRNAs generated by Dicer have a characteristic 2 nucleotide 3' overhang which is unfavorable for RIG-I end recognition<sup>269</sup>.

During viral infections however, viruses often fail to entirely mask their own RNA and thereby produce species that can be detected by RLRs. Potential RIG-I ligands are the incoming viral genome in the first place<sup>105,117</sup>, but as well replication intermediates or defective interfering genomes harboring 5' triphosphates<sup>119,135</sup>. Nevertheless, more and more evidence, including our own study, also points towards 5' triphosphate independent recognition of viral RNA like internal mRNAs regions and parts of the 3' UTRs<sup>114,122,123,135</sup>. In this regard, also short RNAs generated by RNase L through

cleavage of U-rich cytosolic RNA have been described as RIG-I ligands<sup>115,116</sup>.

Sensing of these ligands happens primarily via a basic surface on the RIG-I CTD and its RNA end-capping loop that provides a strong specificity towards the di- or triphosphate. However, also other RIG-I domains help ensure specificity: The CARDs:domain 2b interface aids in discrimination of blunt-ended and non blunt-ended dsRNA or ssRNA, since it prevents the generation of productive protein:RNA complexes that do not have a high affinity tether towards the CTD<sup>108,109</sup>. In addition, the SF2 helicase domain lowers the general affinity towards dsRNA stems, thereby raising the specificity towards RNA ends as well (discussed in detail in discussion section 2).

The optimal MDA5 ligand, on the other hand, is long dsRNA without bulges and regardless of the presence of a tri- or diphosphate end<sup>270</sup>. The more general appearance of MDA5 ligands without a characteristic feature like phosphate-containing ends, as for instance RIG-I ligands have, renders this RLR more prone to the recognition of endogenous RNA. Most cellular RNAs, however, only contain short dsRNA regions and even if longer parts occur, base pairing is effectively destabilized by converting adenosine ribonucleotides to inosine by ADAR1<sup>234</sup>. This is further supported by the fact that loss of A-to-I editing results in embryonic death through the induction of an autoimmune response against self-RNA by MDA5<sup>235</sup>. Other potential endogenous MDA5 ligands could arise from short interspersed nucleotide elements (SINEs) like repetitive Alu elements that constitute up to 10% of the human genome and that can occur within introns or other non-coding regions of transcripts<sup>271</sup>. Alu elements are approximately 300 bases long, contain an A-rich region and are, if present within inverted repeats, ideal MDA5, but also ADAR, substrates<sup>272</sup>. A-to-I editing and the subsequent loss of base pairing might therefore prevent MDA5-dependent signaling.

Consistent with the preference for long dsRNA stems, viral MDA5 agonists have been found to be for instance the replicative form of viruses<sup>273</sup>. Furthermore, and similar to RIG-I, several sense or anti-sense transcripts were found to be recognized in virus-infected cells by deep sequencing of MDA5 associated RNA<sup>95,123,135</sup>. However, since MDA5 does not signal on ssRNA, the identified transcripts might harbor yet unrecognized double-stranded regions. With conventional RNA folding software, nevertheless, so far no connection between length of potential dsRNA parts and sequencing reads could be established, leaving room for speculations about non-cooperative MDA5 binding and signaling.

In addition, besides RNA length, also AU composition of viral RNA was suggested to have an influence on MDA5 recognition<sup>135</sup>. In the same context, also an decreased ATPase activity of MDA5 upon recognition of AU-rich transcript was found. Since so far no base-specific recognition of MDA5 could be detected within any structural protein analysis, one could speculate, that less stable AU-rich sequences might more likely partially melt, leading to a slow-down of MDA5 translocation. Hereof, any RNA structure that disfavors ATP hydrolysis by at the same time preserving RNA binding might lead to prolonged protein:RNA interactions and therefore to increased immune signaling. Nevertheless, the exact mechanism of MDA5 signaling on shorter dsRNA stems still remains to be analyzed.

## 1.2 Is RIG-I's CTD able to bind dsRNA stems?

A still controversial question within RIG-I *in vivo*-functioning concerns the ability of the protein to bind dsRNA stems similar to MDA5. This, however, is a prerequisite for translocation or binding at internal dsRNA parts without proper end. Whereas different crystal structures of RLRs show interactions of the SF2 domain exclusively with the RNA backbone, the relative CTD position varies<sup>60–62,109,144,145</sup>. All so far published RIG-I:RNA complexes show an RNA end-capping mode of RIG-I's CTD via a positively charged loop that encloses the phosphate groups and stacks to the terminal base pair<sup>61,109</sup>. For MDA5, on the other hand, data showing both RNA end-binding as well as recognition of the dsRNA stem are available<sup>144,145</sup>. In all MDA5:RNA crystal structures, however, the end-capping loop, is found to be disordered. This might be convincing since, the end-capping loop of MDA5, contrary to RIG-I, lacks the aromatic amino acids required for base stacking of the RNA end as well as the lysines contacting the phosphates. This suggests, that when MDA5 accommodates dsRNA stems, this loop has an increased flexibility compared to the end-capping loop of RIG-I.

NMR titration experiments of dsRNA to isolated RIG-I and MDA5 CTDs further report different binding modes of these domains<sup>146,274</sup>: Whereas in solution, the RIG-I CTD was found to bind RNA ends via the end-capping loop as well, the MDA5 CTD was shown to sequester the dsRNA stem via its flat surface. Further, biochemical assays and electron microscopy confirm MDA5 stem binding on long double-stranded RNA<sup>130,149</sup> and the preference of RIG-I for (phosphorylated) dsRNA ends<sup>102,103</sup>.

However, all isolated CTDs are found to adopt similar conformations in solution if no RNA is bound (Figure 17)<sup>146,274</sup>, arguing for an intrinsic flexibility of the CTDs that might allow different conformations according to the appropriate RNA substrate. More and more recent data also point to the ability of RIG-I to translocate and oligomerize on dsRNA stems<sup>110,198,199</sup>. Co-immunoprecipitation studies of RIG-I from different virus-infected or uninfected cells further identified binding sites distant from dsRNA-ends indicating that RIG-I might indeed be able to bind dsRNA stems<sup>123,135,275</sup>. A

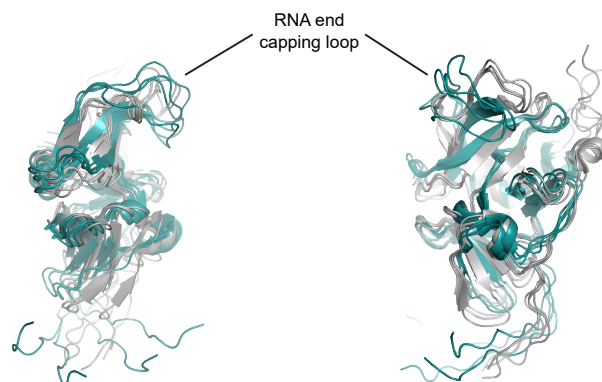


**Figure 17:** Comparison of RIG-I (cyan, RCSB PDB code 2rmj, human) and MDA5 (gray, RCSB PDB code 2rqb, human) CTD NMR structures in solution without presence of RNA. Each 4 out of 20 NMR structures are depicted. The overall root mean square deviation of all RIG-I structures compared to all MDA5 structures equals 2.5 Å as calculated with pymol.

binding mode of the RIG-I CTD similar to the MDA5 CTD might thus be conceivable, but would need to shift the whole domain towards the dsRNA stem followed by an enforced alteration within the RNA capping loop. Nevertheless, structural data supporting the RIG-I stem binding hypothesis are mostly lacking.

In the same regard, also the RIG-I footprint is currently not exactly known and ranges from 8 to 10 nucleotides depending on the crystal structure<sup>61,113</sup>. Otherwise, RIG-I's footprint was suggested to be as small as 6 to 7 nucleotides as known for other SF2 helicases<sup>276</sup>. *In vitro* studies further showed, that even though an 8mer ppp-dsRNA is stably bound by RIG-I via the SF2 helicase domain and CTD, the CARD2:domain 2b interface is not allosterically disrupted<sup>106</sup>. Since those experiments were done in absence of ATP, however, one cannot exclude that ATP binding-dependent structural changes might reduce a potential footprint below 8 nucleotides. The structural integrity of such an RNA under *in vivo* temperature conditions however remains questionable.

Nevertheless, knowledge of the precise minimal binding unit of RIG-I on RNA might help design dsRNA oligos suitable to address questions concerning a RIG-I RNA-stem binding mode.

## 2 What role has ATP in RIG-I-like receptor signaling?

Another question in the field of RLRs addresses the SF2 domain and its ATPase function upon binding to double-stranded RNA. Why do RLRs hydrolyze ATP? Would it not be easier to just release the CARD domains as soon as a suitable ligand is found? Already with the discovery of RIG-I it became clear, that blocking of the ATPase function impedes signaling of the protein<sup>72</sup>. But how is an immune response triggered by RIG-I connected to the ability to hydrolyze ATP? And is it the same for MDA5? Nevertheless, despite intense biochemical and cellular studies over the last years, the exact function of the RLR ATPase domain remained puzzling and only recently it started to be understood.

Several RIG-I constructs co-crystallized with different ATP analogues or ADP and RNA captured different protein conformations during the ATP hydrolysis cycle (Figure 18). Thereby, the main difference in all RIG-I structures is due to different orientations of both domain 1a and 2a to each other depending on the used ATP analogue. This apparent movement of the SF2 domain is further accompanied by changes of the orientation of the insertion domain 2b. The RIG-I CTD however, is so far only caught in one distinct orientation relative to the dsRNA, independent of the presence of a triphosphate or other dsRNA termini.

Recently, three independent groups, including us, dissected the role of ATP binding vs. ATP hydrolysis for the RIG-I immune response by mutating different key amino acids in the Walker A and B motifs, respectively<sup>275,277,278</sup>. Thereby, the Walker A motif lysine (RIG-I K270) was exchanged to a neutral or even acidic amino acid (e.g. alanine, isoleucine or glutamic acid) in order to decrease ATP binding. The ATP bound state, in contrast, was assessed by disturbing the activation of the catalytic water through conversion of a glutamic acid residue of the Walker B motif to glutamine. Thus magnesium binding by neighboring Walker B residues as well as ATP binding stays intact, but ATP hydrolysis is

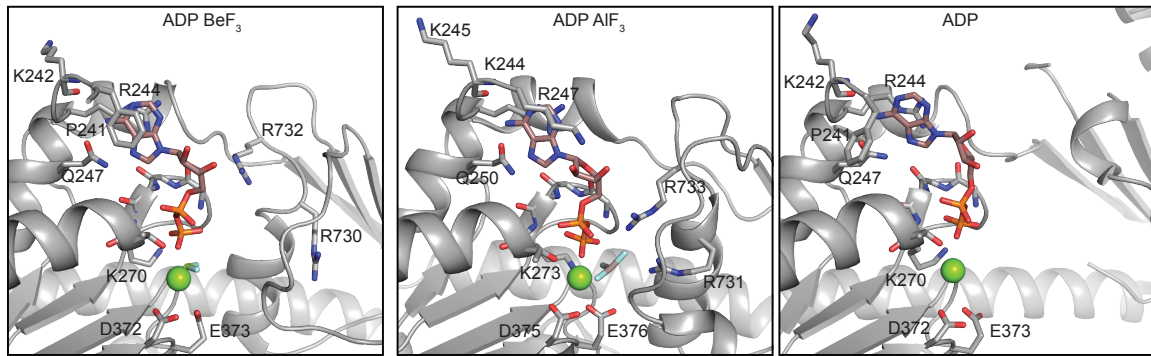


**Figure 18:** Residues involved in coordination of ATP during different states of hydrolysis in RIG-I. ADP·BeF<sub>3</sub> (RCSB PDB code 3tmi, human) resembles the ATP bound state, ADP·AlF<sub>3</sub> (RCSB PDB code 4a36, duck) corresponds to the ATP hydrolysis transition state and ADP (RCSB PDB code 3zd7, human) resembles the reaction product state.

slowed down. This is in contrast to the earlier used aspartate mutation within Walker B motifs that mainly disturbs magnesium ion coordination: Loss of magnesium within the ATP binding pocket, however, disturbs ATP binding as well and therefore is indistinguishable to a Walker A mutation.

Interestingly through different experiments all three studies showed, that ATP binding and hydrolysis for RIG-I and MDA5 have opposing cellular effects: Recognition of both RNA and ATP by RIG-I, or RNA only by MDA5, are sufficient to induce signaling. ATP hydrolysis, in contrast, destabilizes the RLR:RNA complexes and leads to RNA disengagement of the SF2 helicase domain, thereby testing the substrate interactions with the CTD<sup>106,275,277</sup>.

## 2.1 RNA and ATP binding liberate the RIG-I CARDS, whereas MDA5 activation needs RNA only

Blocking of ATP binding in RIG-I through a Walker A lysine mutation in cellular studies with over-expressed proteins resulted in reduced or abrogated signaling even in presence of stimulating RNA or Sendai virus defective interfering genomes<sup>275,277,278</sup>. Interestingly, ATP binding assays of RIG-I K270A/R mutants showed an only two-fold reduced affinity of the protein towards ATP, whereas hydrolysis activity was abolished as expected<sup>278</sup>. RNA binding properties, in contrast, are not altered<sup>73,279</sup>. Immune response signaling on the other hand, as monitored by IRF3 dimerization as well as binding of free ubiquitin chains was shown to be prevented in cell-free systems mimicking viral infections<sup>168</sup>. Thus abrogation or impeding of ATP binding leads to loss of immune signaling, probably through disrupted CARDS release, even in presence of bound RNA. In accordance with this, published crystal structures of RIG-I:RNA complexes bound to ADP with an open helicase state<sup>280</sup> as well as RIG-I with sequestered CARDS to domain 2b<sup>61</sup> can be superimposed without introducing any clash between different domains<sup>192</sup>.

Contrary to RIG-I, the MDA5 CARDS do not entirely fold back to domain 2b and are already partially released even without binding to RNA and ATP as shown in SAXS and deuterium exchange measurements<sup>106,149</sup>. Further, overexpression of MDA5 in cells is already sufficient to induce signaling<sup>73</sup>.

Full activation of an immune response by MDA5 is nevertheless dependent on cooperative MDA5 oligomerization on long dsRNA stretches<sup>130</sup>.

The function of ATP binding in MDA5 signaling might thus differ from RIG-I. In accordance with this and contrary to RIG-I, mutations that disrupt ATP binding are shown to result in constitutive signaling<sup>200,277</sup>. This can be reversed, similar to RIG-I, by additionally disrupting RNA binding sites within the MDA5 SF2 like helicase domain or by abrogating the RNA driven self-assembly of MDA5<sup>277</sup>. Interestingly, a double mutation of the Walker A motif as well as an RNA binding residue within the CTD cannot impede signaling, emphasizing a comparably smaller contribution of the MDA5 CTD towards RNA binding.

## 2.2 ATP hydrolysis by RIG-I and MDA5 impedes signaling on endogenous RNA

Recently, the ATP hydrolysis activity of MDA5's and RIG-I's SF2 helicase domains was found to be required to avoid activation by self-RNA<sup>275,277,278</sup>. In this regard, RIG-I shows enhanced dissociation kinetics for varying RNA substrates already in presence of ADP or the non-hydrolyzable ATP analogue ATP $\gamma$ S *in vitro*<sup>278</sup>.

RIG-I trapped in the ATP bound state, in contrast, constitutive signaled in cellular overexpression studies regardless if cells are stimulated with RIG-I ligands or not<sup>275,277</sup>. Signaling is dependent on RNA binding, since the additional insertion of RNA binding mutations in both helicase or CTD results in loss of signaling<sup>275,277</sup>. Structural changes of the protein that could result in constant CARDs-release without RNA stimulus were ruled-out by SAXS and thermofluor experiments as well as by cellular competition assays with a CARD-less RIG-I construct. Furthermore, co-immunoprecipitation studies revealed an expansion segment of the large ribosomal subunit as a possible abundant endogenous ligand, that might be responsible for the immune response<sup>275</sup>. The relevance of this ligand was further highlighted by transfection into ATPase-deficient RIG-I-expressing cells. Similar to triphosphorylated dsRNA, this endogenous ligand further enhanced the cell's immune response<sup>275,277</sup>. Nevertheless, the idea that RIG-I could not signal from internal duplexes, since they would not efficiently displace the CTD in order to induce a clash with the CARDs<sup>278</sup>, cannot entirely be rejected: Even though *in vitro* and cellular studies confirm binding of RIG-I in absence of ATP or in presence of an ATP analogue to the dsRNA stem, there is still the possibility, that signaling in cellular assays in fact relies on other endogenous ligands that are recognized as well. Further, increased signaling upon transfection of this RNA into RIG-I Walker B mutant-stimulated cells could be induced due to any other upregulated ISG.

Nevertheless, even though nucleotide binding lowers the RIG-I affinity for RNA substrates, it seems not to be enough to restrict activation of an immune response in cells. Therefore, ATP hydrolysis provides the important mechanisms to avoid signaling on endogenous RNA.

An explanation might be, that ATP hydrolysis contributes a proof reading mechanism, that recycles RIG-I on triphosphorylated RNA ends or promotes its dissociation from supposedly non-pathogenic RNA<sup>111,275,277,278</sup>. The CTD of RIG-I might thus serve as an anchor towards tri- or diphosphorylated

dsRNAs, whose binding strength to the protein is constantly challenged by the SF2 helicase domain which in turn weakens the interactions with the RNA stem<sup>111</sup>. By that, ATP hydrolysis of RIG-I enhances specificity towards viral dsRNA and reduces background binding to endogenous RNA. Accordingly, loss of this feature, like e.g. observed in atypical SMS patients, results in the development of autoimmune diseases against cytosolic self-RNA<sup>247</sup>.

MDA5 signaling in contrast is independent of ATP binding, since both ATP binding and ATP hydrolysis-deficient mutants were found to induce a constitutive immune response<sup>277</sup>. Nevertheless, *in vitro* filament formation of MDA5 was shown by electron microscopy to be stabilized in presence of the ATP analogue ADP·AIF<sub>x</sub><sup>281</sup> and in addition ATPase-deficient MDA5 co-purifies with the big ribosomal subunit<sup>275</sup>. Similar to RIG-I, ATP hydrolysis of MDA5 thus seems to be important to disengage MDA5:RNA complexes and to prevent a continuous response<sup>149</sup>. Thereby contrary to RIG-I, not the MDA5 CTD provides the RNA anchor but rather oligomerization on long RNA stems provides the stability needed for signaling.

### 2.3 ATP influences LGP2's regulatory function

In contrast to MDA5 and RIG-I, only limited data concerning the ATP dependency of LGP2 is available. LGP2 is thought to possess regulatory functions in RLR signaling in general<sup>170</sup>. Cellular over-expression assays showed, that low amounts of LGP2 enhance MDA5-dependent signaling, while higher levels of LGP2 inhibit an immune response of both RIG-I and MDA5<sup>94,281</sup>. The increase of MDA5-dependent signaling through LGP2 is realized by attenuating the length of MDA5 filaments<sup>281</sup>. These shorter, but more numerous polymers seem to have higher signal-transducing abilities than longer filaments. Interestingly, LGP2's positive regulatory role depends on the availability of ATP, since ATP binding-deficient LGP2 (Walker A mutant) only retains the ability to inhibit signaling at higher concentrations<sup>97,281</sup>. In addition, the LGP2 Walker A mutant severely suppresses RIG-I signaling even upon transfection with RIG-I ligands<sup>281</sup>.

Since LGP2 lacks the CARDs for immune response signaling, an ATP binding-dependent molecular switch, similar to RIG-I, upon RNA binding might not be necessary. Rather ATP hydrolysis could be important to destabilize the protein:RNA interactions, as in the case of RIG-I and MDA5. This might allow either translocation on long dsRNA and thereby aid in MDA5 cooperative binding, or enhance RNA end recognition in order to turn off an RIG-I mediated immune response<sup>282</sup>. Further, LGP2 was found to have increased RNA recognition abilities in presence of ATP *in vitro*<sup>98</sup>. This could have a broad effect on different cellular RNAs as well, thereby affecting both RIG-I and MDA5 during later stages of infection and in the presence of higher cellular levels of LGP2.

In addition, ATP hydrolysis might drive effector like functions of LGP2 similar to those suggested for RIG-I and MDA5<sup>200</sup> in order to release dsRNA-bound viral factors or even other RLRs and to stop an immune response.

Nevertheless, the effect of ATP onto LGP2's regulatory function is so far less understood and requires further analysis.

### 3 Translocation of RLRs: a model based on the Hepatitis C virus NS3 protein

Related to the ability of RLRs to hydrolyze ATP and due to their assignment to Superfamily 2 helicases, another question concerning their ability to move on RNA emerged. Are RLRs able to translocate on dsRNA? Biochemical studies, mainly conducted on RIG-I, suggested that it binds via the CTD to the 5' triphosphate end of dsRNA and then subsequently moves into the RNA interior in an ATP-dependent manner<sup>110,198,199</sup>. This process might be required to achieve oligomerization of several RLRs on one RNA molecule in order to induce the spatial proximity of the RLR CARDs that is needed for their tetramerization and the subsequent signal transfer. Further, as mentioned, translocation-dependent effector-like functions of RIG-I and MDA5 have been described, proposing a displacement of bound proteins or a remodeling of RNA structures<sup>200</sup>.

Nevertheless, the structural basis for an ATP-dependent translocation of RLRs is still lacking. In order to overcome these limitations, a comparison to other SF2 proteins can be done. In this context, one of the best studied SF2 helicases is the viral non-structural protein 3 (NS3) of which structural data on proteins of different viruses, including Dengue virus, Yellow fever virus, Murray Valley encephalitis virus and Hepatitis C virus (HCV), are available<sup>283–289</sup>. Especially in case of the HCV NS3 protein, a precise model can be established based on several biochemical assays combined with structural data of the protein bound to nucleic acids and varying nucleotide analogues representing different ATP hydrolysis states.

The HCV NS3 protein consists of an N-terminal serine protease as well as a C-terminal helicase domain<sup>290</sup>. The helicase domain contains, similar to the corresponding domain of RLRs, two RecA-like domains (domains 1 and 2, corresponding to domains 1a and 2a of RLRs, see Figure 19), between whose interfaces a nucleotide binding pocket is formed, as well as an  $\alpha$ -helical domain 3. In contrast to RLRs, the NS3 helicase domain can hydrolyze any nucleotide upon nucleic acid binding and further has no preference for DNA or RNA substrates<sup>291–293</sup>.

Based on biochemical and structural studies, a canonical translocation and unwinding mechanism has been proposed. According to the model, NS3 binds to single-stranded regions of nucleic acids and then translocates in an ATP-dependent manner nucleotide-wise in 3' to 5' until it reaches double-stranded regions. Duplexes are subsequently unwound by a "spring-loaded" mechanism after each 3 cycles of ATP hydrolysis via the  $\alpha$ -helical domain of NS3<sup>294</sup>. Mechanistically, domains 1 and 2 step from 3' to 5' direction into the duplex interior, whereas the  $\alpha$ -helical domain 3 lags behind, stays placed at the double-stranded end and accumulates tension towards the protein:nucleic acid complex. After three nucleotide steps, i.e. three cycles of ATP hydrolysis, the created tension relieves in a burst of 3 base pairs unwinding.

The movement of NS3 on the nucleic acid backbone can be linked to different ATP hydrolysis states of the protein<sup>288</sup>: In the ATP-unbound state, the NS3 domains 1 and 2 form an open nucleotide binding cleft. Domain 1 contacts the nucleic acid backbone phosphates (p) 1 and p2 (counted from 3' direction), whereas domain 2 captures p3 to p5. Upon binding of ATP to NS3 (which is resembled by the ADP·BeF<sub>3</sub>-bound state) domain 1 moves one nucleotide towards domain 2, now interacting with p2

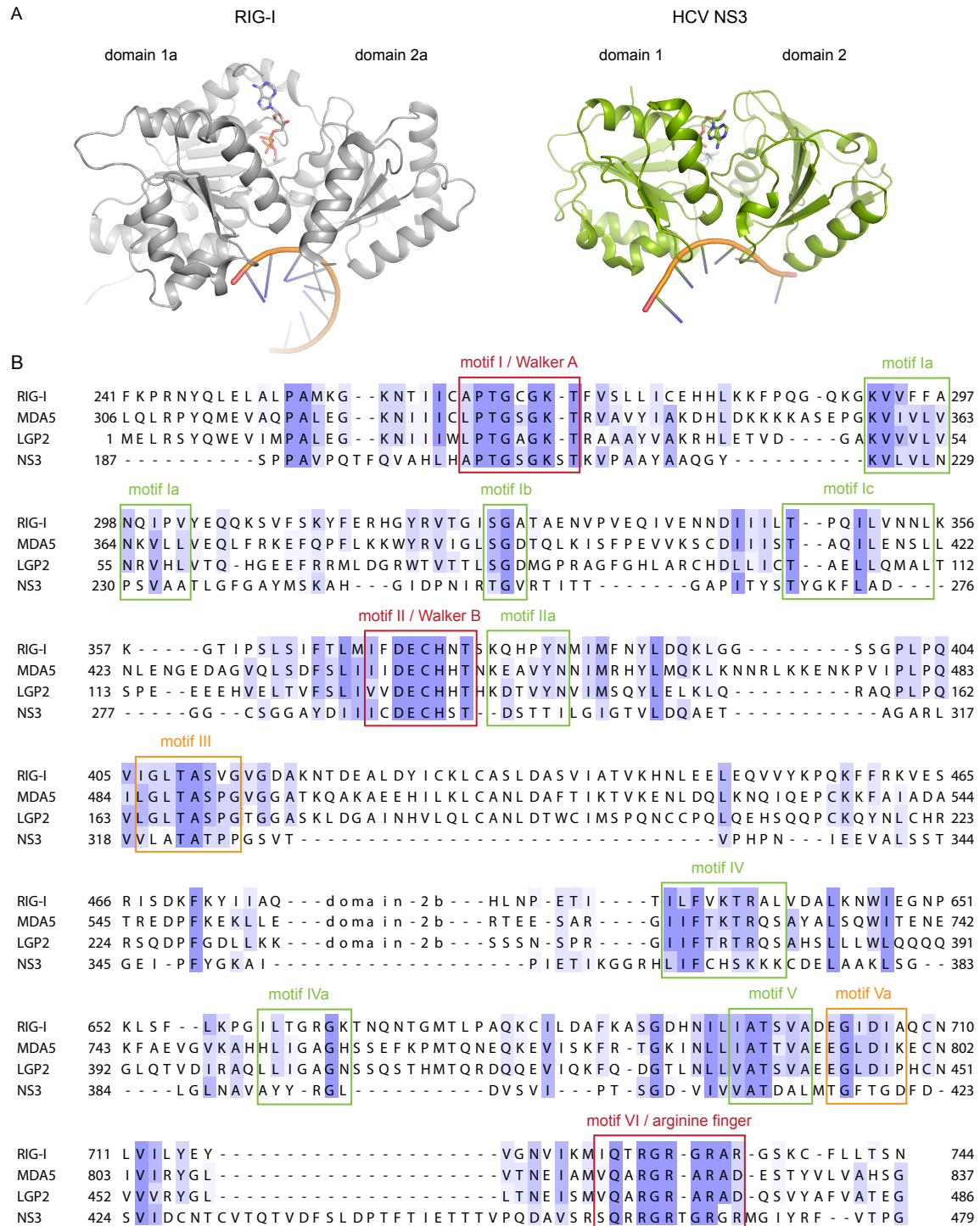


**Figure 19:** Structure and sequence alignment of the SF2 domains of human RLRs and the Hepatitis C virus NS3 protein. (A) Comparison of the RIG-I RecA-like domains 1a and 2a (RCSB PDB code 4a36, duck RIG-I helicase domain) to the NS3 domains 1 and 2 (RCSB PDB code 3kql, HCV NS3). Accessory domains as well as the second RNA strand within the RIG-I structure are hidden for comparison purposes. (B) Sequence alignment of RLRs and HCV NS3 based on a structure alignment of RIG-I and NS3 using pymol. Conserved motifs involved in ATP binding and hydrolysis are marked in red, motifs involved in RNA binding are depicted in green and motifs involved in coupling of ATP hydrolysis to RNA binding are shown in orange (compare with Figure 13).

and p3, whereas domain 2 loses the contact to p3. During the ATP transition state (ADP·AlF<sub>3</sub>-bound state), the distances between domain 1 and the nucleic acid are rearranged, stabilizing the interactions to p2 and p3 via new hydrogen bonds. ATP hydrolysis leads to re-opening of the helicase domain cleft and thereby shifts domain 2 into 5' direction to phosphates p4 to p6.

Since key residues involved in nucleotide hydrolysis, nucleic acid binding and translocation are conserved in SF2 proteins, a similar translocation mechanism might occur in RLRs. In addition, even though RLRs signal only upon binding to double-stranded nucleic acids, domains 1a and 2a almost exclusively contact the bottom RNA strand and could therefore perform a similar movement like NS3. Concerning RIG-I, several binary and ternary structures co-crystallized with RNA and different ATP analogues are available as well. Alignment of these structures based on domain 1 as well identifies movements within the SF2 domain (Figure 20). Interestingly and opposed to NS3, regardless of the co-crystallized nucleotide, no shift of domain 1 relative to the RNA strand is visible. The reason for this could be the high affinity anchor of the CTD, which might relocate the SF2 domain towards the RNA end. The lack of translocation by domain 1a upon ATP binding, however, is compensated by a shift within domain 2a motif V (Figure 20 residues V699 and T697). Yet, in accordance with NS3, nucleotide binding seems to destabilize RIG-I:RNA interactions as well, as emphasized by a reduced affinity of the protein towards RNA<sup>278</sup>. Nevertheless, if the ATP-bound state (ADP·BeF<sub>3</sub>) is compared to the ATP hydrolysis transition state (ADP·AlF<sub>3</sub>) a clear compaction of the whole helicase domain is visible, bringing domain 2a into close contact to domain 1a and decreasing the footprint of both domains on RNA from 5 nucleotides to 4 (Figure 20A). Compared to NS3, translocation of RIG-I in presence of an RNA end might thus be prevented by the CTD leading to stumbling of domain 1a and a subsequent 5' to 3' shift of domain 2a rather than a translocation into 3' to 5' direction. In order to avoid RNA end binding, further studies with hairpin RNAs or RLR constructs lacking the CTD in the presence of different ATP analogues would therefore give important evidence whether domain 1a of RIG-I is able to move or not.

After ATP hydrolysis, i.e. in the ADP bound state, the RIG-I SF2 domain is open again, leading to a loss of RNA contacts within domain 2a, while domain 1a still stays bound (Figure 20B). Repeated cycles of ATP hydrolysis, however, might due to the intramolecular movements facilitate the disruption of the CTD:RNA end interface and could thus help establish a translocation competent binding state.

Contrary to that and as discussed earlier, ATP hydrolysis by RIG-I and MDA5 was shown to lead to disengagement of the SF2 domain from RNA, and thereby helps restore the open helicase state and enables rebinding of the CARDs to domain 2b<sup>106,275,280</sup>. All those scenarios, however, are not mutually exclusive and could happen during different states of infection.

Moreover ATP-dependent translocation of RIG-I and MDA5 could even help dissociate both proteins from endogenous RNA<sup>275</sup>. In that regard, translocation and subsequent running into bulges on endogenous dsRNA could help release protein:RNA complexes. Evidence for this is provided by studies of amino acid residues contacting the RNA backbone. A prominent amino acid pair are e.g. two conserved threonine residues within domain 1a and 2a which are shown to reduce RNA binding and unwinding in NS3<sup>295</sup> (compare to RIG-I in Figure 20C). According to that finding, mutation of the corresponding threonine T347 in RIG-I results in loss of signaling due to decreased RNA binding<sup>275</sup>.

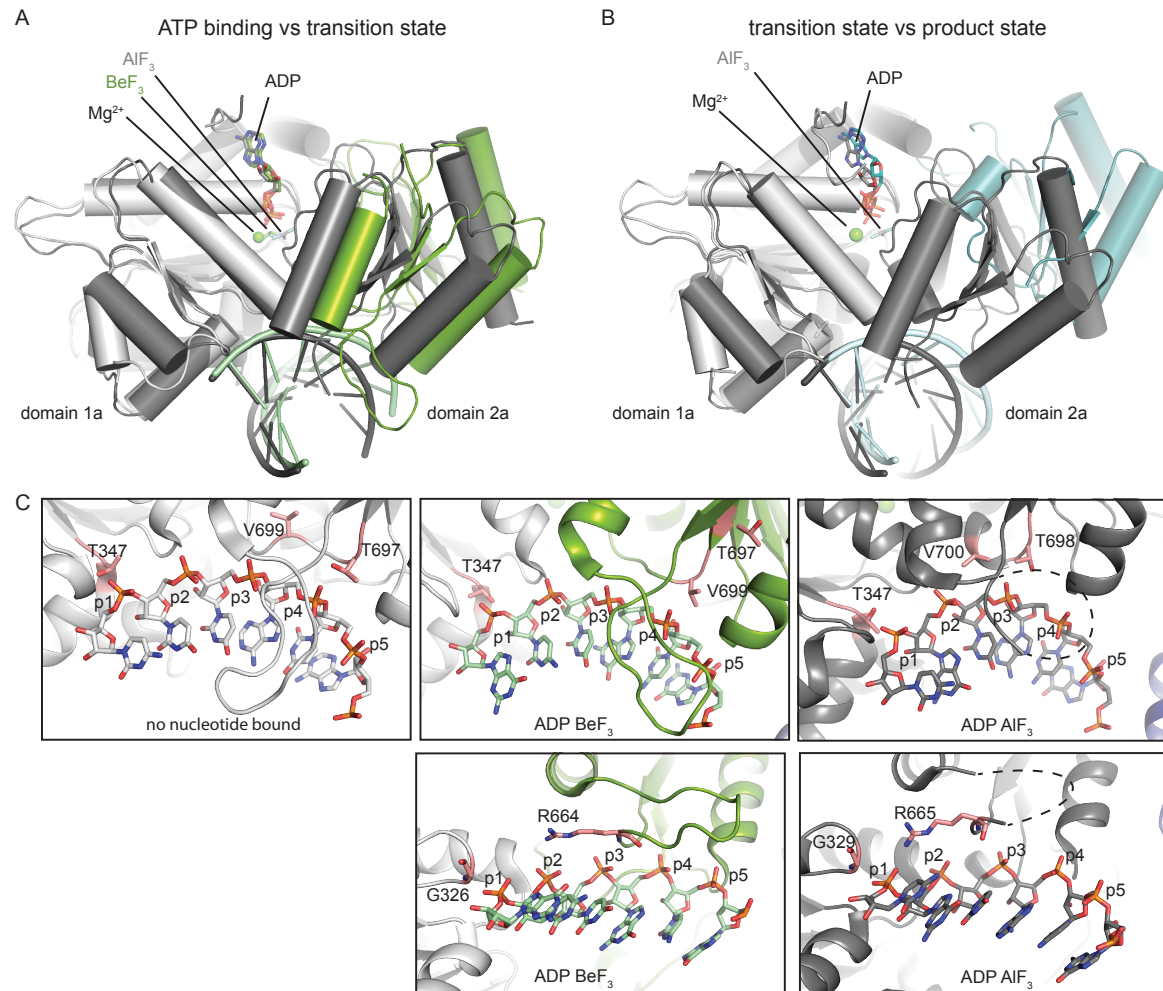


**Figure 20:** RIG-I domain movements. For comparison reasons only domains 1a and 2a are shown. (A) Comparison of the ATP bound state ( $\text{ADP} \cdot \text{BeF}_3$ , light gray: domain 1a, green: domain 2a) with the ATP hydrolysis transition state ( $\text{ADP} \cdot \text{AlF}_3$ , dark gray: domain 1a and 2a). (B) Comparison of the ATP hydrolysis transition state ( $\text{ADP} \cdot \text{AlF}_3$ , dark gray: domain 1a and 2a) with reaction product state ( $\text{ADP}$ , light gray: domain 1a, light blue: domain 2a). (C) RNA coordination of domain 1a motif Ic and domain 2a motif V (upper panels) and domain 1a motif Ib and domain 2a motif IVa (lower panels) during different states of ATP hydrolysis.

RCSB PDB codes for the depicted structures are: 5f9f (RIG-I  $\Delta$ CARDs without nucleotide, human), 3tmi (RIG-I  $\Delta$ CARDs,  $\text{ADP} \cdot \text{BeF}_3$ , human), 4a36 (RIG-I helicase,  $\text{ADP} \cdot \text{AlF}_3$ , duck), 3zd7 (RIG-I  $\Delta$ CARDs,  $\text{ADP}$ , human).

Interestingly, if a valine residue (V699) near the domain 2a-located threonine (T697) is mutated, signaling is not prevented but rather slightly enhanced even under non-infected conditions. V699 does not initially bind to the RNA backbone, but is later relocated and helps coordinating the RNA during the ATP reaction cycle. An explanation for increased signaling might be, that not RNA binding, but translocation is affected. This might result in a slipping of domain 2a on the RNA backbone rather than a distinct one-nucleotide translocation step and could lead to prolonged binding of domain 1a. If the theory holds, this finding would emphasize the importance of translocation on non-perfect dsRNA stems in non-infected cells for protein dissociation and prevention of signaling on endogenous RNA.

## 4 The current model of RNA- and ATP-dependent activation of RIG-I and MDA5

The current view on regulation of signaling by RIG-I and MDA5 in uninfected and virus-infected cells can be updated, based on the presented literature. Thereby, crucial structural differences between both RLRs lead to distinct activation and signaling suppression mechanisms.

In healthy and uninfected cells several instances ensure inactivation of RIG-I but allow surveillance of the cytoplasm in order to detect optimal ligands. In this regard, the RIG-I CARDs are folded back to the insertion domain 2b in order to prevent a stochastic communication with the MAVS CARDs in absence of an RNA stimulus<sup>61</sup>. Thereby, especially CARD2 is shielded from the cytosol since this is the domain to provide the template surface for MAVS activation<sup>152,153</sup>. The RIG-I CTD, however, is flexibly linked to the rest of the protein and free to interact with RNA<sup>61,62</sup>. In addition, several post-translational modifications impede signaling in uninfected cells: examples are phosphorylation of the CARDs that prevents ubiquitination and therefore tetramer stabilization in case of a release of the CARD domains, and acetylation of the CTD that decreases RNA binding<sup>69,178</sup>. Furthermore, unspecific binding to endogenous RNA is decreased through ATP hydrolysis, which leads to either immediate dissociation or to translocation and subsequent disengagement on nearby bulges<sup>275</sup> (Figure 21A). On the other hand compartmentalization of eukaryotic cells shields triphosphate containing unmethylated mRNAs from the cytosol which also helps to avoid the immune activation by those RNAs.

Upon viral infection, the RIG-I CTD captures 5' phosphorylated ends of double-stranded RNA and presents it to the helicase domain<sup>102-104</sup> (Figure 21B). Thereby, even a capped 5' end is tolerated, but not methylation of the first nucleotide<sup>105,109</sup>. RNA-binding again stimulates the ATPase function of the SF2 domain. Since the phosphorylated RNA end now provides a strong anchor to the CTD, ATP hydrolysis still leads to a widening of both domain 1a and 2a of the SF2 helicase domain, therefore decreasing RNA stem recognition, while CTD-mediated binding is not disturbed. Subsequently, the SF2 helicase domain could rebind as before, or might bind with a slightly different orientation, helping to reposition the CTD in order to start translocation on the duplex. Translocation itself might function to dislocate bound viral proteins or to load several RIG-I molecules onto the RNA double-strand in order to enhance downstream signaling<sup>198-200</sup>.

Release of the CARDs is, besides being dependent on dsRNA binding, coupled to ATP and is triggered by a molecular switch upon ATP binding that compacts the SF2 helicase domain. This induces a clash between CARDs and RNA bound to the CTD, and either liberates the CARDs or leads, in case of non tri- or diphosphorylated dsRNA, to dissociation<sup>61</sup>. Successfully freed CARDs, in turn, interact with adjacent CARDs to form tetramers and build a scaffold for the recruitment of MAVS CARDs in order to start an immune response<sup>152,153</sup>. Released RIG-I CARDs or CARDs-tetramers are further dephosphorylated and either bind polyubiquitin chains, ubiquitin-like proteins or domains, or are covalently polyubiquitinated<sup>69,70,166,296</sup>. Ubiquitination, itself is not strictly required for an immune response<sup>199</sup>, but it stabilizes the RIG-I signaling competent complex, especially if no oligomers can be formed on an RNA double-strand, and thus impedes CARDs complex dissociation. In ad-

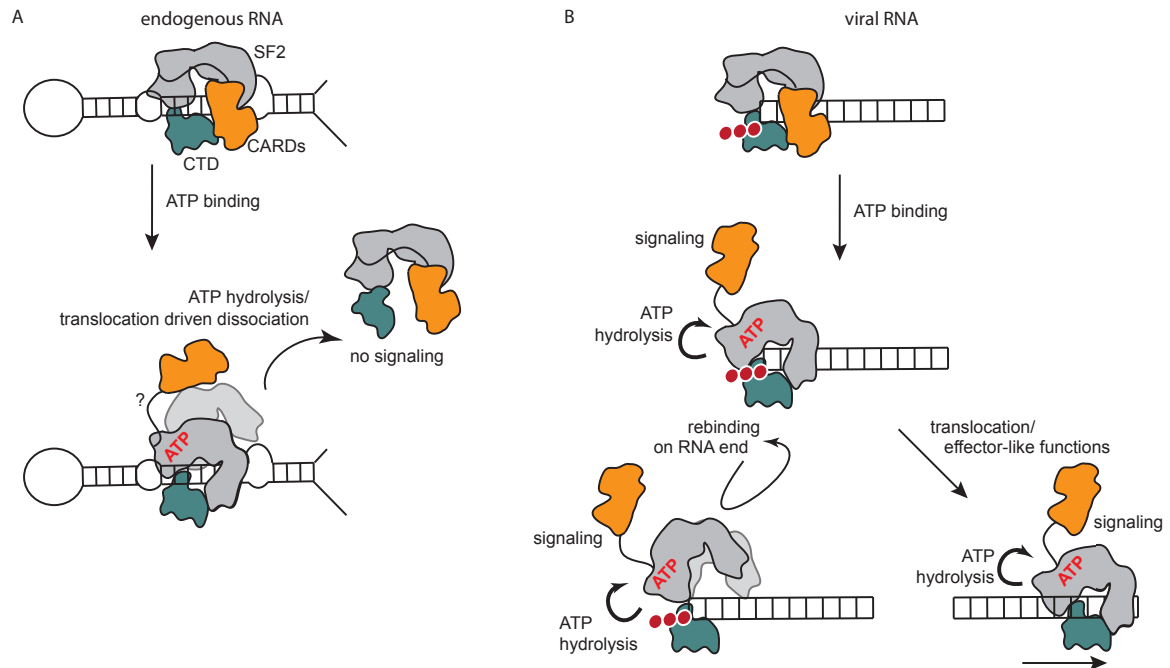


**Figure 21:** RIG-I ATP- and RNA-dependent signaling. (A) RNA binding alone is not sufficient to induce signaling and needs subsequent ATP. ATP hydrolysis and translocation, however, result in rapid dissociation, prevent prolonged protein binding and therefore enable refolding of the CARDs. (B) RIG-I binds phosphorylated dsRNA ends via its CTD. Subsequent ATP binding releases the CARDs and allows immune response signaling. ATP hydrolysis displaces the SF2 domain from the RNA strand, but leads to either rebinding on the RNA end caused by the CTD anchor, or to translocation on the stem. RIG-I SF2 domain: gray, CTD: cyan, CARDs: orange, phosphates: red dots. Figure adopted from Lässig et al.<sup>275</sup>.

dition, deacetylation of the RIG-I CTD further stimulates RNA binding and enhances the immune response<sup>178</sup>. Activation of the downstream signaling cascade ultimately leads to expression of hundreds of ISGs including RLRs themselves in order to boost or fine-tune the immune response.

MDA5 is like RIG-I autoinhibited by phosphorylation of its CARDs<sup>166</sup>. Nevertheless, the CARDs themselves do not as tightly associate with domain 2b as in RIG-I, which leads to partially exposed CARDs and higher background activity of MDA5<sup>106</sup> (Figure 22A). Phosphorylation and its suppressive role in immune response activation through decreased binding of free ubiquitin chains might thus even play a more crucial role for MDA5 compared with RIG-I. The MDA5 CTD is as well flexible, but preferentially captures dsRNA stems<sup>144</sup>. In addition and contrary to RIG-I, also the MDA5 SF2 domain alone is able to bind dsRNA<sup>277</sup>. The MDA5 CTD might therefore have an especially crucial role in stabilizing the MDA5 ring-like structure on dsRNA by docking onto domain 2b via the convex zinc-ion containing surface<sup>144</sup>.

If bound to dsRNA, MDA5 cooperatively forms large filaments and thus scans the RNA length<sup>130</sup> (Figure 22B). Thereby, MDA5 preferentially nucleates within the RNA interior. In contrast to RIG-I and because of the higher flexibility of the MDA5 CARDs, ATP binding is not as essential in order to start

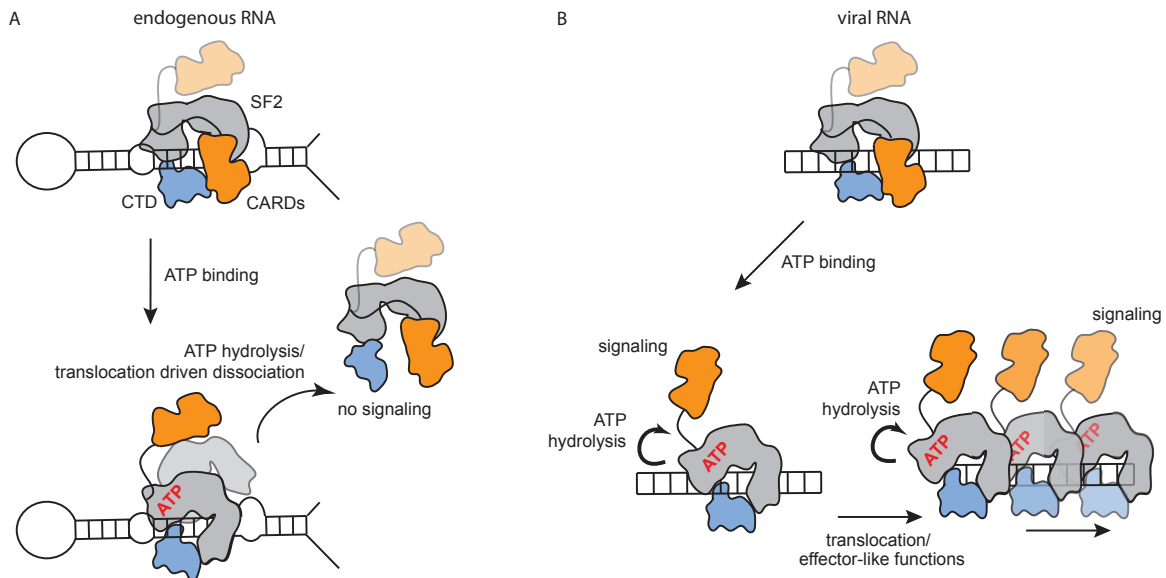


**Figure 22:** MDA5 ATP- and RNA-dependent signaling. (A) The MDA5 CARDS are partially opened and RNA binding alone is sufficient to induce signaling. ATP hydrolysis and translocation, however, prevent prolonged protein binding and result in rapid dissociation from endogenous RNA, thus reducing background signaling. (B) MDA5 binds to viral dsRNA stems. Subsequent ATP binding entirely releases the CARDS and allows increased immune response signaling. ATP hydrolysis leads to translocation and cooperative binding of MDA5 on the RNA stem thereby filling gaps. MDA5 SF2 domain: gray, CTD: blue, CARDS: orange. Figure adopted from Lässig et al. <sup>275</sup>.

an immune response<sup>277</sup>. Nevertheless, RNA binding induces ATP hydrolysis similar to RIG-I, which leads to disassembly of the filaments and therefore displays immunosuppressive effects as well<sup>130</sup>. Since MDA5 lacks the high affinity anchor of the CTD towards phosphorylated RNA ends, translocation might happen easier compared with RIG-I and might lead to faster loading of several molecules onto the dsRNA strand, thereby filling gaps. Cooperative protein binding provides filament stability, whereas ATP hydrolysis-driven disassembly might primarily happen at RNA ends<sup>199</sup>. In addition MDA5 might have a preference for U or A/U-rich dsRNA, which show lower ATP hydrolysis rates and thus could result in more stable filaments through decreased translocation or dissociation. Spatial proximity of several MDA5 molecules on longer dsRNA further induces CARD oligomerization and immune response activation via MAVS.

Importantly, the ATPase function of both RIG-I and MDA5 indirectly prevents immune signaling by disturbing the CARDS-tetramer formation needed for MAVS activation until post-translational modifications are exchanged or the CARDS are ubiquitinated. In that regard, RNA dissociation from non-phosphorylated dsRNA of RIG-I allows CARDS rebinding to domain 2b. Translocation or dissociation on short RNA stems by MDA5 disturbs the spatial proximity. Further, ATP hydrolysis of both RIG-I and MDA5 reduces signaling on short internal dsRNA stems by challenging the helicase:RNA backbone interactions and highlighting additional RNA features but the mere double-stranded nature: In case of RIG-I the SF2 domain tests for the presence of a tri- or diphosphate and for MDA5 it restricts signaling to long dsRNAs.

## References

- [1] Max D Cooper and Brantley R Herrin. How did our complex immune system evolve? *Nature Reviews Immunology*, 10(1):2–3, 2010.
- [2] Charles Janeway, Kenneth P Murphy, Paul Travers, and Mark Walport. *Janeway's Immunobiology*. Garland Science, 2008.
- [3] Jonathan DG Jones and Jeffery L Dangl. The plant immune system. *Nature*, 444(7117): 323–329, 2006.
- [4] Carrie L Lucas and Michael J Lenardo. Identifying genetic determinants of autoimmunity and immune dysregulation. *Current Opinion in Immunology*, 37:28–33, 2015.
- [5] Charles A Janeway. Approaching the asymptote? Evolution and revolution in immunology. In *Cold Spring Harbor Symposia on Quantitative Biology*, volume 54, pages 1–13. Cold Spring Harbor Laboratory Press, 1989.
- [6] Polly Matzinger. Tolerance, danger, and the extended family. *Annual Review of Immunology*, 12(1):991–1045, 1994.
- [7] Akiko Iwasaki and Ruslan Medzhitov. Control of adaptive immunity by the innate immune system. *Nature Immunology*, 16(4):343–353, 2015.
- [8] Andrea Ablasser, Carola Hertrich, Ruth Waßermann, and Veit Hornung. Nucleic acid driven sterile inflammation. *Clinical Immunology*, 147(3):207–215, 2013.
- [9] Taro Kawai and Shizuo Akira. The role of pattern-recognition receptors in innate immunity: update on toll-like receptors. *Nature Immunology*, 11(5):373–384, 2010.
- [10] David Sancho and Caetano Reis e Sousa. Signaling by myeloid C-type lectin receptors in immunity and homeostasis. *Annual Review of Immunology*, 30:491, 2012.
- [11] Jiayi Wu and Zhijian J Chen. Innate immune sensing and signaling of cytosolic nucleic acids. *Annual Review of Immunology*, 32:461–488, 2014.
- [12] Vijay AK Rathinam, Sivapriya Kailasan Vanaja, and Katherine A Fitzgerald. Regulation of inflammasome signaling. *Nature Immunology*, 13(4):333–342, 2012.
- [13] Kiyoshi Takeda, Tsuneyasu Kaisho, and Shizuo Akira. Toll-like receptors. *Annual Review of Immunology*, 21(1):335–376, 2003.
- [14] Akiko Iwasaki and Ruslan Medzhitov. Toll-like receptor control of the adaptive immune responses. *Nature Immunology*, 5(10):987–995, 2004.
- [15] Maximiliano Javier Jiménez-Dalmaroni, M Eric Gerswhin, and Iannis E Adamopoulos. The critical role of Toll-like receptors, from microbial recognition to autoimmunity, a comprehensive review. *Autoimmunity Reviews*, 15(1):1–8, 2016.

- [16] Dong Hyun Song and Jie-Oh Lee. Sensing of microbial molecular patterns by Toll-like receptors. *Immunological Reviews*, 250(1):216–229, 2012.
- [17] Tobias Junt and Winfried Barchet. Translating nucleic acid-sensing pathways into therapies. *Nature Reviews Immunology*, 2015.
- [18] Qian Yin, Tian-Min Fu, Jixi Li, and Hao Wu. Structural biology of innate immunity. *Annual Review of Immunology*, 33:393, 2015.
- [19] Osamu Takeuchi, Taro Kawai, Peter F Mührlradt, Michael Morr, Justin D Radolf, Arturo Zychlinsky, Kiyoshi Takeda, and Shizuo Akira. Discrimination of bacterial lipoproteins by Toll-like receptor 6. *International Immunology*, 13(7):933–940, 2001.
- [20] Osamu Takeuchi, Shintaro Sato, Takao Horiuchi, Katsuaki Hoshino, Kiyoshi Takeda, Zhongyun Dong, Robert L Modlin, and Shizuo Akira. Cutting edge: role of Toll-like receptor 1 in mediating immune response to microbial lipoproteins. *The Journal of Immunology*, 169(1):10–14, 2002.
- [21] Marije Oosting, Shih-Chin Cheng, Judith M Bolscher, Rachel Vestering-Stenger, Theo S Plantinga, Ineke C Verschueren, Peer Arts, Anja Garritsen, Hans van Eenennaam, Patrick Sturm, et al. Human TLR10 is an anti-inflammatory pattern-recognition receptor. *Proceedings of the National Academy of Sciences*, 111(42):E4478–E4484, 2014.
- [22] Alexander Poltorak, Xiaolong He, Irina Smirnova, Mu-Ya Liu, Christophe Van Huffel, Xin Du, Dale Birdwell, Erica Alejos, Maria Silva, Chris Galanos, et al. Defective LPS signaling in C3H/HeJ and C57BL/10ScCr mice: mutations in Tlr4 gene. *Science*, 282(5396):2085–2088, 1998.
- [23] Salman T Qureshi, Line Larivière, Gary Leveque, Sophie Clermont, Karen J Moore, Philippe Gros, and Danielle Malo. Endotoxin-tolerant mice have mutations in Toll-like receptor 4 (Tlr4). *The Journal of Experimental Medicine*, 189(4):615–625, 1999.
- [24] Katsuaki Hoshino, Osamu Takeuchi, Taro Kawai, Hideki Sanjo, Tomohiko Ogawa, Yoshifumi Takeda, Kiyoshi Takeda, and Shizuo Akira. Cutting edge: Toll-like receptor 4 (TLR4)-deficient mice are hyporesponsive to lipopolysaccharide: evidence for TLR4 as the Lps gene product. *The Journal of Immunology*, 162(7):3749–3752, 1999.
- [25] Fumitaka Hayashi, Kelly D Smith, Adrian Ozinsky, Thomas R Hawn, C Yi Eugene, David R Goodlett, Jimmy K Eng, Shizuo Akira, David M Underhill, and Alan Aderem. The innate immune response to bacterial flagellin is mediated by Toll-like receptor 5. *Nature*, 410(6832):1099–1103, 2001.
- [26] Florian Heil, Hiroaki Hemmi, Hubertus Hochrein, Franziska Ampenberger, Carsten Kirschning, Shizuo Akira, Grayson Lipford, Hermann Wagner, and Stefan Bauer. Species-specific recognition of single-stranded RNA via toll-like receptor 7 and 8. *Science*, 303(5663):1526–1529, 2004.
- [27] Sandra S Diebold, Tsuneyasu Kaisho, Hiroaki Hemmi, Shizuo Akira, and Caetano Reis e Sousa. Innate antiviral responses by means of TLR7-mediated recognition of single-stranded RNA. *Science*, 303(5663):1529–1531, 2004.
- [28] Jennifer M Lund, Lena Alexopoulou, Ayuko Sato, Margaret Karow, Niels C Adams, Nicholas W Gale, Akiko Iwasaki, and Richard A Flavell. Recognition of single-stranded RNA viruses by Toll-like receptor 7. *Proceedings of the National Academy of Sciences of the United States of America*, 101(15):5598–5603, 2004.

- [29] Veit Hornung, Margit Guenther-Biller, Carole Bourquin, Andrea Ablasser, Martin Schlee, Satoshi Uematsu, Anne Noronha, Muthiah Manoharan, Shizuo Akira, Antonin de Fougerolles, et al. Sequence-specific potent induction of IFN- $\alpha$  by short interfering RNA in plasmacytoid dendritic cells through TLR7. *Nature Medicine*, 11(3):263–270, 2005.
- [30] Lena Alexopoulou, Agnieszka Czopik Holt, Ruslan Medzhitov, and Richard A Flavell. Recognition of double-stranded RNA and activation of NF- $\kappa$ B by Toll-like receptor 3. *Nature*, 413(6857):732–738, 2001.
- [31] Hiroaki Hemmi, Osamu Takeuchi, Taro Kawai, Tsuneyasu Kaisho, Shintaro Sato, Hideki Sanjo, Makoto Matsumoto, Katsuaki Hoshino, Hermann Wagner, Kiyoshi Takeda, et al. A Toll-like receptor recognizes bacterial DNA. *Nature*, 408(6813):740–745, 2000.
- [32] Kei Yasuda, Mark Rutz, Beatrix Schlatter, Jochen Metzger, Peter B Lippa, Frank Schmitz, Tobias Haas, Antje Heit, Stefan Bauer, and Hermann Wagner. CpG motif-independent activation of TLR9 upon endosomal translocation of “natural” phosphodiester DNA. *European Journal of Immunology*, 36(2):431–436, 2006.
- [33] Tobias Haas, Jochen Metzger, Frank Schmitz, Antje Heit, Thomas Müller, Eicke Latz, and Hermann Wagner. The DNA sugar backbone 2' deoxyribose determines toll-like receptor 9 activation. *Immunity*, 28(3):315–323, 2008.
- [34] Akinori Takaoka, ZhiChao Wang, Myoung Kwon Choi, Hideyuki Yanai, Hideo Negishi, Tatsuma Ban, Yan Lu, Makoto Miyagishi, Tatsuhiko Kodama, Kenya Honda, et al. DAI (DLM-1/ZBP1) is a cytosolic DNA sensor and an activator of innate immune response. *Nature*, 448(7152):501–505, 2007.
- [35] Zhiqiang Zhang, Bin Yuan, Musheng Bao, Ning Lu, Taeil Kim, and Yong-Jun Liu. The helicase DDX41 senses intracellular DNA mediated by the adaptor STING in dendritic cells. *Nature Immunology*, 12(10):959–965, 2011.
- [36] Leonie Unterholzner, Sinead E Keating, Marcin Baran, Kristy A Horan, Søren B Jensen, Shruti Sharma, Cherilyn M Sirois, Tengchuan Jin, Eicke Latz, T Sam Xiao, et al. IFI16 is an innate immune sensor for intracellular DNA. *Nature Immunology*, 11(11):997–1004, 2010.
- [37] Lijun Sun, Jiayi Wu, Fenghe Du, Xiang Chen, and Zhijian J Chen. Cyclic GMP-AMP synthase is a cytosolic DNA sensor that activates the type I interferon pathway. *Science*, 339(6121):786–791, 2013.
- [38] Zhe Ma and Blossom Damania. The cGAS-STING Defense Pathway and Its Counteraction by Viruses. *Cell Host & Microbe*, 19(2):150–158, 2016.
- [39] Anna-Maria Herzner, Cristina Amparo Hagmann, Marion Goldeck, Steven Wolter, Kirsten Kübler, Sabine Wittmann, Thomas Gramberg, Liudmila Andreeva, Karl-Peter Hopfner, Christina Mertens, et al. Sequence-specific activation of the DNA sensor cGAS by Y-form DNA structures as found in primary HIV-1 cDNA. *Nature Immunology*, 16(10):1025–1033, 2015.
- [40] John W Schoggins, Donna A MacDuff, Naoko Imanaka, Maria D Gainey, Bimmi Shrestha, Jennifer L Eitson, Katrina B Mar, R Blake Richardson, Alexander V Ratushny, Vladimir Litvak, et al. Pan-viral specificity of IFN-induced genes reveals new roles for cGAS in innate immunity. *Nature*, 505(7485):691–695, 2014.
- [41] Jiayi Wu, Lijun Sun, Xiang Chen, Fenghe Du, Heping Shi, Chuo Chen, and Zhijian J Chen. Cyclic

- GMP-AMP is an endogenous second messenger in innate immune signaling by cytosolic DNA. *Science*, 339(6121):826–830, 2013.
- [42] Filiz Civril, Tobias Deimling, Carina C de Oliveira Mann, Andrea Ablasser, Manuela Moldt, Gregor Witte, Veit Hornung, and Karl-Peter Hopfner. Structural mechanism of cytosolic DNA sensing by cGAS. *Nature*, 498(7454):332–337, 2013.
- [43] Philip J Kranzusch, Amy Si-Ying Lee, James M Berger, and Jennifer A Doudna. Structure of human cGAS reveals a conserved family of second-messenger enzymes in innate immunity. *Cell Reports*, 3(5):1362–1368, 2013.
- [44] Xin Li, Chang Shu, Guanghui Yi, Catherine T Chaton, Catherine L Shelton, Jiasheng Diao, Xiaobing Zuo, C Cheng Kao, Andrew B Herr, and Pingwei Li. Cyclic GMP-AMP synthase is activated by double-stranded DNA-induced oligomerization. *Immunity*, 39(6):1019–1031, 2013.
- [45] Xu Zhang, Jiayi Wu, Fenghe Du, Hui Xu, Lijun Sun, Zhe Chen, Chad A Brautigam, Xuewu Zhang, and Zhijian J Chen. The cytosolic DNA sensor cGAS forms an oligomeric complex with DNA and undergoes switch-like conformational changes in the activation loop. *Cell Reports*, 6(3):421–430, 2014.
- [46] Pu Gao, Manuel Ascano, Yang Wu, Winfried Barchet, Barbara L Gaffney, Thomas Zillinger, Artem A Serganov, Yizhou Liu, Roger A Jones, Gunther Hartmann, et al. Cyclic [G (2', 5') pA (3', 5') p] is the metazoan second messenger produced by DNA-activated cyclic GMP-AMP synthase. *Cell*, 153(5):1094–1107, 2013.
- [47] Elie J Diner, Dara L Burdette, Stephen C Wilson, Kathryn M Monroe, Colleen A Kellenberger, Mamoru Hyodo, Yoshihiro Hayakawa, Ming C Hammond, and Russell E Vance. The innate immune DNA sensor cGAS produces a noncanonical cyclic dinucleotide that activates human STING. *Cell Reports*, 3(5):1355–1361, 2013.
- [48] Andrea Ablasser, Marion Goldeck, Taner Cavlar, Tobias Deimling, Gregor Witte, Ingo Röhl, Karl-Peter Hopfner, Janos Ludwig, and Veit Hornung. cGAS produces a 2'-5'-linked cyclic dinucleotide second messenger that activates STING. *Nature*, 498(7454):380–384, 2013.
- [49] Dara L Burdette, Kathryn M Monroe, Katia Sotelo-Troha, Jeff S Iwig, Barbara Eckert, Mamoru Hyodo, Yoshihiro Hayakawa, and Russell E Vance. STING is a direct innate immune sensor of cyclic di-GMP. *Nature*, 478(7370):515–518, 2011.
- [50] Hiroki Ishikawa, Zhe Ma, and Glen N Barber. STING regulates intracellular DNA-mediated, type I interferon-dependent innate immunity. *Nature*, 461(7265):788–792, 2009.
- [51] Tilmann Bürckstümmer, Christoph Baumann, Stephan Blüml, Evelyn Dixit, Gerhard Dürnberger, Hannah Jahn, Melanie Planyavsky, Martin Bilban, Jacques Colinge, Keiryn L Bennett, et al. An orthogonal proteomic-genomic screen identifies AIM2 as a cytoplasmic DNA sensor for the inflammasome. *Nature Immunology*, 10(3):266–272, 2009.
- [52] Teresa Fernandes-Alnemri, Je-Wook Yu, Pinaki Datta, Jianghong Wu, and Emad S Alnemri. AIM2 activates the inflammasome and cell death in response to cytoplasmic DNA. *Nature*, 458(7237):509–513, 2009.
- [53] Veit Hornung, Andrea Ablasser, Marie Charrel-Dennis, Franz Bauernfeind, Gabor Horvath, Daniel R Caffrey, Eicke Latz, and Katherine A Fitzgerald. AIM2 recognizes cytosolic dsDNA and forms a caspase-1-activating inflammasome with ASC. *Nature*, 458(7237):514–518, 2009.

- [54] David Wallach, Tae-Bong Kang, Christopher P Dillon, and Douglas R Green. Programmed necrosis in inflammation: Toward identification of the effector molecules. *Science*, 352(6281): aaf2154, 2016.
- [55] Tengchuan Jin, Andrew Perry, Jiansheng Jiang, Patrick Smith, James A Curry, Leonie Unterholzner, Zhaozhao Jiang, Gabor Horvath, Vijay A Rathinam, Ricky W Johnstone, et al. Structures of the HIN domain: DNA complexes reveal ligand binding and activation mechanisms of the AIM2 inflammasome and IFI16 receptor. *Immunity*, 36(4):561–571, 2012.
- [56] Seamus R Morrone, Mariusz Matyszewski, Xiong Yu, Michael Delannoy, Edward H Egelman, and Jungsan Sohn. Assembly-driven activation of the AIM2 foreign-dsDNA sensor provides a polymerization template for downstream ASC. *Nature Communications*, 6, 2015.
- [57] Mohamed Lamkanfi and Vishva M Dixit. Mechanisms and functions of inflammasomes. *Cell*, 157(5):1013–1022, 2014.
- [58] Tuo Li, Benjamin A Diner, Jin Chen, and Ileana M Cristea. Acetylation modulates cellular distribution and DNA sensing ability of interferon-inducible protein IFI16. *Proceedings of the National Academy of Sciences*, 109(26):10558–10563, 2012.
- [59] Megan H Orzalli, Nicole M Broekema, Benjamin A Diner, Dustin C Hancks, Nels C Elde, Ileana M Cristea, and David M Knipe. cGAS-mediated stabilization of IFI16 promotes innate signaling during herpes simplex virus infection. *Proceedings of the National Academy of Sciences*, 112(14):E1773–E1781, 2015.
- [60] Dahai Luo, Steve C Ding, Adriana Vela, Andrew Kohlway, Brett D Lindenbach, and Anna Marie Pyle. Structural insights into RNA recognition by RIG-I. *Cell*, 147(2):409–422, 2011.
- [61] Eva Kowalinski, Thomas Lunardi, Andrew A McCarthy, Jade Louber, Joanna Brunel, Boyan Grigorov, Denis Gerlier, and Stephen Cusack. Structural basis for the activation of innate immune pattern-recognition receptor RIG-I by viral RNA. *Cell*, 147(2):423–435, 2011.
- [62] Fuguo Jiang, Anand Ramanathan, Matthew T Miller, Guo-Qing Tang, Michael Gale, Smita S Patel, and Joseph Marcotrigiano. Structural basis of RNA recognition and activation by innate immune receptor RIG-I. *Nature*, 479(7373):423–427, 2011.
- [63] Stephanie Bechtel, Heiko Rosenfelder, Anny Duda, Christian Schmidt, Ute Ernst, Ruth Wellenreuther, Alexander Mehrle, Claudia Schuster, Andre Bahr, Helmut Blöcker, et al. The full-ORF clone resource of the German cDNA Consortium. *BMC genomics*, 8(1):1, 2007.
- [64] Rashu B Seth, Lijun Sun, Chee-Kwee Ea, and Zhijian J Chen. Identification and characterization of MAVS, a mitochondrial antiviral signaling protein that activates NF- $\kappa$ B and IRF3. *Cell*, 122(5):669–682, 2005.
- [65] Taro Kawai, Ken Takahashi, Shintaro Sato, Cevayir Coban, Himanshu Kumar, Hiroki Kato, Ken J Ishii, Osamu Takeuchi, and Shizuo Akira. IPS-1, an adaptor triggering RIG-I and Mda5-mediated type I interferon induction. *Nature Immunology*, 6(10):981–988, 2005.
- [66] Etienne Meylan, Joseph Curran, Kay Hofmann, Darius Moradpour, Marco Binder, Ralf Bartenschlager, and Jürg Tschopp. Cardif is an adaptor protein in the RIG-I antiviral pathway and is targeted by hepatitis C virus. *Nature*, 437(7062):1167–1172, 2005.
- [67] Liang-Guo Xu, Yan-Yi Wang, Ke-Jun Han, Lian-Yun Li, Zhonghe Zhai, and Hong-Bing Shu. Visa is an adapter protein required for virus-triggered ifn- $\beta$  signaling. *Molecular Cell*, 19(6):727–740,

- 2005.
- [68] Mitsutoshi Yoneyama, Mika Kikuchi, Kanae Matsumoto, Tadaatsu Imaizumi, Makoto Miyagishi, Kazunari Taira, Eileen Foy, Yueh-Ming Loo, Michael Gale, Shizuo Akira, et al. Shared and unique functions of the DExD/H-box helicases RIG-I, MDA5, and LGP2 in antiviral innate immunity. *The Journal of Immunology*, 175(5):2851–2858, 2005.
- [69] Michaela U Gack, Young C Shin, Chul-Hyun Joo, Tomohiko Urano, Chengyu Liang, Lijun Sun, Osamu Takeuchi, Shizuo Akira, Zhijian Chen, Satoshi Inoue, et al. TRIM25 RING-finger E3 ubiquitin ligase is essential for RIG-I-mediated antiviral activity. *Nature*, 446(7138):916–920, 2007.
- [70] Xiaomo Jiang, Lisa N Kinch, Chad A Brautigam, Xiang Chen, Fenghe Du, Nick V Grishin, and Zhijian J Chen. Ubiquitin-induced oligomerization of the rna sensors rig-i and mda5 activates antiviral innate immune response. *Immunity*, 36(6):959–973, 2012.
- [71] Helene Minyi Liu, Yueh-Ming Loo, Stacy M Horner, Gregory A Zornetzer, Michael G Katze, and Michael Gale. The mitochondrial targeting chaperone 14-3-3 $\epsilon$  regulates a RIG-I translocon that mediates membrane association and innate antiviral immunity. *Cell Host & Microbe*, 11(5):528–537, 2012.
- [72] Mitsutoshi Yoneyama, Mika Kikuchi, Takashi Natsukawa, Noriaki Shinobu, Tadaatsu Imaizumi, Makoto Miyagishi, Kazunari Taira, Shizuo Akira, and Takashi Fujita. The RNA helicase RIG-I has an essential function in double-stranded RNA-induced innate antiviral responses. *Nature Immunology*, 5(7):730–737, 2004.
- [73] Takeshi Saito, Reiko Hirai, Yueh-Ming Loo, David Owen, Cynthia L Johnson, Sangita C Sinha, Shizuo Akira, Takashi Fujita, and Michael Gale. Regulation of innate antiviral defenses through a shared repressor domain in RIG-I and LGP2. *Proceedings of the National Academy of Sciences*, 104(2):582–587, 2007.
- [74] Evelyn Dixit, Steeve Boulant, Yijing Zhang, Amy SY Lee, Charlotte Odendall, Bennett Shum, Nir Hacohen, Zhijian J Chen, Sean P Whelan, Marc Fransen, et al. Peroxisomes are signaling platforms for antiviral innate immunity. *Cell*, 141(4):668–681, 2010.
- [75] Fajian Hou, Lijun Sun, Hui Zheng, Brian Skaug, Qiu-Xing Jiang, and Zhijian J Chen. MAVS forms functional prion-like aggregates to activate and propagate antiviral innate immune response. *Cell*, 146(3):448–461, 2011.
- [76] Charlotte Odendall, Evelyn Dixit, Fabrizia Stavru, Helene Bierne, Kate M Franz, Ann Fiegen Durbin, Steeve Boulant, Lee Gehrke, Pascale Cossart, and Jonathan C Kagan. Diverse intracellular pathogens activate type III interferon expression from peroxisomes. *Nature Immunology*, 15(8):717–726, 2014.
- [77] Siqi Liu, Jueqi Chen, Xin Cai, Jiayi Wu, Xiang Chen, You-Tong Wu, Lijun Sun, and Zhijian J Chen. MAVS recruits multiple ubiquitin E3 ligases to activate antiviral signaling cascades. *eLife*, 2:e00785, 2013.
- [78] Chuan-Jin Wu, Dietrich B Conze, Tao Li, Srinivasa M Srinivasula, and Jonathan D Ashwell. Sensing of Lys 63-linked polyubiquitination by NEMO is a key event in NF- $\kappa$ B activation. *Nature Cell Biology*, 8(4):398–406, 2006.
- [79] Chee-Kwee Ea, Li Deng, Zong-Ping Xia, Gabriel Pineda, and Zhijian J Chen. Activation of IKK by

- TNF $\alpha$  requires site-specific ubiquitination of RIP1 and polyubiquitin binding by NEMO. *Molecular Cell*, 22(2):245–257, 2006.
- [80] Daqi Tu, Zehua Zhu, Alicia Y Zhou, Cai-hong Yun, Kyung-Eun Lee, Angela V Toms, Yiqun Li, Gavin P Dunn, Edmond Chan, Tran Thai, et al. Structure and ubiquitination-dependent activation of TANK-binding kinase 1. *Cell Reports*, 3(3):747–758, 2013.
- [81] Michael Hinz and Claus Scheidereit. The I $\kappa$ B kinase complex in NF- $\kappa$ B regulation and beyond. *EMBO Reports*, 15(1):46–61, 2014.
- [82] Siqi Liu, Xin Cai, Jiayi Wu, Qian Cong, Xiang Chen, Tuo Li, Fenghe Du, Junyao Ren, You-Tong Wu, Nick V Grishin, et al. Phosphorylation of innate immune adaptor proteins MAVS, STING, and TRIF induces IRF3 activation. *Science*, 347(6227):aaa2630, 2015.
- [83] Finlay McNab, Katrin Mayer-Barber, Alan Sher, Andreas Wack, and Anne O’Garra. Type I interferons in infectious disease. *Nature Reviews Immunology*, 15(2):87–103, 2015.
- [84] Lionel B Ivashkiv and Laura T Donlin. Regulation of type I interferon responses. *Nature Reviews Immunology*, 14(1):36–49, 2014.
- [85] Michaela U Gack, Axel Kirchhofer, Young C Shin, Kyung-Soo Inn, Chengyu Liang, Sheng Cui, Sua Myong, Taekjip Ha, Karl-Peter Hopfner, and Jae U Jung. Roles of RIG-I N-terminal tandem CARD and splice variant in TRIM25-mediated antiviral signal transduction. *Proceedings of the National Academy of Sciences*, 105(43):16743–16748, 2008.
- [86] Sky W Brubaker, Anna E Gauthier, Eric W Mills, Nicholas T Ingolia, and Jonathan C Kagan. A bicistronic MAVS transcript highlights a class of truncated variants in antiviral immunity. *Cell*, 156(4):800–811, 2014.
- [87] Koji Onomoto, Michihiko Jogi, Ji-Seung Yoo, Ryo Narita, Shiho Morimoto, Azumi Takemura, Suryaprakash Sambhara, Atushi Kawaguchi, Suguru Osari, Kyosuke Nagata, et al. Critical role of an antiviral stress granule containing RIG-I and PKR in viral detection and innate immunity. *PLoS One*, 7(8):e43031, 2012.
- [88] Randal J Kaufman. *The double-stranded RNA-activated protein kinase PKR. In: dsRNA genetic elements – concepts and applications in agriculture, forestry, and medicine*. CRC Press, 2000.
- [89] Juan J Berlanga, Ivan Ventoso, Heather P Harding, Jing Deng, David Ron, Nahum Sonenberg, Luis Carrasco, and Cesar de Haro. Antiviral effect of the mammalian translation initiation factor 2 $\alpha$  kinase GCN2 against RNA viruses. *The EMBO Journal*, 25(8):1730–1740, 2006.
- [90] Koji Onomoto, Mitsutoshi Yoneyama, Gabriel Fung, Hiroki Kato, and Takashi Fujita. Antiviral innate immunity and stress granule responses. *Trends in Immunology*, 35(9):420–428, 2014.
- [91] Mitsutoshi Yoneyama, Michihiko Jogi, and Koji Onomoto. Regulation of antiviral innate immune signaling by stress-induced RNA granules. *Journal of biochemistry*, page mvv122, 2016.
- [92] Kristina M Okonski and Charles E Samuel. Stress granule formation induced by measles virus is protein kinase PKR dependent and impaired by RNA adenosine deaminase ADAR1. *Journal of Virology*, 87(2):756–766, 2013.
- [93] Yongzhi Cui, Minglin Li, Katherine D Walton, Kailai Sun, John A Hanover, Priscilla A Furth, and Lothar Hennighausen. The Stat3/5 locus encodes novel endoplasmic reticulum and helicase-like proteins that are preferentially expressed in normal and neoplastic mammary tissue. *Ge-*

- nomics*, 78(3):129–134, 2001.
- [94] Simon Rothenfusser, Nadege Goutagny, Gary DiPerna, Mei Gong, Brian G Monks, Annett Schoenemeyer, Masahiro Yamamoto, Shizuo Akira, and Katherine A Fitzgerald. The RNA helicase Lgp2 inhibits TLR-independent sensing of viral replication by retinoic acid-inducible gene-1. *The Journal of Immunology*, 175(8):5260–5268, 2005.
- [95] Safia Deddouche, Delphine Goubau, Jan Rehwinkel, Probir Chakravarty, Sharmin Begum, Pierre V Maillard, Annabel Borg, Nik Matthews, Qian Feng, Frank JM van Kuppeveld, et al. Identification of an LGP2-associated MDA5 agonist in picornavirus-infected cells. *eLife*, 3:e01535, 2014.
- [96] Thiagarajan Venkataraman, Maikel Valdes, Rachel Elsby, Shigeru Kakuta, Gisela Caceres, Shinobu Saijo, Yoichiro Iwakura, and Glen N Barber. Loss of DExD/H box RNA helicase LGP2 manifests disparate antiviral responses. *The Journal of Immunology*, 178(10):6444–6455, 2007.
- [97] Takashi Satoh, Hiroki Kato, Yutaro Kumagai, Mitsutoshi Yoneyama, Shintaro Sato, Kazufumi Matsushita, Tohru Tsujimura, Takashi Fujita, Shizuo Akira, and Osamu Takeuchi. LGP2 is a positive regulator of RIG-I–and MDA5-mediated antiviral responses. *Proceedings of the National Academy of Sciences*, 107(4):1512–1517, 2010.
- [98] Annie M Bruns, Darja Pollpeter, Nastaran Hadizadeh, Sua Myong, John F Marko, and Curt M Horvath. ATP hydrolysis enhances RNA recognition and antiviral signal transduction by the innate immune sensor, laboratory of genetics and physiology 2 (LGP2). *Journal of Biological Chemistry*, 288(2):938–946, 2013.
- [99] Kay S Childs, Richard E Randall, and Stephen Goodbourn. LGP2 plays a critical role in sensitizing mda-5 to activation by double-stranded RNA. *PLoS One*, 8(5):e64202, 2013.
- [100] Mehul S Suthar, Hilario J Ramos, Margaret M Brassil, Jason Netland, Craig P Chappell, Gabriele Blahnik, Aimee McMillan, Michael S Diamond, Edward A Clark, Michael J Bevan, et al. The RIG-I-like receptor LGP2 controls CD8+ T cell survival and fitness. *Immunity*, 37(2):235–248, 2012.
- [101] Michaela U Gack. Mechanisms of RIG-I-like receptor activation and manipulation by viral pathogens. *Journal of Virology*, 88(10):5213–5216, 2014.
- [102] Martin Schlee, Andreas Roth, Veit Hornung, Cristina Amparo Hagmann, Vera Wimmenauer, Winfried Barchet, Christoph Coch, Markus Janke, Aleksandra Mihailovic, Greg Wardle, et al. Recognition of 5′ triphosphate by RIG-I helicase requires short blunt double-stranded RNA as contained in panhandle of negative-strand virus. *Immunity*, 31(1):25–34, 2009.
- [103] Andreas Schmidt, Tobias Schwerd, Wolfgang Hamm, Johannes C Hellmuth, Sheng Cui, Michael Wenzel, Franziska S Hoffmann, Marie-Cecile Michallet, Robert Besch, Karl-Peter Hopfner, et al. 5′-triphosphate RNA requires base-paired structures to activate antiviral signaling via RIG-I. *Proceedings of the National Academy of Sciences*, 106(29):12067–12072, 2009.
- [104] Delphine Goubau, Martin Schlee, Safia Deddouche, Andrea J Pruijssers, Thomas Zillinger, Marion Goldeck, Christine Schuberth, Annemarie G Van der Veen, Tsutomu Fujimura, Jan Rehwinkel, et al. Antiviral immunity via RIG-I-mediated recognition of RNA bearing 5′-diphosphates. *Nature*, 514(7522):372–375, 2014.
- [105] Christine Schuberth-Wagner, Janos Ludwig, Ann Kristin Bruder, Anna-Maria Herzner, Thomas

- Zillinger, Marion Goldeck, Tobias Schmidt, Jonathan L Schmid-Burgk, Romy Kerber, Steven Wolter, et al. A Conserved Histidine in the RNA Sensor RIG-I Controls Immune Tolerance to N 1-2'-O-Methylated Self RNA. *Immunity*, 43(1):41–51, 2015.
- [106] Jie Zheng, Hui Yee Yong, Nantika Panutdaporn, Chuanfa Liu, Kai Tang, and Dahai Luo. High-resolution HDX-MS reveals distinct mechanisms of RNA recognition and activation by RIG-I and MDA5. *Nucleic Acids Research*, 43(2):1216–1230, 2015.
- [107] Yanli Wang, Janos Ludwig, Christine Schuberth, Marion Goldeck, Martin Schlee, Haitao Li, Stefan Juranek, Gang Sheng, Ronald Micura, Thomas Tuschl, et al. Structural and functional insights into 5'-ppp RNA pattern recognition by the innate immune receptor RIG-I. *Nature Structural & Molecular Biology*, 17(7):781–787, 2010.
- [108] Anand Ramanathan, Swapnil C Devarkar, Fuguo Jiang, Matthew T Miller, Abdul G Khan, Joseph Marcotrigiano, and Smita S Patel. The autoinhibitory CARD2-Hel2i Interface of RIG-I governs RNA selection. *Nucleic Acids Research*, page gkv1299, 2015.
- [109] Swapnil C Devarkar, Chen Wang, Matthew T Miller, Anand Ramanathan, Fuguo Jiang, Abdul G Khan, Smita S Patel, and Joseph Marcotrigiano. Structural basis for m7G recognition and 2'-O-methyl discrimination in capped RNAs by the innate immune receptor RIG-I. *Proceedings of the National Academy of Sciences*, 113(3):596–601, 2016.
- [110] Sua Myong, Sheng Cui, Peter V Cornish, Axel Kirchhofer, Michaela U Gack, Jae U Jung, Karl-Peter Hopfner, and Taekjip Ha. Cytosolic viral sensor RIG-I is a 5'-triphosphate-dependent translocase on double-stranded RNA. *Science*, 323(5917):1070–1074, 2009.
- [111] Stéphanie Anchisi, Jessica Guerra, and Dominique Garcin. RIG-I ATPase Activity and Discrimination of Self-RNA versus Non-Self-RNA. *mBio*, 6(2):e02349–14, 2015.
- [112] Daisy W Leung and Gaya K Amarasinghe. When your cap matters: structural insights into self vs non-self recognition of 5' RNA by immunomodulatory host proteins. *Current Opinion in Structural Biology*, 36:133–141, 2016.
- [113] Andrew Kohlway, Dahai Luo, David C Rawling, Steve C Ding, and Anna Marie Pyle. Defining the functional determinants for RNA surveillance by RIG-I. *EMBO Reports*, 14(9):772–779, 2013.
- [114] Takeshi Saito, David M Owen, Fuguo Jiang, Joseph Marcotrigiano, and Michael Gale Jr. Innate immunity induced by composition-dependent RIG-I recognition of hepatitis C virus RNA. *Nature*, 454(7203):523–527, 2008.
- [115] Krishnamurthy Malathi, Beihua Dong, Michael Gale, and Robert H Silverman. Small self-RNA generated by RNase L amplifies antiviral innate immunity. *Nature*, 448(7155):816–819, 2007.
- [116] Krishnamurthy Malathi, Takeshi Saito, Nannette Crochet, David J Barton, Michael Gale, and Robert H Silverman. RNase L releases a small RNA from HCV RNA that refolds into a potent PAMP. *RNA*, 16(11):2108–2119, 2010.
- [117] Michaela Weber, Ali Gawanbacht, Matthias Habjan, Andreas Rang, Christoph Borner, Anna Mareike Schmidt, Sophie Veitinger, Ralf Jacob, Stéphanie Devignot, Georg Kochs, et al. Incoming RNA virus nucleocapsids containing a 5'-triphosphorylated genome activate RIG-I and antiviral signaling. *Cell Host & Microbe*, 13(3):336–346, 2013.
- [118] GuanQun Liu, Hong-Su Park, Hyun-Mi Pyo, Qiang Liu, and Yan Zhou. Influenza A virus pan-handle structure is directly involved in RIG-I activation and interferon induction. *Journal of*

- Virology*, 89(11):6067–6079, 2015.
- [119] Alina Baum, Ravi Sachidanandam, and Adolfo García-Sastre. Preference of RIG-I for short viral RNA molecules in infected cells revealed by next-generation sequencing. *Proceedings of the National Academy of Sciences*, 107(37):16303–16308, 2010.
- [120] Jie Xu, Xiomara Mercado-López, Jennifer T Grier, Won-keun Kim, Lauren F Chun, Edward B Irvine, Yoandris Del Toro Duany, Alison Kell, Sun Hur, Michael Gale, et al. Identification of a natural viral RNA motif that optimizes sensing of viral RNA by RIG-I. *mBio*, 6(5):e01265–15, 2015.
- [121] Min-Hi Lee, Pritesh Lalwani, Martin J Raftery, Markus Matthaei, Nina Lütteke, Sina Kirsanovs, Marco Binder, Rainer G Ulrich, Thomas Giese, Thorsten Wolff, et al. RNA helicase retinoic acid-inducible gene I as a sensor of Hantaan virus replication. *Journal of General Virology*, 92(9):2191–2200, 2011.
- [122] Hong-Xin Zhang, Zi-Xing Liu, Yue-Ping Sun, Jiang Zhu, Shun-Yuan Lu, Xue-Song Liu, Qiu-Hua Huang, Yin-Yin Xie, Hou-Bao Zhu, Su-Ying Dang, et al. Rig-I regulates NF- $\kappa$ B activity through binding to Nf- $\kappa$ b1 3'-UTR mRNA. *Proceedings of the National Academy of Sciences*, 110(16):6459–6464, 2013.
- [123] Raul Y Sanchez David, Chantal Combredet, Odile Sismeiro, Marie-Agnès Dillies, Bernd Jagla, Jean-Yves Coppée, Marie Mura, Mathilde Guerbois Galla, Philippe Despres, Frédéric Tangy, et al. Comparative analysis of viral RNA signatures on different RIG-I-like receptors. *eLife*, 5:e11275, 2016.
- [124] Andrea Ablasser, Franz Bauernfeind, Gunther Hartmann, Eicke Latz, Katherine A Fitzgerald, and Veit Hornung. RIG-I-dependent sensing of poly (dA:dT) through the induction of an RNA polymerase III-transcribed RNA intermediate. *Nature Immunology*, 10(10):1065–1072, 2009.
- [125] Yu-Hsin Chiu, John B MacMillan, and Zhijian J Chen. RNA polymerase III detects cytosolic DNA and induces type I interferons through the RIG-I pathway. *Cell*, 138(3):576–591, 2009.
- [126] Takeharu Minamitani, Dai Iwakiri, and Kenzo Takada. Adenovirus virus-associated RNAs induce type I interferon expression through a RIG-I-mediated pathway. *Journal of Virology*, 85(8):4035–4040, 2011.
- [127] Mirco Schmolke, Jenish R Patel, Elisa de Castro, Maria T Sánchez-Aparicio, Melissa B Uccellini, Jennifer C Miller, Balaji Manicassamy, Takashi Satoh, Taro Kawai, Shizuo Akira, et al. RIG-I detects mRNA of intracellular *Salmonella enterica* serovar Typhimurium during bacterial infection. *MBio*, 5(2):e01006–14, 2014.
- [128] Hiroki Kato, Osamu Takeuchi, Eriko Mikamo-Satoh, Reiko Hirai, Tomoji Kawai, Kazufumi Matsushita, Akane Hiiragi, Terence S Dermody, Takashi Fujita, and Shizuo Akira. Length-dependent recognition of double-stranded ribonucleic acids by retinoic acid-inducible gene-I and melanoma differentiation-associated gene 5. *The Journal of Experimental Medicine*, 205(7):1601–1610, 2008.
- [129] Andreas Pichlmair, Oliver Schulz, Choon-Ping Tan, Jan Rehwinkel, Hiroki Kato, Osamu Takeuchi, Shizuo Akira, Michael Way, Giampietro Schiavo, and Caetano Reis e Sousa. Activation of MDA5 requires higher-order RNA structures generated during virus infection. *Journal of Virology*, 83(20):10761–10769, 2009.

- [130] Alys Peisley, Cecilie Lin, Bin Wu, McGhee Orme-Johnson, Mengyuan Liu, Thomas Walz, and Sun Hur. Cooperative assembly and dynamic disassembly of MDA5 filaments for viral dsRNA recognition. *Proceedings of the National Academy of Sciences*, 108(52):21010–21015, 2011.
- [131] Roland Züst, Luisa Cervantes-Barragan, Matthias Habjan, Reinhard Maier, Benjamin W Neuman, John Ziebuhr, Kristy J Szretter, Susan C Baker, Winfried Barchet, Michael S Diamond, et al. Ribose 2 [prime]-O-methylation provides a molecular signature for the distinction of self and non-self mRNA dependent on the RNA sensor Mda5. *Nature Immunology*, 12(2):137–143, 2011.
- [132] Peter Liehl, Vanessa Zuzarte-Luís, Jennie Chan, Thomas Zillinger, Fernanda Baptista, Daniel Carapau, Madlen Konert, Kirsten K Hanson, Céline Carret, Caroline Lassnig, et al. Host-cell sensors for Plasmodium activate innate immunity against liver-stage infection. *Nature Medicine*, 20(1):47–53, 2014.
- [133] Gretja Schnell, Yueh-Ming Loo, Joseph Marcotrigiano, and Michael Gale Jr. Uridine composition of the poly-U/UC tract of HCV RNA defines non-self recognition by RIG-I. *PLoS Pathogens*, 8(8):e1002839, 2012.
- [134] William G Davis, J Bradford Bowzard, Suresh D Sharma, Mayim E Wiens, Priya Ranjan, Shivaprasaksh Gangappa, Olga Stuchlik, Jan Pohl, Ruben O Donis, Jacqueline M Katz, et al. The 3' untranslated regions of influenza genomic sequences are 5' PPP-independent ligands for RIG-I. *PLoS One*, 7(3):e32661, 2012.
- [135] Simon Runge, Konstantin MJ Sparrer, Charlotte Lässig, Katharina Hembach, Alina Baum, Adolfo García-Sastre, Johannes Söding, Karl-Klaus Conzelmann, and Karl-Peter Hopfner. In vivo ligands of MDA5 and RIG-I in measles virus-infected cells. *PLoS Pathogens*, 10(4):e1004081, 2014.
- [136] Brenda L Fredericksen, Brian C Keller, Jamie Fornek, Michael G Katze, and Michael Gale. Establishment and maintenance of the innate antiviral response to West Nile Virus involves both RIG-I and MDA5 signaling through IPS-1. *Journal of Virology*, 82(2):609–616, 2008.
- [137] John S Errett, Mehul S Suthar, Aimee McMillan, Michael S Diamond, and Michael Gale. The essential, nonredundant roles of RIG-I and MDA5 in detecting and controlling West Nile virus infection. *Journal of Virology*, 87(21):11416–11425, 2013.
- [138] Diana A Pippig, Johannes C Hellmuth, Sheng Cui, Axel Kirchhofer, Katja Lammens, Alfred Lammens, Andreas Schmidt, Simon Rothenfusser, and Karl-Peter Hopfner. The regulatory domain of the RIG-I family ATPase LGP2 senses double-stranded RNA. *Nucleic Acids Research*, page gkp059, 2009.
- [139] Tatsuya Nishino, Kayoko Komori, Daisuke Tsuchiya, Yoshizumi Ishino, and Kosuke Morikawa. Crystal structure and functional implications of Pyrococcus furiosus hef helicase domain involved in branched DNA processing. *Structure*, 13(1):143–153, 2005.
- [140] Sheng Cui, Katharina Eisenächer, Axel Kirchhofer, Krzysztof Brzózka, Alfred Lammens, Katja Lammens, Takashi Fujita, Karl-Klaus Conzelmann, Anne Krug, and Karl-Peter Hopfner. The C-terminal regulatory domain is the RNA 5'-triphosphate sensor of RIG-I. *Molecular Cell*, 29(2):169–179, 2008.
- [141] Kristof Kersse, Jelle Verspurten, Tom Vanden Berghe, and Peter Vandenabeele. The death-fold superfamily of homotypic interaction motifs. *Trends in Biochemical Sciences*, 36(10):541–552,

- 2011.
- [142] David C Rawling and Anna Marie Pyle. Parts, assembly and operation of the RIG-I family of motors. *Current Opinion in Structural Biology*, 25:25–33, 2014.
- [143] Martin R Singleton, Mark S Dillingham, and Dale B Wigley. Structure and mechanism of helicases and nucleic acid translocases. *Annual Reviews of Biochemistry*, 76:23–50, 2007.
- [144] Bin Wu, Alys Peisley, Claire Richards, Hui Yao, Xiaohui Zeng, Cecilie Lin, Feixia Chu, Thomas Walz, and Sun Hur. Structural basis for dsRNA recognition, filament formation, and antiviral signal activation by MDA5. *Cell*, 152(1):276–289, 2013.
- [145] Emiko Uchikawa, Mathilde Lethier, H  l  ne Malet, Joanna Brunel, Denis Gerlier, and Stephen Cusack. Structural Analysis of dsRNA Binding to Anti-viral Pattern Recognition Receptors LGP2 and MDA5. *Molecular Cell*, 62(4):586–602, 2016.
- [146] Kiyohiro Takahasi, Mitsutoshi Yoneyama, Tatsuya Nishihori, Reiko Hirai, Hiroyuki Kumeta, Ryo Narita, Michael Gale, Fuyuhiko Inagaki, and Takashi Fujita. Nonself RNA-sensing mechanism of RIG-I helicase and activation of antiviral immune responses. *Molecular Cell*, 29(4):428–440, 2008.
- [147] Filiz Civril, Matthew Bennett, Manuela Moldt, Tobias Deimling, Gregor Witte, Stefan Schiesser, Thomas Carell, and Karl-Peter Hopfner. The RIG-I ATPase domain structure reveals insights into ATP-dependent antiviral signalling. *EMBO Reports*, 12(11):1127–1134, 2011.
- [148] Tobias Deimling, Sheng Cui, Katja Lammens, K-P Hopfner, and Gregor Witte. Crystal and solution structure of the human RIG-I SF2 domain. *Structural Biology and Crystallization Communications*, 70(8), 2014.
- [149] Ian C Berke and Yorgo Modis. MDA5 cooperatively forms dimers and ATP-sensitive filaments upon binding double-stranded RNA. *The EMBO Journal*, 31(7):1714–1726, 2012.
- [150] David C Rawling, Andrew S Kohlway, Dahai Luo, Steve C Ding, and Anna Marie Pyle. The RIG-I ATPase core has evolved a functional requirement for allosteric stabilization by the Pincer domain. *Nucleic Acids Research*, 42(18):11601–11611, 2014.
- [151] Cheng Lu, Hengyu Xu, CT Ranjith-Kumar, Monica T Brooks, Tim Y Hou, Fuqu Hu, Andrew B Herr, Roland K Strong, C Cheng Kao, and Pingwei Li. The structural basis of 5' triphosphate double-stranded RNA recognition by RIG-I C-terminal domain. *Structure*, 18(8):1032–1043, 2010.
- [152] Alys Peisley, Bin Wu, Hui Xu, Zhijian J Chen, and Sun Hur. Structural basis for ubiquitin-mediated antiviral signal activation by RIG-I. *Nature*, 509(7498):110–114, 2014.
- [153] Bin Wu, Alys Peisley, David Tetrault, Zongli Li, Edward H Egelman, Katharine E Magor, Thomas Walz, Pawel A Penczek, and Sun Hur. Molecular imprinting as a signal-activation mechanism of the viral rna sensor rig-i. *Molecular Cell*, 55(4):511–523, 2014.
- [154] Su-Chang Lin, Yu-Chih Lo, and Hao Wu. Helical assembly in the MyD88–IRAK4–IRAK2 complex in TLR/IL-1R signalling. *Nature*, 465(7300):885–890, 2010.
- [155] A Lu, Y Li, FI Schmidt, Q Yin, S Chen, TM Fu, AB Tong, HL Ploegh, Y Mao, and H Wu. Molecular basis of caspase-1 polymerization and its inhibition by a new capping mechanism. *Nature Structural & Molecular Biology*, 2016.

- [156] Ian C Berke, Xiong Yu, Yorgo Modis, and Edward H Egelman. MDA5 assembles into a polar helical filament on dsRNA. *Proceedings of the National Academy of Sciences*, 109(45):18437–18441, 2012.
- [157] Xiaojun Li, Cheng Lu, Mikaela Stewart, Hengyu Xu, Roland K Strong, Tatyana Igumenova, and Pingwei Li. Structural basis of double-stranded RNA recognition by the RIG-I like receptor MDA5. *Archives of Biochemistry and Biophysics*, 488(1):23–33, 2009.
- [158] Meredith E Davis and Michaela U Gack. Ubiquitination in the antiviral immune response. *Virology*, 479:52–65, 2015.
- [159] Michaela U Gack, Estanislao Nistal-Villán, Kyung-Soo Inn, Adolfo García-Sastre, and Jae U Jung. Phosphorylation-mediated negative regulation of RIG-I antiviral activity. *Journal of Virology*, 84(7):3220–3229, 2010.
- [160] Natalya P Maharaj, Effi Wies, Andrej Stoll, and Michaela U Gack. Conventional protein kinase C- $\alpha$  (PKC- $\alpha$ ) and PKC- $\beta$  negatively regulate RIG-I antiviral signal transduction. *Journal of Virology*, 86(3):1358–1371, 2012.
- [161] Zhiguo Sun, Hongwei Ren, Yan Liu, Jessica L Teeling, and Jun Gu. Phosphorylation of RIG-I by casein kinase II inhibits its antiviral response. *Journal of Virology*, 85(2):1036–1047, 2011.
- [162] Philipp Mertins, Jana W Qiao, Jinal Patel, Namrata D Udeshi, Karl R Clauser, DR Mani, Michael W Burgess, Michael A Gillette, Jacob D Jaffe, and Steven A Carr. Integrated proteomic analysis of post-translational modifications by serial enrichment. *Nature Methods*, 10(7):634–637, 2013.
- [163] Xiaoqing Zhang, Haiyang Yu, Jun Zhao, Xiuqing Li, Jiada Li, Jiantai He, Zanzhan Xia, and Jinfeng Zhao. IKK $\epsilon$  negatively regulates RIG-I via direct phosphorylation. *Journal of Medical Virology*, 2015.
- [164] Chunaram Choudhary, Chanchal Kumar, Florian Gnad, Michael L Nielsen, Michael Rehman, Tobias C Walther, Jesper V Olsen, and Matthias Mann. Lysine acetylation targets protein complexes and co-regulates major cellular functions. *Science*, 325(5942):834–840, 2009.
- [165] Woong Kim, Eric J Bennett, Edward L Huttlin, Ailan Guo, Jing Li, Anthony Possemato, Mathew E Sowa, Ramin Rad, John Rush, Michael J Comb, et al. Systematic and quantitative assessment of the ubiquitin-modified proteome. *Molecular Cell*, 44(2):325–340, 2011.
- [166] Effi Wies, May K Wang, Natalya P Maharaj, Kan Chen, Shenghua Zhou, Robert W Finberg, and Michaela U Gack. Dephosphorylation of the RNA sensors RIG-I and MDA5 by the phosphatase PP1 is essential for innate immune signaling. *Immunity*, 38(3):437–449, 2013.
- [167] Estanislao Nistal-Villán, Michaela U Gack, Gustavo Martínez-Delgado, Natalya P Maharaj, Kyung-Soo Inn, Heyi Yang, Rong Wang, Aneel K Aggarwal, Jae U Jung, and Adolfo García-Sastre. Negative role of RIG-I serine 8 phosphorylation in the regulation of interferon- $\beta$  production. *Journal of Biological Chemistry*, 285(26):20252–20261, 2010.
- [168] Wenwen Zeng, Lijun Sun, Xiaomo Jiang, Xiang Chen, Fajian Hou, Anirban Adhikari, Ming Xu, and Zhijian J Chen. Reconstitution of the RIG-I pathway reveals a signaling role of unanchored polyubiquitin chains in innate immunity. *Cell*, 141(2):315–330, 2010.
- [169] Jesper Melchjorsen, Helle Kristiansen, Rune Christiansen, Johanna Rintahaka, Sampsa Matikainen, Søren R Paludan, and Rune Hartmann. Differential regulation of the OASL and

- OAS1 genes in response to viral infections. *Journal of Interferon and Cytokine Research*, 29(4):199–208, 2009.
- [170] Jianzhong Zhu, Yugen Zhang, Arundhati Ghosh, Rolando A Cuevas, Adriana Forero, Jayeeta Dhar, Mikkel Søres Ibsen, Jonathan Leo Schmid-Burgk, Tobias Schmidt, Madhavi K Ganapathiraju, et al. Antiviral activity of human OASL protein is mediated by enhancing signaling of the RIG-I RNA sensor. *Immunity*, 40(6):936–948, 2014.
- [171] Mikkel Søres Ibsen, Hans Henrik Gad, Line Lykke Andersen, Veit Hornung, Ilkka Julkunen, Saumendra N Sarkar, and Rune Hartmann. Structural and functional analysis reveals that human OASL binds dsRNA to enhance RIG-I signaling. *Nucleic Acids Research*, page gkv389, 2015.
- [172] Zhiqiang Mi, Jihuan Fu, Yanbao Xiong, and Hong Tang. SUMOylation of RIG-I positively regulates the type I interferon signaling. *Protein & Cell*, 1(3):275–283, 2010.
- [173] Dong Gao, Yong-Kang Yang, Rui-Peng Wang, Xiang Zhou, Fei-Ci Diao, Min-Dian Li, Zhong-He Zhai, Zheng-Fan Jiang, and Dan-Ying Chen. REUL is a novel E3 ubiquitin ligase and stimulator of retinoic-acid-inducible gene-1. *PLoS One*, 4(6):e5760, 2009.
- [174] Jie Yan, Qi Li, Ai-Ping Mao, Ming-Ming Hu, and Hong-Bing Shu. TRIM4 modulates type I interferon induction and cellular antiviral response by targeting RIG-I for K63-linked ubiquitination. *Journal of Molecular Cell Biology*, 6(2):154–163, 2014.
- [175] Kanako Kuniyoshi, Osamu Takeuchi, Surya Pandey, Takashi Satoh, Hidenori Iwasaki, Shizuo Akira, and Taro Kawai. Pivotal role of RNA-binding E3 ubiquitin ligase MEX3C in RIG-I-mediated antiviral innate immunity. *Proceedings of the National Academy of Sciences*, 111(15):5646–5651, 2014.
- [176] Hiroyuki Oshiumi, Misako Matsumoto, Shigetsugu Hatakeyama, and Tsukasa Seya. Riplet/RNF135, a RING finger protein, ubiquitinates RIG-I to promote interferon- $\beta$  induction during the early phase of viral infection. *Journal of Biological Chemistry*, 284(2):807–817, 2009.
- [177] Hiroyuki Oshiumi, Moeko Miyashita, Misako Matsumoto, and Tsukasa Seya. A distinct role of Riplet-mediated K63-Linked polyubiquitination of the RIG-I repressor domain in human antiviral innate immune responses. *PLoS Pathogens*, 9(8):e1003533, 2013.
- [178] Su Jin Choi, Hyun-Cheol Lee, Jae-Hoon Kim, Song Yi Park, Tae-Hwan Kim, Woon-Kyu Lee, Duk-Jae Jang, Ji-Eun Yoon, Young-Il Choi, Seihwan Kim, et al. HDAC6 regulates cellular viral RNA sensing by deacetylation of RIG-I. *The EMBO Journal*, page e201592586, 2016.
- [179] Kei-ichiro Arimoto, Hitoshi Takahashi, Takayuki Hishiki, Hideyuki Konishi, Takashi Fujita, and Kunitada Shimotohno. Negative regulation of the RIG-I signaling by the ubiquitin ligase RNF125. *Proceedings of the National Academy of Sciences*, 104(18):7500–7505, 2007.
- [180] Qian Hao, Shi Jiao, Zhubing Shi, Chuanchuan Li, Xia Meng, Zhen Zhang, Yanyan Wang, Xiaomin Song, Wenjia Wang, Rongguang Zhang, et al. A non-canonical role of the p97 complex in RIG-I antiviral signaling. *The EMBO Journal*, page e201591888, 2015.
- [181] Lijuan Wang, Wei Zhao, Meng Zhang, Peng Wang, Kai Zhao, Xueying Zhao, Shangru Yang, and Chengjiang Gao. USP4 positively regulates RIG-I-mediated antiviral response through deubiquitination and stabilization of RIG-I. *Journal of Virology*, 87(8):4507–4515, 2013.

- [182] Chen Zhao, Carilee Denison, Jon M Huibregtse, Steven Gygi, and Robert M Krug. Human ISG15 conjugation targets both IFN-induced and constitutively expressed proteins functioning in diverse cellular pathways. *Proceedings of the National Academy of Sciences of the United States of America*, 102(29):10200–10205, 2005.
- [183] Min-Jung Kim, Sun-Young Hwang, Tadaatsu Imaizumi, and Joo-Yeon Yoo. Negative feedback regulation of RIG-I-mediated antiviral signaling by interferon-induced ISG15 conjugation. *Journal of Virology*, 82(3):1474–1483, 2008.
- [184] Kyung-Soo Inn, Michaela U Gack, Fuminori Tokunaga, Mude Shi, Lai-Yee Wong, Kazuhiro Iwai, and Jae U Jung. Linear ubiquitin assembly complex negatively regulates RIG-I-and TRIM25-mediated type I interferon induction. *Molecular Cell*, 41(3):354–365, 2011.
- [185] Minying Zhang, Xuefeng Wu, Andrew J Lee, Wei Jin, Mikyoung Chang, Ato Wright, Tadaatsu Imaizumi, and Shao-Cong Sun. Regulation of I $\kappa$ B kinase-related kinases and antiviral responses by tumor suppressor CYLD. *Journal of Biological Chemistry*, 283(27):18621–18626, 2008.
- [186] Constantin S Friedman, Marie Anne O’Donnell, Diana Legarda-Addison, Aylwin Ng, Washington B Cardenas, Jacob S Yount, Thomas M Moran, Christopher F Basler, Akihiko Komuro, Curt M Horvath, et al. The tumour suppressor CYLD is a negative regulator of RIG-I-mediated antiviral response. *EMBO Reports*, 9(9):930–936, 2008.
- [187] Jun Cui, Yanxia Song, Yinyin Li, Qingyuan Zhu, Peng Tan, Yunfei Qin, Helen Y Wang, and Rong-Fu Wang. USP3 inhibits type I interferon signaling by deubiquitinating RIG-I-like receptors. *Cell Research*, 24(4):400–416, 2014.
- [188] Huan Zhang, Dang Wang, Huijuan Zhong, Rui Luo, Min Shang, Dezhi Liu, Huanchun Chen, Liurong Fang, and Shaobo Xiao. Ubiquitin-specific Protease 15 Negatively Regulates Virus-induced Type I Interferon Signaling via Catalytically-dependent and-independent Mechanisms. *Scientific Reports*, 5, 2015.
- [189] Yihui Fan, Renfang Mao, Yang Yu, Shangfeng Liu, Zhongcheng Shi, Jin Cheng, Huiyuan Zhang, Lei An, Yanling Zhao, Xin Xu, et al. USP21 negatively regulates antiviral response by acting as a RIG-I deubiquitinase. *The Journal of Experimental Medicine*, 211(2):313–328, 2014.
- [190] Peter V Hornbeck, Bin Zhang, Beth Murray, Jon M Kornhauser, Vaughan Latham, and Elzbieta Skrzypek. PhosphoSitePlus, 2014: mutations, PTMs and recalibrations. *Nucleic Acids Research*, 43(D1):D512–D520, 2015.
- [191] Jihuan Fu, Yanbao Xiong, Youli Xu, Genhong Cheng, and Hong Tang. MDA5 is SUMOylated by PIAS2 $\beta$  in the upregulation of type I interferon signaling. *Molecular Immunology*, 48(4):415–422, 2011.
- [192] Dahai Luo, Andrew Kohlway, and Anna Marie Pyle. Duplex RNA activated ATPases (DRAs) Platforms for RNA sensing, signaling and processing. *RNA Biology*, 10(1):111–120, 2013.
- [193] Eckhard Jankowsky, editor. *RNA Helicases*, volume 19. RSC Biomolecular Sciences, 2010.
- [194] Eckhard Jankowsky. RNA helicases at work: binding and rearranging. *Trends in Biochemical Sciences*, 36(1):19–29, 2011.
- [195] Adriana Vela, Olga Fedorova, Steve C Ding, and Anna Marie Pyle. The thermodynamic basis for viral RNA detection by the RIG-I innate immune sensor. *Journal of Biological Chemistry*,

- 287(51):42564–42573, 2012.
- [196] Darja Bamming and Curt M Horvath. Regulation of signal transduction by enzymatically inactive antiviral RNA helicase proteins MDA5, RIG-I, and LGP2. *Journal of Biological Chemistry*, 284(15):9700–9712, 2009.
- [197] Gillian I Rice, Yoandris del Toro Duany, Emma M Jenkinson, Gabriella MA Forte, Beverley H Anderson, Giada Ariaudo, Brigitte Bader-Meunier, Eileen M Baildam, Roberta Battini, Michael W Beresford, et al. Gain-of-function mutations in IFIH1 cause a spectrum of human disease phenotypes associated with upregulated type I interferon signaling. *Nature Genetics*, 46(5):503–509, 2014.
- [198] Jenish R Patel, Ankur Jain, Yi-ying Chou, Alina Baum, Taekjip Ha, and Adolfo García-Sastre. ATPase-driven oligomerization of RIG-I on RNA allows optimal activation of type-I interferon. *EMBO Reports*, 14(9):780–787, 2013.
- [199] Alys Peisley, Bin Wu, Hui Yao, Thomas Walz, and Sun Hur. RIG-I forms signaling-competent filaments in an ATP-dependent, ubiquitin-independent manner. *Molecular Cell*, 51(5):573–583, 2013.
- [200] Hui Yao, Meike Dittmann, Alys Peisley, Hans-Heinrich Hoffmann, Rachel H Gilmore, Tobias Schmidt, Jonathan L Schmid-Burgk, Veit Hornung, Charles M Rice, and Sun Hur. ATP-dependent effector-like functions of RIG-I-like receptors. *Molecular Cell*, 58(3):541–548, 2015.
- [201] Alys Peisley, Myung Hyun Jo, Cecilie Lin, Bin Wu, McGhee Orme-Johnson, Thomas Walz, Sungchul Hohng, and Sun Hur. Kinetic mechanism for viral dsRNA length discrimination by MDA5 filaments. *Proceedings of the National Academy of Sciences*, 109(49):E3340–E3349, 2012.
- [202] Seiichi Sato, Kai Li, Takeshi Kameyama, Takaya Hayashi, Yuji Ishida, Shuko Murakami, Tsunamasa Watanabe, Sayuki Iijima, Yu Sakurai, Koichi Watashi, et al. The RNA sensor RIG-I dually functions as an innate sensor and direct antiviral factor for hepatitis B virus. *Immunity*, 42(1):123–132, 2015.
- [203] Michaela Weber, Hanna Sediri, Ulrike Felgenhauer, Ina Binzen, Sebastian Bänfer, Ralf Jacob, Linda Brunotte, Adolfo García-Sastre, Jonathan L Schmid-Burgk, Tobias Schmidt, et al. Influenza virus adaptation PB2-627K modulates nucleocapsid inhibition by the pathogen sensor RIG-I. *Cell Host & Microbe*, 17(3):309–319, 2015.
- [204] U Schneider, A Martin, M Schwemmler, and P Staeheli. Genome trimming by Borna disease viruses: viral replication control or escape from cellular surveillance? *Cellular and Molecular Life Sciences*, 64(9):1038–1042, 2007.
- [205] Matthias Habjan, Ida Andersson, Jonas Klingström, Michael Schumann, Arnold Martin, Petra Zimmermann, Valentina Wagner, Andreas Pichlmair, Urs Schneider, Elke Mühlberger, et al. Processing of genome 5' termini as a strategy of negative-strand RNA viruses to avoid RIG-I-dependent interferon induction. *PloS One*, 3(4):e2032, 2008.
- [206] Hao Wang, Antti Vaheri, Friedemann Weber, and Alexander Plyusnin. Old World hantaviruses do not produce detectable amounts of dsRNA in infected cells and the 5' termini of their genomic RNAs are monophosphorylated. *Journal of General Virology*, 92(5):1199–1204, 2011.
- [207] Jean-Baptiste Marq, Daniel Kolakofsky, and Dominique Garcin. Unpaired 5' ppp-nucleotides,

- as found in arenavirus double-stranded RNA panhandles, are not recognized by RIG-I. *Journal of Biological Chemistry*, 285(24):18208–18216, 2010.
- [208] Daisy W Leung, Kathleen C Prins, Dominika M Borek, Mina Farahbakhsh, JoAnn M Tufariello, Parameshwaran Ramanan, Jay C Nix, Luke A Helgeson, Zbyszek Otwinowski, Richard B Honzatko, et al. Structural basis for dsRNA recognition and interferon antagonism by Ebola VP35. *Nature Structural & Molecular Biology*, 17(2):165–172, 2010.
- [209] Shridhar Bale, Jean-Philippe Julien, Zachary A Bornholdt, Christopher R Kimberlin, Peter Halfmann, Michelle A Zandonatti, John Kunert, Gerard JA Kroon, Yoshihiro Kawaoka, Ian J MacRae, et al. Marburg virus VP35 can both fully coat the backbone and cap the ends of dsRNA for interferon antagonism. *PLoS Pathogens*, 8(9):e1002916, 2012.
- [210] Parameshwaran Ramanan, Megan R Edwards, Reed S Shabman, Daisy W Leung, Ariel C Endlich-Frazier, Dominika M Borek, Zbyszek Otwinowski, Gai Liu, Juyoung Huh, Christopher F Basler, et al. Structural basis for Marburg virus VP35-mediated immune evasion mechanisms. *Proceedings of the National Academy of Sciences*, 109(50):20661–20666, 2012.
- [211] Kathryn M Hastie, Christopher R Kimberlin, Michelle A Zandonatti, Ian J MacRae, and Erica Ollmann Saphire. Structure of the Lassa virus nucleoprotein reveals a dsRNA-specific 3' to 5' exonuclease activity essential for immune suppression. *Proceedings of the National Academy of Sciences*, 108(6):2396–2401, 2011.
- [212] Michaela Ulrike Gack, Randy Allen Albrecht, Tomohiko Urano, Kyung-Soo Inn, I-Chueh Huang, Elena Carnero, Michael Farzan, Satoshi Inoue, Jae Ung Jung, and Adolfo García-Sastre. Influenza A virus NS1 targets the ubiquitin ligase TRIM25 to evade recognition by the host viral RNA sensor RIG-I. *Cell Host & Microbe*, 5(5):439–449, 2009.
- [213] Kyung-Soo Inn, Sun-Hwa Lee, Jessica Y Rathbun, Lai-Yee Wong, Zsolt Toth, Keigo Machida, Jing-Hsiung James Ou, and Jae U Jung. Inhibition of RIG-I-mediated signaling by Kaposi's sarcoma-associated herpesvirus-encoded deubiquitinase ORF64. *Journal of Virology*, 85(20):10899–10904, 2011.
- [214] Puck B van Kasteren, Corrine Beugeling, Dennis K Ninaber, Natalia Frias-Staheli, Sander van Boheemen, Adolfo García-Sastre, Eric J Snijder, and Marjolein Kikkert. Arterivirus and nairovirus ovarian tumor domain-containing deubiquitinases target activated RIG-I to control innate immune signaling. *Journal of Virology*, 86(2):773–785, 2012.
- [215] Meredith E Davis, May K Wang, Linda J Rennick, Florian Full, Sebastian Gableske, Annelies W Mesman, Sonja I Gringhuis, Teunis BH Geijtenbeek, W Paul Duprex, and Michaela U Gack. Antagonism of the phosphatase PP1 by the measles virus V protein is required for innate immune escape of MDA5. *Cell Host & Microbe*, 16(1):19–30, 2014.
- [216] Jean-Patrick Parisien, Darja Bamming, Akihiko Komuro, Aparna Ramachandran, Jason J Rodriguez, Glen Barber, Robert D Wojahn, and Curt M Horvath. A shared interface mediates paramyxovirus interference with antiviral RNA helicases MDA5 and LGP2. *Journal of Virology*, 83(14):7252–7260, 2009.
- [217] Carina Motz, Kerstin Monika Schuhmann, Axel Kirchofer, Manuela Moldt, Gregor Witte, Karl-Klaus Conzelmann, and Karl-Peter Hopfner. Paramyxovirus V proteins disrupt the fold of the RNA sensor MDA5 to inhibit antiviral signaling. *Science*, 339(6120):690–693, 2013.
- [218] Paola M Barral, Juliet M Morrison, Jennifer Drahos, Pankaj Gupta, Devanand Sarkar, Paul B

- Fisher, and Vincent R Racaniello. MDA-5 is cleaved in poliovirus-infected cells. *Journal of Virology*, 81(8):3677–3684, 2007.
- [219] Paola M Barral, Devanand Sarkar, Paul B Fisher, and Vincent R Racaniello. RIG-I is cleaved during picornavirus infection. *Virology*, 391(2):171–176, 2009.
- [220] Qian Feng, Martijn A Langereis, Marie Lork, Mai Nguyen, Stanleyson V Hato, Kjerstin Lanke, Luni Emdad, Praveen Bhoopathi, Paul B Fisher, Richard E Lloyd, et al. Enterovirus 2Apro targets MDA5 and MAVS in infected cells. *Journal of Virology*, 88(6):3369–3378, 2014.
- [221] Hiroki Kato and Takashi Fujita. RIG-I-like receptors and autoimmune diseases. *Current Opinion in Immunology*, 37:40–45, 2015.
- [222] Insa Buers, Yvonne Nitschke, and Frank Rutsch. Novel interferonopathies associated with mutations in RIG-I like receptors. *Cytokine & Growth Factor Reviews*, 2016.
- [223] Yanick J Crow. Type I interferonopathies: a novel set of inborn errors of immunity. *Annals of the New York Academy of Sciences*, 1238(1):91–98, 2011.
- [224] J Aicardi and F Goutières. A progressive familial encephalopathy in infancy with calcifications of the basal ganglia and chronic cerebrospinal fluid lymphocytosis. *Annals of Neurology*, 15(1):49–54, 1984.
- [225] Yanick J Crow, Diana S Chase, Johanna Lowenstein Schmidt, Marcin Szykiewicz, Gabriella Forte, Hannah L Gornall, Anthony Oojageer, Beverley Anderson, Amy Pizzino, Guy Helman, et al. Characterization of human disease phenotypes associated with mutations in TREX1, RNASEH2A, RNASEH2B, RNASEH2C, SAMHD1, ADAR, and IFIH1. *American Journal of Medical Genetics Part A*, 167(2):296–312, 2015.
- [226] Yanick J Crow and Nicolas Manel. Aicardi-Goutieres syndrome and the type I interferonopathies. *Nature Reviews Immunology*, 15(7):429–440, 2015.
- [227] Yanick J Crow, Bruce E Hayward, Rekha Parmar, Peter Robins, Andrea Leitch, Manir Ali, Deborah N Black, Hans van Bokhoven, Han G Brunner, Ben C Hamel, et al. Mutations in the gene encoding the 3′-5′ DNA exonuclease TREX1 cause Aicardi-Goutières syndrome at the AGS1 locus. *Nature Genetics*, 38(8):917–920, 2006.
- [228] Yanick J Crow, Andrea Leitch, Bruce E Hayward, Anna Garner, Rekha Parmar, Elen Griffith, Manir Ali, Colin Semple, Jean Aicardi, Riyana Babul-Hirji, et al. Mutations in genes encoding ribonuclease H2 subunits cause Aicardi-Goutières syndrome and mimic congenital viral brain infection. *Nature Genetics*, 38(8):910–916, 2006.
- [229] Gillian I Rice, Jacquelyn Bond, Aruna Asipu, Rebecca L Brunette, Iain W Manfield, Ian M Carr, Jonathan C Fuller, Richard M Jackson, Teresa Lamb, Tracy A Briggs, et al. Mutations involved in Aicardi-Goutières syndrome implicate SAMHD1 as regulator of the innate immune response. *Nature Genetics*, 41(7):829–832, 2009.
- [230] Gillian I Rice, Paul R Kasher, Gabriella MA Forte, Niamh M Mannion, Sam M Greenwood, Marcin Szykiewicz, Jonathan E Dickerson, Sanjeev S Bhaskar, Massimiliano Zampini, Tracy A Briggs, et al. Mutations in ADAR1 cause Aicardi-Goutières syndrome associated with a type I interferon signature. *Nature Genetics*, 44(11):1243–1248, 2012.
- [231] Hirotsugu Oda, Kenji Nakagawa, Junya Abe, Tomonari Awaya, Masahide Funabiki, Atsushi Hijikata, Ryuta Nishikomori, Makoto Funatsuka, Yusei Ohshima, Yuji Sugawara, et al. Aicardi-

- Goutieres syndrome is caused by IFIH1 mutations. *The American Journal of Human Genetics*, 95(1):121–125, 2014.
- [232] Jochen C Hartner, Carl R Walkley, Jun Lu, and Stuart H Orkin. ADAR1 is essential for the maintenance of hematopoiesis and suppression of interferon signaling. *Nature Immunology*, 10(1):109–115, 2009.
- [233] Patrice Vitali and ADJ Scadden. Double-stranded RNAs containing multiple IU pairs are sufficient to suppress interferon induction and apoptosis. *Nature Structural & Molecular Biology*, 17(99):1043–1050, 2010.
- [234] Niamh M Mannion, Sam M Greenwood, Robert Young, Sarah Cox, James Brindle, David Read, Christoffer Nellåker, Cornelia Vesely, Chris P Ponting, Paul J McLaughlin, et al. The RNA-editing enzyme ADAR1 controls innate immune responses to RNA. *Cell Reports*, 9(4):1482–1494, 2014.
- [235] Brian J Liddicoat, Robert Piskol, Alistair M Chalk, Gokul Ramaswami, Miyoko Higuchi, Jochen C Hartner, Jin Billy Li, Peter H Seeburg, and Carl R Walkley. RNA editing by ADAR1 prevents MDA5 sensing of endogenous dsRNA as nonself. *Science*, 349(6252):1115–1120, 2015.
- [236] Yogita Ghodke-Puranik and Timothy B Niewold. Genetics of the type I interferon pathway in systemic lupus erythematosus. *International Journal of Clinical Rheumatology*, 8(6):657–669, 2013.
- [237] Daniel Wallace and Bevra Hannahs Hahn. *Dubois' Lupus Erythematosus and related syndromes: Expert Consult-Online*. Elsevier Health Sciences, 2012.
- [238] Emily C Baechler, Franak M Batliwalla, George Karypis, Patrick M Gaffney, Ward A Ortmann, Karl J Espe, Katherine B Shark, William J Grande, Karis M Hughes, Vivek Kapur, et al. Interferon-inducible gene expression signature in peripheral blood cells of patients with severe lupus. *Proceedings of the National Academy of Sciences*, 100(5):2610–2615, 2003.
- [239] Corinna E Weckerle and Timothy B Niewold. The unexplained female predominance of systemic lupus erythematosus: clues from genetic and cytokine studies. *Clinical Reviews in Allergy & Immunology*, 40(1):42–49, 2011.
- [240] Yong Cui, Yujun Sheng, and Xuejun Zhang. Genetic susceptibility to SLE: recent progress from GWAS. *Journal of Autoimmunity*, 41:25–33, 2013.
- [241] Vesela Gateva, Johanna K Sandling, Geoff Hom, Kimberly E Taylor, Sharon A Chung, Xin Sun, Ward Ortmann, Roman Kosoy, Ricardo C Ferreira, Gunnel Nordmark, et al. A large-scale replication study identifies TNIP1, PRDM1, JAZF1, UHRF1BP1 and IL10 as risk loci for systemic lupus erythematosus. *Nature Genetics*, 41(11):1228–1233, 2009.
- [242] Deborah S Cunninghame Graham, David L Morris, Tushar R Bhangale, Lindsey A Criswell, Ann-Christine Syvänen, Lars Rönnblom, Timothy W Behrens, Robert R Graham, and Timothy J Vyse. Association of NCF2, IKZF1, IRF8, IFIH1, and TYK2 with systemic lupus erythematosus. *PLoS Genetics*, 7(10):e1002341, 2011.
- [243] Lien Van Eyck, Lien De Somer, Diana Pombal, Simon Bornschein, Glynis Frans, Stéphanie Humblet-Baron, Leen Moens, Francis de Zegher, Xavier Bossuyt, Carine Wouters, et al. Brief report: IFIH1 mutation causes systemic lupus erythematosus with selective IgA deficiency. *Arthritis & Rheumatology*, 67(6):1592–1597, 2015.

- [244] Julio E Molineros, Amit K Maiti, Celi Sun, Loren L Looger, Shizhong Han, Xana Kim-Howard, Stuart Glenn, Adam Adler, Jennifer A Kelly, Timothy B Niewold, et al. Admixture mapping in lupus identifies multiple functional variants within IFIH1 associated with apoptosis, inflammation, and autoantibody production. *PLoS Genetics*, 9(2):e1003222, 2013.
- [245] Edward B Singleton and David F Merten. An unusual syndrome of widened medullary cavities of the metacarpals and phalanges, aortic calcification and abnormal dentition. *Pediatric Radiology*, 1(1):2–7, 1973.
- [246] Annette Feigenbaum, Christine Müller, Christopher Yale, Johannes Kleinheinz, Peter Jezewski, Hans Gerd Kehl, Mary MacDougall, Frank Rutsch, and Raoul Hennekam. Singleton–Merten syndrome: An autosomal dominant disorder with variable expression. *American Journal of Medical Genetics Part A*, 161(2):360–370, 2013.
- [247] Mi-Ae Jang, Eun Kyoung Kim, Nhung TH Nguyen, Woo-Jong Kim, Joo-Yeon Yoo, Jinhyuk Lee, Yun-Mi Jeong, Cheol-Hee Kim, Ok-Hwa Kim, Seongsoo Sohn, et al. Mutations in DDX58, which encodes RIG-I, cause atypical Singleton-Merten syndrome. *The American Journal of Human Genetics*, 96(2):266–274, 2015.
- [248] Frank Rutsch, Mary MacDougall, Changming Lu, Insa Buers, Olga Mamaeva, Yvonne Nitschke, Gillian I Rice, Heidi Erlandsen, Hans Gerd Kehl, Holger Thiele, et al. A specific IFIH1 gain-of-function mutation causes Singleton-Merten syndrome. *The American Journal of Human Genetics*, 96(2):275–282, 2015.
- [249] Mikael Knip, Riitta Veijola, Suvi M Virtanen, Heikki Hyöty, Outi Vaarala, and Hans K Åkerblom. Environmental triggers and determinants of type 1 diabetes. *Diabetes*, 54(suppl 2):S125–S136, 2005.
- [250] Tom L Van Belle, Ken T Coppieters, and Matthias G Von Herrath. Type 1 diabetes: etiology, immunology, and therapeutic strategies. *Physiological Reviews*, 91(1):79–118, 2011.
- [251] KT Coppieters, A Wiberg, SM Tracy, and MG von Herrath. Immunology in the clinic review series: focus on type 1 diabetes and viruses: the role of viruses in type 1 diabetes: a difficult dilemma. *Clinical & Experimental Immunology*, 168(1):5–11, 2012.
- [252] Didier Hober and Enagnon K Alidjinou. Enteroviral pathogenesis of type 1 diabetes: queries and answers. *Current Opinion in Infectious Diseases*, 26(3):263–269, 2013.
- [253] Wing-Chi G Yeung, William D Rawlinson, and Maria E Craig. Enterovirus infection and type 1 diabetes mellitus: systematic review and meta-analysis of observational molecular studies. *BMJ*, 342:d35, 2011.
- [254] Jennifer P Wang, Anna Cerny, Damon R Asher, Evelyn A Kurt-Jones, Roderick T Bronson, and Robert W Finberg. MDA5 and MAVS mediate type I interferon responses to coxsackie B virus. *Journal of Virology*, 84(1):254–260, 2010.
- [255] K Lind, MH Hühn, and M Flodström-Tullberg. Immunology in the clinic review series; focus on type 1 diabetes and viruses: the innate immune response to enteroviruses and its possible role in regulating type 1 diabetes. *Clinical & Experimental Immunology*, 168(1):30–38, 2012.
- [256] Matthias von Herrath. Diabetes: a virus–gene collaboration. *Nature*, 459(7246):518–519, 2009.
- [257] John A Todd. Etiology of type 1 diabetes. *Immunity*, 32(4):457–467, 2010.

- [258] Deborah J Smyth, Jason D Cooper, Rebecca Bailey, Sarah Field, Oliver Burren, Luc J Smink, Cristian Guja, Constantin Ionescu-Tirgoviste, Barry Widmer, David B Dunger, et al. A genome-wide association study of nonsynonymous SNPs identifies a type 1 diabetes locus in the interferon-induced helicase (IFIH1) region. *Nature Genetics*, 38(6):617–619, 2006.
- [259] Siyang Liu, Hongjie Wang, Yulan Jin, Robert Podolsky, MV Prasad Linga Reddy, Jennifer Pedersen, Bruce Bode, John Reed, Dennis Steed, Steve Anderson, et al. IFIH1 polymorphisms are significantly associated with type 1 diabetes and IFIH1 gene expression in peripheral blood mononuclear cells. *Human Molecular Genetics*, 18(2):358–365, 2009.
- [260] Magdalena Zurawek, Marta Fichna, Piotr Fichna, Bogda Skowronska, Agnieszka Dzikiewicz-Krawczyk, Danuta Januszkiewicz, and Jerzy Nowak. Cumulative effect of IFIH1 variants and increased gene expression associated with type 1 diabetes. *Diabetes Research and Clinical Practice*, 107(2):259–266, 2015.
- [261] Sergey Nejentsev, Neil Walker, David Riches, Michael Egholm, and John A Todd. Rare variants of IFIH1, a gene implicated in antiviral responses, protect against type 1 diabetes. *Science*, 324(5925):387–389, 2009.
- [262] Dimitry A Chistiakov, Natalia V Voronova, Kirill V Savost'Anov, and Rustam I Turakulov. Loss-of-function mutations E627X and I923V of IFIH1 are associated with lower poly (I: C)-induced interferon- $\beta$  production in peripheral blood mononuclear cells of type 1 diabetes patients. *Human Immunology*, 71(11):1128–1134, 2010.
- [263] Taeko Shigemoto, Maiko Kageyama, Reiko Hirai, JiPing Zheng, Mitsutoshi Yoneyama, and Takashi Fujita. Identification of Loss of Function Mutations in Human Genes Encoding RIG-I and MDA5. Implications for resistance to type 1 diabetes. *Journal of Biological Chemistry*, 284(20):13348–13354, 2009.
- [264] Kate Downes, Marcin Pekalski, Karen L Angus, Matthew Hardy, Sarah Nutland, Deborah J Smyth, Neil M Walker, Chris Wallace, and John A Todd. Reduced expression of IFIH1 is protective for type 1 diabetes. *PLoS One*, 5(9):e12646, 2010.
- [265] Konstantin MJ Sparrer and Michaela U Gack. Intracellular detection of viral nucleic acids. *Current Opinion in Microbiology*, 26:1–9, 2015.
- [266] Alison M Kell and Michael Gale. RIG-I in RNA virus recognition. *Virology*, 479:110–121, 2015.
- [267] Agnidipta Ghosh and Christopher D Lima. Enzymology of RNA cap synthesis. *Wiley Interdisciplinary Reviews: RNA*, 1(1):152–172, 2010.
- [268] Heike Betat, Yicheng Long, Jane E Jackman, and Mario Mörl. From end to end: tRNA editing at 5'-and 3'-terminal positions. *International Journal of Molecular Sciences*, 15(12):23975–23998, 2014.
- [269] Joao Trindade Marques, Thalie Devosse, Die Wang, Maryam Zamanian-Daryoush, Paul Serbinowski, Rune Hartmann, Takashi Fujita, Mark A Behlke, and Bryan RG Williams. A structural basis for discriminating between self and nonself double-stranded RNAs in mammalian cells. *Nature Biotechnology*, 24(5):559–565, 2006.
- [270] Axel Roers, Björn Hiller, and Veit Hornung. Recognition of Endogenous Nucleic Acids by the Innate Immune System. *Immunity*, 44(4):739–754, 2016.
- [271] Mark A Batzer and Prescott L Deininger. Alu repeats and human genomic diversity. *Nature*

- Reviews Genetics*, 3(5):370–379, 2002.
- [272] Niamh Mannion, Fabiana Arieti, Angela Gallo, Liam P Keegan, and Mary A O’Connell. New Insights into the Biological Role of Mammalian ADARs; the RNA Editing Proteins. *Biomolecules*, 5(4):2338–2362, 2015.
- [273] Qian Feng, Stanleyson V Hato, Martijn A Langereis, Jan Zoll, Richard Virgen-Slane, Alys Peisley, Sun Hur, Bert L Semler, Ronald P van Rij, and Frank JM van Kuppeveld. MDA5 detects the double-stranded RNA replicative form in picornavirus-infected cells. *Cell Reports*, 2(5): 1187–1196, 2012.
- [274] Kiyohiro Takahasi, Hiroyuki Kumeta, Natsuko Tsuduki, Ryo Narita, Taeko Shigemoto, Reiko Hirai, Mitsutoshi Yoneyama, Masataka Horiuchi, Kenji Ogura, Takashi Fujita, et al. Solution structures of cytosolic RNA sensor MDA5 and LGP2 C-terminal domains identification of the rna recognition loop in RIG-I-like receptors. *Journal of Biological Chemistry*, 284(26): 17465–17474, 2009.
- [275] Charlotte Lässig, Sarah Matheisl, Konstantin MJ Sparrer, Carina C de Oliveira Mann, Manuela Moldt, Jenish R Patel, Marion Goldeck, Gunther Hartmann, Adolfo García-Sastre, Veit Hornung, et al. ATP hydrolysis by the viral RNA sensor RIG-I prevents unintentional recognition of self-RNA. *eLife*, 4:e10859, 2015.
- [276] Harald Dürr, Andrew Flaus, Tom Owen-Hughes, and Karl-Peter Hopfner. Snf2 family ATPases and DExx box helicases: differences and unifying concepts from high-resolution crystal structures. *Nucleic Acids Research*, 34(15):4160–4167, 2006.
- [277] Jade Louber, Joanna Brunel, Emiko Uchikawa, Stephen Cusack, and Denis Gerlier. Kinetic discrimination of self/non-self RNA by the ATPase activity of RIG-I and MDA5. *BMC Biology*, 13(1):54, 2015.
- [278] David C Rawling, Megan E Fitzgerald, and Anna Marie Pyle. Establishing the role of ATP for the function of the RIG-I innate immune sensor. *eLife*, 4:e09391, 2015.
- [279] Peter Gee, Pong Kian Chua, Jirair Gevorkyan, Klaus Klumpp, Isabel Najera, David C Swinney, and Jerome Deval. Essential role of the N-terminal domain in the regulation of RIG-I ATPase activity. *Journal of Biological Chemistry*, 283(14):9488–9496, 2008.
- [280] Dahai Luo, Andrew Kohlway, Adriana Vela, and Anna Marie Pyle. Visualizing the determinants of viral RNA recognition by innate immune sensor RIG-I. *Structure*, 20(11):1983–1988, 2012.
- [281] Annie M Bruns, George P Leser, Robert A Lamb, and Curt M Horvath. The innate immune sensor LGP2 activates antiviral signaling by regulating MDA5-RNA interaction and filament assembly. *Molecular cell*, 55(5):771–781, 2014.
- [282] Xiaojun Li, CT Ranjith-Kumar, Monica T Brooks, Srisathiyannarayanan Dharmiah, Andrew B Herr, Cheng Kao, and Pingwei Li. The RIG-I-like receptor LGP2 recognizes the termini of double-stranded RNA. *Journal of Biological Chemistry*, 284(20):13881–13891, 2009.
- [283] Ting Xu, Aruna Sampath, Alex Chao, Daying Wen, Max Nanao, Patrick Chene, Subhash G Vasudevan, and Julien Lescar. Structure of the dengue virus helicase/nucleoside triphosphatase catalytic domain at a resolution of 2.4 Å. *Journal of Virology*, 79(16):10278–10288, 2005.
- [284] Jinhua Wu, Alope Kumar Bera, Richard J Kuhn, and Janet L Smith. Structure of the Flavivirus helicase: implications for catalytic activity, protein interactions, and proteolytic processing.

- Journal of Virology*, 79(16):10268–10277, 2005.
- [285] Erika J Mancini, Rene Assenberg, Anil Verma, Thomas S Walter, Roman Tuma, Jonathan M Grimes, Raymond J Owens, and David I Stuart. Structure of the Murray Valley encephalitis virus RNA helicase at 1.9 Å resolution. *Protein Science*, 16(10):2294–2300, 2007.
- [286] Dahai Luo, Ting Xu, Randall P Watson, Daniella Scherer-Becker, Aruna Sampath, Wolfgang Jahnke, Sui Sum Yeong, Chern Hoe Wang, Siew Pheng Lim, Alex Strongin, et al. Insights into RNA unwinding and ATP hydrolysis by the flavivirus NS3 protein. *The EMBO Journal*, 27(23):3209–3219, 2008.
- [287] Dahai Luo, Ting Xu, Cornelia Hunke, Gerhard Grüber, Subhash G Vasudevan, and Julien Lescar. Crystal structure of the NS3 protease-helicase from dengue virus. *Journal of Virology*, 82(1):173–183, 2008.
- [288] Meigang Gu and Charles M Rice. Three conformational snapshots of the hepatitis C virus NS3 helicase reveal a ratchet translocation mechanism. *Proceedings of the National Academy of Sciences*, 107(2):521–528, 2010.
- [289] Todd C Appleby, Robert Anderson, Olga Fedorova, Anna M Pyle, Ruth Wang, Xiaohong Liu, Katherine M Brendza, and John R Somoza. Visualizing ATP-dependent RNA translocation by the NS3 helicase from HCV. *Journal of Molecular Biology*, 405(5):1139–1153, 2011.
- [290] Cristina Failla, Licia Tomei, and RAFFAELE De Francesco. Both NS3 and NS4A are required for proteolytic processing of hepatitis C virus nonstructural proteins. *Journal of Virology*, 68(6):3753–3760, 1994.
- [291] JA Suzich, JK Tamura, F Palmer-Hill, P Warrener, A Grakoui, CM Rice, SM Feinstone, and MS Collett. Hepatitis C virus NS3 protein polynucleotide-stimulated nucleoside triphosphatase and comparison with the related pestivirus and flavivirus enzymes. *Journal of Virology*, 67(10):6152–6158, 1993.
- [292] Dong Wook Kim, Yousang Gwack, Jang H Han, and Joonho Choe. C-terminal domain of the hepatitis C virus NS3 protein contains an RNA helicase activity. *Biochemical and Biophysical Research Communications*, 215(1):160–166, 1995.
- [293] Chun-Ling Tai, Wei-Kuang Chi, Ding-Shinn Chen, and Lih-Hwa Hwang. The helicase activity associated with hepatitis C virus nonstructural protein 3 (NS3). *Journal of Virology*, 70(12):8477–8484, 1996.
- [294] Sua Myong, Michael M Bruno, Anna M Pyle, and Taekjip Ha. Spring-loaded mechanism of DNA unwinding by hepatitis C virus NS3 helicase. *Science*, 317(5837):513–516, 2007.
- [295] Chao Lin and Joseph L Kim. Structure-based mutagenesis study of hepatitis C virus NS3 helicase. *Journal of Virology*, 73(10):8798–8807, 1999.
- [296] Ying Kai Chan and Michaela U Gack. RIG-I-like receptor regulation in virus infection and immunity. *Current Opinion in Virology*, 12:7–14, 2015.



## List of abbreviations

ADAR1	adenosine deaminase acting on RNA 1, A-to-I RNA editing enzyme
aa	amino acids
CARDs	caspase activation and recruitment domains, tandem domain of RLRs involved in signal transmission
CTD	C-terminal domain, domain of RLRs that confers substrate specificity
dsRNA	double-stranded RNA
HBV/ HCV	hepatitis B/ C virus
IFN	interferon
IKK	I $\kappa$ B kinase, kinase that phosphorylates I $\kappa$ B
IRF	interferon regulatory factor, transcription factor
ISG	interferon regulated gene
LGP2	laboratory of genetics and physiology 2, RIG-I paralogue involved in viral RNA sensing
MAVS	mitochondrial antiviral signaling protein, adapter protein of RLRs
MDA5	melanoma differentiation-associated gene 5, RIG-I paralogue involved in viral RNA sensing
MeV	measles virus, single-stranded, negative-sense RNA virus
NF- $\kappa$ B	nuclear factor $\kappa$ -light-chain-enhancer of activated B cells, transcription factor
NS3	non-structural protein 3, viral enzyme
PAMP	pathogen-associated molecular pattern
PP1	phosphoprotein phosphatase 1, RIG-I and MDA5 dephosphorylating enzyme
PRR	pathogen recognition receptor
RIG-I	retinoic acid-inducible gene I
RLRs	RIG-I-like receptors
RNase L	ribonuclease L, enzyme that cleaves ssRNA
SF2	Superfamily 2, domain that characterizes Superfamily 2 helicases/ translocases
SMS	Singleton-Merten syndrome, multi-system disease
SNP	single-nucleotide polymorphism
ssRNA	single-stranded RNA
TBK1	TANK-binding kinase 1
TLRs	Toll-like receptors
TRAF	tumor necrosis factor (TNF) receptor-associated factor
TRIM25	tripartite motif 25, a RIG-I ubiquitinating enzyme
UTR	untranslated region, non-coding part of mRNA



# Acknowledgments

An dieser Stelle möchte ich mich bei all jenen bedanken, die mir bei der Umsetzung dieser Arbeit geholfen haben. Ohne die Hilfe und Unterstützung von vielen anderen wäre diese Arbeit nicht möglich gewesen.

Zuallererst gilt mein aufrichtiger Dank meinem Doktorvater Prof. Dr. Karl-Peter Hopfner, dass er sein Vertrauen in mich gesetzt hat und es mir ermöglichte an diesen, wie ich finde sehr spannenden Proteinen zu arbeiten. Ich bin aus den gemeinsamen Besprechungen immer sehr motiviert herausgegangen. Unter seiner Betreuung konnte ich viel lernen und habe die Entscheidung in seinem Labor zu arbeiten nie bereut.

Ebenfalls möchte ich mich bei Prof. Dr. Karl-Klaus Conzelmann ganz herzlich bedanken. Ohne seine Unterstützung und die Zusammenarbeit mit seiner netten Gruppe wäre ein Großteil dieser Arbeit nicht entstanden.

Ein großer Dank gilt natürlich Simon Runge, der mich in das Thema und die Arbeiten im Labor eingeführt hat. Ebenso möchte ich mich bei Konstantin Sparrer für seine Hilfe und sein Interesse ganz herzlich bedanken.

Sarah Matheisl, Carina Mann und Manuela Moldt möchte ich vor allem für die großartige Hilfe während des so stressigen letzten Jahres danken. Stefan Krebs danke außerdem für die nette Hilfe bei der Analyse meiner RNA Proben sowie Phillipp Torkler und Katharina Hembach für die Einarbeitung in die Analyse von Sequenzierungsdaten.

Ich danke weiterhin allen Labormitgliedern für die angenehme Arbeitsatmosphäre und vielseitige Hilfe. Allen dauerhaft Angestellten im Hopfner Labor, allen voran Katja und Gregor, aber auch Brigitte, Olga, Alex und Claudia möchte ich besonders danken, dass sie uns viele kleine und große Aufgaben abnehmen, und sich um alle Fragen gewissenhaft kümmern. Ihr ermöglicht erst ein unbeschwertes Arbeiten.

Meiner Familie, insbesondere meinen Eltern, und meinen Freunden, danke ich von ganzem Herzen, dass sie mich alle jederzeit unterstützt haben wo sie nur konnten und geduldig zu mir halten. Ebenso möchte ich meinem Freund Mathias danken, der mich mit viel Verständnis begleitet und auf den ich mich jedes mal zu Hause freue.



